

---

# Brief Encounters

Binary Correlations among Bosons

---

Ph.D. Thesis

Ole Sørensen



Department of Physics and Astronomy  
University of Aarhus

January 2004



## Preface

This thesis is presented for the Faculty of Science at the University of Aarhus, Denmark, in order to fulfil the requirements for the Ph.D. degree in physics.

The thesis gives an account of the work done during my Ph.D. studies at the Department of Physics and Astronomy at the University of Aarhus. First of all, I thank my supervisors Aksel Jensen and Dmitri Fedorov. I am grateful to their encouragement and our many discussions through the four years. Also a thank you to Esben Nielsen, Han Guangze, and Takaaki Sogo, and thanks to the people at the institute, at conferences, and at other physics meetings. Thanks to Karen Marie Hilligsøe for proof-reading.

Thanks to fellow students and friends.

*Tak til familie og venner.*

Ole Sørensen  
Århus, January 2004



## List of publications and preprints

Most subjects in this thesis are also discussed in the following publications and preprints:

1. **“Two-body correlations in Bose-Einstein condensates”**;  
Ole Sørensen, Dmitri V. Fedorov, Aksel S. Jensen, and Esben Nielsen;  
Phys. Rev. A **65**, 051601(R) (2002);  
*Internet*: <http://arxiv.org/abs/cond-mat/0110069>.
2. **“Towards Treating Correlations in Bose Condensates”**;  
Aksel S. Jensen, Ole Sørensen, Dmitri V. Fedorov, and Esben Nielsen;  
Few-Body Systems **31**, 261 (2002);  
*Internet*: <http://link.springer.de/link/service/journals/00601/bibs/2031002/20310261.htm>.
3. **“Correlated Trapped Bosons and the Many-Body Efimov Effect”**;  
Ole Sørensen, Dmitri V. Fedorov, and Aksel S. Jensen;  
Phys. Rev. Lett. **89**, 173002 (2002);  
*Internet*: <http://arxiv.org/abs/cond-mat/0203400>.
4. **“Two-body correlations in  $N$ -body boson systems”**;  
Ole Sørensen, Dmitri V. Fedorov, and Aksel S. Jensen;  
Phys. Rev. A **66**, 032507 (2002);  
*Internet*: <http://arxiv.org/abs/cond-mat/0210095>.
5. **“Decay of boson systems with large scattering length”**;  
Ole Sørensen, Dmitri V. Fedorov, and Aksel S. Jensen;  
J. Opt. B: Quantum Semiclass. Opt. **5**, S388 (2003);  
*Internet*: <http://www.iop.org/EJ/abstract/1464-4266/5/3/374>.
6. **“Two-Body Correlations and the Structure of Bose-Einstein Condensates”**;  
Ole Sørensen, Dmitri V. Fedorov, and Aksel S. Jensen;  
Few-Body Systems Suppl. **14**, 373 (2003);  
Proceedings of the XVIIIth European Conference on Few-Body Problems in Physics, Bled, Slovenia, 2002;  
*Internet*: <http://www.springer.at/main/book.jsp?bookID=3-211-83900-3&categoryID=13>.

7. **“Correlated  $N$ -boson systems for arbitrary scattering length”**;  
Ole Sørensen, Dmitri V. Fedorov, and Aksel S. Jensen;  
Phys. Rev. A **68**, 063618 (2003);  
*Internet*: <http://arxiv.org/abs/cond-mat/0305040>.
8. **“Structure of boson systems beyond the mean-field”**;  
Ole Sørensen, Dmitri V. Fedorov, and Aksel S. Jensen;  
J. Phys. B: At. Mol. Opt. Phys. **37**, 93 (2004);  
*Internet*: <http://arxiv.org/abs/cond-mat/0306564>.
9. **“Condensates and Correlated Boson Systems”**;  
Ole Sørensen, Dmitri V. Fedorov, and Aksel S. Jensen;  
to be published in Few-Body Systems;  
Conference on Critical Stability III, Trento, Italy, 2003;  
*Internet*: <http://arxiv.org/abs/cond-mat/0310304>.
10. **“Stability, effective dimensions, and interactions for bosons in deformed fields”**;  
Ole Sørensen, Dmitri V. Fedorov, and Aksel S. Jensen;  
revised version will be submitted to Phys. Rev. A;  
*Internet*: <http://arxiv.org/abs/cond-mat/0310462>.

# Contents

<b>Preface</b>	<b>iii</b>
<b>List of publications and preprints</b>	<b>v</b>
<b>1 Introduction</b>	<b>1</b>
1.1 Bosons . . . . .	1
1.2 Two-body properties . . . . .	2
1.3 Few-body physics . . . . .	3
1.4 The thesis work . . . . .	4
1.5 Thesis outline . . . . .	6
<b>2 Hyperspherical description of correlations</b>	<b>7</b>
2.1 Jacobi vectors and hyperspherical coordinates . . . . .	8
2.2 Schrödinger equation for $N$ identical particles . . . . .	10
2.2.1 Hamiltonian in hyperspherical coordinates . . . . .	10
2.2.2 Adiabatic expansion and equations of motion . . . . .	11
2.3 Wave function for identical particles . . . . .	13
2.3.1 Hartree: single-particle product . . . . .	14
2.3.2 Faddeev-Yakubovskii: cluster expansion . . . . .	15
2.3.3 Jastrow: two-body factorization . . . . .	16
2.3.4 Hyperharmonic expansion of two-body components . . . . .	17
2.3.5 Fermion antisymmetry . . . . .	19
2.3.6 Two-boson direction-independent correlations . . . . .	19
2.3.7 Three-body correlations . . . . .	21
2.4 Angular eigenvalue equation for two-boson correlations . . . . .	22
2.4.1 Faddeev-like equation . . . . .	22
2.4.2 Variational angular equation . . . . .	24
2.4.3 Short-range approximation . . . . .	26
2.4.4 Variational equation for three-body correlations . . . . .	28
<b>3 Interactions and the hyperangular spectrum</b>	<b>29</b>
3.1 Interactions between neutral bosons . . . . .	29
3.2 Analytical angular properties . . . . .	33
3.2.1 Kinetic-energy eigenfunctions . . . . .	34

3.2.2	Asymptotic spectrum for two-body states . . . . .	35
3.2.3	Zero-range approximation . . . . .	36
3.2.4	Average, non-correlated effects of interactions . . . . .	38
3.3	Numerical angular solutions . . . . .	40
3.3.1	Numerical method . . . . .	40
3.3.2	Angular potentials . . . . .	41
3.3.3	Angular wave function . . . . .	45
3.4	Summary . . . . .	48
3.4.1	Parametrization . . . . .	48
3.4.2	At the threshold . . . . .	50
3.4.3	Discussion . . . . .	51
<b>4</b>	<b>Hyperradial confinement and condensates</b>	<b>53</b>
4.1	Trapped bosons . . . . .	53
4.2	Radial potential and solutions . . . . .	55
4.3	Self-bound many-body states . . . . .	57
4.4	Efimov-like many-body states . . . . .	59
4.5	Trap states and “the condensate” . . . . .	63
4.5.1	A definition of “condensate” . . . . .	63
4.5.2	Interaction energy . . . . .	66
4.6	Summary . . . . .	67
<b>5</b>	<b>Mean field and validity</b>	<b>69</b>
5.1	Comparison to mean field . . . . .	69
5.1.1	Two-body interactions . . . . .	70
5.1.2	Density-dependent interactions . . . . .	71
5.1.3	Properties of the wave functions . . . . .	74
5.2	Validity conditions . . . . .	76
<b>6</b>	<b>Macroscopic stability and decay</b>	<b>79</b>
6.1	Stability criterion . . . . .	79
6.2	Decay . . . . .	82
6.2.1	Three-body recombination . . . . .	83
6.2.2	Macroscopic tunneling and recombination . . . . .	84
6.2.3	Macroscopic collapse . . . . .	86
6.2.4	Observation of Efimov-like states . . . . .	89
6.3	Summary . . . . .	89
<b>7</b>	<b>Deformed boson system</b>	<b>91</b>
7.1	Hyperspherical description of deformation . . . . .	92
7.2	Stability criterion for bosons in a deformed trap . . . . .	95
7.3	Effective dimension . . . . .	98
7.4	Deformation-dependent interactions . . . . .	99
7.5	Discussion . . . . .	102
<b>8</b>	<b>Conclusions and perspectives</b>	<b>103</b>



<b>9</b>	<b>Sammendrag på dansk (Summary in Danish)</b>	<b>107</b>
<b>A</b>	<b>Coordinate transformations</b>	<b>109</b>
A.1	Jacobi coordinates for $N$ identical particles . . . . .	109
A.2	Hyperspherical coordinates . . . . .	110
A.2.1	Three particles in three dimensions . . . . .	110
A.2.2	$N$ particles in three dimensions . . . . .	111
A.2.3	$N$ particles in $d$ dimensions . . . . .	112
A.3	“Hypercylindrical” coordinates . . . . .	113
<b>B</b>	<b>Hyperangular matrix elements</b>	<b>115</b>
B.1	Alternative Jacobi trees . . . . .	115
B.2	Matrix elements: Faddeev . . . . .	117
B.3	Matrix elements: variational . . . . .	118
B.3.1	Numbers of different terms . . . . .	118
B.3.2	Evaluation of terms . . . . .	121
B.3.3	Results in the short-range limit . . . . .	123
<b>C</b>	<b>Properties of Jacobi functions</b>	<b>125</b>
<b>D</b>	<b>Numerical scalings of angular potential</b>	<b>127</b>
D.1	Effective dependence on the scattering length . . . . .	127
D.2	Dependence on the number of particles . . . . .	129
D.3	Bound two-body state . . . . .	133
<b>E</b>	<b>Derivation of effective dimension</b>	<b>135</b>
<b>F</b>	<b>List of notations</b>	<b>141</b>
	<b>List of figures</b>	<b>145</b>
	<b>Bibliography</b>	<b>147</b>



# Chapter I

## Introduction

A description of a large system of particles is often sought in a derivation from the detailed behaviour of just a few of the particles. The present thesis deals with the connection between such microscopic features and the nature of a collection of many particles. A study of identical bosons is an obvious first investigation of this link, but the ideas might also be applied to fermion systems or to systems with mixed symmetry. The relatively well-known, flexible properties of cold alkali gases have presented questions which might be addressed by a study of few-body correlations. In this chapter we comment on basic features of bosonic systems and motivate a description of few-body correlations within a many-particle system.\*

### 1.1 Bosons

All particles can be classified as either bosons or fermions. The distinction is important when identical particles approach each other. Electrons, nucleons, and quarks are fermions and obey the Fermi-Dirac statistics, while force carriers like photons and gluons are bosons and obey the Bose-Einstein statistics. Atomic nuclei, atoms, and molecules obey one of the statistics depending on the number of contained fermions. In this thesis we as far as possible consider bosons generally, but often relate to bosonic neutral atoms with an even number of neutrons, in particular alkali atoms like  $^{87}\text{Rb}$  or  $^{23}\text{Na}$ . Although bosons are the main objects, we will a couple of times consider extensions of the methods to deal with fermions.

At most one fermion can occupy the same quantum state, whereas bosons are not restricted. An example is Bose-Einstein condensation of a vast number of bosons in the same single-particle state, which was experimentally achieved in 1995 by cooling dilute alkali gases [AEM<sup>+</sup>95, BSTH95, DMA<sup>+</sup>95].

A mean field is the basis for the description of dilute alkali gases by the Gross-Pitaevskii equation [EB95, BP96]. In mean-field self-consistent theories [BJ83]

---

\*The use of “we” refers to the author with the reader's participation.

the influence from interactions is included as an average, hence the name mean field. Such a description is reasonable when the interaction between particles is so weak that each particle only feels the other particles as an average background cloud in which they move. The rigorous criterion is that the mean free path is long compared to the spatial extension of the system. Reviews of theoretical developments before and after the experimental realization of Bose-Einstein condensation are given in the references [DGPS99, PS02, PS03].

At strong interaction or large densities each particle might interact strongly with one or a few of the other particles. The particles then adapt to the local environment, but still feel the (weaker) mean-field influence from the remaining particles. This competition between the background and the local surroundings is important when we formulate the theory in chapter 2.

When the attraction is too large, for example when condensates collapse [SSH98, SGWH99, DCC<sup>+</sup>01, RCC<sup>+</sup>01], correlations beyond the mean field are crucial. Descriptions based on the mean-field Gross-Pitaevskii equation [Adh02b, US03] can account for this collapse, but avoid direct relations to underlying microscopic processes.

Some methods go beyond the mean field, but still avoid the explicit inclusion of correlations. An example is the Skyrme-Hartree-Fock method with density-dependent interactions [SJ87]. Related are low-density expansions of the total energy for a many-boson system [LY57, BHM02].

For large densities particle encounters are more frequent and at least two-body correlations need to be explicitly included. This cannot be done directly on top of the usual mean field with a two-body contact interaction, i.e. of zero range, which would lead to a wave function with zero separation and diverging energy [FJ01a]. On the other hand, the use of realistic potentials in self-consistent mean-field calculations leads to disastrous results because the Hilbert space does not include correlations as needed to describe both the short- and long-range asymptotic behaviour [EG99].

An explicit inclusion of correlations is done by the Jastrow method [Jas55] where the many-body wave function is written as a product of two-body amplitudes instead of one-body amplitudes. With a few assumptions about the asymptotic behaviour of the amplitudes, this results in variational numerical procedures that can be carried through for many-boson systems also for large densities [MM01, CHM<sup>+</sup>02].

## 1.2 Two-body properties

A study of the properties of a many-particle system requires understanding of the two-body problem. The interaction between neutral atoms is repulsive at short distances and attractive at large distances. There may for alkali atoms be a large number of bound two-body states that are sensitive to the details of the interaction. However, when two atoms approach each other slowly from afar, their encounter can be described in a universal way irrespective of the short-distance details of the interaction. The determining parameter is then the

scattering length. This is infinitely large in the presence of a two-body bound state with vanishing energy. Then the two particles correlate in all space, which is the opposite limit than assumed by a mean field where no correlations are allowed.

At a Feshbach resonance, when the energy in a scattering channel coincides with the energy of a bound state in another channel [PS02], the scattering length diverges in the same way as when a two-body bound state occurs. In recent years such a Feshbach resonance has been investigated for both sodium [IAS<sup>+</sup>98, SIA<sup>+</sup>99] and rubidium gases [RCB<sup>+</sup>98, RBC<sup>+</sup>01]. For <sup>85</sup>Rb atoms an external magnetic field can slightly change the effective two-body potential curves, which have resulted in a tool for tuning the two-body scattering length [CCR<sup>+</sup>00].

Mean-field studies of dilute boson systems often include a two-body contact interaction with a coupling strength given by the scattering length. At large densities this becomes a problem since the interaction energy for the bosons then diverges. It is also difficult to handle large scattering lengths close to a Feshbach resonance. The alternative use of a boundary condition given by the scattering length at zero separation between the bosons allows larger density and scattering length [FJ01b].

Ultimately, the best description of the physics properties could be obtained by using realistic potentials which besides the correct large-distance two-body behaviour also incorporate high-energy features and the correct nature of bound states. However, this is especially difficult when the two-body system contains innumerable bound states, as is the case for the alkali atoms in experiments. Furthermore, if the goal is a description of the low-energy two-body properties within the many-body system, it would be an investment of too much effort in the wrong place. A more rewarding method is to use a simpler finite-range potential with the correct scattering length, for instance a linear combination of Gaussian potentials [BG01]. Considerations about the two-body interaction return in chapters 3 and 5.

### 1.3 Few-body physics

A system with only a few particles can be described accurately without crude assumptions. The related methods can provide insight into complicated problems, for instance how two or three particles approach each other within a many-body system. If the spatial extension of the system is large, an encounter of two particles can be considered as a pure two-body process with an average background influence from the other particles. Alternatively, it might be considered as a three-body process, the third body being the collection of the other particles. In smaller systems three particles approach each other more frequently, which then demands a description of a true three-body process. Faddeev [Fad60] wrote a wave function as a sum of terms that account for pairwise encounters, which by Yakubovskii [Yak67] was extended to account for the right behaviour of three-body clusters, four-body clusters, and so on. Within each cluster it is

then possible to treat the degrees of freedom rather accurately, while keeping in mind that the present collection of particles moves relative to the particles outside the cluster. The art of these Faddeev-Yakubovskii techniques is to make the proper assumption about the dominating structure of the many-body system; otherwise little is accomplished and the calculations turn out as complicated as for some methods based on a Jastrow ansatz.

Specifically for bosons, but implemented in nuclear physics, an approach with inclusion of two-body correlations was worked out by de la Ripelle *et al.* [dlR84, dlRFS88]. This approach is equivalent to the Faddeev-like equations to be described in chapter 2. The result is an eigenvalue equation in only one variable. Barnea [Bar99b] proposed the inclusion of higher-order correlations in a method which reminded of the Yakubovskii technique.

The hyperspherical adiabatic method, which was formulated for a study of the helium atom by Macek [Mac68], separates the description of the three-body system into a common length scale, i.e. the hyperradius, and an additional hyperangle. The extension of this method is now frequently used in atomic physics for descriptions of many-electron systems [Lin95].

After the experimental realization of Bose-Einstein condensation, most descriptions of this phenomenon were based on the mean-field Gross-Pitaevskii equation. However, Bohn *et al.* [BEG98] introduced a hyperspherical method to study the effect of interactions within the many-boson system. This hyperspherical method was simplified by the inclusion of a contact interaction and the assumption that the only dependence is on the average distance from the centre of mass, i.e. no correlations were allowed, which reminds of a mean field. An advantage of the hyperspherical method is that it provides an effective potential in a linear eigenvalue equation, in contrast to the non-linear nature of the Gross-Pitaevskii equation. In a related study Blume and Greene [BG02] calculated the properties of three bosons in an external trap with no assumptions about the structure of the wave function, and thus confirmed some of the behaviours of the effective potentials in the hyperspherical model for the many-boson system.

The detailed study of three particles provides an important first step in the formulation of a theory for clusterizations within a many-body system. The Faddeev-formalism is often applied within the hyperspherical adiabatic approximation when the emphasis is on the asymptotic two-body properties [JGF97, NFJG01]. The threshold phenomenon of infinitely many bound three-body states in the case of a two-body bound state with zero energy [Efi70] can be described by just the inclusion of two-body correlations [FJ93]. This anticipates that a generalization of the method to a many-boson system might describe the case of large scattering length where non-correlated models become inadequate.

## 1.4 The thesis work

The work for this thesis started from a few-body description of two-body correlations within a many-body system, and it has been centred on solving the

many-boson problem in a hyperspherical frame. Central questions are formulated as follows.

What is the effect of two-body correlations?

The outset for the thesis work was to understand how two-body correlations influence the properties of a many-boson system. This work is closely related to studies of the three-body system, see e.g. Nielsen *et al.* [NFJG01], and to the hyperspherical investigation of the average properties of the many-boson system by Bohn *et al.* [BEG98]. The formulation of the main techniques behind the inclusion of such correlations was given in the publications [SFJN02, SFJ02b]. This is collected in chapter 2 and appendix B. The effects of two-body correlations were mainly discussed in the references [SFJ02b, SFJ03a] and are here collected in chapters 3 and 4.

What happens close to a resonance?

The case of large scattering length provides for the three-body case the Efimov phenomenon of many bound three-body states [Efi70, FJ93]. The possibility of similar threshold effects for the many-boson system was investigated during the thesis work and the results were published in [SFJ02a]. This is discussed mainly in chapters 3 and 4.

Are the deviations from the mean field trustworthy?

The relations to the mean field and the deviations of the results were published in [SFJ04], where also ranges of validity were considered. This is here included in chapter 2 and in chapter 5.

Do two-body correlations influence stability?

The macroscopic stability problems for a many-boson system were briefly discussed in the previous publications, but were further addressed in relation to the observed phenomenon of macroscopic collapse [RCC<sup>+</sup>01, DCC<sup>+</sup>01] in the reference [SFJ03a], which also included a discussion of the competition between three-body recombinations, macroscopic tunneling, and macroscopic collapse. Chapter 6 collects these considerations.

How does the geometry influence the system?

Deformation effects were discussed in a preprint [SFJ03b], which gave stability criteria, effective dimensions, and effective interactions for bosons in a deformed external field. This discussion is continued in chapter 7. Since an inclusion of correlations in the deformed case is not presently implemented, this treatment is somehow similar to a mean-field treatment.

## 1.5 Thesis outline

The structure of the thesis can be summarized as follows. Chapter 2 presents the hyperspherical frame for studying few-body correlations within the many-boson system. This includes a discussion of the structure of the wave function and some comments on the mean-field wave function. We present the necessary assumptions when restricting to two-body correlations and the main features of the resulting equations of motion. Chapter 3 contains a discussion of analytical and numerical solutions to the hyperangular part of the Hamiltonian. Chapter 4 contains a discussion of the hyperradial part of the description of a many-boson system, as well as a discussion of Bose-Einstein condensation in the hyperspherical model. In chapter 5 we compare results from the previous chapters to the results from the mean-field Gross-Pitaevskii equation and ranges of validity are estimated. In chapter 6 we discuss stability criteria, approaches to the dynamical evolution of the many-boson system, and relevant time scales. Chapter 7 deals with the effects of a deformed external trap. Finally, chapter 8 contains conclusions and discussions of the results.



## Chapter II

### Hyperspherical description of correlations

Hyperspherical methods are used in studies of both few-body and many-body problems, for example in atomic physics [Mac68], nuclear physics [JGF97], and within atomic physics especially for many-electron systems [Lin95]. Especially relevant in the present context is a study of a many-boson system in a hyperspherical frame performed by Bohn *et al.* [BEG98]. A large number of degrees of freedom are described in terms of one length, the hyperradius, and some angles called hyperangles. This reminds of the characterization of a two-body system by the relative two-body distance and the angular degrees of freedom. In the hyperspherical description, the angular degrees of freedom are usually integrated or averaged such that the many-body system is described by only the hyperradius. An effective potential depending on the hyperradius then carries the information about the average angular properties. This is once more analogous to the description of the two-body problem by only the radial distance with inclusion of the angular momentum in an effective centrifugal potential.

In section 2.1 we first define a set of coordinates appropriate for a study of correlations in the many-body system. The steps are similar to the ones written by Barnea [Bar99b, Bar99a]. For clarity we formulate this in three spatial dimensions, but it can as well be written in lower dimensions. We then rewrite the Hamiltonian and the Schrödinger equation according to this choice of coordinate system in section 2.2. Appendix A contains further details. As basic input we need an ansatz for the many-body wave function. We discuss the basis for assuming a Faddeev-like decomposition of the wave function and relate this to other common approaches in section 2.3. We also discuss possible extensions to fermion symmetry and three-body correlations. We are then equipped to solve the angular equation in section 2.4, which is done with the inclusion of two-body correlations both by a Faddeev-like equation and by a variational equation. Some details of the derivations are given in appendix B. We end the chapter by considering the complications involved in an angular equation with the inclusion of three-body correlations.

## 2.1 Jacobi vectors and hyperspherical coordinates

The system of  $N$  identical particles may be described by  $N$  coordinate vectors  $\mathbf{r}_i$  and momenta  $\mathbf{p}_i$ , labeling the particles by the index  $i = 1, \dots, N$ . Here a more suitable choice of coordinates is the centre-of-mass coordinates  $\mathbf{R} = \sum_{i=1}^N \mathbf{r}_i / N$ , the  $N - 1$  relative Jacobi vectors  $\boldsymbol{\eta}_k$  with

$$\boldsymbol{\eta}_k = \sqrt{\frac{N-k}{N-k+1}} \left( \mathbf{r}_{N-k+1} - \frac{1}{N-k} \sum_{j=1}^{N-k} \mathbf{r}_j \right) \quad (2.1)$$

and  $k = 1, 2, \dots, N-1$ , and their associated momenta. These Jacobi coordinates are illustrated for the first six particles in figure 2.1. The notation is  $\eta_k \equiv |\boldsymbol{\eta}_k|$ ,

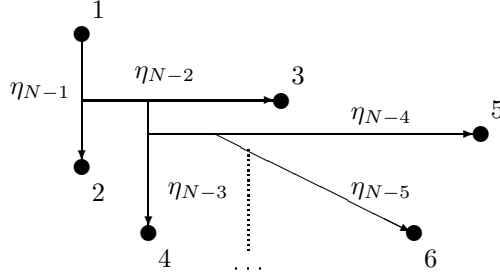


Figure 2.1: Jacobi vectors connecting the first six particles.

so  $\eta_{N-1}$  is proportional to the distance between particles 1 and 2,  $\eta_{N-2}$  is proportional to the distance between particle 3 and the centre of mass of 1 and 2,  $\eta_{N-3}$  is proportional to the distance between particle 4 and the centre of mass of the first three particles, and so on.\*

Hyperspherical coordinates are now defined in relation to the Jacobi vectors. One length, the hyperradius  $\rho$ , is defined by

$$\rho_l^2 \equiv \sum_{k=1}^l \eta_k^2, \quad \rho^2 \equiv \rho_{N-1}^2 = \frac{1}{N} \sum_{i < j}^N r_{ij}^2 = \sum_{i=1}^N (\mathbf{r}_i - \mathbf{R})^2, \quad (2.2)$$

where  $r_{ij} \equiv |\mathbf{r}_i - \mathbf{r}_j|$ . The last two equalities show that the hyperradius can be interpreted either as  $\sqrt{(N-1)/2}$  times the root-mean-square (rms) distance between particles or as  $\sqrt{N}$  times the rms distance between particles and the centre of mass.

In three spatial dimensions, the  $N - 2$  hyperangles  $\alpha_k \in [0, \pi/2]$  for  $k = 2, 3, \dots, N - 1$  relate the length of the Jacobi vectors to the hyperradius via the definition

$$\sin \alpha_k \equiv \frac{\eta_k}{\rho}. \quad (2.3)$$

---

\*Throughout the thesis normal font for a corresponding vector denotes the length of that vector, i.e.  $\eta_k = |\boldsymbol{\eta}_k|$ ,  $r_i = |\mathbf{r}_i|$ , etc.

Since  $\rho_1 = \eta_1$ , the fixed angle  $\alpha_1 = \pi/2$  is superfluous, but is for convenience often included in the notation. Remaining are the  $2(N-1)$  angles  $\Omega_\eta^{(k)} = (\vartheta_k, \varphi_k)$ , for  $k = 1, 2, \dots, N-1$ , that define the directions of the  $N-1$  vectors  $\boldsymbol{\eta}_k$ , that is  $\vartheta_k \in [0, \pi]$  and  $\varphi_k \in [0, 2\pi]$ . All angles are collectively denoted by  $\Omega \equiv \{\alpha_k, \vartheta_k, \varphi_k\}$  with  $k = 1, 2, \dots, N-1$ . In total the hyperangles  $\Omega$  and the hyperradius  $\rho$  amount to  $3(N-1)$  degrees of freedom and the centre-of-mass coordinates  $\mathbf{R}$  amount to three. These coordinates are also related by

$$\sum_{i=1}^N r_i^2 = \frac{1}{N} \sum_{i < j}^N r_{ij}^2 + \frac{1}{N} \left( \sum_{i=1}^N r_i \right)^2 = \rho^2 + NR^2. \quad (2.4)$$

The total volume element is

$$\prod_{i=1}^N d\mathbf{r}_i = N^{3/2} d\mathbf{R} \prod_{k=1}^{N-1} d\boldsymbol{\eta}_k, \quad (2.5)$$

where the part depending on relative coordinates is  $\prod_{k=1}^{N-1} d\boldsymbol{\eta}_k$ .<sup>†</sup> In hyperspherical coordinates this relative part becomes

$$\prod_{k=1}^{N-1} d\boldsymbol{\eta}_k = d\rho \rho^{3N-4} d\Omega_{N-1}, \quad (2.6)$$

$$d\Omega_k = d\Omega_\alpha^{(k)} d\Omega_\eta^{(k)} d\Omega_{k-1}, \quad d\Omega_1 = d\Omega_\eta^{(1)}, \quad (2.7)$$

$$d\Omega_\alpha^{(k)} = d\alpha_k \sin^2 \alpha_k \cos^{3k-4} \alpha_k, \quad d\Omega_\eta^{(k)} = d\vartheta_k \sin \vartheta_k d\varphi_k, \quad (2.8)$$

where  $d\Omega_\eta^{(k)}$  is the familiar angular volume element in spherical coordinates. Since the angle  $\alpha_{N-1}$  is related directly to the two-body distance  $r_{12}$  by  $\sin \alpha_{N-1} = \eta_{N-1}/\rho_{N-1} = r_{12}/(\sqrt{2}\rho)$ , the volume element in equation (2.8) related to this angle is especially important, that is  $d\Omega_\alpha^{(N-1)} = d\alpha_{N-1} \sin^2 \alpha_{N-1} \cos^{3N-7} \alpha_{N-1}$ .

The angular volume integrals can be computed to

$$\int d\Omega_\alpha^{(k)} = \frac{\sqrt{\pi} \Gamma[3(k-1)/2]}{4\Gamma(3k/2)}, \quad \int d\Omega_\eta^{(k)} = 4\pi, \quad (2.9)$$

where  $\Gamma$  is the gamma function [Spi68]. An angular matrix element of an operator  $\hat{O}$  with two arbitrary functions  $\Psi$  and  $\Phi$  is with equation (2.6) for fixed  $\rho$  then given by

$$\langle \Psi | \hat{O} | \Phi \rangle_\Omega = \int d\Omega_{N-1} \Psi^*(\rho, \Omega) \hat{O} \Phi(\rho, \Omega), \quad (2.10)$$

which in general is a function of  $\rho$ .

In this section the many-body system is described by a straightforward ordering of particles as  $\{1, 2, 3, \dots, N\}$ . Furthermore, we use the configuration

<sup>†</sup>The notation is  $d\mathbf{r}_i = dr_{ix} dr_{iy} dr_{iz}$  with  $\mathbf{r}_i = (r_{ix}, r_{iy}, r_{iz})$ .

principle that a Jacobi vector connects one particle with the centre of mass of some other particles. Both the ordering of particles and the recursive configurations have to be done differently when we later evaluate matrix elements. However, the present formulation of the basic equations is independent of such considerations and therefore the simplest structure is presented.

## 2.2 Schrödinger equation for $N$ identical particles

With the preceding choice of coordinates we obtain the Hamiltonian and next rewrite the Schrödinger equation by an adiabatic expansion, which was first used in a study of a helium atom [Mac68].

### 2.2.1 Hamiltonian in hyperspherical coordinates

We consider  $N$  identical particles of mass  $m$  interacting only through two-body potentials  $V_{ij} = V(\mathbf{r}_{ij})$ . We do not consider effects due to spin, and thus omit explicit spin dependence throughout this thesis.

An external trapping field  $V_{\text{trap}}$  confines all particles to a limited region of space. This is written explicitly as an isotropic harmonic-oscillator potential of angular frequency  $\omega$ , i.e. for particle  $i$  it is given by  $V_{\text{trap}}(\mathbf{r}_i) = m\omega^2 r_i^2/2$ . This confining field is relevant for studying trapped atomic gases, but can later be omitted from the general results by putting  $\omega = 0$ . The total Hamiltonian is here given by

$$\hat{H}_{\text{total}} = \sum_{i=1}^N \left( \frac{\hat{\mathbf{p}}_i^2}{2m} + \frac{1}{2}m\omega^2 r_i^2 \right) + \sum_{i<j}^N V(\mathbf{r}_{ij}), \quad (2.11)$$

which with equation (2.4) is separable into a part only involving the centre-of-mass coordinates and a part only involving relative coordinates. The centre-of-mass Hamiltonian is

$$\hat{H}_R \equiv \frac{\hat{\mathbf{P}}_R^2}{2M} + \frac{1}{2}M\omega^2 R^2, \quad (2.12)$$

where  $\mathbf{P}_R \equiv \sum_{i=1}^N \mathbf{p}_i$  is the total momentum and  $M = Nm$  is the total mass of the system. We subtract this from the total Hamiltonian and get

$$\begin{aligned} \hat{H} &\equiv \hat{H}_{\text{total}} - \hat{H}_R \\ &= \sum_{i=1}^N \frac{\hat{\mathbf{p}}_i^2}{2m} - \frac{\hat{\mathbf{P}}_R^2}{2M} + \sum_{i=1}^N \frac{1}{2}m\omega^2 r_i^2 - \frac{1}{2}M\omega^2 R^2 + \sum_{i<j}^N V_{ij}. \end{aligned} \quad (2.13)$$

Using equation (2.4) we can write this as

$$\hat{H} = \hat{T} + \frac{1}{2}m\omega^2 \rho^2 + \sum_{i<j}^N V_{ij}, \quad \hat{T} \equiv \sum_{i=1}^N \frac{\hat{\mathbf{p}}_i^2}{2m} - \frac{\hat{\mathbf{P}}_R^2}{2M}. \quad (2.14)$$

Here  $\hat{T}$  is the intrinsic kinetic-energy operator which in hyperspherical coordinates can be rewritten as

$$\hat{T} = -\frac{\hbar^2}{2m} \left( \frac{1}{\rho^{3N-4}} \frac{\partial}{\partial \rho} \rho^{3N-4} \frac{\partial}{\partial \rho} - \frac{\hat{\Lambda}_{N-1}^2}{\rho^2} \right). \quad (2.15)$$

The dimensionless angular kinetic-energy operator  $\hat{\Lambda}_{N-1}^2$  is recursively defined by

$$\hat{\Lambda}_k^2 = \hat{\Pi}_k^2 + \frac{\hat{\Lambda}_{k-1}^2}{\cos^2 \alpha_k} + \frac{\hat{\mathbf{l}}_k^2}{\sin^2 \alpha_k}, \quad \hat{\Lambda}_1^2 = \hat{\mathbf{l}}_1^2, \quad (2.16)$$

$$\hat{\Pi}_k^2 = -\frac{\partial^2}{\partial \alpha_k^2} + \frac{3k-6 - (3k-2) \cos 2\alpha_k}{\sin 2\alpha_k} \frac{\partial}{\partial \alpha_k}, \quad (2.17)$$

where  $\hat{\mathbf{l}}_k$  is the angular-momentum operator associated with  $\boldsymbol{\eta}_k$ . Thus, the angular kinetic-energy operator is a sum of derivatives with respect to the various hyperspherical angles. Convenient transformations to avoid first derivatives in equations (2.15) and (2.17) are

$$\begin{aligned} -\frac{2m}{\hbar^2} \hat{T}_\rho &\equiv \rho^{-(3N-4)} \frac{\partial}{\partial \rho} \rho^{3N-4} \frac{\partial}{\partial \rho} \\ &= \rho^{-(3N-4)/2} \left[ \frac{\partial^2}{\partial \rho^2} - \frac{(3N-4)(3N-6)}{4\rho^2} \right] \rho^{(3N-4)/2}, \end{aligned} \quad (2.18)$$

$$\begin{aligned} \hat{\Pi}_k^2 &= \sin^{-1} \alpha_k \cos^{-(3k-4)/2} \alpha_k \left[ -\frac{\partial^2}{\partial \alpha_k^2} - \frac{9k-10}{2} + \right. \\ &\quad \left. \frac{(3k-4)(3k-6)}{4} \tan^2 \alpha_k \right] \sin \alpha_k \cos^{(3k-4)/2} \alpha_k. \end{aligned} \quad (2.19)$$

The Hamiltonian  $\hat{H}$  can now be collected as

$$\hat{H} = \hat{T}_\rho + \frac{1}{2} m \omega^2 \rho^2 + \frac{\hbar^2}{2m\rho^2} \hat{h}_\Omega, \quad (2.20)$$

$$\hat{h}_\Omega \equiv \hat{\Lambda}_{N-1}^2 + \sum_{i < j}^N v_{ij}, \quad v_{ij} = \frac{2m\rho^2}{\hbar^2} V_{ij}, \quad (2.21)$$

where  $\hat{T}_\rho$  is the radial kinetic-energy operator,  $\hat{h}_\Omega$  is a dimensionless angular Hamiltonian, and  $v_{ij}$  is a dimensionless potential. Thus, the intrinsic Hamiltonian  $\hat{H}$  contains a part which only depends on  $\rho$  and a part  $\hat{h}_\Omega$  which depends on  $\Omega$  and on  $\rho$  through the two-body potentials  $v_{ij}$ .

### 2.2.2 Adiabatic expansion and equations of motion

Since the total Hamiltonian is given as  $\hat{H}_{\text{total}} = \hat{H}_R + \hat{H}$ , the total wave function for the  $N$ -particle system can be written as a product of a function  $\Upsilon$  depending

only on  $\mathbf{R}$  and a function  $\Psi$  depending on  $\rho$  and the  $3N - 4$  angular degrees of freedom collected in  $\Omega$ , i.e.

$$\Psi_{\text{total}} = \Upsilon(\mathbf{R})\Psi(\rho, \Omega) . \quad (2.22)$$

The centre-of-mass motion for the total mass  $M = Nm$  is determined by

$$\hat{H}_R \Upsilon(\mathbf{R}) = E_R \Upsilon(\mathbf{R}) . \quad (2.23)$$

From equation (2.12) the corresponding energy spectrum is obtained as that of a harmonic oscillator, that is  $E_{R,n} = \hbar\omega(2n + 3/2)$  with  $n = 0, 1, 2, \dots$

The relative wave function  $\Psi(\rho, \Omega)$  obeys the stationary Schrödinger equation

$$\hat{H}\Psi(\rho, \Omega) = E\Psi(\rho, \Omega) , \quad (2.24)$$

where  $E$  is the energy in the centre-of-mass system. This is solved in two steps. First, for a fixed value of the hyperradius  $\rho$  we solve the angular eigenvalue equation

$$(\hat{h}_\Omega - \lambda_\nu)\Phi_\nu(\rho, \Omega) = 0 . \quad (2.25)$$

The angular eigenvalue  $\lambda_\nu(\rho)$  depends on  $\rho$ . Second, the collection of angular eigenfunctions  $\Phi_\nu(\rho, \Omega)$  is used as a complete set of basis functions in an expansion of the relative wave function. This is for each value of the hyperradius  $\rho$  written as

$$\Psi(\rho, \Omega) = \sum_{\nu=0}^{\infty} F_\nu(\rho)\Phi_\nu(\rho, \Omega) , \quad F_\nu(\rho) = \rho^{-(3N-4)/2} f_\nu(\rho) , \quad (2.26)$$

where the factor  $\rho^{-(3N-4)/2}$  is introduced to eliminate first derivatives in  $\rho$ , see equation (2.18). The expansion coefficients for fixed  $\rho$ ,  $f_\nu$  or  $F_\nu$ , are then considered as hyperradial wave functions.

In analogy to the technique for  $N = 3$  [JGF97], equation (2.26) is inserted in equation (2.24), equations (2.20) and (2.25) are used, and the resulting equation is projected onto an angular eigenfunction  $\Phi_\nu$ . The result is a set of radial equations

$$\begin{aligned} & \left[ -\frac{d^2}{d\rho^2} - \frac{2mE}{\hbar^2} + \frac{\lambda_\nu(\rho)}{\rho^2} + \frac{(3N-4)(3N-6)}{4\rho^2} + \frac{\rho^2}{b_t^4} - Q_{\nu\nu}^{(2)}(\rho) \right] f_\nu(\rho) \\ & = \sum_{\nu' \neq \nu} \left[ 2Q_{\nu\nu'}^{(1)}(\rho) \frac{d}{d\rho} + Q_{\nu\nu'}^{(2)}(\rho) \right] f_{\nu'}(\rho) , \end{aligned} \quad (2.27)$$

that couple the different angular channels. Here  $b_t$  is the trap length given by  $b_t \equiv \sqrt{\hbar/(m\omega)}$ , and the coupling terms  $Q_{\nu\nu'}^{(i)}$  are defined as

$$Q_{\nu\nu'}^{(i)}(\rho) \equiv \frac{\langle \Phi_\nu(\rho, \Omega) | \left( \frac{\partial}{\partial \rho} \right)^i | \Phi_{\nu'}(\rho, \Omega) \rangle_\Omega}{\langle \Phi_\nu(\rho, \Omega) | \Phi_\nu(\rho, \Omega) \rangle_\Omega} . \quad (2.28)$$

A special result is  $Q_{\nu\nu}^{(1)} = 0$  [NFJG01]. The angular eigenvalues  $\lambda_\nu$  enter these coupled equations as a part of a radial potential. The total radial potential  $U_\nu(\rho)$ , entering on the left hand side of equation (2.27), is:

$$\frac{2mU_\nu(\rho)}{\hbar^2} \equiv \frac{\lambda_\nu(\rho)}{\rho^2} + \frac{(3N-4)(3N-6)}{4\rho^2} + \frac{\rho^2}{b_t^4} - Q_{\nu\nu}^{(2)}(\rho). \quad (2.29)$$

This includes a  $\rho^2$ -term due to the external harmonic field, a  $\rho^{-2}$  centrifugal barrier-term due to the transformation of the radial kinetic-energy operator, the angular potential  $\lambda_\nu$ , and the diagonal term  $Q_{\nu\nu}^{(2)}$ .

The expansion in equation (2.26) is called the hyperspherical adiabatic expansion. Its efficiency relies on small coupling terms  $Q_{\nu\nu'}^{(i)}$ , which then requires inclusion of fewer channels  $\nu$ . In the following investigations of the dilute boson system, the non-diagonal terms are often found to be smaller than 1% of the diagonal terms. Without these couplings the right-hand side of equation (2.27) vanishes, and the equation simplifies significantly to

$$\left[ -\frac{\hbar^2}{2m} \frac{d^2}{d\rho^2} + U_\nu(\rho) - E \right] f_\nu(\rho) = 0. \quad (2.30)$$

In this thesis small couplings are generally assumed and only results of this non-coupled treatment are shown.

Thus, the centre-of-mass motion is separated out and the hyperspherical adiabatic method turns out to be promising for a sufficiently dilute system due to small coupling terms. The remaining problem is the determination of the angular potential  $\lambda$  from the angular eigenvalue equation.

### 2.3 Wave function for identical particles

So far no specific structures are assumed. The allowed Hilbert space for the many-body wave function in principle includes any structure of the system. However, at this point an ansatz for or approximation of the angular wave function  $\Phi_\nu(\rho, \Omega)$  is necessary.

The Hartree wave function with a product of single-particle amplitudes [BJ83] is the basis for mean-field treatments of many-particle systems. In contrast, Faddeev-Yakubovskii formulations [Fad60, Yak67] contain additive decompositions of the wave function which explicitly reflect the possible asymptotic large-distance behaviours of cluster subsystems. A different starting point is the Jastrow factorization into products of two-body amplitudes [Jas55]. The Jastrow form is more efficient for large densities, while Faddeev-Yakubovskii methods are more successful for smaller densities where the system separates into smaller clusters.

In the present hyperspherical formulation, the angular wave function can be written as a general expansion in the full angular space and subsequently be reduced to yield a practical wave function. The result of such considerations is an

ansatz which is well suited for the low densities encountered for Bose-Einstein condensates. Two-body correlations are expected to be most important. Possible extensions of the method to include three-body correlations or fermion antisymmetry are briefly discussed.

### 2.3.1 Hartree: single-particle product

The Hartree ansatz with a product of single-particle amplitudes [BJ83] is

$$\Psi_{\text{H}}(\mathbf{r}_1, \mathbf{r}_2, \dots, \mathbf{r}_N) = \prod_{i=1}^N \psi_{\text{H}}(\mathbf{r}_i). \quad (2.31)$$

For the ground state of non-interacting bosons trapped by the spherically symmetric external field of trap length  $b_{\text{t}}$ , the amplitudes are given by

$$\psi_{\text{H}}(\mathbf{r}_i) = C e^{-r_i^2/(2b_{\text{t}}^2)}, \quad C^{-1} = \pi^{3/4} b_{\text{t}}^{3/2}. \quad (2.32)$$

With the relation  $\sum_{i=1}^N r_i^2 = \rho^2 + NR^2$  this is rewritten as

$$\begin{aligned} \Psi_{\text{H}}(\mathbf{r}_1, \mathbf{r}_2, \dots, \mathbf{r}_N) &= C^N \exp\left(-\sum_{i=1}^N \frac{r_i^2}{2b_{\text{t}}^2}\right) \\ &= C^N e^{-\rho^2/(2b_{\text{t}}^2)} e^{-NR^2/(2b_{\text{t}}^2)} = \Upsilon_0(\mathbf{R}) F_0(\rho) \Phi_0, \end{aligned} \quad (2.33)$$

which turns out as a product similar to equations (2.22) and (2.26). The separation of the centre-of-mass motion assures that the ground-state centre-of-mass function always is  $\Upsilon_0(\mathbf{R}) = CN^{3/4} \exp[-NR^2/(2b_{\text{t}}^2)]$ . Then equation (2.33) is a product of the ground-state wave function for the motion of the centre-of-mass in a trap and the lowest hyperspherical wave function  $F_0\Phi_0$  in equation (2.26), where  $F_0(\rho) \propto \exp[-\rho^2/(2b_{\text{t}}^2)]$  and the angular part  $\Phi_0$  is a constant. This implies equivalence between a Hartree-Gaussian wave function and lack of dependence on the hyperangles  $\Omega$ .

The interactions produce correlations in such a way that the hyperspherical wave function  $\Psi$  deviates from a hyperradial Gaussian multiplied by a constant hyperangular part. Therefore the Hartree product wave function is strictly not exact. However, a measure can be obtained by calculating the single-particle density  $n$  from the obtained function  $\Psi$ , that is

$$n(\mathbf{r}_1) = \int d\mathbf{r}_2 d\mathbf{r}_3 \cdots d\mathbf{r}_N |\Upsilon_0(\mathbf{R}) \Psi(\rho, \Omega)|^2. \quad (2.34)$$

This can then be compared with the Hartree analogue  $|\psi_{\text{H}}(\mathbf{r}_1)|^2$ . When the numerical hyperspherical solution is inserted, the  $3(N-1)$ -dimensional integral in equation (2.34) is rather complicated. In order to get an idea of the possible relations, we instead assume a constant angular part  $\Phi_0$ . Then the hyperradial



density distribution is expanded on Gaussian amplitudes with different length parameters  $a_j$

$$|F(\rho)|^2 = \sum_j c_j \frac{2}{\Gamma\left(\frac{3N-3}{2}\right) a_j^{3N-3}} e^{-\rho^2/a_j^2}, \quad (2.35)$$

where  $\sum_j c_j = 1$  assures that  $F(\rho)$  is properly normalized as  $\int_0^\infty d\rho \rho^{3N-4} |F(\rho)|^2 = 1$ . This yields the single-particle density

$$n(\mathbf{r}_1) = \sum_j c_j \frac{1}{\pi^{3/2} B_j^3} e^{-r_1^2/B_j^2}, \quad B_j^2 \equiv \frac{(N-1)a_j^2 + b_t^2}{N}, \quad (2.36)$$

which is equivalent to  $\langle r_1^2 \rangle = \int d\mathbf{r}_1 n(\mathbf{r}_1) r_1^2$  since

$$\langle r_1^2 \rangle = \frac{1}{N} \langle \rho^2 \rangle + \langle R^2 \rangle = \frac{3}{2} \left(1 - \frac{1}{N}\right) \sum_j c_j a_j^2 + \frac{3}{2} \frac{1}{N} b_t^2 \quad (2.37)$$

and

$$\begin{aligned} \int d\mathbf{r}_1 n(\mathbf{r}_1) r_1^2 &= \frac{3}{2} \sum_j c_j B_j^2 \\ &= \frac{3}{2} \left(1 - \frac{1}{N}\right) \sum_j c_j a_j^2 + \frac{3}{2} \frac{1}{N} b_t^2 \sum_j c_j = \langle r_1^2 \rangle. \end{aligned} \quad (2.38)$$

The mean-square distance between the particles is then obtained by the relation

$$\langle r_{12}^2 \rangle = \frac{2N}{N-1} \left( \langle r_1^2 \rangle - \langle R^2 \rangle \right) = \frac{2N}{N-1} \left( \langle r_1^2 \rangle - \frac{1}{N} \frac{3}{2} b_t^2 \right). \quad (2.39)$$

These relations are derived and valid only for Gaussian wave functions. However, the true Hartree solution is not strictly a Gaussian although such an approximation rather efficiently describes the dilute boson system [PS02]. The above results relate a Hartree density distribution to a similar hyperradial distribution provided that the angular wave function is assumed to be a constant which corresponds to an uncorrelated structure.

### 2.3.2 Faddeev-Yakubovskii: cluster expansion

The effect of correlations is beyond a mean field where particles only feel each other on average and do not correlate. With the Faddeev-Yakubovskii techniques the proper asymptotic behaviours of the wave functions are directly taken into account [Fad60, Yak67]. These formulations are well suited when the large-distance asymptotics are crucial, as expected for low-density systems.

Faddeev [Fad60] studied three-particle systems where one of the two-body subsystems was bound and the other subsystems were unbound. The wave

function was written as  $\Phi = \Phi_{12} + \Phi_{13} + \Phi_{23}$  with the three terms given by suitable permutations of

$$\Phi_{23} = \phi_{23}(\mathbf{r}_{23})e^{i\boldsymbol{\kappa}_1\mathbf{r}_1+i\boldsymbol{\kappa}_{23}\mathbf{R}_{23}} , \quad (2.40)$$

where  $\mathbf{R}_{23} = (m_2\mathbf{r}_2 + m_3\mathbf{r}_3)/(m_2 + m_3)$  is the centre of mass of the bound subsystem and  $\hbar\boldsymbol{\kappa}_1$  and  $\hbar\boldsymbol{\kappa}_{23}$  are the momenta of particle 1 and of particle pair 2-3, respectively.<sup>‡</sup> This form accounts for the details of the possibly bound pair 2-3 and considers other effects as low-energy plane waves. A generalization of this three-body wave function is

$$\Phi_{ij} = \phi_{ij}(\mathbf{r}_{ij}) \exp\left(i \sum_{\kappa \neq i,j} \boldsymbol{\kappa}_k \mathbf{r}_k + i\boldsymbol{\kappa}_{ij}\mathbf{R}_{ij}\right) , \quad \Phi = \sum_{i<j}^N \Phi_{ij} . \quad (2.41)$$

When all relative energies are small, that is when  $\boldsymbol{\kappa}_{ij} \simeq 0$  and  $\boldsymbol{\kappa}_k \simeq 0$ , the result is  $\Phi_{ij} \simeq \phi_{ij}(\mathbf{r}_{ij})$ .

A generalization to an  $N$ -particle system was formulated by Yakubovskii [Yak67], who arranged the particles into possible groups of subsystems and thereby included the correct large-distance asymptotic behaviour for all cluster divisions. The decisive physical properties are related to the division into clusters, which for  $N = 3$  amounts to three possibilities. The three Faddeev components are related to the number of divisions and not the number of particles. For  $N > 3$  the number of cluster divisions is much larger than  $N$ . For  $N$  particles the wave function is therefore written as a sum over possible clusters

$$\Psi_Y = \sum_{\text{clusters}} \Phi_Y(\text{cluster}) . \quad (2.42)$$

This method is often applied in nuclear physics [CC98, FG02]. In a dilute system two close-lying particles are found more frequently than other cluster configurations. Then the dominating terms in the cluster expression in equation (2.42) are due to the two-body clusters, and the remaining particles are considered uncorrelated and described by plane waves or as a mean-field background. The Yakubovskii wave function then reduces to a Faddeev-like form similar to equation (2.41)

$$\Psi_Y \rightarrow \Phi(\rho, \Omega) = \sum_{i<j}^N \Phi_{ij}(\rho, \Omega) . \quad (2.43)$$

### 2.3.3 Jastrow: two-body factorization

The Jastrow variational formulation [Bij40, Din49, Jas55] was designed to account for correlations in a Bose system. The Jastrow ansatz

$$\Psi_J = \prod_{i<j}^N \psi_J(\mathbf{r}_{ij}) , \quad \mathbf{r}_{ij} \equiv \mathbf{r}_j - \mathbf{r}_i , \quad (2.44)$$

---

<sup>‡</sup>The complex number  $\sqrt{-1}$  is here denoted by  $i$ .

provides an argument for writing the wave function as a sum of two-body terms in the dilute limit. The two-body Jastrow component can be written as a Gaussian term, which corresponds to mean-field amplitudes, multiplied by a modification expected to be important only at small separation, i.e.

$$\psi_J(\mathbf{r}_{ij}) = e^{-r_{ij}^2/(2Nb_t^2)}[1 + \phi_J(\mathbf{r}_{ij})], \quad \phi_J(\mathbf{r}_{ij}) = 0 \quad \text{for } r_{ij} > r_0. \quad (2.45)$$

Beyond some length scale  $r_0$ , deviations due to correlations vanish. With equation (2.4) this leads to the relative wave function

$$\begin{aligned} \Psi_J &= e^{-\rho^2/(2b_t^2)} \prod_{i<j}^N [1 + \phi_J(\mathbf{r}_{ij})] \\ &= e^{-\rho^2/(2b_t^2)} \left[ 1 + \sum_{i<j}^N \phi_J(\mathbf{r}_{ij}) + \sum_{i<j \neq k < l}^N \phi_J(\mathbf{r}_{ij})\phi_J(\mathbf{r}_{kl}) + \dots \right]. \end{aligned} \quad (2.46)$$

For a non-interacting system the sums are zero and the Gaussian mean-field Hartree ansatz from equation (2.33) is obtained. For a sufficiently dilute system it is unlikely that more than two particles simultaneously are close in space, that is when both  $r_{ij} < r_0$  and  $r_{kl} < r_0$ . Therefore the expansion in equation (2.46) can be truncated after the first two terms, i.e.

$$\prod_{i<j}^N [1 + \phi_J(\mathbf{r}_{ij})] \simeq 1 + \sum_{i<j}^N \phi_J(\mathbf{r}_{ij}) = \sum_{i<j}^N \left[ \frac{1}{N(N-1)/2} + \phi_J(\mathbf{r}_{ij}) \right]. \quad (2.47)$$

A redefinition of the two-body amplitude results in a Faddeev-like sum as in equation (2.43).

### 2.3.4 Hyperharmonic expansion of two-body components

The sum of two-body terms can be formally obtained as the  $s$ -wave reduction of an expansion on a properly symmetrized complete set of basis functions. Appropriate are the hyperspherical harmonics  $\mathcal{Y}$  that are eigenfunctions of the grand angular kinetic-energy operator  $\hat{\Lambda}_{N-1}^2$ , equation (2.16) [Smi60]. These are for collective angular momentum  $L_k$  and projection  $M_k$  given by [Bar99a]

$$\hat{\Lambda}_k^2 \mathcal{Y}_{[K_k, L_k, M_k]}^{\{q_k\}} = K_k(K_k + 3k - 2) \mathcal{Y}_{[K_k, L_k, M_k]}^{\{q_k\}}, \quad (2.48)$$

where  $q_k$  denotes the set of quantum numbers  $\{q_k\} = \{l_1, \dots, l_k, \nu_2, \dots, \nu_k\}$ , and the hyperangular momentum  $K_k$  is given by

$$K_k = 2\nu_k + K_{k-1} + l_k, \quad K_1 = l_1. \quad (2.49)$$

The expression for  $\mathcal{Y}$  is

$$\begin{aligned} \mathcal{Y}_{[K_k, L_k, M_k]}^{\{q_k\}} &= \left[ Y_{l_1}(\vartheta_1, \varphi_1) \otimes Y_{l_2}(\vartheta_2, \varphi_2) \otimes \dots \otimes Y_{l_k}(\vartheta_k, \varphi_k) \right]_{L_k, M_k} \times \\ &\left\{ \prod_{j=2}^k \sin^{l_j} \alpha_j \cos^{K_{j-1}} \alpha_j \mathcal{P}_{\nu_j}^{[l_j+1/2, K_{j-1}+(3j-5)/2]}(\cos 2\alpha_j) \right\}. \end{aligned} \quad (2.50)$$

Here the  $Y_{l,m}$ 's are the usual spherical harmonics,  $\mathcal{P}_\nu$  is the Jacobi function, and the coupling of angular momenta is given by the Clebsch-Gordan coefficients through

$$\begin{aligned} & \left[ Y_{l_1}(\vartheta_1, \varphi_1) \otimes Y_{l_2}(\vartheta_2, \varphi_2) \otimes \cdots \otimes Y_{l_k}(\vartheta_k, \varphi_k) \right]_{L_k, M_k} = \\ & \left[ \sum_{m_1, m_2, \dots, m_k} \langle l_1 m_1 l_2 m_2 | L_2 M_2 \rangle \langle L_2 M_2 l_3 m_3 | L_3 M_3 \rangle \cdots \times \right. \\ & \left. \cdots \langle L_{k-1} M_{k-1} l_k m_k | L_k M_k \rangle \prod_{j=1}^k Y_{l_j, m_j}(\vartheta_j, \varphi_j) \right]. \end{aligned} \quad (2.51)$$

Omitting dependence on  $\alpha_k$ , we also define a reduced function  $\tilde{\mathcal{Y}}$  by

$$\begin{aligned} \tilde{\mathcal{Y}}_{[K_{k-1}, L_k, M_k]}^{\{\tilde{q}_k\}} &= \left[ Y_{l_1}(\vartheta_1, \varphi_1) \otimes Y_{l_2}(\vartheta_2, \varphi_2) \otimes \cdots \otimes Y_{l_k}(\vartheta_k, \varphi_k) \right]_{L_k, M_k} \times \\ & \left\{ \prod_{j=2}^{k-1} \sin^{l_j} \alpha_j \cos^{K_{j-1}} \alpha_j \mathcal{P}_{\nu_j}^{[l_j+1/2, K_{j-1}+(3j-5)/2]}(\cos 2\alpha_j) \right\}, \end{aligned} \quad (2.52)$$

where  $\{\tilde{q}_k\} = \{l_1, \dots, l_k, \nu_2, \dots, \nu_{k-1}\}$ .

The wave function for each fixed value of  $\rho$  is for fixed relative angular momentum  $\tilde{L} \equiv L_{N-1}$  and projection  $\tilde{M} \equiv M_{N-1}$  decomposed as

$$\Phi_{[\tilde{L}, \tilde{M}]}(\rho, \Omega) = \sum_{i < j}^N \Phi_{ij}[\tilde{L}, \tilde{M}](\rho, \Omega), \quad (2.53)$$

where the component  $\Phi_{ij}$  is focused on the particle pair  $i$ - $j$ . Each of these components, for instance  $\Phi_{12}$ , can be written as the complete expansion

$$\Phi_{12}[\tilde{L}, \tilde{M}](\rho, \Omega) = \sum_{\{\tilde{q}_{N-1}\}} \phi_{12}^{\{\tilde{q}_{N-1}\}}[\tilde{L}, \tilde{M}](\rho, r_{12}) \tilde{\mathcal{Y}}_{[\tilde{K}, \tilde{L}, \tilde{M}]}^{\{\tilde{q}_{N-1}\}}, \quad (2.54)$$

where the sum runs over all possible quantum numbers  $\tilde{q}_{N-1}$ . Analogies are given in [NFJG01, Bar99a].<sup>§</sup> The number  $\tilde{K} = K_{N-2}$  is used for reference to the kinetic-energy eigenvalue. No assumptions are made yet.

In order to obtain an explicitly symmetric boson wave function in equation (2.53), we need to rewrite equation (2.54) as

$$\Phi_{12}[\tilde{L}, \tilde{M}](\rho, \Omega) = \sum_{\{\tilde{q}_{N-1}\}} \phi_{12}^{\{\tilde{q}_{N-1}\}}[\tilde{L}, \tilde{M}](\rho, r_{12}) \sum_{P_{12}} \hat{P}_{12} \tilde{\mathcal{Y}}_{[\tilde{K}, \tilde{L}, \tilde{M}]}^{\{\tilde{q}_{N-1}\}}, \quad (2.55)$$

where the second sum accounts for all possible permutations  $\hat{P}_{12}$  of particles apart from the pair 1-2.

<sup>§</sup>See page 384 in [NFJG01] and page 1137 in [Bar99a].

Zero angular momenta  $\tilde{L} = \tilde{M} = 0$  is reasonable in the short-range limit. Vanishing hyperangular quantum number  $\tilde{K} = 0$  for the remaining degrees of freedom yields only zero quantum numbers  $\{\tilde{q}_{N-1}\} = \{0\}$ , and the sum is truncated to include only the term

$$\Phi_{12 [0,0]}(\rho, \Omega) = \phi_{12 [0,0]}^{\{0\}}(\rho, r_{12}) \tilde{\mathcal{Y}}_{[0,0,0]}^{\{0\}}. \quad (2.56)$$

The remaining terms  $\Phi_{ij \neq 12}$  are obtained in similar ways, so the angular wave function is

$$\Phi(\rho, \Omega) = \sum_{i < j}^N \phi_{ij}(\rho, r_{ij}), \quad (2.57)$$

omitting the constant  $\tilde{\mathcal{Y}}_{[0,0,0]}$  and superfluous indices.

### 2.3.5 Fermion antisymmetry

For identical fermions the total wave function has to be antisymmetric under permutation of any two particles. If the spin wave function is symmetric, then the spatial wave function can be antisymmetrized by an extension of the method written for bosons

$$\Phi_{[\tilde{L}, \tilde{M}]}(\rho, \Omega) = \sum_{i \neq j}^N \sum_{P_{ij}} (-1)^p \hat{P}_{ij} \Phi_{ij [\tilde{L}, \tilde{M}]}(\rho, \Omega), \quad (2.58)$$

$$\Phi_{12 [\tilde{L}, \tilde{M}]}(\rho, \Omega) = \sum_{\{\tilde{q}_{N-1}\}} \phi_{12 [\tilde{L}, \tilde{M}]}^{\{\tilde{q}_{N-1}\}}(\rho, r_{12}) \tilde{\mathcal{Y}}_{[\tilde{K}, \tilde{L}, \tilde{M}]}^{\{\tilde{q}_{N-1}\}}. \quad (2.59)$$

The second sum of the first line accounts for all different permutations  $\hat{P}_{ij}$  of the  $N - 2$  particles apart from  $i$  and  $j$ . We assume that a specific permutation resulted in the particles ordered as  $ijkl \dots$ . The number  $p$  is then the total number of permutations of two particles needed to transform the straightforward ordering  $1234 \dots$  into the ordering  $ijkl \dots$ .

If no term depends on more than  $N - 2$  particles' positions, it is not possible to write a properly symmetrized wave function for a system of identical fermions as a sum of terms. Therefore, the dependences can not be truncated as roughly as was done for bosons in the steps leading to equation (2.56). However, the antisymmetric function with lowest possible quantum numbers might provide a useful fermion wave function which can be implemented in calculations. In this thesis we do not discuss fermions further, but restrict ourselves to the case of bosons.

### 2.3.6 Two-boson direction-independent correlations

As seen in the preceding sections, a relative wave function of the form

$$\Psi(\rho, \Omega) = F(\rho) \sum_{i < j}^N \Phi_{ij}(\rho, \Omega) \quad (2.60)$$

incorporates both mean-field properties through  $F(\rho)$  and correlations beyond the mean field through the Faddeev-components  $\Phi$ . We therefore decompose the angular wave function  $\Phi$ , equation (2.26), into the symmetric expression of Faddeev components  $\Phi_{ij}$  for fixed values of the hyperradius  $\rho$

$$\Phi(\rho, \Omega) = \sum_{i < j}^N \Phi_{ij}(\rho, \Omega), \quad (2.61)$$

where each term  $\Phi_{ij}$  is a function of  $\rho$  and all angular coordinates  $\Omega$ . Since each term in itself is sufficient when all  $\Omega$  degrees of freedom are allowed, this decomposition is exact. At first this ansatz seems clumsy by introducing an overcomplete basis. However, the indices  $i$  and  $j$  indicate a special emphasis on the particle pair  $i$ - $j$ . The component  $\Phi_{ij}$  is expected to carry the information associated with binary correlations of this particular pair.

This wave function is a natural choice for the trivial case of  $N = 2$ . A wave function rewritten as a sum of terms has also been successful in three-body computations. The advantage is that the correct boundary conditions are simpler to incorporate, as expressed in the original formulation by Faddeev [Fad60] intended for scattering. Still, mathematically nothing is gained or lost in this Faddeev-type of decomposition. For weakly bound and spatially extended three-body systems,  $s$ -waves in each of the Faddeev components are sufficient to describe the system [NFJG01]. This is exceedingly pronounced for large scattering lengths where the Efimov states appear [FJ93, JGF97, NFJG01].

The present  $N$ -body problem is in general more complicated. However, for dilute systems essential similarities remain, i.e. the relative motion of two particles that on average are far from each other is most likely dominated by  $s$ -wave contributions. Each particle cannot detect any directional preference arising from higher partial waves. Implementation of these ideas in the present context implies that each amplitude  $\Phi_{ij}$  for a fixed  $\rho$  only should depend on the distance  $r_{ij}$  between the two particles. Thus, we assume

$$\Phi_{ij}(\rho, \Omega) \simeq \phi_{ij}(\rho, \alpha_{ij}), \quad (2.62)$$

where the two-index parameter  $\alpha_{ij}$  is defined by

$$\sin \alpha_{ij} \equiv \frac{r_{ij}}{\sqrt{2}\rho}. \quad (2.63)$$

These  $\alpha_{ij}$ 's are distinctively different from the  $\alpha_k$ 's of equation (2.3).

The boson symmetry implies that the functions  $\phi_{ij}$  are non-distinguishable, so the indices are omitted. The resulting angular wave function is

$$\Phi(\rho, \Omega) = \sum_{i < j}^N \phi(\rho, \alpha_{ij}) = \sum_{i < j}^N \phi(\alpha_{ij}), \quad (2.64)$$

where  $\phi_{ij}(\rho, \alpha_{ij}) = \phi(\rho, \alpha_{ij}) \equiv \phi(\alpha_{ij})$  with the notational convenient omission of the coordinate  $\rho$ . The wave function in equation (2.64) is symmetric with

respect to the interchange of two particles,  $i \leftrightarrow j$ , since  $\alpha_{ij} = \alpha_{ji}$  and since terms like  $\phi(\alpha_{ik}) + \phi(\alpha_{jk})$  always appear symmetrically.

This ansatz of only  $s$ -waves dramatically simplifies the angular wave function. The original overcomplete Hilbert space is reduced such that some angular wave functions can not be expressed in this remaining basis. Thus, the reduction resulted in an incomplete basis, but the degrees of freedom remaining in equation (2.64) are expected to be those needed to describe the features of a dilute system.

In section 2.3.4 the Faddeev ansatz equation (2.43) was formally established as a generalized partial wave expansion in terms of the hyperspherical harmonic kinetic-energy eigenfunctions. The two-body  $s$ -wave simplification then appears as a truncation of this expansion, which also leads to equation (2.64).

In conclusion, when the system is dilute, the Faddeev ansatz with two-body amplitudes is expected to account sufficiently for the correlations and at the same time keep the mean-field-like information about motion relative to the remaining particles.

### 2.3.7 Three-body correlations

An extension of the inclusion of pairwise correlations to study three-body correlations in denser systems is possible and could yield insight into the process of three-body recombination within  $N$ -boson systems. Since all degrees of freedom are kept in every term, the Faddeev-like decomposition of the wave function can describe all kinds of clusterizations in a particle system. The indices  $ij$  just refer to the correct asymptotic behaviour of the two-body scattering properties between particle  $i$  and  $j$  in a given amplitude  $\phi_{ij}$ . A higher-order correlated wave function is in that sense included in the general expansion. However, for actual application it does not provide any solvable method. Therefore, we proceed as follows with what might be an applicable three-body expansion of the many-body wave function.

A symmetric boson wave function with three-body amplitudes is

$$\Phi(\rho, \Omega) = \sum_{i < j}^N \sum_{k \neq i, j} \phi_{ij,k}, \quad (2.65)$$

where  $\phi_{ij,k}$  depends on the distances between the three particles  $i$ ,  $j$ , and  $k$ . In hyperspherical coordinates the dependence, exemplified for the term  $\phi_{12,3}$ , can be reduced to be on  $\rho$ ,  $\alpha_{N-1}$  ( $\equiv \alpha_{12}$ ),  $\alpha_{N-2}$  ( $\equiv \alpha_{12,3}$ ), and  $\vartheta_{N-2}$  ( $\equiv \vartheta_{12,3}$ ), where  $\vartheta_{N-2}$  is the angle between  $\boldsymbol{\eta}_{N-1}$  and  $\boldsymbol{\eta}_{N-2}$ . A general term  $\phi_{ij,k}$  depends on  $\rho$ ,  $\alpha_{ij}$ ,  $\alpha_{ij,k}$ , and  $\vartheta_{ij,k}$ . It is written as

$$\phi_{ij,k}(\rho, \alpha_{ij}, \alpha_{ij,k}, \vartheta_{ij,k}) = \phi_2(\rho, \alpha_{ij}) + \phi_3(\rho, \alpha_{ij}, \alpha_{ij,k}, \vartheta_{ij,k}), \quad (2.66)$$

where the term  $\phi_n$  accounts for an  $n$ -body correlation. This is analogous to a proposal by Barnea [Bar99b]. Since the functional dependence is the same for all terms, the symmetry is explicitly included. The two-body correlated

method reappears with  $\phi_3 = 0$  since then  $\phi_{ij,k} \rightarrow \phi_2 \rightarrow \phi(\rho, \alpha_{ij})$ . However,  $\phi_3$  provides the three-body correlation on top of the two-body correlation. Terms with  $k < j$  are responsible for an overdetermined expansion since three terms, in principle, describe the same three-body correlation. In the case  $i < j < k$  the three similar terms are  $\phi_{ij,k}$ ,  $\phi_{ik,j}$ , and  $\phi_{jk,i}$ . With only one term  $\phi_{ij,k}$  we would have to impose other symmetry restrictions on this single term such that  $\phi_{ij,k} = \phi_{ik,j} = \phi_{jk,i}$ . With the sum  $\phi_{ij,k} + \phi_{ik,j} + \phi_{jk,i}$  in the ansatz for the wave function, the symmetry is explicitly built in and is independent of the amplitude's functional form. A simpler description is obtained when neglecting  $\vartheta_{ij,k}$  in  $\phi_3$ , and thus yielding a term that accounts for one particle's relations to the pair of particles.

## 2.4 Angular eigenvalue equation for two-boson correlations

Since the eigenvalue  $\lambda$  from equation (2.25) carries information about the two-body interactions and kinetic energy due to internal structure and as well about possible correlations, the techniques and approximations used to find  $\lambda$  are especially important.

This section contains the essential rewritings of the angular equation with the ansatz from equation (2.64) for two-body correlations. We first present the Faddeev-like equations and next construct a variational equation as an alternative which is solvable under the additional assumption of short-range interactions, i.e. the system must be relatively dilute. The Faddeev-like equations were previously written in this form for a boson system by de la Ripelle *et al.* [dIRFS88], whereas the angular variational equation according to the author's knowledge is an original contribution by the author and co-workers and first presented in [SFJN02]. We end the section by briefly considering the inclusion of higher-order correlations.

### 2.4.1 Faddeev-like equation

Insertion of the ansatz for the boson wave function in equation (2.64) along with equation (2.21) into equation (2.25) yields

$$\left( \hat{\Lambda}_{N-1}^2 + \sum_{k<l}^N v_{kl} - \lambda \right) \sum_{i<j}^N \phi_{ij} = 0, \quad (2.67)$$

with  $\phi_{ij} = \phi(\alpha_{ij})$ . Rearrangement of summations leads to

$$\sum_{k<l}^N \left[ \left( \hat{\Lambda}_{N-1}^2 - \lambda \right) \phi_{kl} + v_{kl} \sum_{i<j}^N \phi_{ij} \right] = 0. \quad (2.68)$$

For three particles and with the assumption that each term in the square brackets separately is zero, the Faddeev equations are obtained. They have been



applied for the three-body case to describe particularly the regime of large scattering length [JGF97]. The same assumption for the  $N$ -particle system results in the  $N(N-1)/2$  Faddeev-like equations

$$\left(\hat{\Lambda}_{N-1}^2 - \lambda\right)\phi_{kl} + v_{kl} \sum_{i < j}^N \phi_{ij} = 0, \quad (2.69)$$

which are identical due to symmetry. A description of the many-boson system with such Faddeev-like equations was previously performed by de la Ripelle *et al.* [dlRFS88], who concentrated on systems within the realms of nuclear physics.

With  $k = 1$  and  $l = 2$  the kinetic-energy operator  $\hat{\Lambda}_{N-1}^2$  from equation (2.16) reduces to  $\hat{\Pi}_{N-1}^2$  because  $\hat{\Lambda}_{N-2}^2\phi_{12} = 0$  and  $\hat{\mathbf{l}}_{N-1}^2\phi_{12} = 0$ . Since  $\boldsymbol{\eta}_{N-1} = (\mathbf{r}_2 - \mathbf{r}_1)/\sqrt{2}$  and  $\rho_{N-1} = \rho$ , then equations (2.3) and (2.63) yield  $\alpha_{N-1} = \alpha_{12}$ . Therefore, only derivatives with respect to  $\alpha_{12}$  remain, and it is convenient to introduce the notation  $\hat{\Pi}_{12}^2 \equiv \hat{\Pi}_{N-1}^2$ .

In the sum over angular wave function components in equation (2.69), only three different types of terms appear. When  $k = 1$  and  $l = 2$ , these types are classified by the set  $\{i, j\}$  either having two, one, or zero numbers coinciding with the set  $\{1, 2\}$ . Then equation (2.69) is rewritten as

$$0 = \left[\hat{\Pi}_{12}^2 + v(\alpha_{12}) - \lambda\right]\phi(\alpha_{12}) + \quad (2.70)$$

$$v(\alpha_{12}) \left[ \sum_{j=3}^N \phi(\alpha_{1j}) + \sum_{j=3}^N \phi(\alpha_{2j}) + \sum_{3 \leq i < j}^N \phi(\alpha_{ij}) \right],$$

$$v(\alpha_{kl}) = \frac{2m\rho^2}{\hbar^2} V(\sqrt{2}\rho \sin \alpha_{kl}), \quad (2.71)$$

for a central potential  $V(r)$ . Multiplication of equation (2.70) from the left by  $\phi(\alpha_{12})$  followed by integration over all angular space except  $\alpha_{12}$  results in an integro-differential equation in  $\alpha \equiv \alpha_{12}$  of the form<sup>¶</sup>

$$0 = \left[\hat{\Pi}_{12}^2 + v(\alpha) - \lambda\right]\phi(\alpha) + v(\alpha)2(N-2) \int d\tau \phi(\alpha_{13}) \\ + v(\alpha)\frac{1}{2}(N-2)(N-3) \int d\tau \phi(\alpha_{34}). \quad (2.72)$$

Here  $d\tau \propto d\Omega_{N-2}$  is the angular volume element, excluding the  $\alpha$  dependence, with the normalization  $\int d\tau = 1$ . Due to symmetry between the first and second sums in equation (2.70), this projection leaves for every value of  $\alpha$  only two different integrals. Both can analytically be reduced to one-dimensional integrals. The results are collected in appendix B.2. For brevity here the terms are denoted by

$$\int d\tau \phi(\alpha_{34}) \equiv \hat{\mathbf{R}}_{34}^{(N-2)}\phi(\alpha), \quad (2.73)$$

<sup>¶</sup>Throughout we interchange  $\alpha$ ,  $\alpha_{N-1}$ , and  $\alpha_{12}$ .

$$\int d\tau \phi(\alpha_{13}) \equiv \hat{\mathbf{R}}_{13}^{(N-2)} \phi(\alpha) , \quad (2.74)$$

where  $\hat{\mathbf{R}}_{ij}^{(N-2)}$  is an operator acting on the function  $\phi$  resulting in a function of  $\alpha$ .<sup>||</sup> Equation (2.72) can now be written as

$$\begin{aligned} 0 = & \left[ \hat{\Pi}_{12}^2 + v(\alpha) - \lambda + 2(N-2)v(\alpha)\hat{\mathbf{R}}_{13}^{(N-2)} \right. \\ & \left. + \frac{1}{2}(N-2)(N-3)v(\alpha)\hat{\mathbf{R}}_{34}^{(N-2)} \right] \phi(\alpha) , \end{aligned} \quad (2.75)$$

which is linear in the function  $\phi$ . An advantage of this equation is that it does not become more complicated as the number  $N$  of particles increases.

In this equation, the potential  $v$  and the kinetic-energy operator  $\hat{\Pi}^2$  are diagonal in the sense that they only act in the space of particle pair 1-2, whereas the angular wave function is also evaluated for other two-body pairs. In the Faddeev-like equation (2.75) for the many-body case, all wave-function components are projected onto  $s$  waves in the 1-2 system. This means that effective contributions from higher partial waves in the hyperangular space are omitted.

Another problem is that the Faddeev approximation is not variational, i.e. the energy may be underestimated [NFJG01]. This is explicitly obvious when we add and subtract a constant  $v_0$  from the interaction potential to rewrite equation (2.67) as

$$\left( \hat{\Lambda}_{N-1}^2 + \sum_{k<l}^N v'_{kl} - \lambda' \right) \sum_{i<j}^N \phi_{ij} = 0 , \quad (2.76)$$

$$v'_{kl} = v_{kl} - v_0 , \quad \lambda' = \lambda - \frac{1}{2}N(N-1)v_0 . \quad (2.77)$$

The Faddeev approximation then results in an angular eigenvalue  $\lambda$  which depends on the choice of  $v_0$ . This shows that the Faddeev-like equation has to be handled with care and at worst that it is inconsistent with the present assumption of  $s$  waves.

## 2.4.2 Variational angular equation

Proceeding with the Faddeev-like equation (2.75) is one option, but as discussed this equation shows inadequacies under the required assumptions about the many-body wave function. In this section we therefore rely on the full angular equation and discuss a variational equation where the Faddeev approximation is not necessary. Thus, we might effectively catch influences due to higher partial waves from the different subsystems in the many-body system and benefit from the maintained validity of the variational principle. However, in some of the model calculations in the following chapters, we study results obtained from the

---

<sup>||</sup>Mathematically  $\hat{\mathbf{R}}$  resembles a rotation operator, hence the choice of notation.

Faddeev-like equation and then compare to results from the following variational equation.

First the optimal angular equation is derived within the Hilbert space defined by the form of the angular wave function in equation (2.64). The very short range of the two-body interaction compared with the size of the system simplifies the problem as we shall see in the next section.

The angular Schrödinger equation for fixed  $\rho$  in equation (2.25) and the ansatz for the wave function in equation (2.64) allow the eigenvalue expressed as an expectation value, i.e.

$$\lambda = \frac{\langle \Phi | \hat{h}_\Omega | \Phi \rangle_\Omega}{\langle \Phi | \Phi \rangle_\Omega} = \frac{\langle \sum_{i' < j'}^N \phi_{i'j'} | \hat{h}_\Omega | \Phi \rangle_\Omega}{\langle \sum_{i' < j'}^N \phi_{i'j'} | \Phi \rangle_\Omega}. \quad (2.78)$$

For an operator  $\hat{O}$  which is invariant when interchanging any two particles, the terms  $\langle \phi_{i'j'} | \hat{O} | \Phi \rangle_\Omega = \langle \phi_{i''j''} | \hat{O} | \Phi \rangle_\Omega$  are identical since the possible differences vanish when averaging over all angles  $\Omega$ . Since  $\hat{h}_\Omega$  is invariant with respect to interchange of particles, this identity holds for both numerator and denominator, so equation (2.78) simplifies to

$$\lambda = \frac{\langle \phi_{12} | \hat{h}_\Omega | \sum_{i < j}^N \phi_{ij} \rangle_\Omega}{\langle \phi_{12} | \sum_{i < j}^N \phi_{ij} \rangle_\Omega}. \quad (2.79)$$

The total angular volume element is  $d\Omega_{N-1} = d\Omega_\alpha^{(N-1)} d\Omega_\eta^{(N-1)} d\Omega_{N-2}$ , see equation (2.7). Since the integrands are independent of  $\Omega_\eta^{(N-1)}$ , then  $d\Omega_\eta^{(N-1)}$  can be omitted from the integrations. Using equation (2.10) we then obtain

$$\int d\Omega_\alpha^{(N-1)} \phi_{12}^* \int d\Omega_{N-2} (\hat{h}_\Omega - \lambda) \sum_{i < j}^N \phi_{ij} = 0. \quad (2.80)$$

The wave-function component  $\phi_{12}^*$  is varied until the lowest eigenvalue is obtained. This gives the integro-differential equation

$$\int d\Omega_{N-2} \sum_{k < l}^N \left[ (\hat{\Pi}_{N-1}^2 - \lambda) \phi_{kl} + v_{kl} \sum_{i < j}^N \phi_{ij} \right] = 0, \quad (2.81)$$

where the unknown functions  $\phi_{ij} = \phi(\alpha_{ij})$  all are the same identical function of the different coordinates  $\alpha_{ij}$ . Many terms are identical, e.g.  $\int d\Omega_{N-2} v_{12} \phi_{34} = \int d\Omega_{N-2} v_{12} \phi_{56}$ , since particles 1 and 2 cannot distinguish between other pairs of particles, see appendix B.3.1 for the details. Collecting all terms yields

$$\int d\Omega_{N-2} \left[ (\hat{\Pi}_{12}^2 + v_{12} - \lambda) \phi_{12} + G(\tau, \alpha_{12}) \right] = 0, \quad (2.82)$$

where  $\tau$  denotes angular coordinates apart from  $\alpha_{12}$ . The kernel  $G$  contains all non-diagonal parts involving other particles than 1 and 2. This is given by

$$G(\tau, \alpha_{12}) = \frac{1}{2} n_2 \left[ \hat{\Pi}_{34}^2 + v(\alpha_{12}) + v(\alpha_{34}) - \lambda \right] \phi(\alpha_{34})$$

$$\begin{aligned}
& + \frac{1}{2} n_2 v(\alpha_{34}) \phi(\alpha_{12}) + 2n_1 v(\alpha_{13}) [\phi(\alpha_{12}) + \phi(\alpha_{23})] \\
& + 2n_1 \left[ \hat{\Pi}_{13}^2 + v(\alpha_{12}) + v(\alpha_{13}) - \lambda \right] \phi(\alpha_{13}) \\
& + n_3 \left\{ v(\alpha_{34}) [\phi(\alpha_{35}) + \phi(\alpha_{15})] + v(\alpha_{13}) \phi(\alpha_{45}) \right\} \\
& + 2n_2 v(\alpha_{13}) [\phi(\alpha_{14}) + \phi(\alpha_{24}) + \phi(\alpha_{34})] \\
& + 2n_2 v(\alpha_{34}) \phi(\alpha_{13}) + \frac{1}{4} n_4 v(\alpha_{34}) \phi(\alpha_{56}) , \tag{2.83}
\end{aligned}$$

where  $n_i = \prod_{j=1}^i (N - j - 1)$  and  $\hat{\Pi}_{ij}^2$  is defined from equation (2.17) with  $k = N - 1$  and with  $\alpha_k$  replaced by  $\alpha_{ij}$ . In equation (2.83) all terms depend at most on coordinates of the six particles 1-6. The first three terms in equation (2.82) do not depend on the integration variables  $\tau$  leaving only  $G(\tau, \alpha_{12})$  for integration.

By appropriate choices of Jacobi systems [SS77], the relevant degrees of freedom can be expressed in terms of the five vectors  $\boldsymbol{\eta}_{N-1}, \dots, \boldsymbol{\eta}_{N-5}$ . One is the argument of the variational function and not an integration variable. The remaining twelve-dimensional integral is then evaluated with the corresponding volume element  $d\tau \propto \prod_{i=2}^5 d\Omega_\alpha^{(N-i)} d\Omega_\eta^{(N-i)}$  where the normalization is  $\int d\tau = 1$ . Then equation (2.82) becomes

$$\left[ \hat{\Pi}_{12}^2 + v(\alpha_{12}) - \lambda \right] \phi(\alpha_{12}) + \int d\tau G(\tau, \alpha_{12}) = 0 , \tag{2.84}$$

where the first terms are independent of the integration variables. Equation (2.84) is a linear integro-differential equation in one variable containing up to five-dimensional integrals, see appendix B.3.2. As is the case for the Faddeev-like equation, this equation does not complicate further at large  $N$ , i.e. when  $N$  increases beyond  $N = 6$ , the structure does not change.

### 2.4.3 Short-range approximation

The two-body potentials  $V(r_{ij})$  are assumed to be characterized by a length scale  $b$  beyond which the interaction vanishes, that is when  $r_{ij} \gg b$ . The angular eigenvalue equation (2.84) simplifies in the limit when this two-body interaction range  $b$  is much smaller than  $\rho$ . Then the integrals are either analytical or reduce to one-dimensional integrals. This reduction could in principle be accounted for by substituting the interaction potential with a  $\delta$  function, but is done generally for any finite-range interaction as long as the range is small compared to the hyperradius. However, this is only possible for the potentials appearing under the integrals. Thus, apart from the local terms containing  $v(\alpha)$ , the results mainly depend on a parameter  $a_B$  related to the volume average of the potential by the definition

$$a_B \equiv \frac{m}{4\pi\hbar^2} \int d\mathbf{r} V(\mathbf{r}) . \tag{2.85}$$

A finite value of this volume integral is essential for the validity of the method. This is obeyed for short-range potentials that fall off faster than  $1/r^2$ .

As an example of the reductions, when  $\rho \cos \alpha \gg b$ , the  $\int d\tau v(\alpha_{34})$ -term reduces to

$$\int d\tau v(\alpha_{34}) \equiv v_1(\alpha) \simeq 2\sqrt{\frac{2}{\pi}} \frac{\Gamma(\frac{3N-6}{2})}{\Gamma(\frac{3N-9}{2})} \frac{a_B}{\rho \cos^3 \alpha}. \quad (2.86)$$

Similarly the  $\int d\tau v(\alpha_{13})$ -term reduces to

$$\int d\tau v(\alpha_{13}) \equiv v_2(\alpha) \simeq \frac{8}{3\sqrt{3}} \cos^{3N-11} \beta_0 \Theta(\alpha < \pi/3) v_1(\alpha) \quad (2.87)$$

in the limit when  $\rho \cos \alpha \cos \beta_0 \gg b$ , where  $\sin \beta_0 \equiv \tan \alpha / \sqrt{3}$ . Here  $\Theta$  is the truth function, i.e. it equals unity when the argument is true and zero otherwise. The remaining terms can in this limit be expressed through  $v_1(\alpha)$ ,  $v_2(\alpha)$ ,  $\hat{R}_{ij}^{(k)}$  from equations (2.73) and (2.74), and other related operators  $\hat{R}_{ijkl}^{(n)}$ . Corresponding definitions are given in appendix B.3.3.

The reductions can be understood qualitatively via figure 2.2 which shows the geometry when the short-range interaction contributes to the integrals. In the integral  $\int d\tau v(\alpha_{13})\phi(\alpha_{34})$ , see figure 2.2a, the dominant contributions occur when particles 1 and 3 are close together as shown in figure 2.2b. Then the distance between particles 3 and 4 appearing in  $\phi_{34}$  is approximately equal to the distance between particles 1 and 4. Therefore  $\int d\tau v(\alpha_{13})\phi(\alpha_{34}) \simeq \int d\tau v(\alpha_{13})\phi(\alpha_{14})$ .

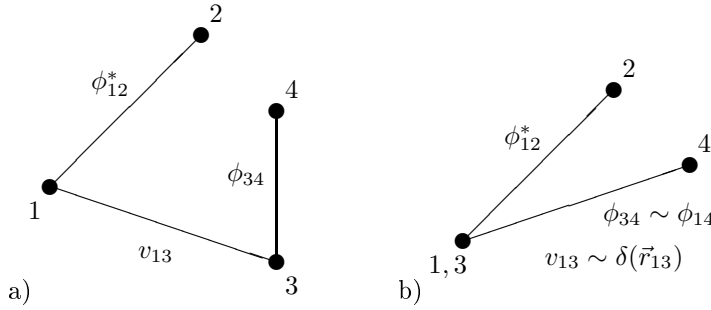


Figure 2.2: Simplifications due to short-range potentials.

So, for  $b \ll \rho$  the exact short-range shapes of the potential are not important and the integral in equation (2.84) of equation (2.83) can be written as

$$\begin{aligned} \int d\tau G(\tau, \alpha) &\simeq \left[ \frac{n_2}{2} v_1(\alpha) + 4n_1 v_2(\alpha) \right] \phi(\alpha) \\ &+ \frac{n_2}{2} \hat{R}_{34}^{(N-2)} v\phi(\alpha) + 2n_1 \hat{R}_{13}^{(N-2)} v\phi(\alpha) \\ &+ \frac{n_2}{2} \left\{ \hat{R}_{34}^{(N-2)} \hat{\Pi}_{34}^2 \phi(\alpha) + [v(\alpha) - \lambda] \hat{R}_{34}^{(N-2)} \phi(\alpha) \right\} \end{aligned}$$

$$\begin{aligned}
& +2n_1 \left\{ \hat{\mathbf{R}}_{13}^{(N-2)} \hat{\Pi}_{13}^2 \phi(\alpha) + [v(\alpha) - \lambda] \hat{\mathbf{R}}_{13}^{(N-2)} \phi(\alpha) \right\} \\
& + \frac{n_4}{4} v_1(\alpha) \hat{\mathbf{R}}_{34}^{(N-3)} \phi(\alpha) + n_3 v_1(\alpha) \hat{\mathbf{R}}_{3435}^{(1)} \phi(\alpha) + n_3 v_2(\alpha) \hat{\mathbf{R}}_{1345}^{(1)} \phi(\alpha) \\
& + n_3 v_1(\alpha) \hat{\mathbf{R}}_{13}^{(N-3)} \phi(\alpha) + 2n_2 v_1(\alpha) \hat{\mathbf{R}}_{3413}^{(2)} \phi(\alpha) \\
& + 2n_2 v_2(\alpha) [2\hat{\mathbf{R}}_{1314}^{(2)} \phi(\alpha) + \hat{\mathbf{R}}_{1324}^{(2)} \phi(\alpha)] . \tag{2.88}
\end{aligned}$$

The variational equation with these reductions is the basis for the calculations in chapter 3.

#### 2.4.4 Variational equation for three-body correlations

The ansatz for the angular wave function from equation (2.66) includes a general correlation within all three-body subsystems. We choose a trial wave function and write the angular potential  $\lambda$  as an expectation value analogous to equation (2.78)

$$\int d\Omega_{N-1} \sum_{i' < j'}^N \sum_{k' \neq i', j'} \phi_{i'j'k'}^* \left( \hat{\Lambda}_{N-1}^2 + \sum_{i'' < j''}^N v_{i''j''} - \lambda \right) \sum_{i < j}^N \sum_{k \neq i, j} \phi_{ij,k} = 0 . \tag{2.89}$$

The calculation of these expectation values requires at most twelve degrees of freedom which with a short-range potential for  $b \ll \rho$  reduces to at most nine degrees of freedom.

Performing the variation  $\phi_{12,3}^* \rightarrow \phi_{12,3}^* + \delta\phi_{12,3}^*$  leads to the angular variational integro-differential equation in  $\alpha_{N-1}$ ,  $\alpha_{N-2}$ , and  $\vartheta_{N-2}$ :

$$\int d\tilde{\tau} \left( \hat{\Lambda}_{N-1}^2 + \sum_{i' < j'}^N v_{i'j'} - \lambda \right) \sum_{i < j}^N \sum_{k \neq i, j} \phi_{ij,k} = 0 , \tag{2.90}$$

where  $d\tilde{\tau}$  denotes the angular volume element for all angles apart from  $\alpha_{N-1}$ ,  $\alpha_{N-2}$ , and  $\vartheta_{N-2}$ . There are 126 different  $V$ -terms (38 for  $N = 4$ ), 12 different  $\hat{\Lambda}^2$ -terms, and 12 different  $\lambda$ -terms. In the short-range limit many terms are identical and thus reduce the complications. The integrals in the integro-differential equation are three dimensions lower than those in the expectation value since three angles are fixed. Thus, the short-range approximation results in an integro-differential equation in three variables with up to six-dimensional integrals. This is beyond the scope of the present work, but indicates the complications when including higher-order correlations.

## Chapter III

### Interactions and the hyperangular spectrum

In the hyperspherical formulation of the many-body problem in chapter 2, the tedious problems are “hidden” in the angular equation. The angular solutions carry essential information about interactions between the particles and about internal kinetic energy. The correlations were assumed to be two-body for sufficiently dilute systems, and this was built into the wave function. The key quantity is then the function  $\lambda$ , equation (2.25), which determines the properties of the radial potential, equation (2.29). The angular wave functions potentially carry information about couplings between the different adiabatic channels.

First, in section 3.1 we discuss how to model two-body interactions in the  $N$ -particle system. Analytical derivations of angular potentials in various regimes are given in section 3.2. Then we comment on the numerical procedure before solving the angular variational equation. Section 3.3 presents the attributes of the found wave functions and angular potentials for various kinds of interaction strengths. Section 3.4 summarizes the nature of the angular potentials, which can be parametrized by the interaction parameters and the number of particles. The details behind this parametrization were previously published [SFJ03a] and hence collected in appendix D.

#### 3.1 Interactions between neutral bosons

The effective two-body interactions vary enormously for different boson systems depending both on the nature of the bosons in question and on the surroundings. Here we consider bosons with short-range interactions in the sense that the volume integral of the two-body interaction potential is finite. Neutral atoms, that are frequently encountered in experiments with dilute boson systems, interact via a potential of sufficiently short range and can be considered by this method.

The interaction between atoms is repulsive at short distances due to the Pauli exclusion principle which forbids overlapping centres. Neutral atoms attract each other at longer distances due to mutual polarization which induces a dipole moment. The interaction between two particles, e.g. 1 and 2, can be modelled

by the two-body potential [GB01]

$$V_{\text{vdW}}(r) = \frac{C_6}{r_0^6} \left[ e^{-c(r-r_0)} - \left( \frac{r_0}{r} \right)^6 \right], \quad \mathbf{r} \equiv \mathbf{r}_2 - \mathbf{r}_1. \quad (3.1)$$

This potential has the van der Waals (vdW) tail  $-C_6/r^6$  when  $r \gg r_0$ , and is thus of short range in the sense that it decays faster than  $1/r^2$ . The important part of this potential is illustrated in figure 3.1 for some choice of the parameters  $C_6$ ,  $r_0$ , and  $c$ .

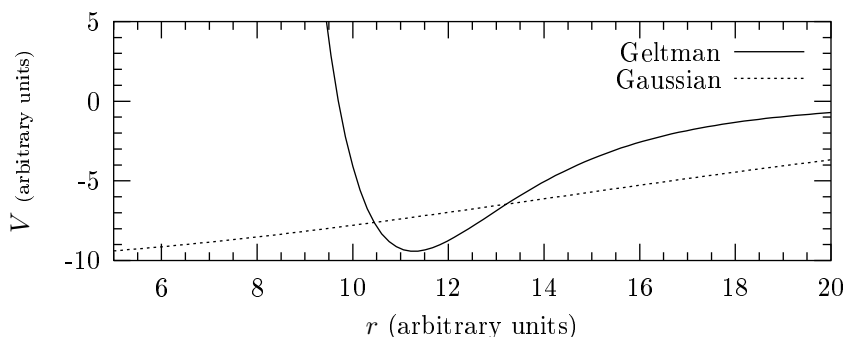


Figure 3.1: Two-body potentials. The solid line is the potential in equation (3.1) from Geltman and Bambini [GB01], and the dotted line is the Gaussian potential from equation (3.7).

At large particle separations, a direction-independent behaviour is expected, which means that zero relative angular momentum is preferred. Then the asymptotic two-body wave function for particles interacting via short-range potentials behaves as

$$u(r) = \sin[\kappa r + \chi(\kappa)], \quad (3.2)$$

where  $\chi$  is the phase shift and  $\hbar\kappa$  is the relative momentum. The phase shift depends on the relative energy  $\hbar^2\kappa^2/m$  and is at low energy given by the expansion

$$\kappa \cot [\chi(\kappa)] = -\frac{1}{a_s} + \frac{1}{2}\kappa^2 R_{\text{eff}} + \mathcal{O}(\kappa^4), \quad (3.3)$$

where  $a_s$  is the  $s$ -wave scattering length and  $R_{\text{eff}}$  is the effective range. The convention applied here is that for a purely repulsive interaction the scattering length is positive, while for a purely attractive interaction without any bound states the scattering length is negative. The effective range and higher-order terms can be neglected at sufficiently low relative energy. Thus, at low energy the properties of the two-body system are basically determined by the scattering length  $a_s$ .



The  $s$ -wave scattering length for a given two-body potential  $V(r)$  can be obtained by solving the radial Schrödinger equation for two identical particles of mass  $m$  for zero angular momentum, zero energy ( $\kappa = 0$ ), and boundary condition  $u(0) = 0$ :

$$\left[ -\frac{\hbar^2}{m} \frac{d^2}{dr^2} + V(r) \right] u(r) = 0 . \quad (3.4)$$

Outside the two-body potential the solution is a straight line. According to a Taylor expansion of equation (3.2), the wave function for small  $\kappa$  is

$$u(r) \simeq \left\{ 1 + \kappa r \cot [\chi(\kappa)] \right\} \sin [\chi(\kappa)] \propto 1 - \frac{r}{a_s} . \quad (3.5)$$

Thus, the scattering length can be determined by the intersection of the asymptotic wave function with zero, that is  $u(a_s) = 0$ .

It is often convenient to also define the parameter  $a_B$  by

$$a_B \equiv \frac{m}{4\pi\hbar^2} \int d\mathbf{r} V(\mathbf{r}) = \frac{m}{\hbar^2} \int_0^\infty dr r^2 V(r) , \quad (3.6)$$

which is the Born approximation to the scattering length  $a_s$ . The last equality holds for a central potential. The strength of the interaction is then proportional to  $a_B$ .

Since the finer details of the interaction potential are superfluous, a finite-range Gaussian potential

$$V_G(r) = V_0 e^{-r^2/b^2} , \quad V_0 = \frac{4\hbar^2 a_B}{\sqrt{\pi} m b^3} , \quad (3.7)$$

see dotted line in figure 3.1, is sufficient for a study of the dependence on the scattering length and possibly a few more of the low-energy parameters in the expansion of the phase shift. The strength  $V_0$  is then related to  $a_B$  as indicated.

Figure 3.2a shows  $a_s$  as a function of the strength parameter  $a_B$  for the Gaussian potential. When the parameter  $a_B$  decreases from zero to negative values, the scattering length varies slowly and roughly linearly with  $a_B$  for small  $a_B$ , until a value  $a_B^{(0)}$  where  $a_s$  diverges as a signal of the appearance of the first two-body bound state. For increasing attraction  $a_s$  turns positive when this state is slightly bound. Then the scattering length decreases and turns negative again. This pattern repeats itself as the second bound state appears, and so on at each subsequent threshold.

For a square-well potential  $V_{sw}(r) = V_{sw,0} \Theta(r < b)$  the threshold value of  $a_B^{(0)}$  differs from the value for the Gaussian potential, but  $a_s/a_B$  as a function of  $a_B/a_B^{(0)}$  results in virtually the same curves, see figure 3.2b. This indicates that for simple potentials the behaviour is approximately independent of the shape.

Table 3.1 shows the scattering length  $a_s$  for different potential strengths  $a_B$  for the Gaussian potential, primarily for the cases studied in this work where

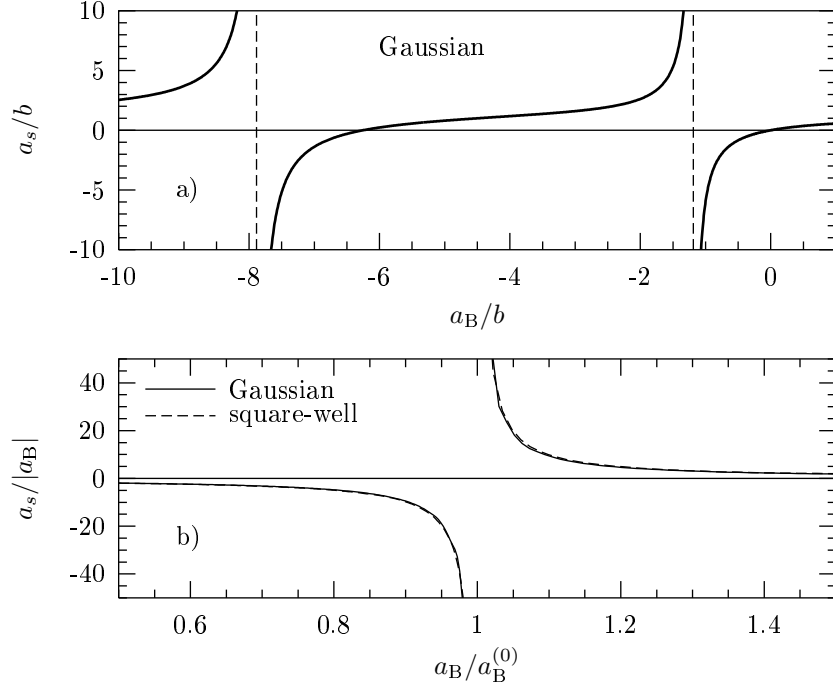


Figure 3.2: a) Scattering length  $a_s$  divided by the potential range  $b$  as a function of  $a_B$  divided by  $b$  for the Gaussian potential from equation (3.7). b) Scattering length  $a_s$  divided by  $a_B$  as a function of  $a_B$  divided by  $a_B^{(0)}$ , defined as the value of  $a_B$  where the first bound state occurs. Results are shown for the Gaussian potential with  $a_B^{(0)}/b = -1.1893$  and for the square-well potential  $V_{\text{sw}}(r) = V_{\text{sw},0}\Theta(r < b)$  with  $a_B^{(0)}/b = -0.8225$ .

$|a_B|/b$  is close to unity. The Born approximation equals the correct scattering length only in the limit of weak attraction where the magnitude of the scattering length  $a_s$  is much smaller than the interaction range  $b$ .

To exemplify, in experimental work  $^{87}\text{Rb}$  atoms have a scattering length of  $a_s \simeq 100$  a.u.\* Assuming an interaction range around  $b = 1$  nm we obtain  $a_s/b = 5.29$ . This can be modelled by a Gaussian two-body interaction with  $a_B/b \simeq -1.5$ , where the lowest solution corresponds to two-body bound states and the next accounts for the properties of the dilute gas. However, by applying an external magnetic field it is possible to change the internal energy levels in alkali atoms, e.g. in  $^{85}\text{Rb}$  [CCR<sup>+</sup>00], and thereby change the scattering length to almost any desired value. This allows experimental studies of a large range of scattering lengths.

\*The scattering lengths for relevant spin states of  $^{87}\text{Rb}$  atoms are according to Pethick and Smith [PS02] all close to 100 a.u., where 1 a.u. =  $0.529 \cdot 10^{-10}$  m.

$a_B/b$	$a_s/b$	$\mathcal{N}_B$	$a_B/b$	$a_s/b$	$\mathcal{N}_B$
+3.625	+1.00	0	-1.18765	-799	0
+1.00	+0.565	0	-1.1890	-4212	0
-0.3560	-0.50	0	-1.1893	-85601	0
-0.500	-0.84	0	-1.2028	+100	1
-0.551	-1.00	0	-1.220	+44.5	1
-1.00	-5.98	0	-1.3380	+10.0	1
-1.069	-10.0	0	-1.35	+9.32	1
-1.110	-15.7	0	-1.50	+5.31	1
-1.1761	-100	0	-6.868	-1.00	1
-1.1860	-401	0	-7.6612	-10.0	1

Table 3.1: The scattering length  $a_s$  in units of  $b$  for various strengths of a Gaussian potential measured as  $a_B/b$ . The number  $\mathcal{N}_B$  is the number of bound two-body states.

The short-range two-body interaction with  $s$ -wave scattering length  $a_s$  has in mean-field contexts [DGPS99], i.e. with a Hartree ansatz as in equation (2.31), been modelled by the three-dimensional zero-range potential

$$V_\delta(\mathbf{r}) = \frac{4\pi\hbar^2 a_s}{m} \delta(\mathbf{r}), \quad (3.8)$$

where  $\delta$  is the Dirac delta function. Only the scattering length enters as the parameter characterizing the two-body interaction. This is usually assumed to be successful when  $n|a_s|^3 \ll 1$ , where  $n$  is the density of the system. For this zero-range interaction equation (3.6) yields  $a_B = a_s$ , which is rarely the case for finite-range interactions, as is obvious for the cases illustrated in figure 3.2.

The finite-range Gaussian potential from equation (3.7) is used in the following calculations. In order to test the dependence on the short-range details of the interaction, a linear combination of different Gaussians was also used in some cases, although these results are not shown here.

## 3.2 Analytical angular properties

Before solving numerically we investigate various limits analytically. In the non- or weakly-interacting limit, the kinetic-energy eigenfunctions are relevant for understanding the properties of the many-body system. When a two-body bound state is present, there is a signature of it in the angular spectrum, which can also be studied analytically. A zero-range treatment incorporates the well-known asymptotic two-body behaviour into the many-body wave function. This leads to an equation which has an analytic solution for a very dilute system. Finally, we average the interactions in a way that resembles the mean field, i.e. all correlations are neglected. These different analytic approaches provide

a basis for understanding the numerical solutions, which we turn to in section 3.3.

### 3.2.1 Kinetic-energy eigenfunctions

First, non-interacting particles, that is  $v = 0$ , are considered. With the transformation in equation (2.20), equation (2.75) becomes

$$\left[ -\frac{d^2}{d\alpha^2} + \frac{(3N-7)(3N-9)}{4} \tan^2 \alpha - \frac{9N-19}{2} - \lambda \right] \tilde{\phi}(\alpha) = 0. \quad (3.9)$$

Here  $\tilde{\phi}(\alpha)$  is a reduced angular wave function

$$\tilde{\phi}(\alpha) \equiv \sin \alpha \cos^{(3N-7)/2} \alpha \phi(\alpha), \quad (3.10)$$

in analogy to the transformation from radial to reduced radial wave function for the two-body problem. Since  $\phi$  for a physical state cannot diverge at  $\alpha = 0$  or  $\alpha = \pi/2$ , the boundary condition for the reduced angular wave function is  $\tilde{\phi}(0) = \tilde{\phi}(\pi/2) = 0$ .

Non-reduced solutions to equation (3.9) are given by the Jacobi polynomials  $\mathcal{P}$  [AS65] as

$$\phi_K(\alpha) = \mathcal{P}_\nu^{[1/2, (3N-8)/2]}(\cos 2\alpha). \quad (3.11)$$

See further details in appendix C. The hyperspherical quantum number  $K$  is given by  $K = 2\nu = 0, 2, 4, \dots$  and denotes the angular kinetic-energy eigenfunction with  $\nu$  nodes in  $\alpha$  space. The corresponding angular eigenvalues are  $\lambda_K = K(K + 3N - 5)$ . This notation is consistent with the general hyperspherical harmonics from equations (2.48) and (2.50). The lowest eigenvalue is zero corresponding to a constant eigenfunction  $\mathcal{P}_0 = 1$ .

Figure 3.3a shows the reduced angular kinetic-energy eigenfunctions for  $N = 100$  and the lowest three eigenvalues. The constant wave function  $\phi_{K=0}$  is in the figure represented by  $\tilde{\phi}_0(\alpha) = \sin \alpha \cos^{(3N-7)/2} \alpha$ , where  $|\tilde{\phi}_0|^2$  then is the volume element in  $\alpha$  space. The oscillations are located at relatively small  $\alpha$  values. As seen in figure 3.3b, the location of the maximum changes as  $1/\sqrt{N}$  due to the centrifugal barrier proportional to  $\tan^2 \alpha$  in equation (3.9). Thus, as  $N$  increases, the probability becomes increasingly concentrated in a smaller and smaller region of  $\alpha$  space around  $\alpha = 0$ .

Some solutions may be spurious, i.e. each component  $\phi$  is non-vanishing, but the full wave function  $\Phi$  in equation (2.64) is identically zero:

$$\Phi = \sum_{i < j}^N \phi_{ij} = 0. \quad (3.12)$$

Equation (2.69) shows that such a component  $\phi$  with zero sum is an eigenfunction of the angular kinetic-energy operator. Here the  $K = 2$  eigenfunction from

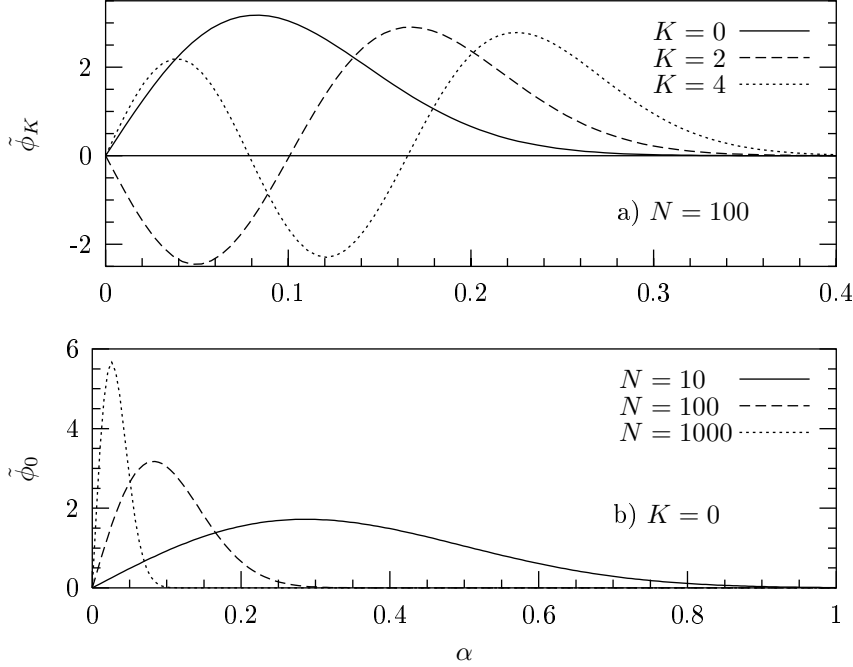


Figure 3.3: The reduced angular wave function  $\tilde{\phi}_K$ , defined in equations (3.10) and (3.11), for a)  $N = 100$  and  $K = 0, 2, 4$  and b)  $K = 0$  and  $N = 10, 100, 1000$ . The normalization is  $\int_0^{\pi/2} d\alpha |\tilde{\phi}_K(\alpha)|^2 = 1$ .

equation (3.11) has a vanishing angular average, i.e.

$$\int d\tau \sum_{i<j}^N \phi_{K=2}(\alpha_{ij}) = 0, \quad (3.13)$$

see appendix C. This criterion is not identical to equation (3.12), but functions  $\phi$  that obey equation (3.13) are nevertheless inert to the interaction potential as it occurs in the Faddeev-like equation (2.72) and in the angular variational equation (2.84). Solutions like  $\phi_{K=2}$  obtained by solving equations (2.72) or (2.84) are therefore independent of the interactions and the eigenvalue is independent of  $\rho$ . Since the  $K = 2$  function is spurious in this sense, it must be avoided when obtaining the solutions.

### 3.2.2 Asymptotic spectrum for two-body states

For large values of  $\rho$ , the short-range two-body potential  $v$  with range  $b$  is non-vanishing only when  $\alpha$  is smaller than a few times  $b/\rho$ . For larger values of  $\alpha$ ,

the ‘‘potential-rotation’’ terms  $v\hat{R}\phi$  in the angular Faddeev-like equation (2.75) can therefore be omitted.

We first assume that the rotation terms  $\hat{R}\phi$  can be neglected for smaller  $\alpha$ . For  $\alpha \ll 1$  substitution of  $r \simeq \sqrt{2}\rho\alpha$  instead of  $\alpha$  in equation (2.75) then leads to the two-body equation with energy  $E^{(2)}$ :

$$\left[ -\frac{\hbar^2}{m} \frac{d^2}{dr^2} + V(r) - E^{(2)} \right] u(r) = 0, \quad (3.14)$$

where  $2m\rho^2 E^{(2)}/\hbar^2 = \lambda + 9N/2 - 9$  and  $u(\sqrt{2}\rho \sin \alpha) = \tilde{\phi}(\alpha)$ . A two-body bound state with  $E^{(2)} < 0$  corresponds to an eigenvalue  $\lambda$  diverging towards  $-\infty$  as  $-\rho^2$ . Moreover, the wave function will be concentrated around  $r \sim b$ , which in terms of  $\alpha$  means  $\alpha \sim b/\rho \ll 1$ . Such solutions do not produce significant rotation terms, which is consistent with the omission in the derivation. The structure of the  $N$ -body system is given by the fully symmetrized wave function for two particles in the bound state, while all other particles are far away, thus producing the large average distance.

A solution to equation (2.75) that does not correspond to a two-body bound state has a wave function distributed over larger regions of  $\alpha$  space. As the potentials then vanish for large  $\rho$ , we are left with the free solutions, i.e. the free spectrum of non-negative  $\lambda$  values is obtained in this limit of large  $\rho$ .

A two-body state with energy slightly below zero forces  $\lambda$  to diverge slowly as  $-\rho^2$ . On the other hand, if the two-body system is slightly unbound,  $\lambda$  instead converges slowly to zero which is the lowest eigenvalue of the free solutions. Precisely at the threshold, it seems that  $\lambda$  should not be able to decide and therefore must remain constant. Thus, for infinitely large two-body  $s$ -wave scattering length we are led to expect that one angular eigenvalue approaches a negative constant for large  $\rho$ . Similar predicted behaviours have been confirmed for three particles [NFJG01]. In section 3.3.2 we turn to the numerical verification for  $N > 3$ .

### 3.2.3 Zero-range approximation

A zero-range treatment of three-body systems leads to an equation which can be easily solved for the angular eigenvalue [NFJG01, FJ01b]. The basic assumption is that when the hyperradius is large compared to the range of the interaction, two interacting particles in the many-body system consider each other as point particles. Therefore, the details of the interaction potential can be replaced by a boundary condition at zero separation. Moreover, it is seen from the Faddeev-like equation (2.75) that outside the potential range the angular equation is just the kinetic-energy eigenvalue equation with the solutions from section 3.2.1. Combination of these observations leads to an analytic solution as follows.

The many-body wave function at small two-particle separation approaches the two-body wave function. The two-body wave function at low energy accord-

ing to equation (3.5) then behaves as

$$\frac{1}{u(r)} \frac{du(r)}{dr} \Big|_{r=0} = -\frac{1}{a_s}. \quad (3.15)$$

In order to compare consistently, we use the many-body wave function including the volume element in the angle  $\alpha$  where  $\alpha$  is related to the two-body distance  $r$  by  $r = \sqrt{2}\rho \sin \alpha$ , i.e. we assume that at small separations the two-body wave function  $u(r)$  is represented by  $\alpha\Phi(\rho, \Omega)$ . Equation (3.15) then becomes

$$\frac{\partial[\alpha\Phi(\rho, \Omega)]}{\partial\alpha} \Big|_{\alpha=0} = -\frac{\sqrt{2}\rho}{a_s} \alpha\Phi(\rho, \Omega) \Big|_{\alpha=0}. \quad (3.16)$$

By averaging over all angular coordinates except  $\alpha$  we obtain

$$\Phi(\rho, \Omega) = \phi(\alpha) + 2(N-2)\hat{\mathbf{R}}_{13}^{(N-2)}\phi(\alpha) + \frac{1}{2}(N-2)(N-3)\hat{\mathbf{R}}_{34}^{(N-2)}\phi(\alpha). \quad (3.17)$$

Outside the diagonal potential  $v(\alpha)$  the solutions and eigenvalues, with proper boundary condition at  $\alpha = \pi/2$ , are

$$\phi_\nu(\alpha) = \tilde{\mathcal{P}}_\nu(-\cos 2\alpha), \quad \tilde{\mathcal{P}}_\nu(x) \equiv \mathcal{P}_\nu^{[(3N-8)/2, 1/2]}(x), \quad (3.18)$$

$$\lambda = 2\nu(2\nu + 3N - 5). \quad (3.19)$$

Since we do not restrict  $\phi_\nu$  for  $\alpha \rightarrow 0$ , non-integer values of  $\nu$  are allowed. For small  $\alpha$  the solutions behave as [NFJG01], see also appendix C,

$$\phi_\nu(\alpha) \simeq \frac{A}{\alpha} + B, \quad A \equiv -\frac{\sin(\pi\nu)}{\sqrt{\pi}} \frac{\Gamma(\nu + \frac{3N-6}{2})}{\Gamma(\nu + \frac{3N-5}{2})}, \quad (3.20)$$

$$B \equiv \cos(\pi\nu) \frac{2}{\sqrt{\pi}} \frac{\Gamma(\nu + \frac{3}{2})}{\Gamma(\nu + 1)}. \quad (3.21)$$

Then at the edge of the zero-range potential we get

$$\alpha\Phi(\rho, \Omega) \Big|_{\alpha=0} = \alpha\phi_\nu(\alpha) \Big|_{\alpha=0} = A, \quad (3.22)$$

$$\begin{aligned} \frac{\partial[\alpha\Phi(\rho, \Omega)]}{\partial\alpha} \Big|_{\alpha=0} &= B + 2(N-2)\hat{\mathbf{R}}_{13}^{(N-2)}\phi_\nu(0) \\ &+ \frac{1}{2}(N-2)(N-3)\hat{\mathbf{R}}_{34}^{(N-2)}\phi_\nu(0), \end{aligned} \quad (3.23)$$

$$\hat{\mathbf{R}}_{34}^{(N-2)}\phi_\nu(0) = \frac{2\Gamma(\frac{3N-6}{2})\Gamma(\nu + \frac{3}{2})}{\sqrt{\pi}\Gamma(\nu + \frac{3N-6}{2})} \xrightarrow{\nu \rightarrow 0} 1, \quad (3.24)$$

$$\hat{\mathbf{R}}_{13}^{(N-2)}\phi_\nu(0) = \frac{2\Gamma(\frac{3N-6}{2})}{\sqrt{\pi}\Gamma(\frac{3N-9}{2})} \left(\frac{2}{3}\right)^{(3N-8)/2} \times \quad (3.25)$$

$$\int_{-1}^{1/2} dx \sqrt{1+x} \left(\frac{1}{2} - x\right)^{(3N-11)/2} \tilde{\mathcal{P}}_\nu(x) \xrightarrow{\nu \rightarrow 0} 1 \quad \text{for } N > 3,$$

$$\hat{\mathbf{R}}_{13}^{(N-2)}\phi_\nu(0) = \frac{2 \sin[(\nu+1)\pi/3]}{(\nu+1)\sqrt{3}} \xrightarrow{\nu \rightarrow 0} 1 \quad \text{for } N = 3. \quad (3.26)$$

Combination of these results leads to  $\rho/a_s$  as a function of  $\nu$ :

$$\frac{\rho}{a_s} = \frac{\sqrt{2}\Gamma(\nu + \frac{3}{2})}{\sin(\pi\nu)} \frac{\Gamma(\frac{3N-6}{2})\Gamma(\nu + \frac{3N-5}{2})}{\Gamma(\nu + \frac{3N-6}{2})^2} \times \quad (3.27)$$

$$\left[ \frac{\cos(\pi\nu)\Gamma(\nu + \frac{3N-6}{2})}{\Gamma(\nu + 1)\Gamma(\frac{3N-6}{2})} + 2(N-2) \frac{\hat{R}_{13}^{(N-2)}\phi_\nu(0)}{\hat{R}_{34}^{(N-2)}\phi_\nu(0)} + \frac{(N-2)(N-3)}{2} \right].$$

At small  $|\nu| \ll 1$ , the square bracket yields  $N(N-1)/2$ , and then  $\nu$  becomes

$$\nu(\rho) \simeq \frac{N(N-1)}{2\sqrt{2\pi}} \frac{\Gamma(\frac{3N-5}{2})}{\Gamma(\frac{3N-6}{2})} \frac{a_s}{\rho}. \quad (3.28)$$

The angular eigenvalue  $\lambda$  from equation (3.19) is then

$$\lambda(\rho) \simeq 2\nu(3N-5) = \sqrt{\frac{2}{\pi}} N(N-1) \frac{\Gamma(\frac{3N-3}{2})}{\Gamma(\frac{3N-6}{2})} \frac{a_s}{\rho}. \quad (3.29)$$

This derivation is valid when  $\nu \ll 1$ , or equivalently when  $\rho \gg N^{5/2}|a_s|$ .

As we shall see in the following section, the result in equation (3.29) can be obtained otherwise. However, when the treatment of equation (3.27) is numerically extended to smaller hyperradii, unmistakably wrong results are encountered. Whether this is reminiscent of the initially expected deficiencies of the Faddeev-like equation or it is a mistake in the treatment of equation (3.27) is presently not sorted out.

### 3.2.4 Average, non-correlated effects of interactions

As discussed in section 2.3.1, a mean-field wave function corresponds to a constant angular wave function where no correlations are included. With a non-correlated, constant angular wave function  $\Phi_{K=0} = \sum_{i<j}^N \phi_{K=0}(\alpha_{ij})$ , the expectation value of the angular Hamiltonian  $\hat{h}_\Omega$  becomes

$$\lambda_{K=0} = \langle \Phi_{K=0} | \hat{h}_\Omega | \Phi_{K=0} \rangle_\Omega = \left\langle \Phi_{K=0} \left| \sum_{k<l}^N v_{kl} \right| \Phi_{K=0} \right\rangle_\Omega, \quad (3.30)$$

without contribution from angular kinetic energy. Proceeding in the manner of the mean field we then have to assume the same ansatz for the two-body interaction, i.e. the  $\delta$  function from equation (3.8). With this zero-range interaction, equation (3.30) becomes

$$\lambda_\delta \equiv \sqrt{\frac{2}{\pi}} N(N-1) \frac{\Gamma(\frac{3N-3}{2})}{\Gamma(\frac{3N-6}{2})} \frac{a_s}{\rho} \xrightarrow{N \gg 1} \frac{3}{2} \sqrt{\frac{3}{\pi}} N^{7/2} \frac{a_s}{\rho}. \quad (3.31)$$

Bohn *et al.* [BEG98] did a similar calculation, but since they did not separate out the centre-of-mass motion, the present result for  $\lambda_\delta$  is effectively that of



[BEG98] with  $N$  replaced by  $N - 1$  in the  $\Gamma$  function. For  $N \gg 1$  the results are identical.

We note that the angular potential from equation (3.31) coincides with equation (3.29), i.e. the large-hyperradii derivation from the zero-range model in section 3.2.3. This indicates that the structure of the two-body correlated ansatz for the many-body wave function catches the essential information in agreement with the low-density result, equation (3.31), which corresponds to the mean field.

Thus, the zero-range interaction from equation (3.8) leads to reasonable energies in the dilute limit. However, at larger densities (smaller  $\rho$ ) a negative scattering length  $a_s$  potentially leads to unphysical behaviours. We can understand this problem by putting  $\lambda_\delta \propto a_s/\rho$  into the radial potential, equation (2.29), which yields a term  $a_s/\rho^3$  that diverges faster than other terms as  $\rho \rightarrow 0$ . We return to this problem in chapter 6.

Thus, a zero-range two-body interaction in mean-field computations can lead to a collapse. This problem is not present for finite-range interactions, and the present method allows the use of strongly attractive potentials. The  $\delta$  interaction furthermore does not allow a study of short-range properties such as bound two-body systems and similar clusterizations. Both problems are overcome by using a finite-range potential in the present model. When  $\rho$  is much larger than the potential range  $b$ , the expectation value of a finite-range potential is of the same form as  $\lambda_\delta$  in equation (3.31)

$$\lambda_{K=0}^{\text{finite}} \xrightarrow{\rho \gg b} \sqrt{\frac{2}{\pi}} N(N-1) \frac{\Gamma(\frac{3N-3}{2})}{\Gamma(\frac{3N-6}{2})} \frac{a_B}{\rho}, \quad (3.32)$$

with the Born approximation  $a_B$  from equation (3.6) instead of the real scattering length  $a_s$ .

In the opposite limit, when  $\rho \ll b$ , the result is strongly dependent on the shape of the potential. For example, the Gaussian potential from equation (3.7) yields

$$\lambda_{K=0}^{\text{finite}} \xrightarrow{\rho \ll b} \frac{4}{\sqrt{\pi}} N(N-1) \frac{a_B}{b} \left(\frac{\rho}{b}\right)^2. \quad (3.33)$$

As seen from these two limits there are some scaling properties for finite-range potentials. The angular eigenvalue at a given  $N$  value depends only on  $a_B/b$  and  $\rho/b$ . For a Gaussian potential we have

$$v_{kl} = \frac{2m\rho^2 V_0}{\hbar^2} e^{-r_{kl}^2/b^2} = \frac{8a_B}{\sqrt{\pi}b} \left(\frac{\rho}{b}\right)^2 e^{-2(\rho/b)^2 \sin^2 \alpha_{kl}}, \quad (3.34)$$

which implies that for a given value of  $a_B/b$ , the angular eigenvalue  $\lambda$  is only a function of  $\rho/b$ . The radial potential  $U$  from equation (2.29), which we return to in chapter 4, can be scaled as

$$\frac{2mb^2 U(\rho)}{\hbar^2} = \frac{\lambda}{(\rho/b)^2} + \frac{(3N-4)(3N-6)}{4(\rho/b)^2} + \frac{(\rho/b)^2}{(b_t/b)^4}, \quad (3.35)$$

where  $b_t = \sqrt{\hbar/(m\omega)}$  is the characteristic length for a harmonic trap of angular frequency  $\omega$ . The scaled energy  $2mb^2E/\hbar^2$  is then for a given  $N$  value only a function of  $a_B/b$  and  $b_t/b$ . These scaling properties are useful in model calculations.

### 3.3 Numerical angular solutions

In the previous section we discussed solutions to the angular equation in the presence of no interactions, in the case of two-body bound states, and in the zero-range limit. However, solutions with general two-body interactions have to be obtained numerically, which is the quest of the present section. We first comment on the numerical procedure before discussing properties of the angular eigenvalues and wave functions.

#### 3.3.1 Numerical method

The angular eigenvalue equation was rewritten in chapter 2 by a variational technique as the second-order integro-differential equation (2.84) in the variable  $\alpha$ , where  $r_{12} = \sqrt{2}\rho \sin\alpha$ . For neutral atoms in recent trapping experiments the interaction range is very short compared to the spatial extension of the  $N$ -body system. Then this equation simplifies to contain at most one-dimensional integrals. The validity of the approximations only relies on the small *range*  $b$  of the potential, whereas the scattering length  $a_s$  can be as large as desired.

Even though the complexity of the angular equation does not increase as the number of particles increases, the numerical solutions become harder to handle for large  $N$ . The origin of this problem is the sharp peak in the angular volume element for large  $N$ , see section 3.2.1.

#### Expansion on kinetic-energy eigenfunctions

A usual method within the hyperspherical formalism is to expand the angular wave function on kinetic-energy eigenfunctions [Lin95, BEG98]. Such an expansion is successful when the physical extension of the system is comparable to the interaction range. The hyperspherical harmonics contain oscillations at angles of the order of magnitude  $\alpha \sim \mathcal{O}(1/K)$ , so for a given hyperradius we need  $K$  values of the order of  $K_{\max} \sim \mathcal{O}(\rho/b)$  to describe potentials limited to  $\alpha < b/\rho$ . Thus, the angular kinetic-energy eigenfunctions constitute an ineffective basis at large hyperradii since the diagonal potential in this case will be sharply peaked around  $\alpha = 0$ , and a huge number of terms is necessary to account for the correct behaviour of the wave function around  $\alpha = 0$ .

For trapped particles the scale of the system is determined by the trap length  $b_t$  which for atomic gases usually is of order  $\mu\text{m}$ . Since the interaction range  $b$  usually is in the nm region, an expansion on kinetic-energy eigenfunctions converges slowly and is not appropriate for the present treatment.

### Finite differences

Instead of an expansion on hyperspherical harmonics we choose a basis of discrete mesh points distributed in  $\alpha$  space  $\phi(\alpha) \rightarrow \underline{\phi} \equiv [\phi(\alpha_1), \dots, \phi(\alpha_M)]$  to take into account the short range of the potential and to keep sufficient information about small  $\alpha$ . Derivatives are then written as finite differences [KM90] and integrations like  $\hat{R}\phi(\alpha)$  of equation (2.88) can be expressed in matrix form, i.e.  $\hat{R}\phi(\alpha) \rightarrow \underline{R}\underline{\phi}$ .

Numerical computation of the integrals becomes increasingly difficult with decreasing interaction range. This can be understood in terms of the  $\alpha$  coordinate, since the potential at a given  $\rho$  and a given range  $b$  of the interaction, is confined to an  $\alpha$  region of size  $\Delta\alpha \sim b/\rho$ , which for Bose-Einstein condensates easily becomes very small and thus cannot be handled directly numerically.

Recently the method of finite elements was applied to the Faddeev-like equation (2.75). With finite elements the basis functions are smooth and yield more reliable matrix elements, especially those involving derivatives due to the kinetic energy. This proves easier to handle, but is presently not implemented for the angular variational equation (2.84). For details about finite-elements methods see references in Press *et al.* [PFTV89].

Unless stated otherwise, the following numerical results are obtained with the method of finite differences.

#### 3.3.2 Angular potentials

The angular eigenvalue depends on the number of particles, on the size of the system through the hyperradius, and on the two-body potential. Figure 3.4 shows the angular eigenvalue for the particle number  $N = 20$  and various Gaussian potential strengths. Only the lowest  $\lambda_0$  is shown unless otherwise indicated.

The long-dashed line shows the calculation for a purely repulsive interaction with positive scattering length. Here the angular eigenvalue approaches zero at large hyperradii approximately as  $1/\rho$ . The thin, solid line shows  $\lambda_\delta \propto a_s/\rho$  from equation (3.31) for the same scattering length. These two curves almost coincide at large hyperradii. The short-dashed curve shows the angular eigenvalue for a slightly attractive two-body interaction without any two-body bound state and with negative scattering length. This angular potential approaches zero from below as  $1/\rho$ , also in agreement with equation (3.31). For a larger attraction, when the scattering length becomes very large, the angular eigenvalue (thick, solid line) is almost constant for a large region of hyperradii. This agrees with the expectations in section 3.2.2. For a slightly larger attraction the scattering length turns positive and a two-body bound state forms. Then (dot-dashed line) the lowest angular eigenvalue at some point diverges to minus infinity. For even larger attraction the binding energy of the bound state increases and  $\lambda$  diverges faster, see the sequence of the dot-dashed, double-dashed, and triple-dashed lines.

The dotted line shows the angular eigenvalue for the next angular solution for the strongest attraction. This approaches zero from above as  $1/\rho$ , which

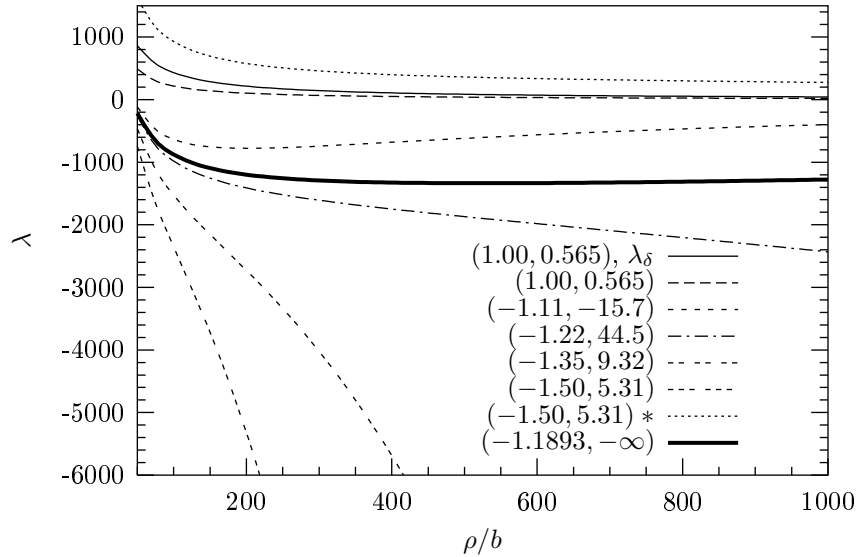


Figure 3.4: Angular eigenvalues for  $N = 20$  and parameters  $(a_B/b, a_s/b)$  as shown on the figure. A star refers to the first excited state. For  $a_B/b = -1.1893$  we have  $a_s/b = -85601$ , see table 3.1, which here is denoted by  $-\infty$ .

resembles the behaviour for a purely repulsive interaction (long-dashed line). This illustrates the use of the terms “effectively repulsive” or “effectively attractive” in the mean field, depending on the sign of  $a_s$  even though the interaction potential might be purely attractive. See related comments by Geltman and Bambini [GB01].

For one hundred particles figure 3.5 shows the lowest angular potential for various attractive interactions. Qualitatively the same behaviours as for  $N = 20$  are observed. When  $a_s = -b$  (solid line) the system has no bound two-body states. The lowest angular eigenvalue is zero at  $\rho = 0$ , decreases then through a minimum as a function of  $\rho$ , and approaches zero at large hyperradii as  $a_s/\rho$ . A larger attraction (broken lines) decreases all angular eigenvalues for all  $\rho$  values. The details at smaller hyperradii hardly change with large variations of the scattering length. However, at larger distances the approach towards zero is converted into a parabolic divergence as soon as the scattering length jumps from negative (dotted line) to positive (dot-dashed line) corresponding to the appearance of a bound two-body state. The faster divergence (double-dashed line) is again observed for increasing binding energy.

The characteristic feature for both cases  $N = 20, 100$  is the large-distance asymptotic behaviours. For repulsive potentials all eigenvalues are positive and the lowest approaches zero from above. The higher eigenvalues would then converge to  $K(K + 3N - 5)$  as  $1/\rho$ , where  $K = 4, 6, 8, \dots$ . The solution for  $K = 2$

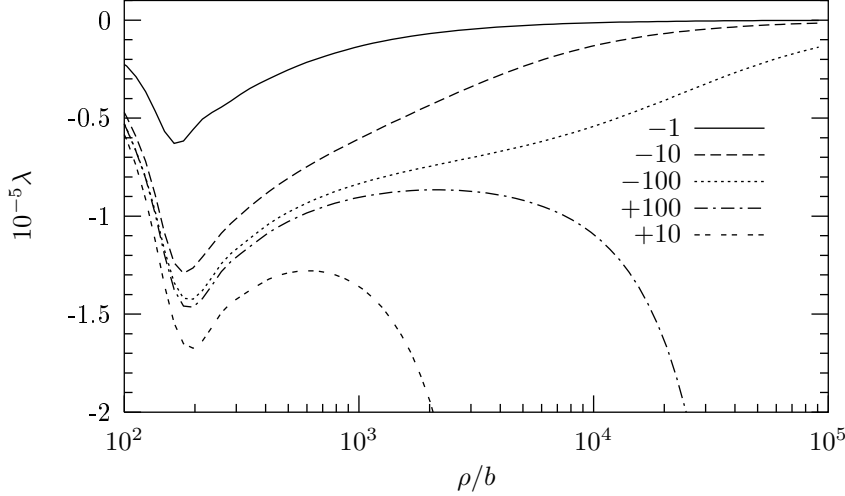


Figure 3.5: The lowest angular eigenvalues  $\lambda$  for  $N = 100$  bosons interacting via a Gaussian two-body potential  $V(r) = V_0 \exp(-r^2/b^2)$  with zero or one bound two-body states. The scattering lengths  $a_s/b$  are indicated on the figure.

is not allowed, corresponding to removal of the non-physical spurious solution, see section 3.2.1.

For weak attractions the lowest  $\lambda$  is negative and approaches zero from below as  $1/\rho$ . The higher angular eigenvalues approach, again,  $K(K + 3N - 5)$  corresponding to the spectrum for free particles. The constant of proportionality to  $\rho^{-1}$  for the lowest eigenvalue is qualitatively recovered as the predicted dependence on  $a_s$ . Calculations with a two-body potential as a linear combination of different Gaussians (not shown) confirm that the large-distance angular potential only depends on the scattering length  $a_s$  as in  $\lambda_\delta$ .

In the presence of a two-body bound state the divergence as  $-\rho^2$  reflects the corresponding two-body binding energy, see equation (3.14). Generally, an attractive finite-range interaction can support a certain number  $\mathcal{N}_B$  of two-body bound states for both positive and negative scattering lengths. Then the lowest angular eigenvalues,  $\lambda_0, \lambda_1, \dots, \lambda_{\mathcal{N}_B-1}$ , describe these bound two-body states within the many-body system at large hyperradii, i.e. they diverge to  $-\infty$  as seen in figure 3.5.

The next eigenvalue  $\lambda_{\mathcal{N}_B}$  converges to zero at large distance and corresponds to the first “two-body-unbound” mode. The higher eigenvalues would then, once more, converge to  $K(K + 3N - 5)$ . Increasing the attraction to allow another bound two-body state would then shift the asymptotic spectrum such that one more eigenvalue diverges while the non-negative energy spectrum remains unchanged. This yields qualitatively the same asymptotic spectrum for the unbound modes irrespective of the number of bound states below. This invaluablely

eases the computations, i.e. all the bound states of the two-body system are not needed in order to describe the unbound modes of the many-body system. Therefore, the two-body interaction does not have to be the real two-body interaction, which allows all the two-body bound states that are known to exist, but the interaction potential can be written in a way that accounts for the investigated properties. This is the case for the potential from Geltman *et al.* [GB01], equation (3.1), and also for the Gaussian potential, equation (3.7), applied in the present work.

These properties of the two lowest eigenvalues in the presence of one two-body bound state are evident in figure 3.6. The lowest eigenvalue (dashed curve) diverges to minus infinity proportional to  $\rho^2$ . This corresponds to the bound state. The second eigenvalue (solid curve) is negative at small hyperradii, but turns positive at larger and approaches the asymptotic behaviour of  $\lambda_\delta \propto a_s/\rho$  (dotted curve, see details in the inset). Since the second eigenvalue at

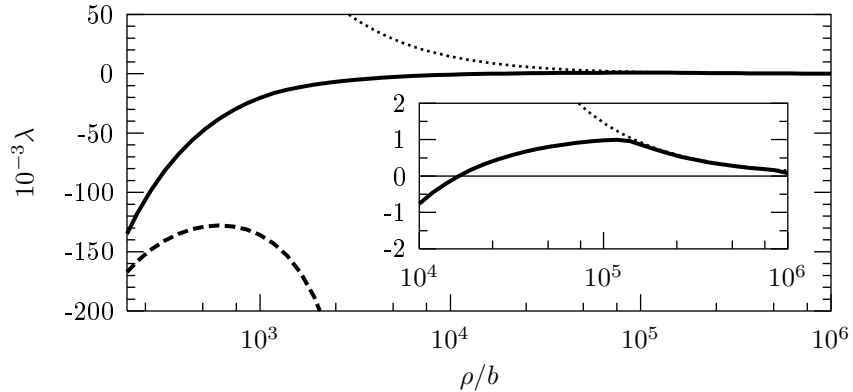


Figure 3.6: The two lowest angular eigenvalues (dashed and solid curves) for  $N = 100$ ,  $a_s/b = +10$ , and one bound two-body state. The dotted curve is  $\lambda_\delta$  for the same scattering length.

small and intermediate hyperradii is negative, this might allow a self-bound system located at distances far inside and independent of a confining external trap potential. This feature is absent in a description with overall repulsive potentials, corresponding to positive scattering lengths, for example the zero-range interaction with  $a_s > 0$ . Then no attractive part is possible.

At each threshold for the appearance of a new bound two-body state, one eigenvalue asymptotically approaches a negative constant as in figure 3.4. This eigenvalue is responsible for the structure of the  $N$ -body system for very large scattering lengths. This reflects the transition from unbound to bound two-body states, that is the transition from convergence towards zero as  $-1/\rho$  to divergence as  $-\rho^2$ , see section 3.2.2.

We finish the discussion of the angular eigenvalue from the variational equa-

tion (2.84) by comparing with the results from a finite-element treatment of the Faddeev-like equation (2.75). Figure 3.7 shows the results from the Faddeev-like equation for the same parameters as in figure 3.4. At large hyperradius the results agree, whereas they differ as  $\rho \rightarrow 0$ . This is probably due to the short-range approximation of section 2.4.3, although we recall the non-variational nature of the Faddeev-like equation, as discussed in section 2.4.1, as another possible source. However, due to the importance of correlations higher than two-body in

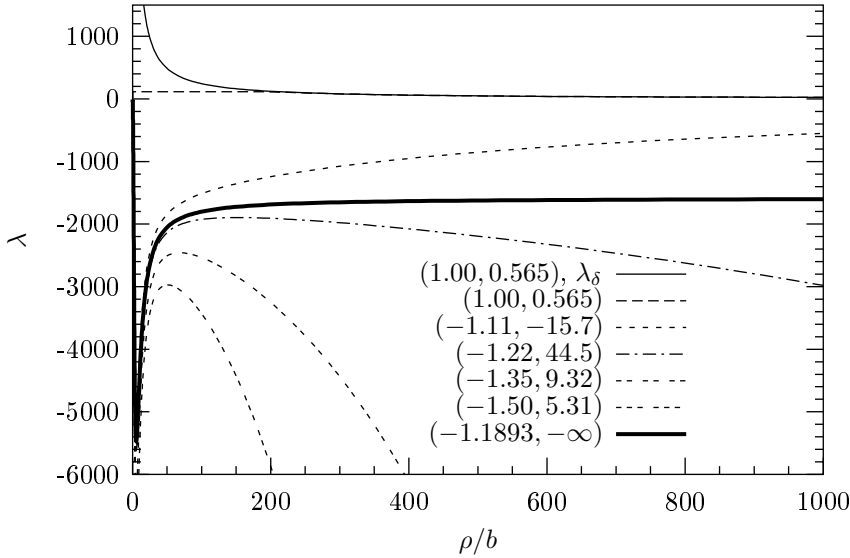


Figure 3.7: Angular eigenvalues for  $N = 20$  and parameters  $(a_B/b, a_s/b)$  as shown on the figure obtained from the Faddeev-like equation (2.75).

the denser regions, corrections to these short-distance results would be in order even without the short-range approximation. Moreover, for a description of a dilute many-boson system we do not need the details at such short distances, so they are not considered in the following.

### 3.3.3 Angular wave function

The total angular wave function is determined as the sum of two-body components in equation (2.64). Figure 3.8 shows the lowest component wave function, reduced as in equation (3.10), for a two-body potential with one bound two-body state. With increasing  $\rho$  the amplitude concentrates at smaller and smaller values of  $\alpha$ . This reflects the convergence towards the two-body bound state in agreement with the transformation  $r_{12} = \sqrt{2}\rho \sin \alpha$ , see section 3.2.2. The numerical recovery of this behaviour is essential, since otherwise the large-distance properties cannot be described.

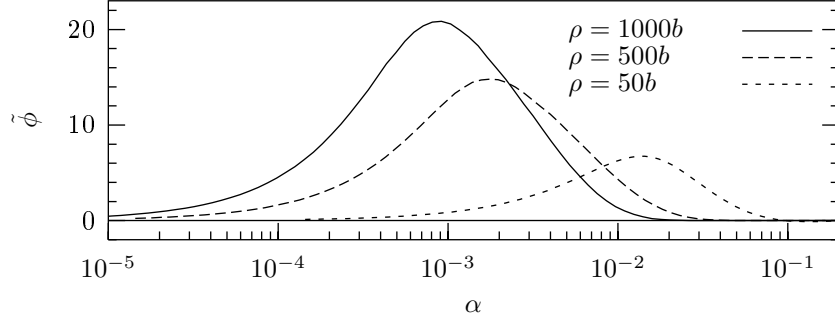


Figure 3.8: The lowest reduced angular wave functions for  $N = 20$  and  $a_B = -1.50b$ ,  $a_s = 5.31b$  for three values of the hyperradius. This potential has one bound two-body state.

The angular eigenfunction varies with the strength of the interaction. Examples of this variation are shown in figure 3.9a. The lowest non-interacting wave function (thin, solid line) has only nodes at the endpoints. The repulsive case shows an oscillation (dashed line) which lowers the angular energy due to the rotation terms. The fast change at small  $\alpha$ , which is emphasized in figure 3.9b, is typical for interacting particles. The wave function for the excited state (dotted line) has an additional node. The corresponding lower-lying wave function was shown as the dashed line in figure 3.8.

The wave function for infinite scattering length (thick, solid line in figure 3.9) corresponds to an interaction where the two-body bound state is at the threshold for occurrence. This eigenfunction resembles those where a bound two-body state is present, compare with the results shown in figure 3.8. However, now (thick curve of figure 3.9b) the wave function is located at larger  $\alpha$  values.

The properties of the component of the angular wave function is further illustrated by the second moment defined by

$$\langle r_{12}^2 \rangle_\phi \equiv 2\rho^2 \langle \phi_{12} | \sin^2 \alpha | \phi_{12} \rangle. \quad (3.36)$$

A number of these moments for different interactions are shown in figure 3.10 as functions of  $\rho$ . For states obtained from repulsive potentials, moderately attractive potentials without bound two-body states, and for excited states of positive  $\lambda$ , the moment  $\langle r_{12}^2 \rangle_\phi$  increases proportional to  $\rho^2$  for large  $\rho$ . This resembles the behaviour of the expectation value in the lowest angular state for a non-interacting system, i.e.  $K = 0$ , where  $\langle r_{12}^2 \rangle_\phi = 2\rho^2/(N - 1)$ . The qualitative explanation is that large  $\rho$  implies the limit of a non-interacting spectrum with the corresponding non-correlated wave functions.

In contrast, a different behaviour is observed when the potential can bind two particles, i.e.  $\langle r_{12}^2 \rangle_\phi$  approaches a constant at large  $\rho$ . The angular equation in this limit approaches the two-body equation (3.14). The wave function in



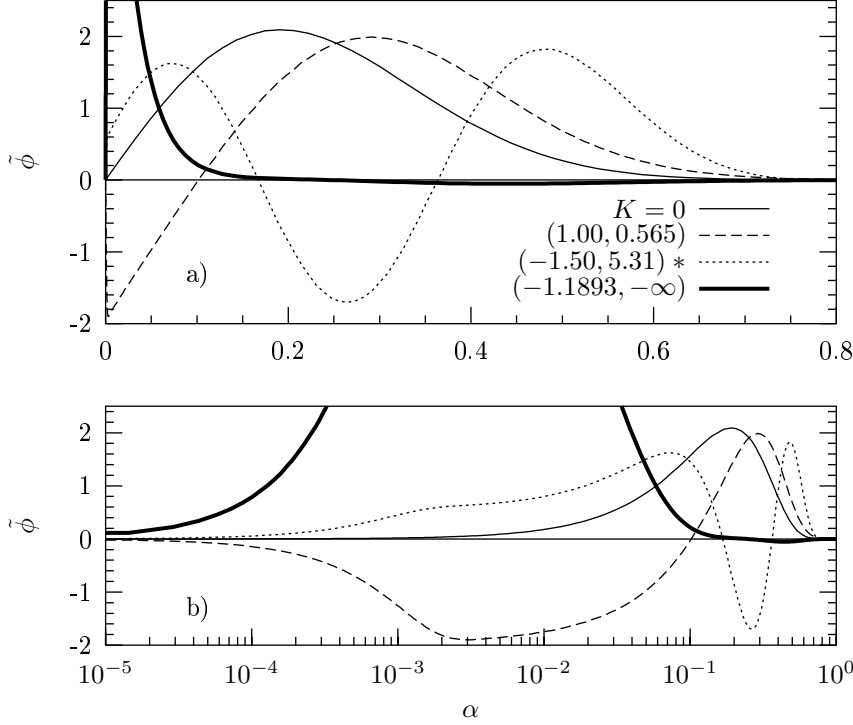


Figure 3.9: a) Angular wave functions for  $N = 20$  and  $\rho = 500b$  for different interaction parameters  $(a_B/b, a_s/b)$  as shown on the figure. The  $K = 0$  curve corresponds to a non-interacting system. A star refers to the first excited state. b) The same as a), but with logarithmic  $\alpha$  axis.

the zero-range limit converges to  $u(r) = \exp(-r/a_s)$ . The second moment is then found as  $\langle u|r^2|u \rangle = a_s^2/2$ , which in the limit of large  $\rho$  reproduce the constant values for  $\langle r_{12}^2 \rangle_\phi$  when  $a_s/b = 9.32$  and  $a_s/b = 5.31$ , i.e. the double- and triple-dashed lines in figure 3.10 approach  $9.32^2/2 \simeq 43$  and  $5.31^2/2 \simeq 14$ , respectively.

Expressed differently, when a two-body bound state is present, the angular wave function is at increasing  $\rho$  squeezed inside the potential since the range in  $\alpha$  space decreases proportional to  $\rho^{-1}$ . This implies  $\langle \phi_{12} | \sin^2 \alpha | \phi_{12} \rangle \propto 1/\rho^2$ . The distance between a pair of particles is therefore independent of  $\rho$  at large values of  $\rho$ . This means that pairwise the two-body bound state is approached while all other particles are far away. The symmetrization does not affect this conclusion. Thus, apart from this symmetrization of the many-boson wave function, the attributes of the many-body system in the presence of this two-body bound state show only small deviations from the well-known properties of

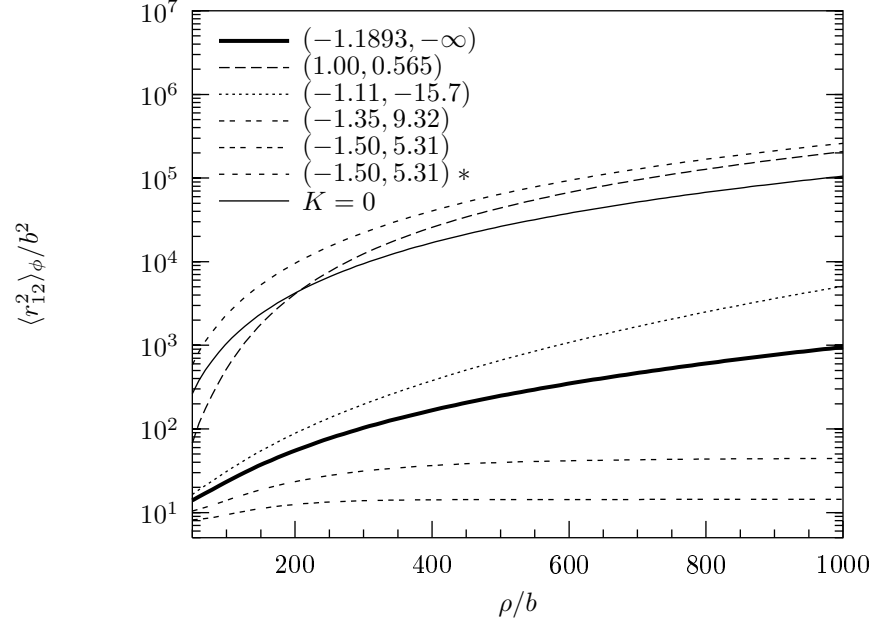


Figure 3.10: The second moment  $\langle r_{12}^2 \rangle_\phi$  as a function of hyperradius for  $N = 20$  for solutions to the angular variational equation with different interaction parameters specified in the figure by  $(a_B/b, a_s/b)$ . Also shown is the  $K = 0$  value. A star refers to the first excited state.

the isolated two-body bound state.

At the threshold for two-body binding, that is for infinite scattering length, the intermediate behaviour once again emphasizes the transition from bound to unbound, see the thick, solid line in figure 3.10.

### 3.4 Summary

Further numerical analysis allows us to construct a parametrization for the behaviour of the lowest angular eigenvalue for attractive two-body interactions in two different regimes: i) no bound two-body states and  $a_s < 0$ , and ii)  $a_s > 0$  and one bound two-body state of energy  $E^{(2)}$ . These details are previously published [SFJ03a] and collected in appendix D. Here we summarize the results, illustrate them, and then comment on them in relation to the previous observations.

#### 3.4.1 Parametrization

For small hyperradii  $\rho < \rho_0 \equiv 0.87N^{1/2}(b/|a_s|)^{1/3}b$  we use for all  $a_s$  the perturbation result obtained as the expectation value of the two-body interaction

$V(r)$  in a constant angular wave function, i.e. for  $N \gg 1$

$$\lambda_a = \frac{mV(0)N^2\rho^2}{\hbar^2} \quad \text{for } \rho < \rho_0. \quad (3.37)$$

For hyperradii exceeding the lower limit  $\rho_0$  the analytic expressions from equations (D.3), (D.4), (D.9), and (D.10) are expressed as

$$\lambda_a(N, \rho) = -|\lambda_\delta(N, \rho)| \left( 1 + \frac{0.92N^{7/6}b}{\rho} \right) \quad (3.38)$$

$$\times \begin{cases} 1 - \exp \left[ -\frac{|\lambda_\infty(N)|}{|\lambda_\delta(N, \rho)|} \right] & \text{when } a_s < 0, \\ \frac{|\lambda_\infty(N)|}{|\lambda_\delta(N, \rho)|} + \frac{|\lambda^{(2)}(\rho)|}{|\lambda_\delta(N, \rho)|} & \text{when } a_s > 0, \end{cases} \quad \text{for } \rho > \rho_0,$$

with  $\lambda_\delta$  from equation (3.31) and

$$\lambda_\infty(N) = -1.59N^{7/3}, \quad (3.39)$$

$$\lambda^{(2)}(\rho) = \frac{2m\rho^2}{\hbar^2} E^{(2)}, \quad E^{(2)} = -\frac{\hbar^2}{m|a_s|^2} c. \quad (3.40)$$

The number  $c$  approaches unity when the scattering length becomes very large. The factor  $(1 + 0.92N^{7/6}b/\rho)$  reflects dependence on the finite range  $b$  of the Gaussian two-body interaction. At  $\rho \sim N^{7/6}|a_s|$  we find  $\lambda_\delta \sim \lambda_\infty \sim \lambda^{(2)}$ .

The results of the parametrizations in equations (3.37) and (3.38) are illustrated in figure 3.11 for  $N = 100$  and various scattering lengths. The pronounced

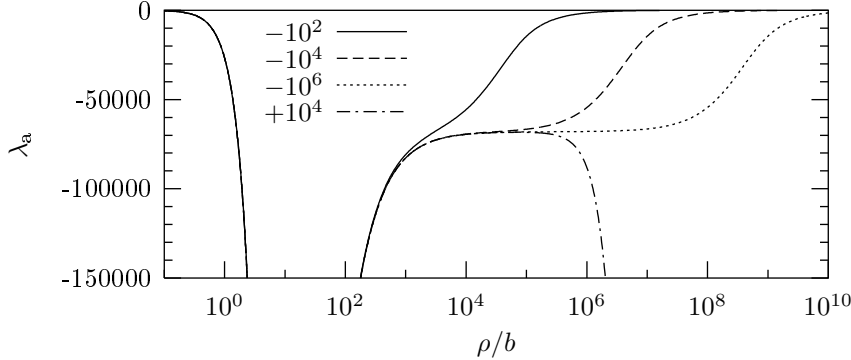


Figure 3.11: The angular eigenvalue  $\lambda$ , equations (3.38) and (3.37), for  $N = 100$  as function of  $\rho$  for the different scattering lengths given on the figure in units of the range  $a_s/b$ .

deep minimum at  $\rho \sim \rho_0$  is in the region depending on the two-body potential and reflects the qualitative behaviour of the lowest angular eigenvalue. After this strongly attractive region at small  $\rho$  the eigenvalues approach zero. As the

size of the scattering length increases, the eigenvalue develops a plateau at a constant value  $\lambda_\infty$  independent of  $a_s$ . Eventually at large  $\rho$  the eigenvalues vanish as  $\lambda_\delta$  when  $a_s < 0$  and diverge to  $-\infty$  when  $a_s > 0$ . This is comparable with the sequence of the short-dashed, thick-solid, and dot-dashed lines in figure 3.4.

When  $a_s < 0$ , the analytic and the correct eigenvalues both exceed the asymptotic zero-range result, i.e.  $\lambda_a \geq \lambda_\delta$  for all hyperradii. This means that the ground-state energy is higher than the energy obtained with the zero-range interaction. Thus, the ground state energy from the present model is higher than the mean-field energy. The origin of this sequence of energies is that the zero-range interaction inevitably leads to diverging energies for smaller distances. The present model avoids this non-physical short-range collapse.

When  $a_s > 0$  the interaction is effectively repulsive at large hyperradii and an analytical expression in this case for the second angular eigenvalue obeys  $\lambda_a \leq \lambda_\delta$  for all hyperradii, due to the divergence of  $\lambda_\delta \rightarrow +\infty$  as  $\rho \rightarrow 0$ . Correspondingly, the energies are smaller than the zero-range mean-field result in the positive- $a_s$  case.

### 3.4.2 At the threshold

At intermediate hyperradii, that is when

$$b < \frac{\rho}{N^{7/6}} < |a_s|, \quad (3.41)$$

the angular eigenvalue as obtained from equation (3.38) is independent of both the short-range details of the two-body interaction and the scattering length. Then  $\lambda$  approaches a constant value given by equation (3.39) as  $\lambda_\infty \simeq -1.59N^{7/3}$ . This plateau value can be estimated by considering the angular eigenvalue for a two-body bound state:

$$\lambda^{(2)}(\rho) \simeq -\frac{2\rho^2}{a_s^2}. \quad (3.42)$$

The plateau terminates at a hyperradius  $\rho_a$  where this two-body angular potential intersects with  $\lambda_\delta$  from equation (3.31), i.e.

$$\lambda_\infty(N) = \lambda^{(2)}(\rho_a) = \lambda_\delta(N, \rho_a) \simeq \frac{3}{2} \sqrt{\frac{3}{\pi}} N^{7/2} \frac{a_s}{\rho_a}. \quad (3.43)$$

Combination of equations (3.42) and (3.43) yields

$$\rho_a \simeq \sqrt[3]{\frac{3}{4}} N^{7/6} |a_s|, \quad (3.44)$$

$$\lambda_\infty(N) \simeq -\sqrt[3]{\frac{9}{2}} N^{7/3} \simeq -1.65N^{7/3}, \quad (3.45)$$

which is in agreement with the numerical results in equations (3.39) and (3.41). However, the  $N$  dependence cannot be predicted from the angular equation since the result is an interplay between the various terms in equation (2.84).

The symbol  $\lambda_\infty$  is chosen for this constant since the relevant  $\rho$  region extends to infinity in the limit of infinitely large scattering length. With no bound two-body states ( $a_s < 0$ ) the lowest angular eigenvalue approaches zero at larger hyperradii, whereas it diverges towards  $-\infty$  as  $\rho^2$  when a bound two-body state is present ( $a_s > 0$ ). On the threshold for a two-body bound state  $a_s = \pm\infty$  and the angular eigenvalue therefore remains constant. For finite, but large,  $a_s$  the eigenvalue lingers and cannot decide which way to go until the hyperradius exceeds a size  $\rho_a$  proportional to the scattering length given by equation (3.44).

### 3.4.3 Discussion

The two-body correlations built into the many-body wave function are evident in the properties of the angular wave function. The particles feel pairwise repelled or attracted to each other, which is reflected in the average two-body distance in the two-body amplitude. The presence of a two-body bound state is described by an angular adiabatic potential proportional to the two-body binding energy. The angular wave function in this limit equals the wave function for the two-body bound state.

The angular adiabatic potential reflects the effective interaction between the bosons. We recovered numerically the scattering length as the determining parameter for a dilute system with large average separation. Deviations at larger densities resulted in a parameter-free effective interaction  $\lambda_\infty$  which is interpreted in simple physical terms as the transition between the shape-dependent and the scattering-length-dependent regions. The properties of the lowest angular eigenvalues are collected in table 3.2.

$\mathcal{N}_B$	$a_s$	$\lambda_0$	$\lambda_1$	$\lambda_2$
0	$> 0$	$\lambda_\delta$	$\lambda_{K=4}$	$\lambda_{K=6}$
0	$< 0$	$\lambda_\delta$	$\lambda_{K=4}$	$\lambda_{K=6}$
threshold	$\mp\infty$	$\lambda_\infty$	constant	constant
1	$> 0$	$2m\rho^2 E_0^{(2)}/\hbar^2$	$\lambda_\delta$	$\lambda_{K=4}$
1	$< 0$	$2m\rho^2 E_0^{(2)}/\hbar^2$	$\lambda_\delta$	$\lambda_{K=4}$
threshold	$\mp\infty$	$2m\rho^2 E_0^{(2)}/\hbar^2$	$\lambda_\infty$	constant
2	$> 0$	$2m\rho^2 E_0^{(2)}/\hbar^2$	$2m\rho^2 E_1^{(2)}/\hbar^2$	$\lambda_\delta$
2	$< 0$	$2m\rho^2 E_0^{(2)}/\hbar^2$	$2m\rho^2 E_1^{(2)}/\hbar^2$	$\lambda_\delta$
threshold	$\mp\infty$	$2m\rho^2 E_0^{(2)}/\hbar^2$	$2m\rho^2 E_1^{(2)}/\hbar^2$	$\lambda_\infty$

Table 3.2: The behaviour of the lowest angular eigenvalues at large hyperradii as a function of the number  $\mathcal{N}_B$  of bound two-body states and for different regions of the scattering length. The attraction increases through the sequence.  $E_n^{(2)}$  is the energy of the  $n$ 'th two-body state.

Calculations with a correlated Jastrow wave function with the right behaviour at small interparticle distances and with realistic interactions [CHM<sup>+</sup>02]

and with various finite-range potentials [BG01] confirm that the ground-state energy of a dilute boson system only depends on the scattering length and not on the details of the potential. The advantage of the present model is that it results in a relatively simple one-dimensional differential equation which provides analytical results in some limits, i.e. the scattering-length-only behaviour is recovered analytically in section 3.2.3. Furthermore, from the two-body ansatz for the wave function no further assumptions are necessary in order to obtain the large-distance scattering-length-only signatures.

## Chapter IV

### Hyperradial confinement and condensates

In chapter 3 we studied the attributes of the solutions to the hyperangular equation for a fixed value of the hyperradius. This froze the variation in the average distance between the particles, but nevertheless showed a range of characteristics depending on the nature of the two-body interaction. In this chapter we complete the treatment of the degrees of freedom in the centre-of-mass system by studying the radial equation and the properties of its solutions.

Besides the contributions from kinetic energy and interactions, the radial equation contains a term due to an external field acting on the particles. As shown in chapter 2 this separates for a harmonic field nicely into a centre-of-mass part and a hyperradial part. The inclusion of such a term is discussed in section 4.1. Then the hyperangular contributions due to interactions are included in section 4.2 in a study of the properties of the full radial potential and the solutions to the radial equation. Section 4.3 presents more details about negative-energy states, which include the Efimov-like states that are described further in section 4.4. In section 4.5 we discuss condensation before summing up in section 4.6.

#### 4.1 Trapped bosons

In experiments neutral atoms, for instance evaporated sodium atoms [DMA<sup>+</sup>95], are cooled and trapped by lasers, and then held and further cooled in magnetic fields which interact with the magnetic moments of the particles. In a common set-up, the time-averaged orbiting potential, a static magnetic field is combined with a rotating magnetic field [PS02]. This effectively generates a harmonic-oscillator field in which all particles move, e.g. for particle  $i$  we have

$$V_{\text{trap}}(\mathbf{r}_i) = \frac{1}{2}m(\omega_x^2 x_i^2 + \omega_y^2 y_i^2 + \omega_z^2 z_i^2), \quad (4.1)$$

where the position of particle  $i$  is  $\mathbf{r}_i = (x_i, y_i, z_i)$ , and the angular frequencies along the coordinate directions  $q = x, y, z$  are denoted by  $\omega_q$ . These angular frequencies  $\omega_q$  depend on the magnetic moments of the atoms and on the strengths

of both the stationary field and the time-varying magnetic field. Experimentally it is possible to obtain the same effective frequency along two axes,  $x$  and  $y$ , and a different frequency along the third axis,  $z$ . E.g. for  $^{85}\text{Rb}$  atoms the effective frequencies  $\nu_q = \omega_q/(2\pi)$  in recent experiments are  $\nu_x = \nu_y = 17.5$  Hz, and  $\nu_z \sim \nu_x/2$  [DCC<sup>+</sup>01]. In terms of the trap lengths  $b_q = \sqrt{\hbar/(m\omega_q)}$  this is  $b_x = b_y = 2591$  nm and  $b_z \sim \sqrt{2}b_x$ .

We will address the general geometry in chapter 7 and here restrict ourselves to a spherically symmetric field,  $\omega = \omega_x = \omega_y = \omega_z$ , which leaves a central potential

$$V_{\text{trap}}(r_i) = \frac{1}{2}m\omega^2 r_i^2. \quad (4.2)$$

Put differently, we treat the axial field as spherical with  $\omega = \sqrt[3]{\omega_x\omega_y\omega_z}$  as the geometric mean angular frequency. A set of parameters which we will use frequently is for  $^{87}\text{Rb}$ -atoms with oscillator frequency  $\nu_{\text{trap}} = \omega/(2\pi) = 200$  Hz [BEG98], thus yielding  $b_t \equiv \sqrt{\hbar/(m\omega)} = 763$  nm. All lengths are then scaled in units of the typical interaction range  $b \simeq 10$  a.u., which leads to  $b_t/b \simeq 1442$ .

In the case of the free angular solutions from section 3.2.1, we have  $\lambda_K = K(K + 3N - 5)$  with  $K = 0, 2, 4, \dots$ . In the general case, i.e. when we include dependences beyond the  $s$ -waves in one hyperangle, we can replace  $K$  with  $K_{N-1}$  from equation (2.49). The radial solutions are analytically obtained from equation (2.30) with the radial potential from equation (2.29) with zero coupling terms. The radial wave functions are then given by

$$f_n(\rho) = e^{-\rho^2/(2b_t^2)} \rho^{l_{N,K}+1} \mathcal{L}_n^{(l_{N,K}+1/2)}\left(\frac{\rho^2}{b_t^2}\right), \quad l_{N,K} = \frac{3N-6}{2} + K, \quad (4.3)$$

where  $\mathcal{L}_n$  for  $n = 0, 1, \dots$  is the generalized Laguerre polynomial with  $n$  radial nodes. Here  $l_{N,K}$  plays the role of a generalized angular momentum due to the kinetic energy of the many-body system. Especially,  $l_{2,0} = 0$  reproduces the familiar behaviour of the harmonic-oscillator solutions for the two-particle system [BJ83]. The energy is  $E_n = \hbar\omega[3(N-1)/2 + 2n + K]$  with the subtraction of the centre-of-mass ground-state energy  $3\hbar\omega/2$ .

The ground state with  $n = 0$  is usually associated with the mode of Bose-Einstein condensation, see mean-field approaches [PS02, PS03] or related hyperspherical approaches [BEG98, WM99]. In terms of temperature the condition for onset of Bose-Einstein condensation is that the thermal length scale  $l_T$  given by  $k_B T \sim \hbar^2/(ml_T^2)$  is larger than the average distance  $\bar{r}$  between particles [PS02]. For bosons in a trap  $\bar{r} \sim \sqrt{k_B T/(m\omega^2)}/N^{1/3}$ , which yields that condensation occurs when

$$k_B T < N^{1/3} \hbar\omega. \quad (4.4)$$

When this equation is fulfilled, a large number of atoms prefer the ground state which is a signature of the condensate. The criterion is equivalent to a sufficiently large level spacing of the modes of the harmonic oscillator. In



the present thesis we assume no finite-temperature effects, corresponding to a sufficiently large level spacing.

In this non-interacting picture all quantum modes of the many-boson system are represented by single-particle levels. This means that the Bose-Einstein distribution can be applied to the non-interacting single-particle levels. In general the interactions complicate matters. In the following sections we discuss the structure of the radial solutions when interactions are included, and then in section 4.5 return to this problem.

## 4.2 Radial potential and solutions

The effect of interactions for a fixed value of the hyperradius was discussed in chapter 3 in terms of the angular potentials. These in themselves tell only a part of the story about the many-boson system. As indicated above for the non-interacting case, the radial equation is the next step in obtaining knowledge about the physical properties. The angular potentials and angular wave functions then enter the effective radial potential and transfer information about the interactions to quantities like energy and size of the system.

For a dilute Bose gas the coupling terms of equation (2.28), which in the non-interacting case are identically zero, contribute at most about 1 % compared with other terms of the full radial equation (2.27). In the following all coupling terms are therefore omitted and the solutions to the uncoupled radial equation (2.30) are considered. This way only the angular potential  $\lambda$  itself plays a role and additional information from the angular wave function  $\Phi(\rho, \Omega)$  is neglected. We should however bear in mind that coupling terms might play a role at larger densities or scattering lengths. The radial potential then consists of three terms, where the repulsive centrifugal barrier and the confining external field both are positive. The interaction term can be either repulsive or attractive. The combination has structure depending on the strength of the interaction.

The lowest potential for the non-interacting system, which was discussed in section 4.1, is shown as the thick, dashed line in figure 4.1a for  $N = 20$  particles. This has a global minimum at values of the hyperradius given by the trap length, that is at  $\rho \sim \rho_{\text{trap}} \equiv \sqrt{3N/2}b_t$ . The schematic character of this non-interacting potential is representative also for a very weak two-body attraction and for a purely repulsive two-body potential. Corresponding solutions are confined to the region between the infinitely large potential walls at small and large hyperradii.

Also shown in figure 4.1a are the lowest two radial potentials for a Gaussian interaction with no bound two-body states and a small, negative scattering length. The deviations from the weakly-interacting case are substantial. For the lowest (thick, solid line) a second minimum has developed due to the attraction between the bosons. This dominates at large densities, i.e. at small hyperradii. A barrier separates this global minimum from another minimum at large hyperradii, see details in figure 4.1b. This second minimum almost coincides with

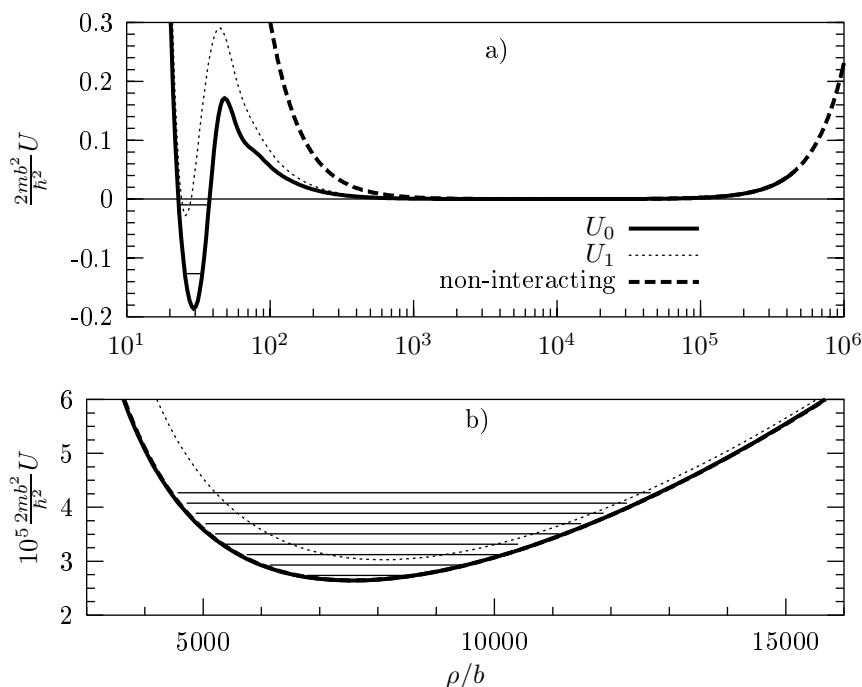


Figure 4.1: a) Radial potentials  $U_0$  (thick, solid line) and  $U_1$  (dotted line) from equation (2.29) corresponding to the lowest two angular potentials for  $N = 20$ ,  $a_s/b = -0.5$ , and  $b_t/b = 1442$ . The thick, dashed line shows the lowest non-interacting potential, that is with  $\lambda = 0$ . Horizontal lines show the lowest two energy levels in  $U_0$ . b) Details at larger hyperradii with the next nine energy levels in  $U_0$ . Here  $U_0$  and the curve for non-interacting particles are hardly distinguishable.

the minimum for the non-interacting case and these are hardly distinguishable in the figure.

With this potential the diagonal radial equation is solved. The solutions can be divided into groups related to either the first or the second minimum. The lowest two radial eigenstates in the lowest potential have negative energies, indicated as horizontal lines in figure 4.1a, and the hyperradial wave function is located in the global minimum at relatively low hyperradii. They are truly bound states as they cannot decay into continuum states at large hyperradii. Their properties are independent of the external trap which only has an influence at much larger distances. These self-bound  $N$ -body states might decay into lower-lying states consisting of various bound cluster states, e.g. a number of diatomic or triatomic clusters. We discuss this further in chapter 6. The possibility of self-bound many-body systems even though the two- and three-body

subsystems are unbound is also discussed by Bulgac [Bul02], who, however, considers a three-body interaction strength as a determining parameter for the properties of the self-bound many-boson system.

The group of states in the higher-lying minimum all have positive energies. These radial eigenstates are located in the trap minimum at larger hyperradii, see figure 4.1b, with approximately equidistant spacing as for the non-interacting oscillator. The lowest of these “trap states” can be interpreted as the state of the condensate. Thus, the structure of the “trap states” is similar for effectively attractive and repulsive interactions, i.e. for positive and negative scattering lengths. However, an attraction produces a series of lower-lying states at smaller hyperradii.

The radial potential  $U_1$  corresponding to the second adiabatic potential  $\lambda_1$  is shown as the dotted line in figure 4.1. This contains larger contributions from hyperangular kinetic energy, but still has a second minimum at small hyperradii. Otherwise the structure is the same with a barrier and a local minimum at larger hyperradii.

Increasing  $N$  leaves quantitatively the same features for pure repulsion. Attraction leads to a decreasing barrier at intermediate hyperradius and at some point this barrier vanishes altogether. At the same time the attractive minimum at smaller hyperradius becomes deeper. This leads to an increasing number of bound states in this minimum as a function of  $N$ . Figure 4.2 shows  $U_0$  for a larger number of particles,  $N = 100$ , and doubled scattering length. The increased effective attraction is pronounced at large densities, that is at small  $\rho$ . The barrier height is now small compared to the potential depth at small hyperradii. The rather deep and narrow minimum occurs for  $N = 100$  about 150 times the range of the interaction. This corresponds to a root-mean-square two-body distance of about 15 times the interaction range  $b$ .

As the scattering length increases, the barrier disappears and the effective potential inside the trap approaches the  $\rho^{-2}$  behaviour characteristic for Efimov states. We return to a discussion of such states in section 4.4.

We also study the hyperradial wave function  $F$  which tells about the root-mean-square displacement  $\bar{r}_R$  from the centre of the system defined by

$$\bar{r}_R^2 \equiv \frac{1}{N} \sum_{i=1}^N (\mathbf{r}_i - \mathbf{R})^2 = \frac{\rho^2}{N}. \quad (4.5)$$

It is shown in figure 4.3 for various scattering lengths. The thick, solid curve shows the non-interacting result. When interactions are included, the expected result turns up, i.e. that repulsion forces the particles away from the centre whereas the opposite holds for attraction.

### 4.3 Self-bound many-body states

Since the external field is negligible when  $\rho \ll \sqrt{N}b_t$ , the radial potential is negative when  $\lambda + (3N - 4)(3N - 6)/4 < 0$  and  $\rho$  is sufficiently small. Then

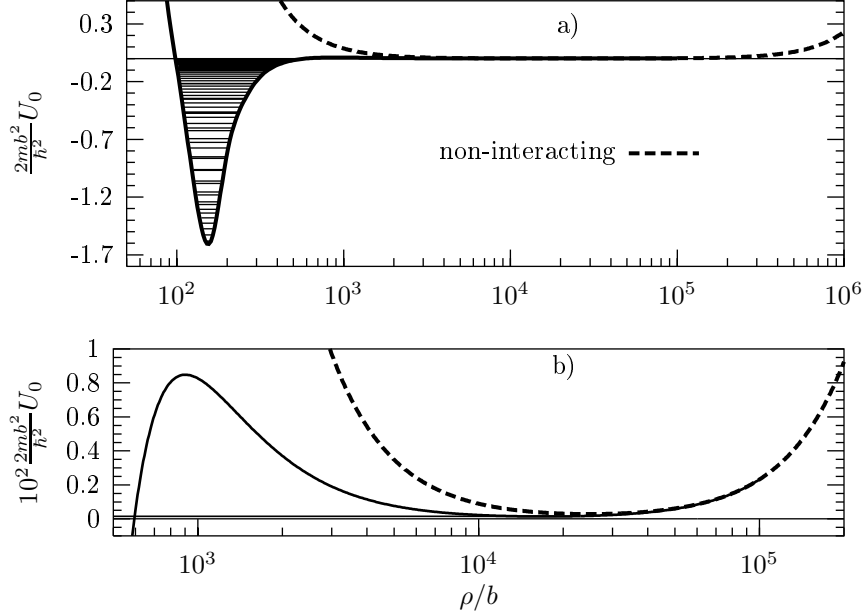


Figure 4.2: a) Radial potential  $U_0$  from equation (2.29) corresponding to the lowest angular potential for  $N = 100$ ,  $a_s/b = -1$ , and  $b_t/b = 1442$ . Also shown as horizontal lines are the negative energies  $E_{0,n}$ ,  $n = 0, \dots, 46$ , in the lowest potential in the uncoupled radial equation (2.27). b) Detail at larger hyperradii. The energy of the first oscillator-like state is shown as a horizontal line close to zero.

self-bound many-body states with negative energies and finite extensions are possible. The radial equation corresponding to the relatively weak attraction between the twenty bosons in the potential shown in figure 4.1 has two negative-energy solutions with the wave function located in the global negative minimum.

With the parametrization in equation (3.38) figure 4.4 shows the analytical radial potential, equation (2.29), corresponding to one of the angular eigenvalues from figure 3.11. The radial potential is negative in a large range of hyperradii, which can be divided into three different regions. For small hyperradii, region 1, the radial potential has a minimum. For intermediate hyperradii, Efimov region, the angular potential is constant and therefore the radial potential behaves as  $-1/\rho^2$ . This is from figure 3.11 seen to appear for  $\rho/b$  between  $10^2$  and  $10^4$ . For large hyperradii, region 2, that is when  $\rho \geq N^{7/6}|a_s|$ , the angular potential behaves as  $-1/\rho$ , so the radial potential vanishes as  $-1/\rho^3$ . Finally the trap  $\propto \rho^2$  dominates with positive contributions at large hyperradii  $\rho \gg \sqrt{N}b_t$ .

With the method described in [KMW02] it is possible to estimate the number

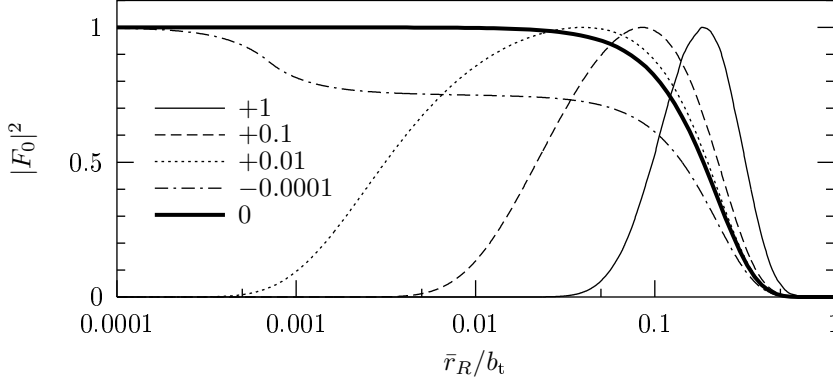


Figure 4.3: The probability distribution  $|F_0|^2$  for the rms separation from the centre of the system  $\bar{r}_R$  defined by  $\bar{r}_R^2 \equiv \sum_{i=1}^N (\mathbf{r}_i - \mathbf{R})^2 / N = \rho^2 / N$  for  $N = 20$ ,  $b_t/b = 1442$ , and scattering lengths indicated as  $a_s/b$ . The angular potential was obtained from the parametrization in equation (3.38) for  $a_s < 0$  and from  $\lambda_\delta$  for  $a_s > 0$ . The normalizations are different.

$\mathcal{N}$  of bound states in the different regions, i.e.

$$\mathcal{N} \simeq \frac{\sqrt{2m}}{\pi\hbar} \int d\rho \sqrt{|U^{(-)}(\rho)|}, \quad (4.6)$$

where  $U^{(-)}(\rho)$  denotes the negative part of the radial potential  $U(\rho)$ . The bound states in this potential can be divided into groups according to their hyperradial extension. The total number of such states is written as  $\mathcal{N} = \mathcal{N}_1 + \mathcal{N}_E + \mathcal{N}_2$  where  $\mathcal{N}_1$ ,  $\mathcal{N}_E$ , and  $\mathcal{N}_2$  are the number of states located respectively in the attractive pocket at small hyperradii, in the intermediate  $-1/\rho^2$  region, and at hyperradii large compared with the scattering length.

The analytic expressions for the angular potential from equations (3.37) and (3.38) yield the crude estimate that the number of self-bound states in the pocket is  $\mathcal{N}_1 \simeq 1.3N^{3/2}$ . The outer region supports bound states when the trap length  $b_t$  is sufficiently large, that is  $b_t \gg N|a_s|$ , and analogously the number is estimated to be  $\mathcal{N}_2 \simeq 0.78N^{7/6}$ . The intermediate region is considered in the following section.

#### 4.4 Efimov-like many-body states

When the scattering length is large, the three-body system exhibits the so-called Efimov effect [Efi70] where many bound three-body state turns up. In the following we investigate the properties of the many-body system in this Efimov regime. Much of the formulation is quite similar to that in a recent description of three-body Efimov states [NFJG01].

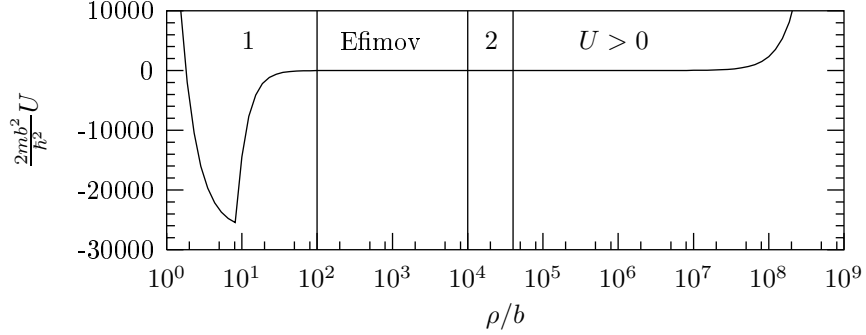


Figure 4.4: Analytic radial potential obtained from equations (2.29) and (3.38) for  $N = 100$ ,  $a_s/b = -10^4$ , and  $b_t/b = 1442$ .

A large scattering length implies through the eigenvalue from equation (3.38) an intermediate region in hyperradius where the angular potential is almost constant, see section 3.4.2. More specifically, when

$$b < \frac{\rho}{N^{7/6}} < |a_s|, \quad (4.7)$$

then equation (3.39) yields  $\lambda \simeq \lambda_\infty = -1.59N^{7/3}$  and two of the terms in the radial equation add to a negative value. At the threshold for binding of the two-body system, i.e.  $|a_s| = \infty$ , the radial potential in equation (2.29) then has the form

$$U(\rho) \simeq \frac{\hbar^2}{2m} \left( \frac{-\xi^2 - 1/4}{\rho^2} + \frac{\rho^2}{b_t^4} \right), \quad (4.8)$$

$$\xi^2 \equiv -\lambda_\infty - \frac{(3N-4)(3N-6)}{4} - \frac{1}{4} \xrightarrow{N \gg 1} 1.59N^{7/3}. \quad (4.9)$$

This implies that no repulsive barrier is present. Then the effective potential behaves as  $-\rho^{-2}$  until the trap dominates.

Figure 4.5 shows the radial potential for  $N = 20$  and infinite scattering length corresponding to  $\lambda_\infty \sim -1340$  or  $\xi^2 \sim 584$ . Deviations from the form in equation (4.8) are only present at small hyperradii due to the finite range of the interaction.

Without the external  $\rho^2$  potential the  $1/\rho^2$  potential in equation (4.8) would produce infinitely many radial solutions to the non-coupled radial equation (2.30). The radial wave function for these states would behave like

$$f_\infty(\rho) = \sqrt{\rho} \sin \left[ |\xi| \ln \left( \frac{\rho}{\rho_{sc}} \right) \right], \quad (4.10)$$

with some hyperradius scale  $\rho_{sc}$ . The energies and mean-square hyperradii for

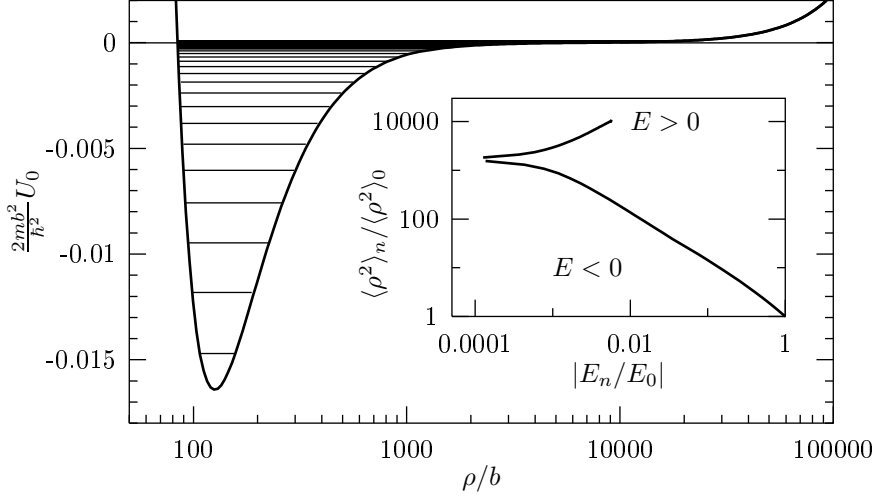


Figure 4.5: The lowest radial potential for  $N = 20$ ,  $|a_s| = \infty$ , and  $b_t/b = 1442$ . The horizontal lines indicate the 69 lowest energy eigenvalues, with 30 below zero and 39 *very* close-lying above zero. The inset relates their mean-square hyperradii with the absolute values of their energies. The lowest state has  $2mb^2 E_0/\hbar^2 \simeq -0.0147$  and  $\sqrt{\langle \rho^2 \rangle_0}/b \simeq 136$ .

such states are related by

$$E_n = -\frac{\hbar^2}{2m\langle \rho^2 \rangle_n} \frac{2}{3}(1 + \xi^2), \quad E_n = E_0 e^{-2\pi n/|\xi|}, \quad (4.11)$$

where the exponential dependence on the strength  $\xi$  of the effective potential and the number  $n$  of the excited state is highlighted. This relation can be written as

$$\frac{E_n}{E_{n+1}} = \frac{\langle \rho^2 \rangle_{n+1}}{\langle \rho^2 \rangle_n} = e^{2\pi/|\xi|}. \quad (4.12)$$

With increasing quantum number these states become exponentially larger with exponentially smaller energies approaching zero.

Around thirty states with this character are obtained for the potential in figure 4.5. The lower curve in the inset of figure 4.5 illustrates the relation in equation (4.12), and accordingly many states are in this log-log plot represented by a point on the straight line with slope  $-1$ . The very lowest states deviate due to the attraction at small  $\rho$ , and the states close to  $E = 0$  deviate due to the external potential. The denser positive energy spectrum in the upper part of the inset approaches a straight line with slope  $+1$  as expected for a harmonic potential. Using equation (2.2) we get  $2\langle \rho^2 \rangle = (N - 1)\langle r_{12}^2 \rangle \simeq 2(N - 1)\langle r_1^2 \rangle$ .

Even the most bound state with  $\langle \rho^2 \rangle^{1/2} \simeq 136b$  then has a root-mean-square (rms) distance between two particles  $\langle r_{12}^2 \rangle^{1/2} \simeq 44b$ , which is much larger than the interaction range. Also the rms distance from the centre of the trap  $\langle r_1^2 \rangle^{1/2} \simeq 31b$  is large.

The intermediate region responsible for the constant  $\lambda$  is only present when the scattering length is relatively large, i.e. when relation (4.7) is obeyed. This corresponds to hyperradii larger than  $\rho_{\min} = N^{7/6}b$  and smaller than  $\rho_{\max} = N^{7/6}|a_s|$ . The number of Efimov-like states  $\mathcal{N}_E$  located in this region is then by equation (4.6) given as

$$\mathcal{N}_E \simeq \frac{|\xi|}{\pi} \ln \left( \frac{\rho_{\max}}{\rho_{\min}} \right) \simeq 0.40N^{7/6} \ln \left( \frac{|a_s|}{b} \right), \quad (4.13)$$

where equation (4.9) yielded the last estimate. The number of Efimov-like states  $\mathcal{N}_E$  increases strongly with  $N$ . This assumes that the external trap has no influence on the hyperradial potential for  $\rho < \rho_{\max}$ . However, when the trap length  $b_t$  is sufficiently small, that is when  $\rho_{\text{trap}} = \sqrt{3N/2}b_t < N^{7/6}|a_s|$ , the extension of the plateau is truncated at large hyperradii. The number of states is then estimated by substituting  $\rho_{\max}$  with  $\rho_{\text{trap}}$  in equation (4.13). This yields

$$\mathcal{N}_E \simeq 0.40N^{7/6} \ln \left( \frac{\sqrt{3/2}b_t}{N^{2/3}b} \right). \quad (4.14)$$

When the trap length is large and does not terminate the plateau at large distances, the mean-square hyperradii of the first and last Efimov-like states are of the order  $\rho_{\min}^2 \sim N^{7/3}b^2$  and  $\rho_{\max}^2 \sim N^{7/3}|a_s|^2$ , respectively. Equation (4.11) then yields the energies of the first and last Efimov-like states

$$E_{\text{first}} \sim -\frac{\hbar^2}{2mb^2}, \quad E_{\text{last}} \sim -\frac{\hbar^2}{2m|a_s|^2}. \quad (4.15)$$

These energies are independent of the particle number  $N$  and remind of the kinetic-energy scale of strongly bound two-body states and the two-body binding energy, respectively. However, the rms distances  $\bar{r}$  between two particles in these many-body states are *not* given by  $b$  and  $a_s$ . In fact,  $\bar{r}$  contains an additional  $N$ -dependent factor, i.e.  $\bar{r} \simeq N^{2/3}b, N^{2/3}|a_s|$  for the two cases. These constant energy limits imply that the density of Efimov-like states increases with the particle number.

These many-body states arise when the two-body scattering length is large. This is the condition for the occurrence of the three-body Efimov states [Efi70, FJ93], that show characteristic properties similar to equations (4.10), (4.11), and (4.12). The author and co-workers therefore proposed to call the many-body states with similar attributes for many-body Efimov states [SFJ02a]. A more correct name is probably Efimov-*like* many-body states since some definitions of the term ‘‘Efimov state’’ read that infinitely many  $N$ -body bound states occur when the  $N - 1$ -body system is on the threshold for binding. According to



Amado *et al.* [AG73] “there is no Efimov effect for four or more particles” in the sense that being on the threshold for binding in the  $N - 1$ -body system does not produce infinitely many  $N$ -body bound states when  $N > 4$ . This statement is not in contradiction with the Efimov-like states discussed here since the present Efimov-like  $N$ -body states occur when the two-body system, and *not* the  $N - 1$ -body system, is on the threshold for binding. However, the quoted remark reminds us that the three-, four-,  $\dots$ ,  $N - 1$ -body systems are also bound and that many of the  $N$ -body states might be resonances embedded in the continua of dimer, trimer, and higher-order cluster states. They could be artifacts of the model where only special degrees of freedom are treated, and where we recall the possible changes due to larger coupling terms for large scattering lengths. However, because the particles are far from each other and couplings to the continuum states therefore could be weak, some of these states might be distinguishable structures which could be relatively stable. We return to such considerations in section 6.2.4.

## 4.5 Trap states and “the condensate”

In the non-interacting case hyperradial many-body states are located in the potential minimum created by a competition between the kinetic energy and the external trap. Similar behaviours were seen in the cases of repulsion and attraction, see for instance in figure 4.1 the excited states above the lowest two located in the minimum at large hyperradii. The corresponding density profile of the lowest trap state is similar to that obtained in experiments creating Bose-Einstein condensates [DGPS99]. We can therefore call this trap state for “the condensate” or define a condensate by the typical signatures of the lowest state located in this minimum due to the external trap.

The attraction produces lower-lying many-body bound states with an average distance between the particles much smaller than in the condensate-like state. The structure of these states could as well be characterized as a condensate (condensed  $N$ -body state), but they are much more unstable due to the much larger density and the larger recombination probability. These lower states have no parallels in mean-field computations.

Through the derived adiabatic potential the two-body unbound mode is responsible for the properties of atomic Bose-Einstein condensation where no clusterization is allowed. We focus on the state of the condensate in the second minimum and in the present work only use the lower-lying negative-energy states in connection with the possible decay of the condensate. However, first we discuss a definition of a condensate state in the present context.

### 4.5.1 A definition of “condensate”

In mean-field treatments, with repulsive two-body potentials and confining trap potentials, the condensate is uniquely defined as a statistical mixture of single-particle states with the ground state dominating [PS02, Pou02]. This many-

body state is mainly determined by the properties of the trap. It is at best only approximately stationary due to the neglected degrees of freedom which allow energetically favored di- and tri-atomic cluster states. This instability is also an experimental fact seen by permanent loss of trapped atoms, e.g. in recombination processes [DCC<sup>+</sup>01].

Without any two-body interaction the properties of the many-body system is determined by the thick, dashed potential curve in figure 4.2. Then the condensate is a physical state dominated by the ground-state component. With attractive interactions (full curve) the deep minimum at small hyperradius is produced. Then the ground state, located in this minimum, has nothing to do with a condensate. The density is so high that couplings to other degrees of freedom would develop higher-order correlations and processes like three-body recombinations would quickly destroy the single-atom nature of the gas. This ground state, before or after recombinations, does not show the signature of a Bose-Einstein condensate where many particles occupy one single-particle level.

The formulation in the present work does not use the concept of single-particle levels. Therefore we cannot talk about a statistical distribution of particles with the majority in the lowest state. However, we can talk about a many-particle system described as a superposition of many-body eigenstates where the lowest states are favored in thermal equilibrium. To clarify, a quantum state is given as the superposition of eigenstates  $\Psi_n(\rho, \Omega)$  from equation (2.26):

$$\Psi_{\text{quantum state}}(\rho, \Omega) = \sum_{n=0}^{\infty} c_n \Psi_n(\rho, \Omega) = \sum_{n=0}^{\infty} c_n \sum_{\nu=0}^{\infty} F_{\nu,n}(\rho) \Phi_{\nu}(\rho, \Omega), \quad (4.16)$$

with the normalization  $\sum_{n=0}^{\infty} |c_n|^2 = 1$ . The spatial extension of a condensate must be sufficiently large in order to exceed a certain minimum interparticle distance  $d_c$  below which the atoms are too close and recombine very fast. This distance depends on the scattering length and on the number of particles. Therefore, a state cannot be characterized as a condensate if components with  $\langle r_{12}^2 \rangle \ll d_c^2$  are dominating contributions in the wave function.

One of the stationary states in this model can be defined as the “ideal condensate state”, i.e. the state of lowest energy with one component, labeled by the quantum numbers  $\nu_c$  and  $n_c$ , which has

$$\langle r_{12}^2 \rangle_{\nu_c, n_c} \gtrsim d_c^2. \quad (4.17)$$

When no bound two-body states are included in the model, this ideal state is determined by the adiabatic component in the lowest angular potential, that is  $\nu_c = 0$ . On the other hand, the states of lowest energy with  $\nu = 0$  might have an average particle distance less than  $d_c$ . The appropriate choice among these excited states depends on the number of particles and on the scattering length. The ideal state is then characterized by one dominating component, that is  $\nu_c = 0$ ,  $|c_{n_c}| \simeq 1$ , and  $|c_{n \neq n_c}| \ll 1$ . If it is impossible to distinguish states with these features, it probably makes little sense to define a condensate. The possible states would be too unstable.

If  $d_c$  is significantly smaller than  $b_t$ , then the state of lowest energy located in the second minimum can be identified as the condensate. This state is characterized by a radial wave function  $F(\rho)$  with the root-mean-square (rms) radius  $\langle \rho^2 \rangle^{1/2}$  approximately equal to the hyperradius at the second minimum of the adiabatic potential  $U_0(\rho)$ .

Figure 4.6a shows the rms interparticle distance  $\bar{r}_n$  given by  $\bar{r}_n^2 \equiv \langle r_{12}^2 \rangle_n = 2\langle \rho^2 \rangle_n / (N - 1)$  for the lowest excited states, labeled by  $n$ , in the potential of figure 4.2. All states with  $n \leq 46$  have  $20b \leq \bar{r}_n \leq 100b$ , which implies that the particles are well outside the range of the interaction with each other. Whether the average distance qualifies a state as a condensate depends on the decay rate of this state. From figure 4.6b it is seen that the abrupt change in rms distance does not influence the energy which changes smoothly for the states in question.

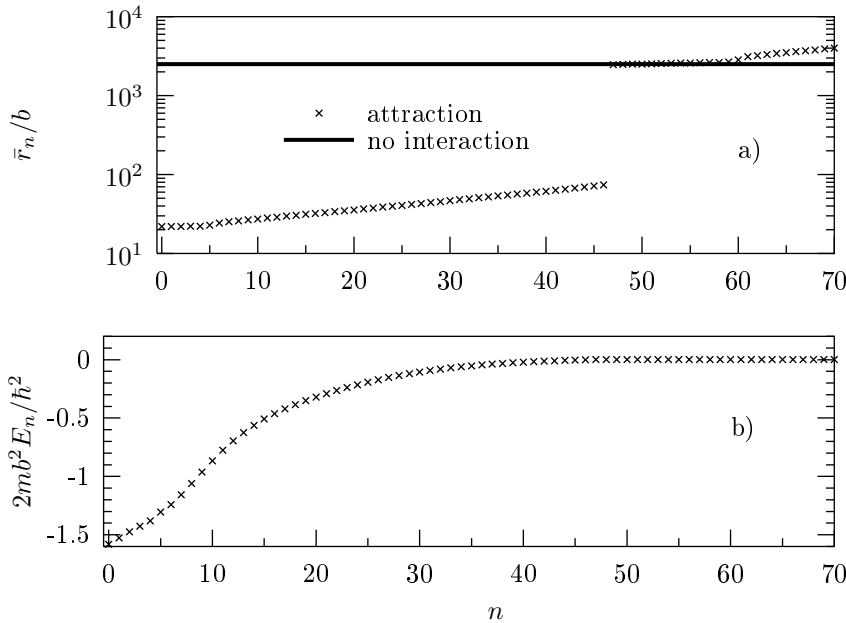


Figure 4.6: a) The root-mean-square distance  $\bar{r}$  for  $\nu = 0$  as a function of the hyperradial quantum number  $n$  for  $N = 100$ ,  $a_s/b = -1$ , and  $b_t/b = 1442$ . b) The energy  $E$  for the same case.

For the positive-energy states ( $n \geq 47$ ) the average particle distance now exceeds  $2000b$ , that is  $\bar{r}^2 \simeq 3b_t^2$  which approximately is obtained in the limit of a non-interacting gas. This investigation repeated for the higher adiabatic potentials  $\nu \geq 1$  results in the same pattern (not shown), although there are fewer states with small interparticle distance.

In section 6.2 we return to a discussion of the appropriate value for  $d_c$ , which then would characterize these states as ideal for a condensate or not.

## 4.5.2 Interaction energy

The total energy of a state in the first minimum only depends on the interaction since this state is bound even in the absence of the external field. Such a state has no analogue in mean-field calculations. Total energies of states in the second minimum are dominated by the contribution from the confining field and therefore are rather insensitive to anything else than this field. It is then more informative to study interaction energies where the large background external-field contribution is removed.

Figure 4.7 shows the interaction energy per particle as a function of the particle number for a relatively weak attraction corresponding to the small scattering length  $a_s/b = -0.84$ . The two crosses for  $N = 20$  (on the left) show the results from the two-body correlated model for the lowest adiabatic channel  $\nu = 0$  with quantum numbers  $n = 7$  and  $n = 8$ . The interaction energy is negative for the lower state, whereas the shown value for the upper state is positive due to the extra internal kinetic energy. This is repeated for the larger  $N$  values  $N = 100$  and  $N = 900$ , i.e. the lowest state characteristic for a condensate is shown along with some of the higher-lying states. For  $N \gtrsim 950$  there are no trap states since the barrier has vanished. However, the correlated solutions are still stable due to the use of the finite-range potential.

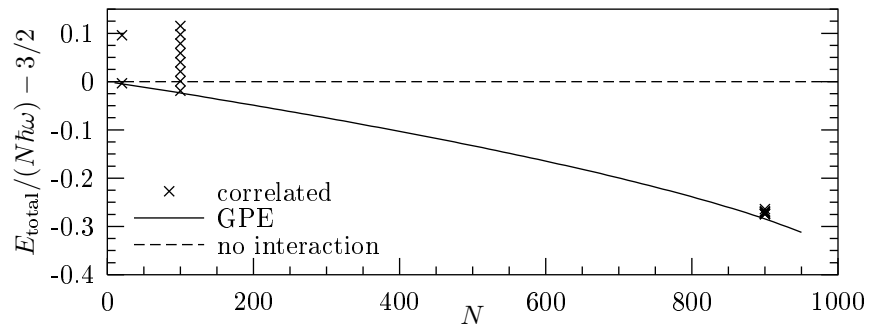


Figure 4.7: Interaction energy as a function of  $N$  for  $a_s/b = -0.84$  and  $b_t/b = 1442$ . The crosses are results of the present hyperspherical calculation for three numbers of particles. The quantum numbers are  $\nu = 0$  and, for the lowest cross in each of the three cases,  $n_c = 7$  for  $N = 20$  ( $N|a_s|/b_t = 0.012$ ),  $n_c = 52$  for  $N = 100$  ( $N|a_s|/b_t = 0.058$ ), and  $n_c = 88$  for  $N = 900$  ( $N|a_s|/b_t = 0.52$ ). The solid curve shows results of the GPE.

We anticipate the mean-field discussion of chapter 5, i.e. an ansatz for the many-body wave function as a product of single-particle amplitudes and a zero-range interaction potential lead to the mean-field Gross-Pitaevskii equation (GPE). Shown as the solid line in figure 4.7 is the interaction energy obtained from the GPE. For small  $N$  values the GPE solution is stable and the related interaction energy is negative due to the attraction between the particles. A

nearly linear behaviour is observed at small particle numbers since each particle interacts with  $N - 1$  other particles. We observe the similarity between the mean-field energy and the energy for the lowest trap state in the hyperspherical model. As  $N$  increases, the mean-field attraction increases and a non-physical collapse is inevitable. This instability occurs for  $N|a_s|/b_t \simeq 0.55$  which corresponds to  $N \simeq 950$  with the present set of parameters. There is no stable solution to the GPE for  $N|a_s|/b_t > 0.55$ .

Thus, using the correlated model we generally observe both condensate-like and collapsed many-boson states. In the present example for relatively few particles  $N$ , it was easy to distinguish due to the presence of the intermediate potential barrier. In chapter 6 we discuss the case of small or vanishing barrier and in chapter 5 compare further to the mean field.

## 4.6 Summary

The radial potential exhibits features from kinetic energy, interactions, and external field, and thus combines the information available within the hyperspherical model. The structure of the system depends mainly on the scattering length and the trap length. Confined many-body states of negative energy may occur even without an external confining potential. This is possible when the effective attraction between the bosons is sufficiently large.

Self-bound states with properties similar to the three-body Efimov states occur when the scattering length is very large compared to the range of the interaction. These states may still have relatively low density and thus avoid the instant collapse due to three-body recombinations. This will be further addressed in chapter 6.

A description of the condensate as effectively a non-self-bound many-body state confined by the external trap is possible within this hyperspherical treatment. Then the average properties are comparable to those of the mean-field treatment, as we shall see in more detail in the following chapter. So, the main effect of correlations is to allow the Efimov-like many-body states, and the finite interaction range prevents an infinite collapse of the system as the density increases.



## Chapter V

### Mean field and validity

The mean field provides a study of the average properties of a many-boson system. Section 5.1 first presents some features of the mean-field method, then discusses density-dependent interactions, and finally compares mean-field results with the results from the correlated model. Section 5.2 contains a discussion of the ranges of validity for both models.

#### 5.1 Comparison to mean field

When studying a dilute system of particles, the first approach is usually to apply a mean-field method where the many-body wave function for identical bosons is factorized into one-particle amplitudes  $\psi$  as described in section 2.3.1. This often leads to the non-linear Gross-Pitaevskii equation (GPE) [Pit61], where the single-particle function enters as a properly normalized single-particle density  $|\psi(\mathbf{r}_1)|^2$ . In the stationary case the GPE is written as

$$\left[ -\frac{\hbar^2}{2m} \frac{\partial^2}{\partial \mathbf{r}_1^2} + \frac{1}{2} m \omega^2 r_1^2 + \frac{4\pi\hbar^2 a_s}{m} (N-1) |\psi(\mathbf{r}_1)|^2 - \mu \right] \psi(\mathbf{r}_1) = 0, \quad (5.1)$$

where  $m$  is the mass of the particles,  $\omega$  is the angular frequency of an external trapping potential, and  $a_s$  is the two-body  $s$ -wave scattering length. The eigenvalue of this equation is the chemical potential  $\mu$  which is related to the total energy  $E_{\text{total}}$  by  $\mu = \partial E_{\text{total}} / \partial N$ .

The GPE was applied to a description of experiments with trapped alkali atoms [EB95, BP96] and is now routinely solved for the density profile of a condensate [DGPS99, PS02, PS03] and for the dynamical evolution of a condensate with the time-dependent version of equation (5.1) [AM02]. Proukakis *et al.* [PBS98] derived a non-linear Schrödinger equation from a microscopic treatment of binary interactions and in the low-density limit obtained the GPE. The under-lying assumptions are valid when the scattering length  $a_s$  is small compared to the inter-particle separations [LS02], i.e. when  $n|a_s|^3 \ll 1$  where

$n$  is the density.\* The mean-field validity condition is then fulfilled, which means that the mean free path  $\bar{\alpha}$  given by  $\bar{\alpha} = 1/(na_s^2)$  is long compared to the average distance which approximately is  $n^{-1/3}$ .† The low-energy scattering properties expressed by the scattering length are then decisive. In the following we first comment on the choice of interaction, then discuss density-dependent interactions, and finally collect some differences between the results from the mean-field method and the hyperspherical adiabatic method.

### 5.1.1 Two-body interactions

The origin of the interaction term in the Gross-Pitaevskii equation (GPE) is the approximation

$$\int d\mathbf{r}_2 V(\mathbf{r}_2 - \mathbf{r}_1) |\psi(\mathbf{r}_2)|^2 \simeq |\psi(\mathbf{r}_1)|^2 \int d\mathbf{r}_2 V(\mathbf{r}_1 - \mathbf{r}_2) \quad (5.2)$$

for an interaction of much shorter range than the average distance. This integral is given by the Born approximation to the scattering length as we saw in section 3.1

$$\int d\mathbf{r}_2 V(\mathbf{r}_1 - \mathbf{r}_2) = \frac{4\pi\hbar^2}{m} a_B, \quad (5.3)$$

where the GPE then occurs with  $a_B$  replaced by  $a_s$ . The smallness of  $a_s$  compared with the average distance between particles is the criterion of validity [Pit61]. This corresponds to a scattering situation where the wave function hardly changes due to the scattering, i.e. the wave length is very large corresponding to low energy and low density.

The mean-field treatment above corresponds to a zero-range interaction with  $a_B$  replaced by  $a_s$

$$V_\delta(\mathbf{r}) = \frac{4\pi\hbar^2 a_s}{m} \delta(\mathbf{r}), \quad \mathbf{r} = \mathbf{r}_2 - \mathbf{r}_1, \quad (5.4)$$

see also section 3.1. This limit can be obtained from a finite-range potential where the range approaches zero and the strength is appropriately adjusted. The finite-range Gaussian interaction of equation (3.7) can be expressed as

$$V_G(\mathbf{r}) = \frac{4\pi\hbar^2 a_B}{m} \delta_G(\mathbf{r}), \quad (5.5)$$

$$\delta_G(\mathbf{r}) \equiv \frac{1}{\pi^{3/2} b^3} e^{-r^2/b^2}, \quad 1 = \int d\mathbf{r} \delta_G(\mathbf{r}). \quad (5.6)$$

---

\*In chapters 5 and 6  $n$  denotes the density and *not* the hyperradial quantum number as in chapter 4.

†The Danish letter “ $\alpha$ ” is pronounced almost like the vowel in the English “them” or “Thames”.



The Gaussian  $\delta_G(\mathbf{r})$  is in the limit when  $b \rightarrow 0$  a representation of the Dirac  $\delta$  function. For  $a_s = a_B$  we then have

$$\lim_{b \rightarrow 0} V_G(\mathbf{r}) = V_\delta(\mathbf{r}) . \quad (5.7)$$

However,  $a_s = a_B$  is only valid when  $|a_B|/b \rightarrow 0$ , which is rarely the case, see figure 3.2.

The aim of computing reliable energies in the mean-field approximation can be achieved with equation (5.4) for dilute systems [EG99]. The interaction and the Hilbert space must be consistent, that is to say that a renormalized interaction follows a restricted space to produce the correct energy. In this case the Hilbert space is restricted to the mean-field product wave function. Any inclusion of features outside this restricted space, for example two-body cluster structures, would be disastrous [FJ01a]. Maintaining the finite-range interaction with the correct scattering length then results in different properties of the interaction even when the range approaches zero on any scale defined by the problem. Thus, the mean-field product wave function with a realistic two-body potential would also lead to wrong results, as we shall see later.

The full Hilbert space with the correct interaction must produce correct answers to any proposed question. Whether a realistic interaction combined with the present inclusion of two-body correlations reproduces the main features is not obvious. However, the investigations in chapter 4 demonstrate that the energy in the mean-field approximation for dilute systems is reproduced. This asymptotic behaviour is determined by the scattering length which only implicitly is contained in a given combination of range and strength of the Gaussian interaction. This implies that the Hilbert space of the model accounts properly for the correlations crucial at large separations.

### 5.1.2 Density-dependent interactions

In section 3.2.4 we studied the angular potential with a zero-range interaction as in equation (5.4). This led to the angular eigenvalue  $\lambda_\delta$  from equation (3.31), which in the limit of large densities clearly is wrong. A possible treatment at large densities is to use a finite-range potential with the correct scattering length as discussed in section 3.1. However, this immediately requires a treatment beyond the mean field, e.g. by the Jastrow or Faddeev approaches. Another common approach, especially in nuclear physics [SJ87, CBB<sup>+</sup>03], but also for atomic many-boson systems [LY57, LHY57, BHM02], is to expand the interaction in density-dependent terms. In the present case the two-body interaction can be written as

$$V(\mathbf{r}) = g_2(n)\delta(\mathbf{r}) , \quad (5.8)$$

where the low-density limit of the coupling strength  $g_2(n)$  is  $g_2(0) = 4\pi\hbar^2 a_s/m$ .

We relate the density  $n$  to the root-mean-square (rms) hyperradius  $\bar{\rho} \equiv \sqrt{\langle \rho^2 \rangle}$ . The density is related to the rms separation  $\bar{r}$ , which is defined by

$\bar{r}^2 \equiv \langle r_{12}^2 \rangle$ , by  $1/n \simeq 4\pi\bar{r}^3/3$ . The relation  $\bar{r}^2 = 2\bar{\rho}^2/(N-1)$ , obtained from equation (2.2), then yields

$$n \simeq \frac{3}{8\sqrt{2}\pi} \frac{N^{3/2}}{\bar{\rho}^3}. \quad (5.9)$$

We then replace  $\bar{\rho}$  by  $\rho$  and for a fixed hyperradius calculate the angular potential as an expectation value of the two-body interactions, equation (5.8), in a constant hyperangular function. This yields

$$\lambda_{\delta n}(n) = \lambda_{\delta} \frac{g_2(n)}{g_2(0)}, \quad \lambda_{\delta n}(0) = \lambda_{\delta}. \quad (5.10)$$

The reverse relation yields an expression for the density-dependent coupling strength, i.e.

$$g_2(n) = g_2(0) \frac{\lambda_{\delta n}(n)}{\lambda_{\delta}}. \quad (5.11)$$

We assume that the numerically obtained angular potentials  $\lambda$ , as calculated in chapter 3 and parametrized in equation (3.38), represent the density-dependent potential rather well, so we identify  $\lambda_{\delta n}$  with the lowest angular potential for the case with no two-body bound states. Here we use the above-mentioned transition between  $n$  and  $\rho$ . So figure 5.1a shows for various  $N$  values  $\lambda_{\delta n}(n)/\lambda_{\delta} = g_2(n)/g_2(0)$  as a function of the density in the combination  $N^2 n |a_s|^3$ .

At low densities the ratio approaches unity which yields the correct limit  $g_2 \simeq g_2(0)$ . At larger densities the deviations are significant, and the coupling strength vanishes altogether as  $n|a_s|^3 \rightarrow \infty$  since the finite-range interaction contains no divergence. Figure 5.1b shows the same quantities for different scattering lengths and the behaviours are confirmed.

When the scattering length is negative and large,  $n|a_s|^3 \gg 1/N^2$ , the angular potential assumes a constant value  $\lambda \simeq \lambda_{\infty}$ , see equation (3.39) in section 3.4. This yields a coupling strength of magnitude

$$\frac{g_2(n)}{g_2(0)} \simeq \frac{\lambda_{\infty}}{\lambda_{\delta}} \simeq \frac{0.48}{N^{2/3} n^{1/3} |a_s|} \simeq \frac{0.77\bar{r}}{N^{2/3} |a_s|}. \quad (5.12)$$

In this region the coupling strength decreases linearly with the rms distance  $\bar{r}$  between the bosons. The interaction energy per particle in this region is given by

$$\frac{E}{N} \simeq \frac{1}{2} g_2(n) n \simeq -\frac{\pi\hbar^2 n^{2/3}}{N^{2/3} m}. \quad (5.13)$$

This is independent of the scattering length. A Jastrow calculation in the denser region for *positive* scattering lengths by Cowell *et al.* [CHM<sup>+</sup>02] yielded  $E/N \simeq 13\hbar^2 n^{2/3}/m$ , which reminds of the present result for negative scattering length.

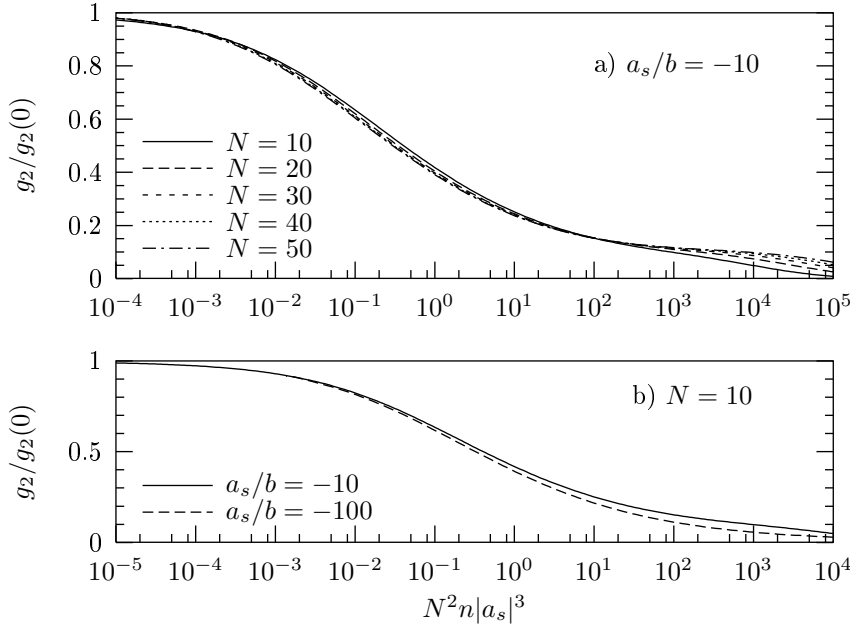


Figure 5.1: a) The coupling strength in units of the zero-density value as a function of the density for  $a_s/b = -10$  and various particle numbers. b) The coupling strength in units of the zero-density value as a function of the density for  $N = 10$  and various scattering lengths. The results are obtained by a finite-element treatment of the Faddeev-like equation (2.75).

Besides the sign change and the different factor, the present result contains an additional dependence on the number of particles.

This expansion in  $(n^{1/3}|a_s|)^{-1}$  is in clear contrast to density-expansions where the energy functional is written as expansions in  $n^{1/3}|a_s|$  [LY57, BHM02]. Such a low-density expansion clearly diverges at large densities where it is not intended to work. The present results also need corrections at large densities due to higher-order correlations, but they might provide a modified zero-range interaction  $V(\mathbf{r}) = g_2(n)\delta(\mathbf{r})$  which could possibly be implemented in a GPE-like treatment of systems denser than usually within reach.

In order to avoid collapse due to an attractive two-body  $\delta$  interaction, some methods apply a repulsive three-body contact interaction. This can be written as

$$V_3(\mathbf{r}_{12}, \mathbf{r}_{13}) = g_3(n)\delta(\mathbf{r}_{12})\delta(\mathbf{r}_{13}), \quad (5.14)$$

where we allow a density-dependent coupling strength  $g_3$ . The expectation value of the three-body interactions in a constant angular wave function yields

the angular potential

$$\lambda_{3\text{-body}}(n) = \frac{\sqrt{3}}{8\pi^2} N(N-1)(N-2)(N-3) \left(N - \frac{5}{3}\right) \left(N - \frac{7}{3}\right) \frac{g_3(n)m}{\hbar^2 \rho^4}. \quad (5.15)$$

Inspired by Gammal *et al.* [GFTC00] we parametrize the coupling strength as

$$g_3(n) = \frac{g_2^2(0)k_3(n)}{\hbar\omega}, \quad (5.16)$$

which for  $N \gg 1$  yields, in units of  $\lambda_\delta$ ,

$$\frac{\lambda_{3\text{-body}}(n)}{\lambda_\delta} = \frac{4\sqrt{\pi}}{3[\rho/(\sqrt{N}b_t)]^3} \frac{Na_s}{b_t} k_3(n). \quad (5.17)$$

Gammal *et al.* [GFTC00] use values  $0 \leq k_3 \leq 0.03$  which yields  $\lambda_{3\text{-body}}/\lambda_\delta \ll 1$  for a system with  $\rho \sim \sqrt{N}b_t$ . However, at larger densities we have  $\lambda_{3\text{-body}} > \lambda_\delta$ . Even though this three-body contact interaction can not account for the details when three particles approach each other, it might provide a step towards an explicit inclusion of three-body correlations.<sup>‡</sup>

A treatment of fermion antisymmetry in the hyperangular equations probably becomes too complicated when many particles are involved. However, the effect of two-body correlations for fermions might be included by a modified zero-range coupling strength as described for bosons above. The density dependence could possibly be extracted for a few fermions and then applied for a large number of particles.

### 5.1.3 Properties of the wave functions

In the dilute limit the Hartree wave function is closely related to the hyper-radial function and the Jastrow correlated wave function is closely related to the Faddeev-like decomposition of the wave function, see section 2.3. A direct comparison of the wave functions is in general not possible as this requires an expansion on a complete set of basis functions in one of the coordinate systems. The necessary calculations involve non-reducible high-dimensional integrals.

Instead we use the indirect relations provided in section 2.3.1 where energy and average distance between particles are characteristic features of the solutions. For a given scattering length the energy  $E$  is numerically obtained for identical bosons as a function of the particle number. The interaction energy is next calculated as  $E - E_0$  where  $E_0 = 3N\hbar\omega/2$  is the energy of the non-interacting trapped gas. The results for  $a_s/b = -0.84$  are shown in figure 5.2a. The discussion of stability which follows in section 6.1 shows that in terms of variational average distance the GPE energy for attractive potentials has a local minimum at large average distances and much lower energies at small

<sup>‡</sup>On this train of thought the work by Bohn *et al.* [BEG98] was an initiation for the present study of two-body correlations.

average distances. The physically meaningful mean-field solution is located in the minimum at large average distance. This minimum becomes unstable for sufficiently large particle numbers. In the example of figure 5.2a no stable mean-field solution (solid, thin line) exists for  $N = 1000$ . This is consistent with the experimentally established stability criterion  $N|a_s|/b_t < 0.55$  [CKT<sup>+</sup>03] as seen from the upper  $N|a_s|/b_t$ -axis.

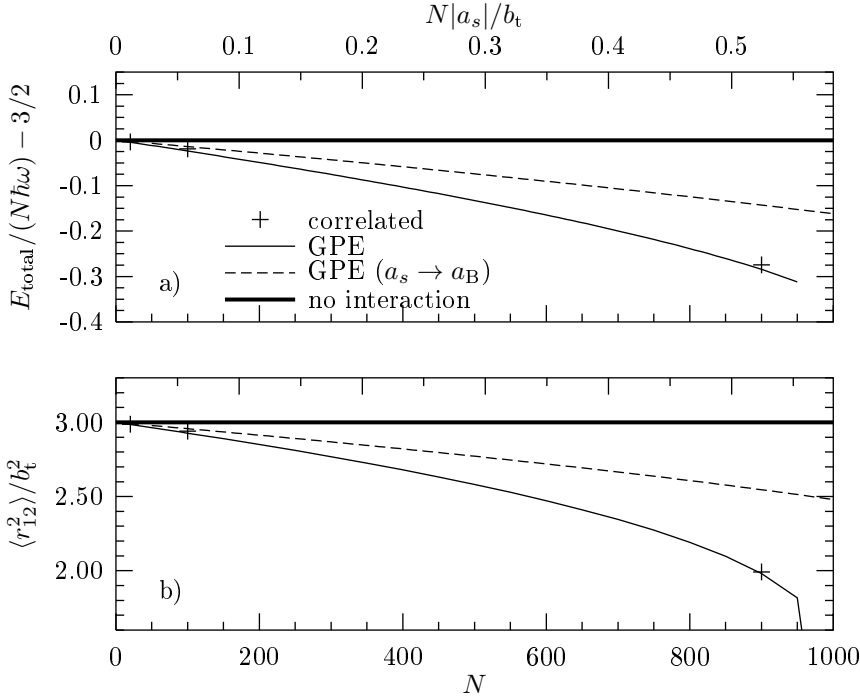


Figure 5.2: a) Interaction energy as a function of  $N$  for  $a_s/b = -0.84$  ( $a_B/b = -0.5$ ) and  $b_t/b = 1442$ . The thin solid line shows GPE results and the plusses are obtained from the two-body correlated model; see also figure 4.7. The dashed line shows the GPE results for  $a_s/b = -0.5$ . The upper  $N|a_s|/b_t$ -axis applies for  $a_s/b = -0.84$ . b) Mean-square distance between the particles for the same cases.

The same figure shows results obtained with the present two-body correlated method for three different particle numbers (plusses). The correlated and mean-field interaction energies are remarkably similar. It may at first appear odd that the mean-field interaction energy is marginally lower than by use of the correlated wave function which includes an extra degree of freedom. The reason is that the mean-field result is obtained with an effective interaction which only in the Born approximation has the correct scattering length, while the correlated solution is obtained for an interaction with the correct scattering length. The

mean-field interaction is effectively more attractive as discussed in section 3.4.

The proper comparison is then a GPE calculation with  $a_s/b = -0.5$ , corresponding to the Born approximation for a Gaussian of  $a_B/b = -0.5$  with true scattering length  $a_s/b = -0.84$ . As seen in figure 5.2a (dashed curve), now the mean-field interaction energies are numerically smaller. This comparison does not include the negative-energy states supported by the attractive pocket at short distance, see e.g. figure 4.1. They would appear far below the “condensate-like” state shown in figure 5.2a.

Using equations (2.2) and (2.39), we compare in figure 5.2b  $\langle r_{12}^2 \rangle$  for the solutions to the mean-field approximation and the hyperspherical methods. Also this quantity is very similar for the two methods, whereas we again observe the discrepancy when we for the GPE method replace  $a_s$  by  $a_B$ . The mean-square distance decreases with increasing particle number for calculations with an attractive potential. As  $N$  approaches 1000, the Gross-Pitaevskii mean-field radius approaches zero due to the unavoidable collapse. The same behaviour is seen for radii and interaction energies, i.e. the average distance between particles decreases until the condensate collapses and the size vanishes in the mean field, while many-body bound states with smaller extension play a role in the present hyperspherical description. Then also higher-order correlations can be expected to be essential and result in recombination processes as will be discussed in section 6.2.

In conclusion, for weak interactions or very small scattering lengths a stationary many-body state can be approximated by a product of single-particle amplitudes. However, stronger attraction between particles must invoke other degrees of freedom like clusterization. Then a single-particle description is not valid. This is in agreement with general expectations, and thus confirmed with the present point of departure.

## 5.2 Validity conditions

We conclude the chapter by estimating validity criteria for the models. Of special importance in relation to trapped atomic gases is a radial wave function with rms hyperradius  $\rho \sim \sqrt{N}b_t$ . Accurate angular eigenvalues in this region are therefore crucial for a proper description. If these hyperradii are sufficiently large, that is  $\rho \sim \sqrt{N}b_t > N^{7/6}|a_s|$ , the angular eigenvalue has reached its asymptotic value  $\lambda \simeq \lambda_\delta$ . This condition is equivalent to  $N|a_s|/b_t < N^{1/3}$ , which is obeyed by stable systems with  $N|a_s|/b_t < 0.55 < N^{1/3}$ .

The different models are valid if appropriately designed, i.e. the present two-body correlated model reproduces the correct effective interaction for the correct scattering length for any short-range interaction, whereas the Gross-Pitaevskii equation (GPE) reproduces this same correct effective interaction by using the Born approximation. Interaction energies and sizes would be very similar for the states corresponding to the condensate.

From equation (5.9) a given rms hyperradius  $\bar{\rho}$  is related to the density  $n$  of the system by  $n \sim N^{3/2}/\bar{\rho}^3$ . The zero-range mean-field method (GPE) is usually

valid for condensates when  $n|a_s|^3 \ll 1$ , see [CHM<sup>+</sup>02, PS03]. Then the number of particles within a scattering volume  $4\pi|a_s|^3/3$  is on average much smaller than one. From the present model, in the zero-range asymptotic region of  $\bar{\rho} > N^{7/6}|a_s|$ , we find that  $n\bar{\rho}^3 > N^{7/2}n|a_s|^3$  or  $n|a_s|^3 < 1/N^2 \ll 1$ , which means that the system is very dilute and both the GPE method and the correlated method are valid.

For  $\bar{\rho} < N^{7/6}|a_s|$  the large-distance asymptotic  $\lambda \simeq \lambda_\delta$  is not valid. This corresponds to that we cannot use a non-correlated model with the zero-range interaction. This is here interpreted as an indication of the inadequacies of the GPE in the region where  $\bar{\rho} < N^{7/6}|a_s|$  or equivalently where  $n|a_s|^3 > 1/N^2$ . This appears different than the usual criterion of validity  $n|a_s|^3 \ll 1$ , but could potentially specify what is meant by “much smaller than unity”.

The present adiabatic hyperspherical method with two-body correlations explicitly allowed in the form of the wave function is valid in the region  $\bar{\rho} > N^{7/6}|a_s|$  where correlations are expected to be insignificant. The inclusion of two-body correlations is expected to allow smaller hyperradii  $\bar{\rho} < N^{7/6}|a_s|$ . When higher-order clusterizations occur, any method without correlations higher than two-body breaks down. The absolute lower criterion must be that the distance between two particles on average exceeds the interaction range  $b$ , i.e.  $\bar{\rho} > N^{1/2}b$ . We quote this as the criterion even though explicit calculations might prove that higher-order correlations alter the lower limit.

In conclusion, the validity regions for the two-body correlated method and the GPE version of the mean field are estimated to be

$$\bar{\rho} > \sqrt{Nb} \quad \text{for two-body correlated method ,} \quad (5.18)$$

$$\bar{\rho} > N^{7/6}|a_s| \quad \text{for GPE (the present result) .} \quad (5.19)$$

These relations can with equation (5.9) be expressed via the density as

$$nb^3 < 1 \quad \text{for two-body correlated method ,} \quad (5.20)$$

$$n|a_s|^3 < \frac{1}{N^2} \quad \text{for GPE (the present result) ,} \quad (5.21)$$

$$n|a_s|^3 \ll 1 \quad \text{for GPE (usual expectation) ,} \quad (5.22)$$

where we also collected the usual criterion for validity of the GPE. When the density is low, both descriptions are valid and the energies are similar. For larger densities the importance of correlations increases and the mean-field approximation breaks down. At even higher density also two-body correlations are insufficient and the particles may clusterize further.

These conclusions are illustrated in figure 5.3 where the lowest angular eigenvalue for a case with no two-body bound state and negative scattering length is compared to the zero-range angular potential for the same scattering length. For low density  $n|a_s|^3 < 1/N^2$  the effective energy of the two methods coincide. For larger densities the GPE energy diverges, while the energy from the finite-range model remains finite. Moreover, it deviates in a region where the density is still relatively low  $n|a_s|^3 < 1$  so higher-order correlations, especially

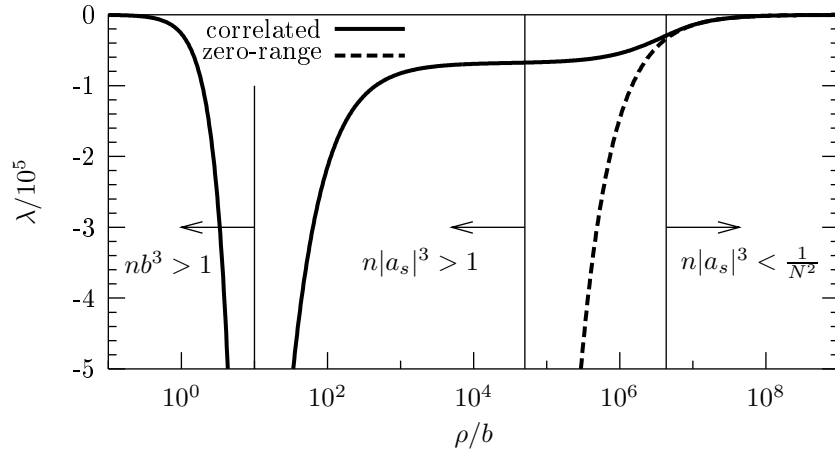


Figure 5.3: The lowest angular eigenvalue for  $a_s/b = -10^4$ ,  $N = 100$ , and no bound two-body states (solid line). The dashed curve is  $\lambda_\delta$  for the same scattering length. The vertical lines indicate regions of different density.

three-body, do not play a role yet. As the average distance becomes smaller, we expect corrections due to higher-order correlations.



## Chapter VI

### Macroscopic stability and decay

Chapter 4 opened a discussion of the macroscopic boson systems known as condensates, and a definition of the condensate was given in the present hyperspherical context. In this chapter we discuss stability and consider possible dynamics, primarily related to this lowest trap state or “condensate”. In terms of the degrees of freedom explicitly included in the two-body correlated model, section 6.1 presents a criterion for macroscopic stability. This is similar to the discussion presented by Bohn *et al.* [BEG98]. Section 6.2 ventures into a discussion of degrees of freedom that in the strictest sense are beyond the present model. This especially involves three-body recombination events that potentially ignite dynamics of the system as one macroscopic whole.

#### 6.1 Stability criterion

Macroscopic instability of systems of bosons has been investigated thoroughly the last eight years. Macroscopic stability for a Bose-Einstein condensate (BEC) means that the BEC state is well defined and has a sufficiently long lifetime when considering possible decay modes. In this sense it was originally expected that Bose-Einstein condensation could not be realized for atoms with effectively attractive interactions. However, this was achieved in 1995 for  ${}^7\text{Li}$  atoms [BSTH95]. Since then numerous experiments, e.g. [RBC<sup>+</sup>01, CKT<sup>+</sup>03], have tested the critical region. Also the collapse process itself has been studied [SGWH99, DCC<sup>+</sup>01, RCC<sup>+</sup>01].

The criterion for stability of a system with negative scattering length  $a_s$  can be expressed as a critical combination of the number of particles, the scattering length, and the trap length  $b_t \equiv \sqrt{\hbar/(m\omega)}$ , where  $\omega$  is a geometric mean, see section 4.1. Recently it was measured that when  $N|a_s|/b_t > 0.55$ , a condensate of  ${}^{85}\text{Rb}$ -atoms is unstable [CKT<sup>+</sup>03]. This can be understood as a competition between the kinetic energy which is effectively repulsive and the two-body attractive interaction. When the kinetic energy subdues the net attraction, a meta-stable system with signatures of a condensate exists. The number of kinetic-energy terms equals the number of particles  $N$  and the num-

ber of interactions equals the number of particle pairs  $N^2/2$ . Therefore, as  $N$  or the scattering length  $a_s$  increases, the interactions at some point win and for attraction lead to collapse. When the trap length  $b_t$  is small, the system is compressed too much and is according to the criterion unstable. This means that the interactions win at larger densities.

In the mean field this can be formulated variationally with a Gaussian-Hartree amplitude with a variational width  $w$ , i.e.  $\psi(r_1) = \exp[-r_1^2/(2w^2)]$ , see also Pethick and Smith [PS02]. The kinetic energy per particle is proportional to  $1/w^2$ , the external field energy  $w^2/b_t^4$ , and the interaction energy  $Na_s/w^3$ . This leads to the variational total energy

$$\frac{2m}{\hbar^2}E_{\text{total}}(w) = \frac{3N}{2w^2} + \frac{3Nw^2}{2b_t^4} + \sqrt{\frac{2}{\pi}}N^2\frac{a_s}{w^3}. \quad (6.1)$$

This yields energy curves in the length scale  $w$ , analogous to the hyperradial potential curves in chapter 4, which has stable points for a sufficiently weak attraction. The critical value is then found to be about 0.67 [DGPS99, PS02]. More detailed analysis of the Gross-Pitaevskii equation (5.1), incorporating time dependence, yields a value of 0.55 [GFT01] in agreement with the experimentally measured value [CKT+03].

By analogy with the mean-field discussion we here take a closer look at the derivation of the stability criterion in the hyperspherical frame. This is also equivalent to the derivation performed by Bohn *et al.* [BEG98]. The criterion is obtained by estimating when the radial barrier disappears. The effective hyperradial potential  $U(\rho)$  from equation (2.29) can in the asymptotic region when  $\rho > N^{7/6}|a_s|$ , that is when  $\lambda \simeq \lambda_\delta$  from equation (3.31), for  $N \gg 1$  be written as

$$\frac{2mU(\rho)}{\hbar^2} = \frac{9N^2}{4\rho^2} + \frac{\rho^2}{b_t^4} + \sqrt{\frac{2}{\pi}}N^2\left(\frac{3N}{2}\right)^{3/2}\frac{a_s}{\rho^3}. \quad (6.2)$$

If we rescale equation (6.2) with  $\rho = \sqrt{3N/2}w$ , this hyperradial potential is identical to the mean-field variational energy from equation (6.1), i.e.  $U(w) = E_{\text{total}}(w)$ . For a large and negative  $a_s$  or a large value of  $N$  there is no stable region in such a potential. In general, a potential of the form

$$u(x) = \frac{A}{x^2} + Bx^2 - \frac{C}{x^p}, \quad \{A, B, C\} > 0, \quad (6.3)$$

diverges to  $+\infty$  as  $x \rightarrow \infty$  and if  $p > 2$  to  $-\infty$  as  $x \rightarrow 0$ . For a sufficiently small constant  $C$  there will always be a local minimum. There will be no local minimum when  $p \geq 2$  and

$$C > \frac{8}{p(p+2)}\frac{A^{(p+2)/4}}{B^{(p-2)/4}}\left(\frac{p-2}{p+2}\right)^{(p-2)/4}. \quad (6.4)$$

For the present case the power  $p$  is given by  $p = 3$  and  $A$ ,  $B$ , and  $C$  are given by comparing equations (6.2) and (6.3). Then the radial potential for negative

scattering length has a local minimum only when

$$\frac{N|a_s|}{b_t} < \frac{2\sqrt{2\pi}}{5^{5/4}} \simeq 0.67. \quad (6.5)$$

This is identical to the value obtained variationally from the mean field since the  $a_s$ -only dependence at large hyperradii corresponds to the mean field with a zero-range interaction, as discussed in chapter 3 and directly evident by comparing equations (6.1) and (6.2). This gives the right order of magnitude of the critical combination of particle number, scattering length, and trap length. The discrepancy from the experimental value can be accounted for by the deformation of the external field and the zero-point energy from motion in the trap. This will be discussed in chapter 7.

The criterion is in figure 6.1 illustrated by the radial potential, with the angular eigenvalue obtained from equation (3.38), as a function of the hyperradius for a series of different particle numbers and scattering lengths. The strongly-varying short-distance dependence is omitted to allow focus on intermediate and large hyperradii. When an intermediate barrier is present, the condensate is described as the state of lowest energy located in the minimum at large hyperradius. This minimum exists for  $a_s < 0$  when  $N|a_s|/b_t < 0.67$  as established above.

In figure 6.1a-6.1d the particle number is fixed at  $N = 6000$  while only the scattering length  $a_s$  varies. In figure 6.1d-6.1f the scattering length is fixed at  $a_s/b = -0.35$  and  $N$  is varied. In figure 6.1a the two-body interaction is zero, that is  $a_s = 0$ , which leads to a vanishing lowest angular eigenvalue  $\lambda = 0$ . The effective radial potential then consists only of the centrifugal barrier and the external field with one minimum. In figure 6.1b an attractive potential with  $a_s = -0.05b$  is sufficiently strong to overcompensate for the centrifugal repulsion and create a second minimum in the radial potential at smaller hyperradius; the final divergence  $U(\rho) \rightarrow +\infty$  when  $\rho \rightarrow 0$  is not included in the scale of the figure. An intermediate barrier is left between the two minima at small and large hyperradii. A further increase of the attraction in figure 6.1c removes the barrier while leaving a smaller flat region. The negative-potential region around the minimum at small hyperradius is now even more pronounced. This tendency is continued in figure 6.1d with a stronger attraction. With the scattering length from figure 6.1d, i.e.  $a_s = -0.35b$ , and a decreasing number of particles the intermediate barrier is slowly restored. In figure 6.1e for  $N = 3000$  a barrier is about to occur, and in figure 6.1f for  $N = 500$  an intermediate barrier is again present between a minimum at small and large hyperradii.

The discussion in this section involved the static properties of states located in the local minimum at large hyperradii. Other factors are important when we in the following section to some extent include time dependence.

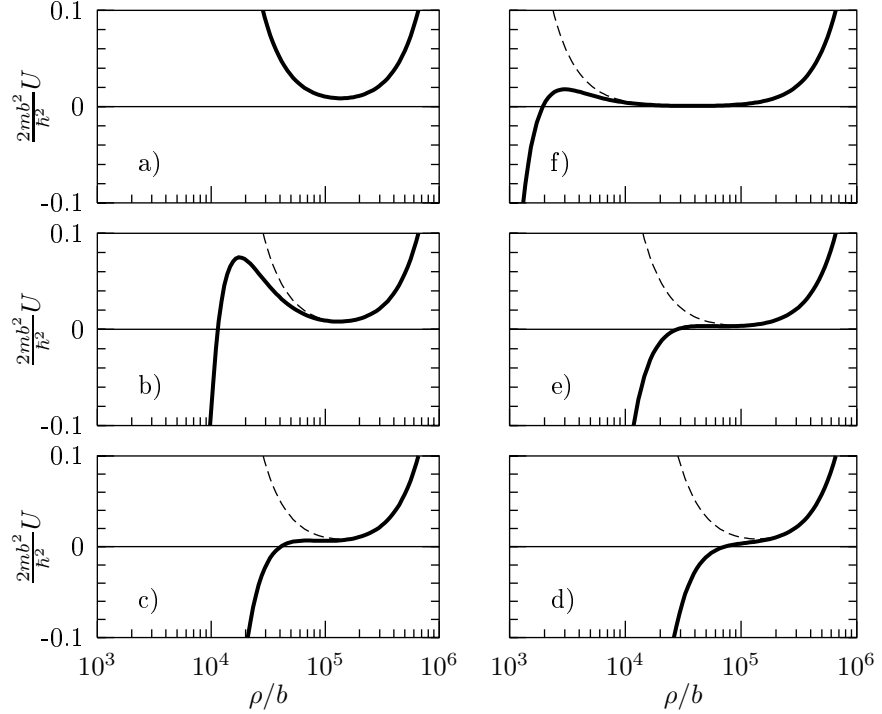


Figure 6.1: Radial potentials with  $b_t/b = 1442$  and a)  $N = 6000$ ,  $a_s = 0$ ; b)  $N = 6000$ ,  $a_s/b = -0.05$ ; c)  $N = 6000$ ,  $a_s/b = -0.18$ ; d)  $N = 6000$ ,  $a_s/b = -0.35$ ; e)  $N = 3000$ ,  $a_s/b = -0.35$ ; f)  $N = 500$ ,  $a_s/b = -0.35$ . The dashed lines are obtained with  $a_s = 0$ .

## 6.2 Decay

The Bose-Einstein condensate (BEC) is intrinsically unstable and decays spontaneously, e.g. into lower-lying dimer states. Recombination of two particles into a lower-lying state is possible by emission of a photon, but the rate is enhanced when a third particle is involved instead of the photon. This three-body recombination process inevitable occurs in a system of bosons when at least one two-body bound state exists. This has been suggested to be important for a BEC [Adh01, US03]. The related change of the surrounding medium could lead to an instability which involves many particles, and thus result in much faster decays which could be described as a collapse [Adh02b].

Figure 6.2 illustrates the different behaviours by using the angular eigenvalues parametrized through equations (3.37) and (3.38). In figure 6.2a the scattering length is relatively small and a large barrier separates the outer minimum from the inner region. When the scattering length increases, the barrier decreases first into a relatively flat region as in figure 6.2b and then disappears

completely as in figure 6.2c when the trap length is exceeded.

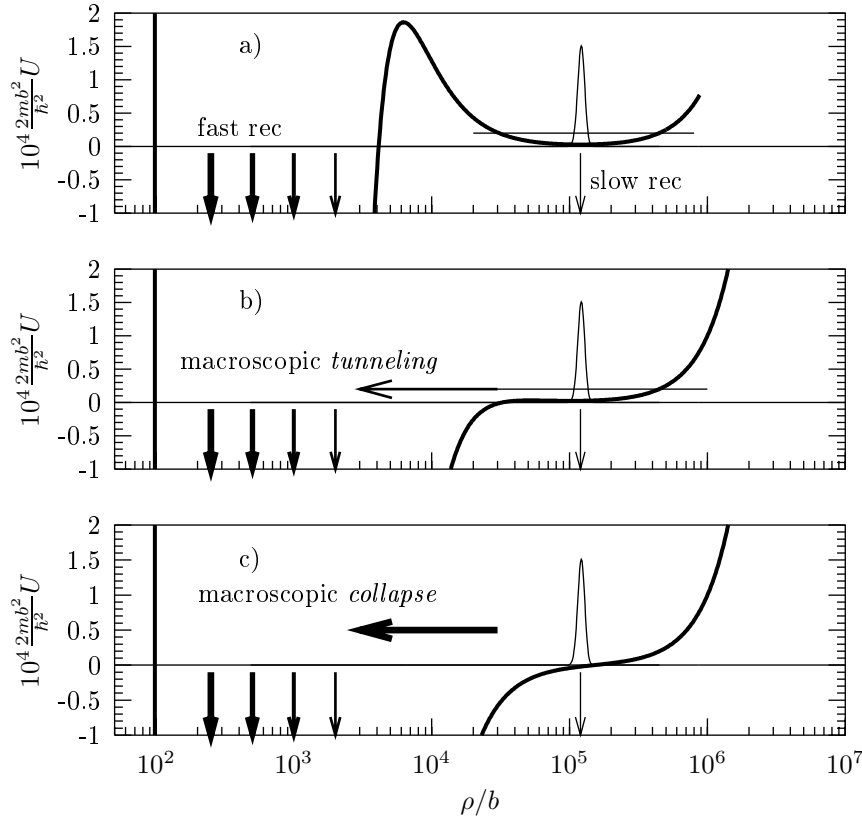


Figure 6.2: The radial potential from the parametrization for  $N = 100$ ,  $b_t/b = 10^4$ , and a)  $a_s/b = -6$ , b)  $a_s/b = -50$ , and c)  $a_s/b \rightarrow -\infty$ . The shown wave function is the lowest radial solution in the non-interacting case. The horizontal lines in parts a) and b) indicate an energy level (not to scale).

The discussion of macroscopic dynamics in this picture involves various isolated ideas which lead to simple decay rates. These are then incorporated in a description of the experimental collapse situation.

### 6.2.1 Three-body recombination

The condensate state is unstable due to the couplings into degrees of freedom different than the coherent many-body mode. The formation of bound-state dimers is possible by a three-body process where the third particle ensures conservation of energy and momentum. The number of these three-body recombination (rec) events per unit volume and time can be estimated by the upper

limit given in [NM99, BBH00]:

$$\nu_{\text{rec}} \simeq 68 \frac{\hbar |a_s|^4 n^3}{m}, \quad (6.6)$$

where  $n$  is the density. This expression can be converted into an estimate of the recombination rate for a given root-mean-square (rms) hyperradius  $\bar{\rho} \equiv \sqrt{\langle \rho^2 \rangle}$  by using the relation between density and rms hyperradius from equation (5.9), i.e.  $n \simeq 3N^{3/2}/(8\sqrt{2}\pi\bar{\rho}^3)$ . With the volume  $\mathcal{V} = N/n$  the total recombination rate then is

$$\frac{\Gamma_{\text{rec}}}{\hbar} = \nu_{\text{rec}} \mathcal{V} \simeq 0.5 \frac{N^4 \hbar |a_s|^4}{m \bar{\rho}^6}. \quad (6.7)$$

The recombination rate increases rapidly with decreasing  $\bar{\rho}$ , as indicated by the vertical arrows in figure 6.2 where we interchange  $\rho$  and  $\bar{\rho}$  to illustrate this effect.

If  $N(t)$  is the number of particles present in the coherent many-body state as time  $t$  goes by, the recombination time scale  $\tau_{\text{rec}}$  can be defined by  $N(t) = N(0) \exp(-t/\tau_{\text{rec}})$ . This leads to the rate  $\Gamma_{\text{rec}}/\hbar = -dN/dt = N/\tau_{\text{rec}}$ , so

$$\tau_{\text{rec}} = \frac{N\hbar}{\Gamma_{\text{rec}}} \simeq \frac{2m\bar{\rho}^6}{N^3\hbar|a_s|^4} \simeq \frac{m\bar{r}^6}{4\hbar|a_s|^4}. \quad (6.8)$$

Since the condensate forms in the external trap, the system must be stable versus recombination events on a time scale  $\tau_{\text{trap}}$  which is given by the oscillator time scale  $2\pi/\omega$ , that is  $\tau_{\text{rec}} > \tau_{\text{trap}} \equiv 2\pi/\omega$ . With the relation  $1/\omega = mb_t^2/\hbar$  the criterion for a stable condensate becomes

$$\bar{r} > \sqrt[6]{8\pi} |a_s|^{2/3} b_t^{1/3} = d_c. \quad (6.9)$$

Here an expression for the minimal separation  $d_c$ , as introduced in section 4.5.1, is obtained. In units of  $b_t$  we have

$$\frac{d_c}{b_t} = \sqrt[6]{8\pi} \left( \frac{|a_s|}{b_t} \right)^{2/3}, \quad (6.10)$$

where the determining combination is  $|a_s|/b_t$ .

Thus, for  $|a_s|/b_t \ll 1$  also  $d_c/b_t \ll 1$ . The rms distance  $\bar{r}$  for a state located in the second minimum is of the order  $b_t$  and therefore  $\bar{r} > d_c$ , i.e. for this state  $\bar{r}$  is larger than the critical stability length  $d_c$ . This state then qualifies as a condensate. For  $^{87}\text{Rb}$  atoms with  $a_s \simeq 100$  a.u. and trapped in a field with  $\nu_{\text{trap}} \simeq 100$  Hz, we obtain  $\tau_{\text{rec}} \sim 7$  days.

### 6.2.2 Macroscopic tunneling and recombination

The second decay process is macroscopic tunneling through the small barrier as indicated in figure 6.2b. The model provides stationary eigenstates which by definition are time independent. Thus, strictly the states do not tunnel through

the barrier. However, an exponentially small tail extends to small hyperradii or large density. All particles thus approaching each other would recombine into molecular clusters because the density is very large in the inner region. The rate of this two-step decay with tunneling through the barrier and subsequent recombination is determined by the bottleneck. The rate of recombination due to macroscopic tunneling can be estimated by [BEG98]

$$\frac{\Gamma_{\text{tunnel}}}{\hbar} \simeq \frac{N\nu_{\text{tunnel}}}{1 + e^{2\sigma}}, \quad \nu_{\text{tunnel}} = \frac{1}{2\pi} \sqrt{\frac{1}{m} \frac{d^2 U(\rho)}{d\rho^2}} \Big|_{\rho_{\text{min}}}, \quad (6.11)$$

$$\sigma = \int_{\rho_{\text{in}}}^{\rho_{\text{out}}} d\rho \sqrt{\frac{2m}{\hbar^2} [U(\rho) - E]}, \quad (6.12)$$

where the multiplication by the factor  $N$  gives the total number of recombined particles. Here  $\rho_{\text{min}}$  is the position of the second minimum of  $U$ , and  $\rho_{\text{in}}$  and  $\rho_{\text{out}}$  are the points where the barrier height equals the energy  $E$ .

When  $N|a_s|/b_t \ll 1$ , the barrier is large and the very small rate can be estimated through equations (6.11) and (6.12). The action integral is then large and given by

$$\sigma \simeq \frac{3}{2} N \ln \left( \frac{b_t}{N|a_s|} \right). \quad (6.13)$$

Classical turning points of the potential are present when  $N|a_s|/b_t \leq 0.53$ . Close to this threshold, i.e. when the barrier is small, the exponent is

$$\sigma \simeq 1.7N \left( 1 - \frac{N|a_s|}{0.53b_t} \right), \quad (6.14)$$

which is valid when  $N|a_s|/(0.53b_t)$  is close to unity.

At the threshold for macroscopic stability then  $N|a_s|/b_t \sim 0.5$ , which due to the factor of  $N$  implies that  $|a_s|/b_t \ll 1$ . Close to this threshold we have  $\bar{r} \sim b_t \gg d_c$ , which means that the average distance between the bosons is so large that the three-body recombination is slow compared to the typical time scale for oscillation in the harmonic-oscillator trap. Therefore, the three-body recombination does not limit the macroscopic stability of a condensate. In the limit  $\sigma \ll 1$  we get explicitly

$$\frac{\Gamma_{\text{rec}}}{\Gamma_{\text{tunnel}}} \simeq \frac{1}{7.0N^4} \ll 1, \quad (6.15)$$

implying that the macroscopic tunneling process dominates. With  $\sigma \ll 1$  then  $\Gamma_{\text{tunnel}}/\hbar \simeq 0.5N\nu_{\text{tunnel}}$  and  $\nu_{\text{tunnel}} \simeq \nu_{\text{trap}}$ , which yields a tunneling time of about  $1/\nu_{\text{trap}}$ . For the case with  $\nu_{\text{trap}} \simeq 100$  Hz the macroscopic tunneling time scale is 10 ms. This is much smaller than the three-body recombination time scale which close to stability is given by the reciprocal of equation (6.15), that is

$$\frac{\tau_{\text{rec}}}{\tau_{\text{tunnel}}} = \frac{\Gamma_{\text{tunnel}}}{\Gamma_{\text{rec}}} \simeq 7.0N^4 \gg 1. \quad (6.16)$$

The three-body recombination rate is in figure 6.3 shown as a function of the hyperradius (solid curve) and compared with the macroscopic tunneling rate (dashed curve) where all particles in the condensate simultaneously disappear during contraction. At small hyperradii the three-body recombination rate is much larger than the macroscopic tunneling rate, whereas the opposite holds for large hyperradii. For the chosen set of parameters the two time scales are roughly equal around the second minimum where the condensate is located. However, the tunneling rate depends strongly on the barrier through the combination  $N|a_s|/b_t$ . Variation of either of the three quantities then moves the

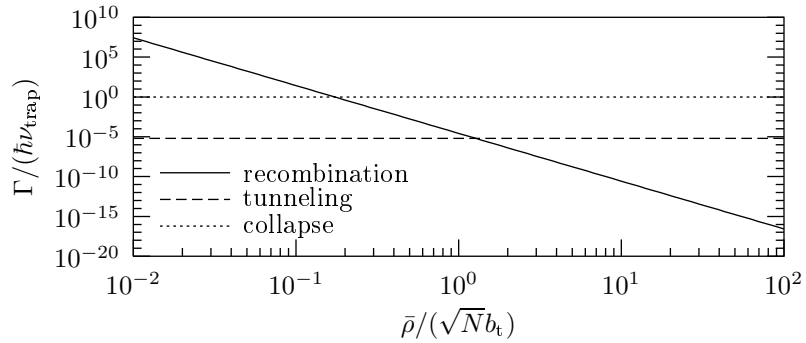


Figure 6.3: The three-body recombination rate from equation (6.7) in units of the oscillator frequency  $\nu_{\text{trap}} = \omega/(2\pi)$ , which typically is 10-100 Hz, as a function of hyperradius for  $N = 100$ ,  $a_s/b = -50$ , and  $b_t/b = 10^4$ . Shown as the horizontal, dashed line is the macroscopic tunneling rate from equation (6.11). Shown as the horizontal, dotted line is the macroscopic collapse rate from equation (6.17) when the scattering length is much larger than the trap length.

tunneling rate up or down in figure 6.3. For a larger barrier the condensate would only decay slowly by recombination. For a smaller barrier macroscopic tunneling would dominate and all the bosons in the condensate would participate in a “collective recombination” in a short time interval.

When a few particles recombine into dimers and leave the condensate, the system is no longer in an eigenstate of the corresponding new Hamiltonian. An adiabatic adjustment of Hamiltonian and wave function could then take place. Since fewer particles and unchanged  $a_s$  and  $b_t$  means a larger barrier, the macroscopic stability of the new system is therefore increased.

### 6.2.3 Macroscopic collapse

Scenarios where the boson system develops with time as one unified body are open for investigations in experiments where the effective interaction almost instantaneously is changed by tuning close to a resonance [IAS<sup>+</sup>98, DCC<sup>+</sup>01, RCC<sup>+</sup>01]. An initially small magnitude of the scattering length, corresponding



to a stable condensate state in the second minimum of the hyperradial potential, can be changed to a value where the barrier is removed.

In one experiment [DCC<sup>+</sup>01] a condensate is first created with effectively zero interaction, i.e. zero scattering length as in figure 6.1a. The radial wave function is then located at relatively large distances in the minimum created by the compromise between centrifugal barrier and external field. The attractive pocket at small distances is not present and the condensate forms as the ground state in this potential. Figure 6.4 shows both the radial potential (thick, dashed line) and the wave function (thin, dashed line) for schematic model parameters.

In the experiment the effective interaction was then suddenly changed by tuning a Feshbach resonance [CCR<sup>+</sup>00] to obtain a large and negative scattering length [DCC<sup>+</sup>01]. The measurement showed a burst and a remnant of coherent atoms. This was interpreted and explained as formation of dimers via the two-body resonance, a burst of dissociating dimers, and a remnant of an oscillating mixture of coherent atoms and coherent molecules [KH02, MSJ02, KGB03].

In the present formulation the effective potential is suddenly altered by a change of the underlying two-body interaction. The corresponding new radial potential, shown as the thick solid line in figure 6.4, has a pronounced attractive region which is able to support a number of self-bound many-body states.

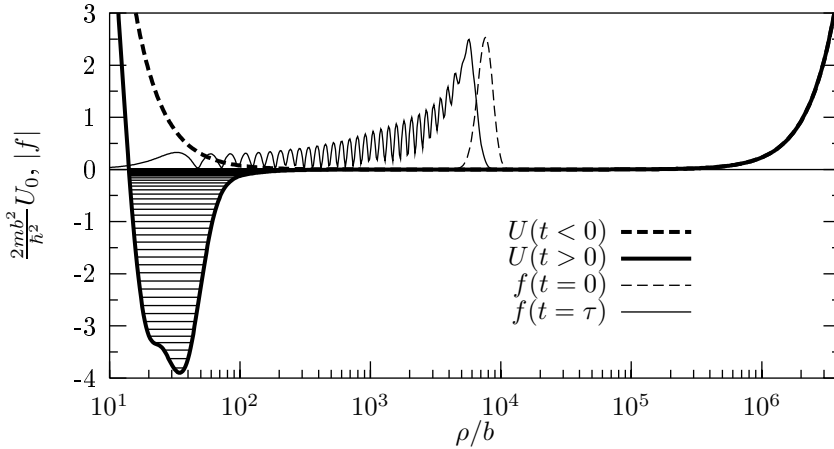


Figure 6.4: Wave functions  $f$  and effective hyperradial potentials  $U$  in dimensionless units as a function of hyperradius for  $N = 20$  and  $b_i/b = 1442$ . The scattering length is zero up to the time  $t = 0$  and then suddenly changes to be large and negative at later times  $t > 0$ . Potentials and the corresponding wave functions are sketched for  $t = 0$  and at a time  $\tau \sim 0.1$  ms after half a period. The horizontal lines show the stationary negative-energy states for  $t > 0$ .

Since the initial wave function is not a stationary state in the new potential, a motion is started towards smaller hyperradii where it would be reflected off the “wall” of the centrifugal term. This macroscopic contraction or collapse is

indicated by the large arrow in figure 6.2c. If no degrees of freedom beyond the model assumptions are involved, the system would then oscillate between the centrifugal repulsion and the wall of the external field. This corresponds to an oscillation in density. However, during the macroscopic contraction the rate for dimer production via the three-body process increases and dimers are produced and subsequently ejected from the trap. Since the rate explodes as the contraction culminates, all particles should recombine instantly. Thus, the relevant time scale, i.e. the bottleneck, is the time scale for macroscopic contraction.

If the only excitations are the degrees of freedom contained in the lowest new hyperspherical potential with  $s$ -waves, we can get quantitative information by expanding on the new eigenfunctions. The dominating states in this expansion are on the transition point between the lowest-lying positive-energy states with energies comparable to the initial condensate and the highest-lying Efimov-like many-body states, now present because of the large scattering length, see section 4.4. These states have a spatial extension as large as that of the initial state. The time scale for evolution of the initial state in the new potential is then determined by the energy differences between such levels. The states of positive energy and large spatial extension confined by the trap are roughly separated by the oscillator quantum of energy  $\hbar\omega$ . The corresponding rate for populating smaller distances with the consequence of immediate recombination is then crudely estimated to be

$$\frac{\Gamma_{\text{collapse}}}{\hbar} \sim \frac{1}{\tau_{\text{trap}}} = \frac{\omega}{2\pi}. \quad (6.17)$$

The resulting non-stationary wave function provides a specific oscillation time. After half a period the extension of the system has reached its minimum. The wave function at this time  $\tau \sim \tau_{\text{trap}}/2 \sim 0.1$  ms is also shown in figure 6.4. Experimentally [DCC+01] the macroscopic-collapse time is verified to be of the order  $\sim 1/\omega$ . These time scales agree on the order-of-magnitude level.

The rate of macroscopic collapse is also shown in figure 6.3. This is larger than the tunneling rate. The motion in the potential is slow compared to the recombination time for distances in the minimum at small  $\rho$ , whereas the opposite holds for distances in the minimum at large  $\rho$ . The time evolution after the sudden removal of the barrier could then be as follows. A macroscopic collapse towards smaller hyperradii sets in. This is followed by emission of dimers which lowers the number of remaining particles and results in a reappearing barrier. The part of the wave function trapped at large distances in the second minimum can then stabilize into a condensate with fewer particles. The time scale for these processes should then be between the macroscopic-collapse time and the recombination time at the second minimum.

This makes the assumption that no other degrees of freedom are exploited, for example the angular dependence of the wave function or molecular bound states described by other adiabatic potentials. Direct population of two-body bound states requires inclusion of the adiabatic potential asymptotically describing these states. This is possible within the model, but constitutes a major

numerical investigation of coherent atoms and molecules, oscillations between them, and three-body recombinations within the same framework. Other time scales due to these neglected degrees of freedom could possibly turn up in such a complete study of the dynamics of a many-boson system.

#### 6.2.4 Observation of Efimov-like states

The recombination probability increases with decreasing hyperradius due to the higher density, i.e. several particles are close in space and therefore much more likely recombine into molecular states. The time scale  $\tau_{\text{rec}}$  for three-body recombination is given by  $N(t) = N(0) \exp(-t/\tau_{\text{rec}})$  where  $N$  is the number of atoms in the condensate. This is as a function of the root-mean-square hyperradius  $\bar{\rho}$  estimated by equation (6.8). This recombination time for the highest-lying Efimov-like states with  $\bar{\rho} \sim N^{7/6}|a_s|$ , see equation (3.41), can then be compared to the time scale for motion in the condensate which is given by  $\tau_{\text{trap}} = 2\pi/\omega$ . With  $\bar{\rho} \simeq N^{7/6}|a_s|$  we obtain

$$\frac{\tau_{\text{rec}}}{\tau_{\text{trap}}} \simeq \frac{N^2}{\pi} \left( \frac{N|a_s|}{b_t} \right)^2. \quad (6.18)$$

Thus, close to the limit of stability, i.e.  $N|a_s|/b_t \sim 0.5$ , we have  $\tau_{\text{rec}} \gg \tau_{\text{trap}}$  for  $N \gg 1$ , so the recombination process is rather slow for these highest-lying Efimov-like states. Even though the lifetime is shorter than for the initially created condensate, it might be long enough for an observation of these states.

If the Efimov-like states are populated in experiments where the potential suddenly is changed from figure 6.1a to figure 6.1d, they could possibly be indirectly observed. A signature of this many-body Efimov effect would be observation of the diatomic molecules formed in the recombination process and with the estimated time scale from equation (6.18). The rate should then be inversely proportional to the square of the scattering length reached after changing the potential. The dimers can probably not be distinguished from this and other processes, but the measured rate can possibly be separated into different characteristic components. Since their lifetime due to recombination processes can be very large compared to the time scale defined by the external field, these negative-energy self-bound many-body states should essentially maintain their spatial extension after the external field is switched off. This is in contrast to positive-energy states where only the trap prevents expansion. Thus, a relatively slow time evolution of the density distribution without external field should be characteristic for these many-body Efimov-like states. A later measurement of a system denser than expected for a positive-energy system could then be a signature of the self-bound many-body state.

### 6.3 Summary

The stability criterion for the many-boson system is verified within the hyperspherical framework. The avoided collapse at large densities, compared to col-

lapse of the Gross-Pitaevskii description, allows a more detailed study of what happens during the macroscopic-collapse process. Time scales are estimated on the basis of three-body recombination at different densities. Macroscopic-tunneling times and oscillation times in a “free-fall” collapse allow the existence of the self-bound states without recombination to other cluster-structures. However, since the critical region occurs when a zero-range interaction in a non-correlated model describes the system rather well, the inclusion of two-body correlations does not alter the criterion for macroscopic stability. This is seen by considering a trapped gas with  $n \sim 1/b_t^3$ . Close to threshold  $N|a_s|/b_t \sim 1$  implies  $n|a_s|^3 \sim 1/N^3$ . This means that  $n|a_s|^3 < 1/N^2$ , which is the asymptotic region where  $\lambda \simeq \lambda_\delta$  and the GPE method is in agreement with the hyperspherical correlated method, see section 5.2. In this sense the correlations do not modify the expectations obtained from a mean-field consideration. However, the possibility for a study of couplings between the coherent many-body system and the bound two-body channels is clearly beyond the mean field. This is a goal for future investigations of decays.

## Chapter VII

### Deformed boson system

The atom traps in experiments are of cylindrical geometry, as described in section 4.1. For  $N$  attractive atoms the stability criterion, as described in section 6.1, is experimentally established to be  $N|a_s|/b_t < 0.55$  [CKT<sup>+</sup>03], where  $a_s$  is the scattering length and  $b_t \equiv \sqrt{\hbar/(m\omega)}$  is the relevant length scale of the harmonic trap of geometric average frequency  $\omega \equiv \sqrt[3]{\omega_x\omega_y\omega_z}$ . A reduction from three dimensions to effectively one or two dimensions was observed experimentally [GVL<sup>+</sup>01] in the limit when the interaction energy is small compared to the level spacing in the tightly-confining dimension. Experiments with continuous variation of the trap geometry from three to either one or two effective dimensions [GVL<sup>+</sup>01], with a two-dimensional structure [GBM<sup>+</sup>01, RENG03], and an effective one-dimensional geometry [TOH<sup>+</sup>03] request a corresponding theoretical description.

Theoretical interpretations and the underlying analyses are frequently based on model assumptions of spherical symmetry [BEG98, Adh02b], as discussed in section 4.1. Confinement to lower dimensions can also be studied directly without the three-dimensional starting point. This has been done with a variational calculation in Gross-Pitaevskii equation (GPE) [BP96] and more recently in the GPE with variational dimensionality [MW02]. Also effects on stability of deformed external fields have been investigated by use of the GPE formulation [BP96, GFT01, Adh02a]. Extreme deformations could result in effective one-dimensional or two-dimensional systems which can be described by effective interactions of corresponding discrete lower dimensions [Ols98, PHS00, PS01, LMDB02].

In the present chapter, which corrects and extends the discussions in reference [SFJ03b], we rewrite the hyperspherical formulation from chapter 2 to account for a general deformation of the external field. Since two-body correlations are not yet included in the wave function, this hyperspherical approach reminds of a mean-field treatment. We investigate the stability criterion in section 7.2. Section 7.3 contains an approach to an effective dimension which depends on the deformation of the external field. Since the interactions are presently not included in this effective dimension, we therefore in section 7.4

introduce them on top of the derived  $d$ -dimensional Hamiltonian. Although the choice of interactions is not unique, we can with some guess obtain an alternative stability criterion and subsequently interpret the results in terms of a deformation-dependent coupling strength, which is finally compared with known results.

## 7.1 Hyperspherical description of deformation

As described in section 4.1 a combination of magnetic fields results in an effective trapping potential, which can be described as the deformed harmonic oscillator potential  $V_{\text{trap}}$  acting on all the identical particles of mass  $m$

$$V_{\text{trap}}(\mathbf{r}_i) = \frac{1}{2}m(\omega_x^2 x_i^2 + \omega_y^2 y_i^2 + \omega_z^2 z_i^2). \quad (7.1)$$

The hyperradius  $\rho$  is the principal coordinate, which is separated into the components  $\rho_x$ ,  $\rho_y$ , and  $\rho_z$  along the different axes, i.e.

$$\rho^2 = \frac{1}{N} \sum_{i < j}^N r_{ij}^2 = \rho_x^2 + \rho_y^2 + \rho_z^2 = \rho_{\perp}^2 + \rho_z^2, \quad \rho_{\perp}^2 \equiv \rho_x^2 + \rho_y^2, \quad (7.2)$$

where  $\mathbf{r}_{ij} = \mathbf{r}_j - \mathbf{r}_i$ . In the centre-of-mass system the remaining coordinates are given as angles collectively denoted by  $\Omega$ , see analogies in chapter 2 and more details in appendix A.3.

An application here of the method presented in chapter 2 is to assume a relative wave function as a sum of two-particle components. In the case of a spherical trapping field each two-body component only needs dependence on  $\rho$  and the two-body distance  $r_{ij} = \sqrt{2}\rho \sin \alpha_{ij}$  through an angle  $\alpha_{ij}$ . For a deformed external field it also needs dependence on the angle  $\vartheta_{ij}$  between the interatomic vector  $\mathbf{r}_{ij}$  and the axis of the external field. The two-body component should in the cylindrical case then be on the form  $\phi(\rho, \alpha_{ij}, \vartheta_{ij})$ , which would lead to an angular equation in the two variables  $\alpha_{12}$  and  $\vartheta_{12}$  with more complicated integrals than those appearing in equations (2.75) and (2.84). We will not investigate this, but here restrict ourselves to no dependence on hyperangles. This is expected to dominate for dilute systems where the large distances average out directional dependence.

Thus, we neglect correlations in analogy to a mean-field treatment, so in the dilute limit the hyperangular average of the relative Hamiltonian is

$$\langle \hat{H} \rangle_{\Omega} \rightarrow \hat{H} = \hat{H}_x + \hat{H}_y + \hat{H}_z + \hat{V}, \quad \hat{V} = \sum_{i < j}^N \langle V_{ij} \rangle_{\Omega}, \quad (7.3)$$

$$\frac{2m\hat{H}_q}{\hbar^2} = -\frac{1}{\rho_q^{d(N-1)-1}} \frac{\partial}{\partial \rho_q} \rho_q^{d(N-1)-1} \frac{\partial}{\partial \rho_q} + \frac{\rho_q^2}{b_q^A}, \quad (7.4)$$

where  $d = 1$  and  $b_q^2 \equiv \hbar/(m\omega_q)$  for  $q = x, y, z$ . The interactions  $V_{ij}$  are averaged over all angles  $\Omega$ , which for the zero-range interaction  $4\pi\hbar^2 a_s \delta(\mathbf{r}_{ij})/m$  from equation (3.8) for  $N \gg 1$  yields

$$\hat{V} = \frac{4\pi\hbar^2 a_s}{m} \sum_{i < j}^N \langle \delta(\mathbf{r}_{ij}) \rangle_{\Omega} = \frac{\hbar^2}{2m} \frac{1}{2\sqrt{\pi}} N^{7/2} \frac{a_s}{\rho_x \rho_y \rho_z}. \quad (7.5)$$

If we replace as  $\rho_x = \rho_y = \rho_z = \rho/\sqrt{3}$ , this is identical to  $\hbar^2 \lambda_{\delta}/(2m\rho^2)$  with  $\lambda_{\delta}$  from equation (3.31).

We define the following dimensionless coordinates and parameters:

$$x \equiv \frac{\rho_x}{b_x} \sqrt{\frac{2}{N}}, \quad y \equiv \frac{\rho_y}{b_y} \sqrt{\frac{2}{N}}, \quad z \equiv \frac{\rho_z}{b_z} \sqrt{\frac{2}{N}}, \quad (7.6)$$

$$\beta \equiv \frac{b_x^2 + b_y^2}{2b_z^2}, \quad \gamma \equiv \frac{b_x^2 - b_y^2}{2b_z^2}, \quad s \equiv \frac{Na_s}{b_t}, \quad b_t^3 \equiv b_x b_y b_z. \quad (7.7)$$

The deformation along the different axes is then described by  $\beta$  and  $\gamma$ , and  $s$  is the effective interaction strength. The Schrödinger equation  $\hat{H}F(\rho_x, \rho_y, \rho_z) = EF(\rho_x, \rho_y, \rho_z)$  is rewritten with the transformation

$$f(x, y, z) \propto (xyz)^{(N-2)/2} F(\rho_x, \rho_y, \rho_z) \quad (7.8)$$

in order to avoid first derivatives. We then obtain

$$\left[ -\frac{1}{\beta + \gamma} \frac{\partial^2}{\partial x^2} - \frac{1}{\beta - \gamma} \frac{\partial^2}{\partial y^2} - \frac{\partial^2}{\partial z^2} + \frac{N^2 u(x, y, z) - \varepsilon}{2^3 \sqrt{\beta^2 - \gamma^2}} \right] f(x, y, z) = 0, \quad (7.9)$$

$$u(x, y, z) = \frac{1}{2} \sqrt[3]{\beta^2 - \gamma^2} \left[ \frac{1}{\beta + \gamma} \left( x^2 + \frac{1}{x^2} \right) + \frac{1}{\beta - \gamma} \left( y^2 + \frac{1}{y^2} \right) + z^2 + \frac{1}{z^2} \right] + \sqrt{\frac{2}{\pi}} \frac{s}{xyz}, \quad (7.10)$$

where  $\varepsilon \equiv 2NE/(\hbar\omega)$ . Without interaction, i.e.  $a_s = 0$ , the ground-state solution is

$$f(x, y, z) = (xyz)^{(N-2)/2} \exp[-N(x^2 + y^2 + z^2)/4], \quad (7.11)$$

which for  $N \gg 1$  is peaked at  $(x, y, z) = (1, 1, 1)$ .

Here we do not solve this equation, but instead investigate the character of the effective potential  $u$ . For axial symmetry around the  $z$  axis the  $x$  and  $y$  directions cannot be distinguished, that is when  $\gamma = 0$  and  $\beta = b_{\perp}^2/b_z^2$  with  $b_{\perp}^2 \equiv b_x b_y$ . This symmetry amounts to replacing  $\rho_x^2$  and  $\rho_y^2$  by  $\rho_{\perp}^2/2$  in the equations. A convenient definition for this case is  $2\varrho^2 \equiv x^2 + y^2$ . Equipotential

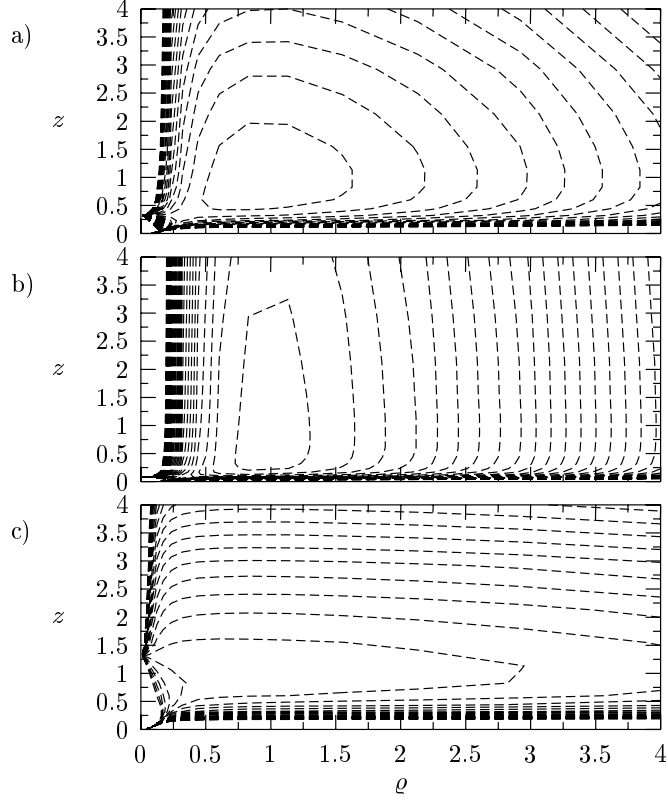


Figure 7.1: Contour plots of  $u(x, y, z)$ , equation (7.10), with  $x = y = \varrho$  as a function of  $(\varrho, z)$  for  $s = -0.4\beta^{1/6}$  corresponding to  $Na_s/b_{\perp} = -0.4$  for three deformations. The values for the contours change by 2, 2, and 5, respectively for a)  $\beta = 1$  (spherical), b)  $\beta = 1/16$  (cigar-shaped or prolate), and c)  $\beta = 16$  (pancake-shape or oblate).

contours of  $u$  in the  $(\varrho, z)$  plane for  $\varrho = x = y$  are shown in figure 7.1 for attractive interactions. For  $a_s < 0$  ( $s < 0$ ) there is always a divergence towards  $-\infty$  when  $(\varrho, z) \rightarrow (0, 0)$ , see equation (7.10). However, a stationary minimum is seen in both figures 7.1a (spherical symmetry) and 7.1b (prolate) close to  $(\varrho, z) = (1, 1)$ , whereas this minimum has disappeared for the oblate system in figure 7.1c. For very weak attraction a stationary minimum is present for all deformations.

Figure 7.2 shows cuts of the potential  $u(\varrho, z)$  along paths close to the bottom of the valleys (see inset). The spherical minimum (full line) is shielded by a relatively small barrier from the divergence for  $\varrho \rightarrow 0$ . The minimum for the prolate deformation (dashed curve) is extremely stable although the divergence for  $\varrho \rightarrow 0$  still exists. For the oblate deformation (dot-dashed line) the local minimum has vanished for this attraction strength.



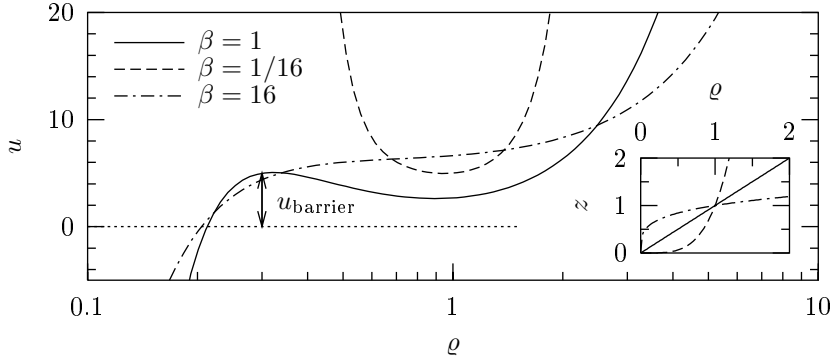


Figure 7.2: The potential  $u(x, y, z)$  for  $s = -0.4\beta^{1/6}$  as a function of  $\varrho = x = y$  along cuts of the  $(\varrho, z)$  plane where  $z = \varrho^{1/\sqrt{\beta}}$ . The height  $u_{\text{barrier}}$  of the local maximum at top of the barrier is indicated for the spherical case  $\beta = 1$ . The inset shows corresponding trajectories in the  $(\varrho, z)$  plane, compare with figure 7.1, for the three deformations.

## 7.2 Stability criterion for bosons in a deformed trap

The barrier height depends on the deformation of the external field, see figures 7.1 and 7.2. Extrema  $(x_0, y_0, z_0)$  of  $u$  in equation (7.10) obey the three equations obtained from

$$\frac{b_t^2}{b_x^2}(x_0^4 - 1) = \sqrt{\frac{2}{\pi}} \frac{s x_0}{y_0 z_0} \quad (7.12)$$

and symmetric permutations of  $x$ ,  $y$ , and  $z$ . This can be used to determine the critical strength  $s$  when a local minimum disappears. The results for axial symmetry are shown as the thin solid line in figure 7.3. In these units the critical strength  $s$  is largest for a geometry very close to spherical. Since  $s = N a_s / b_t$  and  $b_t^3 = b_x b_y b_z$ , this means that at fixed  $b_t^3$ , or fixed volume, the scattering length can assume the largest negative value for the spherical trap. Gammal *et al.* [GFT01] performed a time-dependent study with the Gross-Pitaevskii equation (GPE) which resulted in the critical strengths here shown as the dotted line. This is in large regions lower than the present result, which might be due to our neglect of quantum effects and time dependence. The energy gain due to correlations is not included in the simple expectation value with the assumed angle-independent wave function. The recent value for the experimental stability region [CKT<sup>+</sup>03] is shown as the plus and agrees with the mean-field model. We perform two alternative derivations withing the hyperspherical model in order to see if the assumptions need modifications.

These results can be compared to an analytical “spherical” approximation where the radial motion is described by only  $\rho$  while the deformed external field

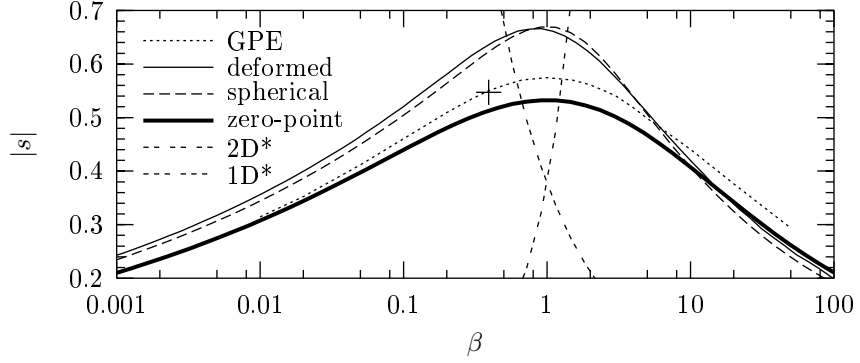


Figure 7.3: The critical strength  $|s| = N|a_s|/b_t$  as a function of the deformation  $\beta = b_{\perp}^2/b_z^2$  from the potential in equation (7.10) (thin solid line), from equation (7.16) (dashed line), and from a mean-field Gross-Pitaevskii computation by Gammal *et al.* [GFT01] (dotted line). The thick solid line is equation (7.18) obtained by considering the zero-point energy. The plus is the experimentally measured value [CKT<sup>+</sup>03]. Regions below curves are considered stable in the separate treatments. The double- and triple-dashed lines indicate the effective cross-overs to two (2D\*) and one (1D\*) dimensions [GVL<sup>+</sup>01].

remains the same. The effective radial potential  $U$  is then obtained by adding centrifugal barrier and the contributions from zero-range interaction and the external field, see equation (2.29). The angular average replaces each of the three components  $\rho_q^2$  and  $R_q^2$  by  $\rho^2/3$  and  $R^2/3$ , where  $\mathbf{R}$  is the centre-of-mass coordinates, i.e.

$$\sum_{i=1}^N \langle V_{\text{trap}}(\mathbf{r}_i) \rangle_{\Omega} = \frac{1}{2} m \frac{\omega_x^2 + \omega_y^2 + \omega_z^2}{3} (\rho^2 + NR^2), \quad (7.13)$$

$$\frac{2m\hat{V}}{\hbar^2} = 8\pi a_s \sum_{i<j}^N \langle \delta(\mathbf{r}_{ij}) \rangle_{\Omega} = \frac{3}{2} \sqrt{\frac{3}{\pi}} N^{7/2} \frac{a_s}{\rho^3}, \quad (7.14)$$

$$\frac{2mU(\rho)}{\hbar^2} = \frac{3}{2} \sqrt{\frac{3}{\pi}} N^{7/2} \frac{a_s}{\rho^3} + \frac{9N^2}{4\rho^2} + \frac{\rho^2}{l_2^4}, \quad (7.15)$$

where  $3l_2^{-4} \equiv b_x^{-4} + b_y^{-4} + b_z^{-4}$ . By comparison with equations (6.2), (6.3), and (6.4) the stability condition becomes

$$\frac{N|a_s|}{b_t} < k(\beta, \gamma), \quad k(1, 0) = \frac{2\sqrt{2\pi}}{5^{5/4}} \simeq 0.67, \quad (7.16)$$

$$k(\beta, \gamma) = k(1, 0) \sqrt[4]{\frac{3(\beta^2 - \gamma^2)^{4/3}}{2\beta^2 + 2\gamma^2 + (\beta^2 - \gamma^2)^2}}. \quad (7.17)$$

The spherical limit corresponds to  $\gamma = 0$  and  $\beta = 1$  where the barrier is present when  $|s| = N|a_s|/b_t < 0.67$ . The result for a cylinder (only  $\gamma = 0$ ) is shown as the dashed line in figure 7.3 and is noticeably different from, but numerically almost coincides with, the “deformed” treatment, thin solid line. An extreme oblate deformation corresponds to the two-dimensional limit where  $b_z \ll b_\perp$  and  $\beta \rightarrow \infty$ . Here equation (7.17) yields the critical strength  $k \simeq 0.4\sqrt[4]{0.6}\sqrt{\pi/2}\beta^{-1/3}$ . As seen from the contour plot in figure 7.1c, the motion is now almost confined at  $z = 1$ . From  $x = y = \varrho$  we see that  $u(\varrho, \varrho, 1)$  only has a local minimum when  $|s| < \sqrt{\pi/2}\beta^{-1/3}$ , which is larger than the value where the  $z$  motion is not fixed. This is reasonable since more degrees of freedom in the model lowers the energy. Baym and Pethick [BP96] obtained with a variational study of the GPE the criterion  $|s| < \sqrt{\pi/2}\beta^{-1/3}$  provided that the variational width in the axial direction does not change due to the interactions. This is identical to the criterion from studying the potential  $u(\varrho, \varrho, 1)$ , i.e. consistent with the fixed value  $z = 1$ . This again emphasizes the equivalence between the present hyperspherical non-correlated model and the mean-field GPE.

Analogously, in the extreme prolate limit (one-dimensional) where  $\beta \rightarrow 0$ , equation (7.17) yields the critical strength  $k \simeq 0.25\sqrt[4]{1.25}\sqrt{\pi}\beta^{1/6}$ . However, fixing  $x = y = 1$  in equation (7.10) yields no critical strength since  $u(1, 1, z)$  always has a global minimum. Therefore, the other degrees of freedom are essential in this prolate limit.

A modified stability criterion can be obtained by considering the ground-state energy  $E_0$  of the boson system, which in the non-interacting case is  $E_0 = \hbar(\omega_x + \omega_y + \omega_z)(N - 1)/2$  where the centre-of-mass energy is subtracted. The system is unstable when this energy is larger than the barrier height  $U_{\text{barrier}}$ , see the indication in figure 7.2 of the corresponding height  $u_{\text{barrier}}$  for the reduced potential. With this condition the criterion of stability is

$$\frac{N|a_s|}{b_t} < \frac{1}{2}\sqrt{\frac{\pi}{3}}\frac{l_1}{b_t}\sqrt{1 + \frac{1}{12}\frac{l_1^4}{l_2^4}}, \quad (7.18)$$

where  $3l_1^{-2} \equiv b_x^{-2} + b_y^{-2} + b_z^{-2}$ . This is seen in figure 7.3 (thick solid line) to be below the GPE calculations [GFT01]. The improvement is here substantial compared to when the zero-point energy is neglected. In particular, for the spherical case we get  $N|a_s|/b_t \simeq 0.53$  instead of  $N|a_s|/b_t \simeq 0.67$ .

The estimate of equation (7.18) describes the stability problem better since it includes the quantum effect due to the zero-point energy. The GPE calculation is time dependent and thus describes the dynamics even better and is also closest to the experimental value. Since we expect the present non-correlated hyperspherical treatment to be in agreement with the mean field, we expect that a time-dependent treatment in this frame would yield the same result as obtained by Gammal *et al.* [GFT01].

A recent variational Monte Carlo investigation of the stability criterion in elongated, almost one-dimensional, traps yielded the stability criterion  $n_{1D}a_{1D} \lesssim 0.35$  [ABGG03b], where  $n_{1D} \sim N/b_z$  is the density in one dimension and

$a_{1D} = -b_{\perp}(b_{\perp}/a_s - 1.0326)$ . Equation (7.18) can in the one-dimensional limit be written as  $N|a_s|/b_{\perp} \lesssim 0.66$ . The deviation between the two results might be due to our use of a three-dimensional zero-range interaction in this non-correlated model, whereas Astrakharchik *et al.* [ABGG03b] used a one-dimensional model with a zero-range interaction with coupling strength proportional to  $1/a_{1D}$  as well as a full 3D correlated model with hard-sphere or finite-range potentials. An effective potential analogous to  $\delta(x)/a_{1D}$  in the general case with intermediate deformations would be a rewarding goal.

According to Görlitz *et al.* [GVL<sup>+</sup>01] the interaction energy is smaller than the energy in the tightly-confining dimension when  $|s| \leq \sqrt{32/225}\beta^{-5/6}$  for the 1D limit and when  $|s| \leq \sqrt{32/225}\beta^{5/3}$  for the 2D limit. These cross-overs are indicated by double-dashed (two-dimensional) and triple-dashed (one-dimensional) lines in figure 7.3. Since the critical region in each limit is below the relevant cross-over, stable and strongly deformed systems can be regarded as effectively one- or two-dimensional in the sense of these energy relations.

### 7.3 Effective dimension

The deformation of the external field effectively changes the dimension  $d$  of the space where the particles move. The field changes continuously and  $d$  could correspondingly vary from three to either two or one. In order to arrive at such a description, we aim at an effective  $d$ -dimensional Hamiltonian analogous to equation (7.4) with only one radial variable  $\rho$ , a deformation-dependent dimension  $d$ , and an effective trap length  $b_d$ , i.e.

$$\frac{2m\hat{H}_d}{\hbar^2} = -\frac{1}{\rho^{d(N-1)-1}} \frac{\partial}{\partial \rho} \rho^{d(N-1)-1} \frac{\partial}{\partial \rho} + \frac{\rho^2}{b_d^4} + \frac{2m\hat{V}}{\hbar^2}, \quad (7.19)$$

where  $\hat{V}$  represents all particle interactions in  $d$  dimensions. The requirement is that the Schrödinger equation  $\hat{H}_d G_d = E_d G_d$  with  $d$ -dimensional eigenfunction  $G_d$  and eigenvalue  $E_d$  is obeyed, at least on average, i.e.

$$\int d\rho \rho^{d(N-1)-1} G_d^*(\rho) (\hat{H}_d - E_d) G_d(\rho) = 0. \quad (7.20)$$

The lowest free solution, that is with  $\hat{V} = 0$ , is given by equation (7.11). In the cylindrical case we can relate the  $d$ -dimensional function  $G_d$  to this by performing the average with respect to the angle  $\theta$  in the parametrization  $(\rho_{\perp}, \rho_z) = \rho(\sin \theta, \cos \theta)$ . With inclusion of the corresponding volume elements, see appendix A.3, this leads to

$$\rho^{d(N-1)-1} |G_d(\rho)|^2 = \rho^{3(N-1)-1} \int_0^{\pi} d\theta \cos^{N-2} \theta \sin^{2N-3} \theta |F(\rho, \theta)|^2, \quad (7.21)$$

where  $F(\rho, \theta)$  can be obtained by rewriting equations (7.11) and (7.8).

The characteristic energy and length can be defined by

$$E_d = \frac{d\hbar^2}{2mb_d^2}(N-1), \quad db_d^2 = 2b_\perp^2 + b_z^2, \quad (7.22)$$

which clearly is correct in the three limits, i.e. spherical:  $d = 3$  and  $b_d = b_z = b_\perp$ , two-dimensional:  $d = 2$  and  $b_\perp \gg b_z$ , and one-dimensional:  $d = 1$  and  $b_z \gg b_\perp$ .

In general it is not possible to find one  $\rho$ -independent set of constants  $(E_d, b_d, d)$  such that  $\hat{H}_d G_d = E_d G_d$ . Instead we insist on the average condition in equation (7.20) with  $G_d$  and  $E_d$  from equations (7.21) and (7.22). The result for axial geometry is a second-degree equation in  $d$  with one physically meaningful root, see details in appendix E. The results for various  $N$  values are shown in figure 7.4. The effective dimension depends on  $N$  for relatively small

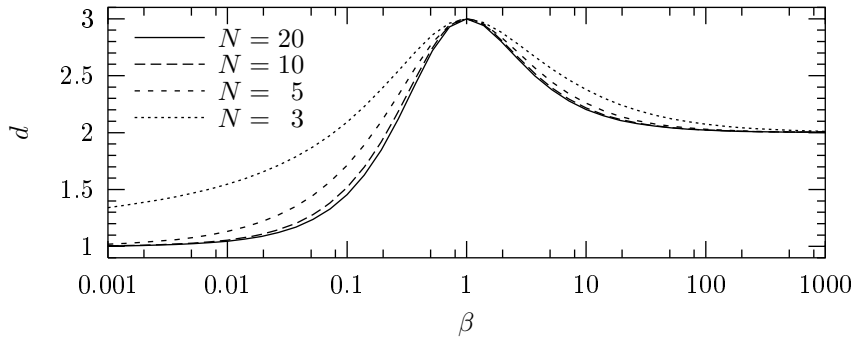


Figure 7.4: The effective dimension  $d$  obtained as a function of the deformation parameter  $\beta = b_\perp^2/b_z^2$ . Curves for larger  $N$  are very close to that for  $N = 20$ .

particle numbers. When  $N > 20$ , the curve is essentially fixed. Furthermore, the asymptotic values of both  $d = 1$  (small  $\beta$ ) and  $d = 2$  (large  $\beta$ ) are reached faster for larger  $N$  since many particles feel the geometric confinement stronger than few particles.\* Since these effective dimensions are obtained as average values over  $\rho$ , the system might look spherical at large distances and strongly deformed at small distances, on average resulting in the curves in figure 7.4.

## 7.4 Deformation-dependent interactions

The effective dimension for the non-interacting system possibly changes when interactions are included. The steps of the previous section should in principle be repeated with the interactions. However, this would be complicated and miss the goal which is a simple effective Hamiltonian with a renormalized interaction in lower dimension, see analogies in the references [Ols98, PHS00, LMDB02].

\*It may be amusing to speculate on the meaning of  $d = 2$  for elongated cigar-shaped confinement ( $0.1 \lesssim \beta \lesssim 0.2$ ).

We therefore start out with a two-body contact interaction with a coupling strength which is modified due to the deformation. This is in line with the renormalization in section 5.1.2 due to the inclusion of two-body correlations. So we write a  $d$ -dimensional zero-range interaction with a dimension-dependent coupling strength  $g(d)$  as

$$V_d(r_{ij}) = g(d)\delta^{(d)}(r_{ij}), \quad g(3) = \frac{\hbar^2 a_s}{m}, \quad (7.23)$$

where this “ $d$ -dimensional  $\delta$  function” is defined by  $\delta^{(d)}(r) = 0$  for  $r \neq 0$  and  $\int_0^\infty dr r^{d-1} \delta^{(d)}(r) = 1$ . The distance between two particles, e.g. particle 1 and 2, is in hyperspherical coordinates defined by  $r_{12} = \sqrt{2}\rho \sin \alpha$ , where the angle  $\alpha$  enters the angular volume element as

$$d\Omega_\alpha = d\alpha \sin^{d-1} \alpha \cos^{d(N-2)-1} \alpha. \quad (7.24)$$

This is valid at least for  $d = 1, 2, 3$ , see appendix A.2.3. The effective interaction  $\hat{V}$  in equation (7.19) is for  $N \gg 1$  then given by the average over all coordinates except  $\rho$ :

$$\hat{V} = \frac{N^2}{2} \frac{\int_0^{\pi/2} d\Omega_\alpha V_d(\sqrt{2}\rho \sin \alpha)}{\int_0^{\pi/2} d\Omega_\alpha} = \frac{\hbar^2}{2m} \frac{2N^2 (Nd/4)^{d/2} a_s g(d)}{\Gamma(d/2) \rho^d g(3)}. \quad (7.25)$$

However, this does not yield instability for  $d < 2$  since the power  $d$  in  $\rho^{-d}$  is smaller than two, see section 6.1.

We therefore pursue another approach. Inspired by the forms of equations (7.14) and (7.25), we write  $\hat{V}$  as

$$\hat{V} = \frac{\hbar^2}{2m} \frac{2N^2 (Nd/4)^{p/2} a_d}{\Gamma(d/2) \rho^p}, \quad a_3 = a_s, \quad (7.26)$$

which with  $a_3 = a_s$  coincides with the result for  $d = 3$  if we choose  $p = 3$ . The effective potential  $U_d$  in the  $d$ -dimensional Schrödinger equation corresponding to equation (7.19) is then

$$\frac{2mU_d(\rho)}{\hbar^2} = \frac{2N^2 (Nd/4)^{p/2} a_d}{\Gamma(d/2) \rho^p} + \frac{d^2 N^2}{4\rho^2} + \frac{\rho^2}{b_d^4}. \quad (7.27)$$

For  $p < 2$  this potential always has a global minimum and thus no collapse is present. For  $p > 2$  there is always divergence to  $-\infty$  when  $\rho \rightarrow 0$ . For weak attraction, i.e. small  $|a_d|$ , there is a local minimum. This disappears at larger  $|a_d|$  when

$$\frac{N|a_d|}{b_t} > \frac{b_d^{p-2}}{b_t} \frac{2^{1+p/2} d(p-2)^{(p-2)/4} \Gamma(d/2)}{p(p+2)^{(p+2)/4}}. \quad (7.28)$$

The criterion in equation (7.16) was also obtained by estimating when the critical point vanished. Equation (7.16) is valid for all deformations, i.e. any  $d$ . In

order to be able to compare equations (7.16) and (7.28), we therefore choose  $p > 2$  such that equation (7.28) always is applicable. When equations (7.28) and (7.16) agree, the effective interaction strength  $a_d$  is given by

$$\frac{a_d}{a_s} = \frac{b_d^{p-2}}{b_t} \frac{2^{(p-1)/2} \Gamma(\frac{d}{2}) 5^{5/4} (p-2)^{(p-2)/4}}{\sqrt{\pi} (p+2)^{(p+2)/4} \beta^{1/6} p/d} \sqrt[4]{\frac{2+\beta^2}{3}}. \quad (7.29)$$

This effective interaction strength is in figure 7.5 shown as a function of the deformation for various choices of the power  $p$ . The solid line shows the result for  $p = 3$ , which is known to be correct for  $\beta = 1$  ( $d = 3$ ). Similarly the dashed line shows the result with  $p = d$ , which does not work for  $d < 2$  ( $\beta \lesssim 0.2$ ). Since the effective coupling strength depends strongly on the power  $p$ , we need

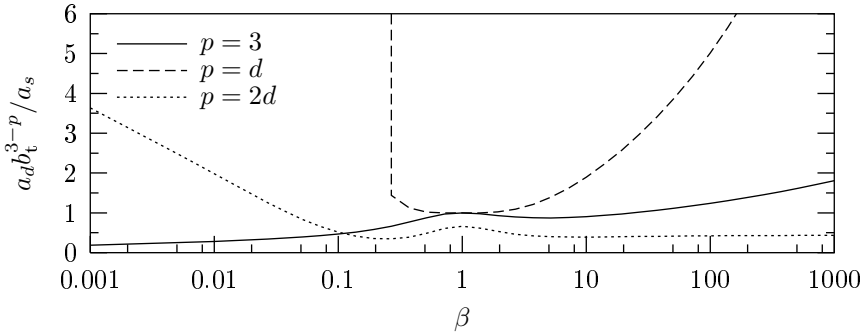


Figure 7.5: The effective interaction strength  $a_d$  from equation (7.29) obtained as a function of the deformation parameter  $\beta = b_{\perp}^2/b_z^2$  in the large- $N$  limit, i.e. the connection between deformation and effective dimension obtained from the calculation for  $N = 20$  is used for this illustration. The vertical divergence of the dashed line indicates the inadequacy of the corresponding method when  $d < 2$ .

further information about how the interactions enter the effective potential.

An extreme deformation might lead to effectively one-dimensional or two-dimensional properties. Pitaevskii and Stringari [PS03] collected results for the effective coupling strength in two dimensions that yields  $g(2) = \sqrt{8\pi\hbar^2} a_s / (mb_z)$ , whereas the result from equation (7.29) in that limit is larger by the factor  $5^{5/4}/4 \simeq 1.9$ . Even though the results differ by a factor close to two, the right combination of lengths shows that we have incorporated the degrees of freedom in the correct manner. This was also the case in the previous comparison of the stability criterion with the one obtained by Baym and Pethick [BP96]. However, as was also mentioned by Pitaevskii and Stringari [PS03], in the low-density limit in two dimensions the coupling constant becomes density-dependent, which is beyond the present model where correlations are neglected.

Since  $p = d$  for  $d = 1$  does not yield a meaningful interpretation of the stability criterion, a one-dimensional system needs a different treatment.

## 7.5 Discussion

In conclusion, the hyperspherical method with a non-correlated approach yielded stability criteria as a function of the deformation of the external field. For constant volume the highest stability was found for spherical traps. Effective dimensions  $d$  continuously varying between 1 and 3 were calculated as a function of the deformation. The system can possibly be described by a  $d$ -dimensional effective radial potential with a  $d$ -dimensional effective interaction. However, this does not have an unambiguous form. Applications to restricted geometries become simpler, where the obtained two-dimensional coupling strength compares reasonably with a coupling strength obtained by an axial average of a three-dimensional contact interaction. For the one-dimensional case an effective coupling strength was not obtained.

A previous approach to a  $d = 1$  treatment by Gammal *et al.* [GFTA00] shows that a three-body contact interaction is necessary for the GPE to produce collapse in one spatial dimension. In the present framework a three-body contact interaction for a constant angular wave function produces a hyperradial potential proportional to  $\rho^{-2d}$ , compare with equation (5.15), which for any  $d \geq 1$  leads to instability if the three-body coupling strength is sufficiently negative. The dotted line in figure 7.5 shows the effective coupling strength for  $p = 2d$ , corresponding to this three-body zero-range interaction.

According to Astrakharchik *et al.* [ABGG03b, ABGG03a] a Jastrow ansatz for a correlated wave function and inclusion of two-body interactions lead to collapse in one spatial dimension. According to preliminary Faddeev calculations with the two-body correlated model presented in chapter 2, a two-body interaction and inclusion of only two-body correlations in one spatial dimension do not lead to collapse. It seems that at least three-body correlations or three-body interactions are necessary in order to achieve a realistic description of collapse in one dimension.



## Chapter VIII

### Conclusions and perspectives

The present thesis studied few-body correlations within a many-body system, especially effects beyond the commonly applied mean field by a method that is usually applied to clusterized systems.

Chapter 2 presented a hyperspherical framework for including two-body correlations explicitly in the wave function. For bosons this was done as a sum of two-body amplitudes, the Faddeev decomposition of the wave function. One advantage of this wave function is that it contains a signature of the average distance between all particles. In this respect it reminds of the mean field, and it is indeed possible to relate the wave functions when the interactions are sufficiently weak. On the other hand, in the dilute limit where three-body encounters are rare, this wave function reminds of the Jastrow factorization into two-body amplitudes. Thus, it catches the information from the encounter of two particles at the same time as remembering the background cloud of other particles. In the shape of a variational equation, the Schrödinger equation was then reduced to a one-dimensional differential equation in a hyperangle, plus a simple one-dimensional equation in the hyperradius. A similar result was previously obtained by de la Ripelle *et al.* [dIRFS88] in terms of Faddeev-like equations. However, the present equation is variational and the complications compared to the simpler Faddeev-like equations are not severe.

In chapter 3 we discussed analytical estimates of the angular eigenvalues. These provide results in the dilute limit in agreement with expectations based on mean-field-like assumptions. Then the numerical solutions confirm these results in the dilute limit and furthermore provide significant deviations at larger densities. In the regime of a very large two-body  $s$ -wave scattering length the angular potential approaches a constant value which only depends on the number of particles. Also the signatures of a two-body bound state are recognized, providing a possible link between the scattering channels and the two-body bound channels within the many-boson system.

The macroscopic properties of a trapped system of bosons were investigated in chapter 4, where the radial equation was solved for the size scale and total energy of the system. Some of the stationary solutions in the hyperradial poten-

tial turn out to have a much smaller spatial extension than the typical size scale of a Bose-Einstein condensate. Furthermore, the total energy of many states might be negative due to a large average attraction at large densities, i.e. when the bosons are close to each other. The Bose-Einstein condensate is usually unstable if the external confinement is removed, whereas these negative-energy modes are self-bound, and thus confined even if the trap is turned off.

Chapter 5 presented the basic assumptions in the mean-field Gross-Pitaevskii (GP) treatment of a dilute boson system. We related the obtained angular potentials to a possible density-dependent zero-range interaction. This allows a possible renormalization of the mean-field interaction for calculations with the GP equation for denser systems. The energies and average distances for a dilute boson system obtained from the mean field are very close to those obtained from the two-body correlated model. However, the states with larger densities and negative energies have no parallels in the mean-field model. In this region we obtained interaction energies independent of the scattering length. Concerning validity, chapter 5 gave estimates of the validity ranges, extending the validity region for the two-body correlated model to larger densities with deviations from the mean field.

The stability criterion for a Bose-Einstein condensate is in the present hyperspherical treatment of pairwise correlations obtained in a way which is similar to the derivation from the mean field. This was evident in chapter 6 where the criterion was derived in terms of the hyperradial potential. Three-body recombination and macroscopic tunneling were discussed qualitatively, estimating the effects of degrees of freedom that are not explicitly included in the two-body correlated model. This is related to discussions by Bohn *et al.* [BEG98]. The discussion of macroscopic collapse when suddenly changing the underlying two-body interactions is possible within the model. This provides an estimate of the collapse time which agrees on the order-of-magnitude level with the measured time scale.

A possible improvement is the explicit inclusion of three-body correlations in the ansatz for the wave function in order to study three-body recombinations in the many-boson system. This can also indicate the validity of the present model, and tell if the self-bound many-body states described in chapter 4 have physical relevance or if they are artificial products of the present ansatz with two-body correlations. A quantitative study of collapse dynamics can be performed by studying the time-dependent problem with inclusion of couplings between the different channels in the adiabatic expansion of the wave function.

The investigation showed that the lifetime of some of the self-bound many-body states might be so large that they can be observed in experiments. This might be done by turning off the trap, waiting for some time, and then altering the two-body interaction such that the particles repel each other and the system expands. By extrapolating back to the density profile before expansion, it might be concluded that the system did not expand in the time period between the external trap was turned off and the two-body interactions were made effectively repulsive.

The effects of deformation were discussed in chapter 7, which described the trapped boson system in a non-correlated hyperspherical frame. The external confining field alters the stability criterion in agreement with the experimentally measured criterion. For a fixed volume any deviation from the spherical geometry decreases the stability. This was also concluded by Gammal *et al.* [GFT01] from a study of the time-dependent GP equation. The present treatment provides an analytical stability criterion as a function of deformation, which agrees well, but not perfectly, with the experimentally measured value. The deviations are probably due to the crudeness of the approximations made for the analytical estimates, but not due to the lack of correlations since these are also absent in a mean-field treatment. We furthermore sought to use only one length scale to describe the deformation. For the non-interacting case this results in an effective dimension, which then enters an effective Hamiltonian in a single length scale. However, the problem is the inclusion of interactions, which does not appear trivial. A proposed effective potential provides a stability criterion, but does so in a non-transparent way where the coupling to the two-body interactions has vanished. It seems that higher-order correlations or higher-order interactions are crucial for a full understanding of stability phenomena in effectively lower dimensions.

An immediate extension of the present work is to complete the treatment of two-body correlations in lower dimensions and in the general deformed system. This could provide the wanted effective interaction in lower dimensions and possibly confirm the results of other approaches, e.g. the references [PHS00, LMDB02] for the two-dimensional cases.

The treatments in this thesis are performed at zero temperature. The effects of a finite temperature can possibly be included as a statistical distribution of many-body states, where couplings between the states then will play a larger role. This might yield information about the effect of pairwise correlations on the condensate fraction and the transition temperature.

Experiments with trapping of fermionic gases raise many questions about the modification of correlations for fermions. Especially the problem of binary correlations between identical fermions is a great challenge, but can potentially be built on top of a hyperspherical frame. Another approach is an extraction of a density-dependent coupling strength for a fermion system. This might also provide answers to questions in other fields of physics, e.g. in molecular physics and nuclear physics, where the mean field is inadequate for studies of exotic problems, for example nuclei close to a drip line.

In conclusion, the present study of two-body correlations yielded insight into mechanisms that in the dilute limit can be accounted for by a mean field, and yielded deviations especially in the presence of a two-body bound state or a resonance. The inclusion of three-body correlations can be the crucial next step which provides answers to questions about three-body recombination and the structure of lower-dimensional systems.



## Chapter IX

### Sammendrag på dansk (Summary in Danish)

*Resumé: Afhandlingen "Korte tilfældige sammenstød. Parvise korrelationer blandt bosoner" omhandler teoretiske modeller for parvise påvirkninger mellem atomer, der befinder sig i en gas af ens partikler ved meget lav temperatur. Teorien bag en model for opdeling af et mangepartikelsystem i små grupper præsenteres, og denne model anvendes i tilfældet hvor kun to partikler skiller sig ud. Specielt undersøges betydningen af store tætheder og kraftig vekselvirkning mellem atomerne. Dette viser afvigelser i forhold til en middelfeltsmodel, hvor atomerne ikke har mulighed for at indrette sig efter hinanden. Studiet af cigarformede eller pandekageformede systemer indikerer, at man må inkludere påvirkningen mellem tre atomer for at forstå disse systemer til bunds.*

Denne afhandling bekræfter sig med korrelationer i bosonsystemer, især relateret til de mange eksperimenter udført med meget kolde alkaligasser (lithium, natrium, rubidium og cæsium) i de seneste 10 år. Specielt studeres afvigelser fra middelfeltet. Efter det introducerende kapitel 1 præsenterede vi i kapitel 2 en hypersfærisk beskrivelse af fåpartikelkorrelationer i et mangepartikelsystem. Til laveste orden inkluderede vi topartikelkorrelationer i form af en sum af topartikelamplituder. Når to partikler kommer tæt på hinanden, ændrer mangepartikelbølgefunktionen sig fra den sædvanlige enkeltpartikelstruktur, som kendes fra en middelfeltsbeskrivelse. På denne måde minder den hypersfæriske bølgefunktion for et tyndt system om en kombination af en Jastrow-beskrivelse og en Hartree-beskrivelse. Schrödinger-ligningen omskrives med sådanne topartikelamplituder til en Faddeev-agtig ligning i en hypervinkel, der relateres til topartikelafstanden, samt en simpel ligning i hyperradius, der beskriver den samlede udstrækning af mangepartikelsystemet. I den ene hypervinkel udledte vi også en mere kompliceret variationsligning, der ses som et alternativ til den Faddeev-agtige ligning. I grænsen, hvor middelfeltet mellem partiklerne er meget større end den typiske vekselvirkingsrækkevidde, er det muligt at reducere komplikationerne ved denne variationsligning, så et anvendeligt redskab fremkommer.

I kapitel 3 diskuteredes analytiske egenskaber af vinkelligningen. For et

fortyndet system giver dette resultat i overensstemmelse med en ukorreleret antagelse for bølgefunktionen sammen med en vekselvirkning, der normalt anvendes i en middelfeltsbeskrivelse. De numeriske løsninger bekræfter denne grænse, men viser også afvigelser ved større tætheder, bl.a. er tilstedeværelsen af en bundet tilstand mellem to partikler bestemmende for en af egenverdierne, hvilket ikke forekommer i middelfeltet. Dette kan muligvis danne grundlaget for en beskrivelse af koblinger mellem kondensatfasen og de bundne tilstande.

I kapitel 4 sammenføjede vi effekten fra vekselvirkningerne med signaturerne fra en ydre fælde. Dette resulterer i forskellige typer løsninger til det fulde radiale problem. Specielt forekommer mangepartikeltilstande, der er bundet selv uden den ydre fældes indflydelse.

I kapitel 5 beskrev vi middelfeltsantagelserne, og løsningerne fra den korrelerede metode sammenlignedes med middelfeltsløsninger. Det er muligt at udlede en tæthedsafhængig vekselvirkning fra de korrelerede beregninger. Slutteligt vist det, at gyldigheden af den korrelerede metode strækker sig til områder med større tætheder og store afvigelser fra middelfeltet.

Stabilitetskriterier og tidsskalaer for forskellige henfaldsmuligheder diskuteres i kapitel 6, dog uden at vi studerede de tidsafhængige ligninger, og uden at vi inkluderede koblinger imellem de forskellige faser eksplicit. Dette er en mulig udvidelse af metoden. Specielt inklusionen af trepartikkelkorrelationer ses som en nærliggende fremtidig undersøgelse. Tilstande med negativ energi kan muligvis observeres i eksperimenter, da deres levetid er tilstrækkeligt stor, og da deres rumlige udstrækning vil udvikle sig anderledes i tiden end for systemer med positiv energi.

Deformationens indvirkning på et bosonsystems egenskaber studeredes i kapitel 7. En ukorreleret fremgangsmåde giver analytiske stabilitetskriterier, hvor det bedste er i nogenlunde overensstemmelse med et tidsafhængigt middelfeltsstudie og med den eksperimentelt målte værdi. Vi udledte en effektiv dimension, der kan anvendes i studiet af effektive vekselvirkninger for deformerede systemer eller i en ekstrem grænse med diskret, lavere dimension. Formen for den effektive vekselvirkning er dog uklar og må i et nøjere studie af korrelationer udledes fra de effektive potentialer. Foreløbige undersøgelser af et éndimensionalt system viser, at topartikelkorrelationer er utilstrækkelige for en beskrivelse af kendte strukturer. Sandsynligvis bør man inkludere trepartikkelkorrelationer for at opnå en tilfredsstillende beskrivelse.

Problematikken omkring fermiongasser kan måske udredes med en form for topartikelkorrelationer indarbejdet i en hypersfærisk beskrivelse. Dette kan også vise sig frugtbart inden for andre områder af fysikken, f.eks. i studiet af driplinie-kerner eller af molekylære klynger.

Umiddelbare udvidelser af de beskrevne metoder er færdiggørelse af studiet af korrelationer i deformerede systemer og inklusion af eksplicit tidsafhængighed. Desuden forventes en model indeholdende trepartikkelkorrelationer at kunne besvare mange spørgsmål, da korrelationer af højere orden sandsynligvis er ubetydelige selv ved forholdsvist store tætheder. Samtidig kan dette teste gyldigheden af resultaterne opnået vha. antagelsen om topartikelkorrelationer.

## Appendix A

### Coordinate transformations

From Schaum's [Spi68] p. 124-125 we generalize transformations between large sets of coordinates. We start with a set of  $M$  coordinates denoted by  $\mathbf{s} = (s_1, s_2, \dots, s_M)$  and replace these by another set of  $M$  coordinates  $\mathbf{q} = (q_1, q_2, \dots, q_M)$ , i.e.  $s_i = s_i(\mathbf{q})$ . We obtain the relation between volume elements and Laplacians as follows. First define

$$h_j \equiv \left| \frac{\partial \mathbf{s}}{\partial q_j} \right|, \quad \mathcal{H} \equiv \prod_{j=1}^M h_j. \quad (\text{A.1})$$

The Laplacian operators and the volume elements are then connected by

$$\sum_{i=1}^M \frac{\partial^2}{\partial s_i^2} = \sum_{j=1}^M \hat{\Delta}_j, \quad \hat{\Delta}_j \equiv \frac{\partial}{\partial q_j} \frac{\mathcal{H}}{h_j^2} \frac{\partial}{\partial q_j}, \quad (\text{A.2})$$

$$\prod_{i=1}^M ds_i = \mathcal{H} \prod_{j=1}^M dq_j. \quad (\text{A.3})$$

#### A.1 Jacobi coordinates for $N$ identical particles

We start with the coordinate vectors  $\mathbf{r}_i$  for  $N$  identical particles in  $d$  spatial dimensions. These are then transformed to the centre-of-mass coordinates

$$\mathbf{R} = \frac{1}{N} \sum_{i=1}^N \mathbf{r}_i \quad (\text{A.4})$$

and  $N - 1$  relative Jacobi coordinates  $\boldsymbol{\eta}_k$  for  $k = 1, 2, \dots, N - 1$ :

$$\begin{aligned} \boldsymbol{\eta}_{N-1} &= \frac{1}{\sqrt{2}}(\mathbf{r}_2 - \mathbf{r}_1), \quad \dots, \\ \boldsymbol{\eta}_k &= \sqrt{\frac{N-k}{N-k+1}} \left( \mathbf{r}_{N-k+1} - \frac{1}{N-k} \sum_{i=1}^{N-k} \mathbf{r}_i \right). \end{aligned} \quad (\text{A.5})$$

The inverse relations are

$$\begin{aligned} \mathbf{r}_i &= \mathbf{R} - \sum_{k=1}^{N-i} \frac{1}{\sqrt{(N-k)(N-k+1)}} \boldsymbol{\eta}_k + \sqrt{\frac{i-1}{i}} \boldsymbol{\eta}_{N-i+1}, \\ \dots, \quad \mathbf{r}_N &= \mathbf{R} - \sqrt{\frac{N-1}{N}} \boldsymbol{\eta}_1. \end{aligned} \quad (\text{A.6})$$

The notation in relation to equation (A.1) is

$$\mathbf{s} = \begin{cases} (r_{1x}, r_{1y}, r_{1z}, r_{2x}, \dots, r_{Nz}) & \text{for } d = 3, \\ (r_{1x}, r_{1y}, r_{2x}, \dots, r_{Ny}) & \text{for } d = 2, \\ (r_{1x}, r_{2x}, \dots, r_{Nx}) & \text{for } d = 1, \end{cases} \quad (\text{A.7})$$

and  $\mathbf{q} = (\mathbf{R}, \boldsymbol{\eta}_{N-1}, \dots, \boldsymbol{\eta}_1)$ . The  $i$ 'th component of the centre-of-mass coordinates obeys  $h_{R_i} = N^{1/2}$  and for the relative components  $h_{\eta_{k,i}} = 1$ . Then the volume element is

$$\prod_{i=1}^N d\mathbf{r}_i = N^{d/2} d\mathbf{R} \prod_{k=1}^{N-1} d\boldsymbol{\eta}_k, \quad (\text{A.8})$$

where each vector denotes  $d$  degrees of freedom. The total Laplacian is

$$\hat{\Delta}_{\text{total}} \equiv \sum_{i=1}^N \frac{\partial^2}{\partial r_i^2} = \hat{\Delta}_R + \sum_{k=1}^{N-1} \frac{\partial^2}{\partial \boldsymbol{\eta}_k^2}, \quad \hat{\Delta}_R \equiv \frac{1}{N} \frac{\partial^2}{\partial \mathbf{R}^2}. \quad (\text{A.9})$$

## A.2 Hyperspherical coordinates

### A.2.1 Three particles in three dimensions

For simplicity we first study the case of hyperspherical coordinates for  $d = 3$  spatial dimensions and  $N = 3$  particles. The Jacobi vectors are

$$\boldsymbol{\eta}_2 = \rho \sin \alpha \begin{pmatrix} \sin \vartheta_2 \cos \varphi_2 \\ \sin \vartheta_2 \sin \varphi_2 \\ \cos \vartheta_2 \end{pmatrix}, \quad \boldsymbol{\eta}_1 = \rho \cos \alpha \begin{pmatrix} \sin \vartheta_1 \cos \varphi_1 \\ \sin \vartheta_1 \sin \varphi_1 \\ \cos \vartheta_1 \end{pmatrix}. \quad (\text{A.10})$$

So, we start with six relative coordinates  $\mathbf{s} = (\eta_{1x}, \dots, \eta_{2z})$  and wish to obtain the volume element and Laplacian operator in the (new) set of hyperspherical coordinates  $\mathbf{q} = (\rho, \alpha, \vartheta_2, \varphi_2, \vartheta_1, \varphi_1)$ . In this case  $h_\rho = 1$ ,  $h_\alpha = \rho$ ,  $h_{\vartheta_2} = \rho \sin \alpha$ ,  $h_{\varphi_2} = \rho \sin \alpha \sin \vartheta_2$ ,  $h_{\vartheta_1} = \rho \cos \alpha$ , and  $h_{\varphi_1} = \rho \cos \alpha \sin \vartheta_1$ , which yields

$$\mathcal{H} = \rho^5 \sin^2 \alpha \cos^2 \alpha \sin \vartheta_2 \sin \vartheta_1. \quad (\text{A.11})$$

The terms in the Laplacian then become

$$\hat{\Delta}_\rho = \frac{1}{\mathcal{H}} \frac{\partial}{\partial \rho} \frac{\mathcal{H}}{\rho^2} \frac{\partial}{\partial \rho} = \frac{1}{\rho^5} \frac{\partial}{\partial \rho} \rho^5 \frac{\partial}{\partial \rho}, \quad (\text{A.12})$$



$$\hat{\Delta}_\alpha = \frac{1}{\mathcal{H}} \frac{\partial \mathcal{H}}{\partial \alpha} \frac{\partial}{\rho^2} \frac{\partial}{\partial \alpha} = \frac{1}{\rho^2 \sin^2 \alpha \cos^2 \alpha} \frac{\partial}{\partial \alpha} \sin^2 \alpha \cos^2 \alpha \frac{\partial}{\partial \alpha}, \quad (\text{A.13})$$

$$\hat{\Delta}_{\vartheta_2} + \hat{\Delta}_{\varphi_2} = -\frac{\hat{\mathbf{i}}_2^2}{\rho^2 \sin^2 \alpha}, \quad (\text{A.14})$$

$$\hat{\mathbf{i}}_k^2 = -\frac{1}{\sin \vartheta_k} \frac{\partial}{\partial \vartheta_k} \sin \vartheta_k \frac{\partial}{\partial \vartheta_k} - \frac{1}{\sin^2 \vartheta_k} \frac{\partial^2}{\partial \varphi_k^2}, \quad (\text{A.15})$$

$$\hat{\Delta}_{\vartheta_1} + \hat{\Delta}_{\varphi_1} = -\frac{\hat{\mathbf{i}}_1^2}{\rho^2 \cos^2 \alpha}, \quad (\text{A.16})$$

$$\hat{\Delta} \equiv \hat{\Delta}_{\text{total}} - \hat{\Delta}_R = \frac{1}{\rho^5} \frac{\partial}{\partial \rho} \rho^5 \frac{\partial}{\partial \rho} - \frac{\hat{\Lambda}_2^2}{\rho^2}, \quad (\text{A.17})$$

$$\hat{\Lambda}_2^2 \equiv -\frac{1}{\sin^2 \alpha \cos^2 \alpha} \frac{\partial}{\partial \alpha} \sin^2 \alpha \cos^2 \alpha \frac{\partial}{\partial \alpha} + \frac{\hat{\mathbf{i}}_2^2}{\sin^2 \alpha} + \frac{\hat{\mathbf{i}}_1^2}{\cos^2 \alpha}. \quad (\text{A.18})$$

In this notation  $\hat{h}_{\mathbf{k}}$  is the angular momentum operator associated with  $\boldsymbol{\eta}_k$ .

### A.2.2 $N$ particles in three dimensions

The hyperspherical coordinates are related to the Jacobi coordinates by

$$\boldsymbol{\eta}_k = \rho_k \sin \alpha_k \begin{pmatrix} \sin \vartheta_k \cos \varphi_k \\ \sin \vartheta_k \sin \varphi_k \\ \cos \vartheta_k \end{pmatrix}, \quad k = 1, 2, \dots, N-1, \quad (\text{A.19})$$

$$\rho_k = \rho_{k+1} \cos \alpha_{k+1} = \rho \prod_{j=k+1}^{N-1} \cos \alpha_j, \quad \rho \equiv \rho_{N-1}. \quad (\text{A.20})$$

The Jacobi coordinates are  $\mathbf{s} = (\eta_{1x}, \dots, \eta_{N-1,z})$ . With  $\alpha_1 = \pi/2$  the new set of coordinates is  $\mathbf{q} = (\rho, \alpha_{N-1}, \alpha_{N-2}, \dots, \alpha_2, \vartheta_k, \varphi_k)$ . This yields  $h_\rho = 1$ ,  $h_{\alpha_k} = \rho_k$ ,  $h_{\vartheta_k} = \rho_k \sin \alpha_k$ ,  $h_{\varphi_k} = \rho_k \sin \alpha_k \sin \vartheta_k$ , and the volume element is

$$\mathcal{H} = \rho^{3N-4} \cdot \left( \prod_{k=1}^{N-1} \sin \vartheta_k \right) \cdot \left( \prod_{k=2}^{N-1} \sin^2 \alpha_k \cos^{3k-4} \alpha_k \right). \quad (\text{A.21})$$

Each degree of freedom contributes to the Laplacian as follows:

$$\hat{\Delta}_\rho = \frac{1}{\mathcal{H}} \frac{\partial \mathcal{H}}{\partial \rho} \frac{\partial}{h_\rho^2} \frac{\partial}{\partial \rho} = \frac{1}{\rho^{3N-4}} \frac{\partial}{\partial \rho} \rho^{3N-4} \frac{\partial}{\partial \rho}, \quad (\text{A.22})$$

$$\hat{\Delta}_{\alpha_k} = \frac{1}{\rho^2 \prod_{j=k+1}^{N-1} \cos^2 \alpha_j} \frac{\cos^{4-3k} \alpha_k}{\sin^2 \alpha_k} \frac{\partial}{\partial \alpha_k} \sin^2 \alpha_k \cos^{3k-4} \alpha_k \frac{\partial}{\partial \alpha_k}, \quad (\text{A.23})$$

$$\hat{\Delta}_{\vartheta_k} = \frac{1}{\rho^2 \cdot \left( \prod_{j=k+1}^{N-1} \cos^2 \alpha_j \right)} \frac{1}{\sin^2 \alpha_k} \frac{1}{\sin \vartheta_k} \frac{\partial}{\partial \vartheta_k} \sin \vartheta_k \frac{\partial}{\partial \vartheta_k}, \quad (\text{A.24})$$

$$\hat{\Delta}_{\varphi_k} = \frac{1}{\rho^2 \cdot \left( \prod_{j=k+1}^{N-1} \cos^2 \alpha_j \right)} \frac{1}{\sin^2 \alpha_k} \frac{1}{\sin^2 \vartheta_k} \frac{\partial^2}{\partial \varphi_k^2}. \quad (\text{A.25})$$

We then note

$$\hat{\Delta}_{\varphi_k} + \hat{\Delta}_{\vartheta_k} = \frac{1}{\rho^2 \cdot \left(\prod_{j=k+1}^{N-1} \cos^2 \alpha_j\right)} \frac{-\hat{l}_k^2}{\sin^2 \alpha_k}. \quad (\text{A.26})$$

All the terms can be collected in

$$\hat{\Delta} = \hat{\Delta}_\rho + \sum_{i=2}^{N-1} \hat{\Delta}_{\alpha_k} + \sum_{i=1}^{N-1} (\hat{\Delta}_{\varphi_k} + \hat{\Delta}_{\vartheta_k}) = \hat{\Delta}_\rho - \frac{\hat{\Lambda}_{N-1}^2}{\rho^2}, \quad (\text{A.27})$$

$$\hat{\Lambda}_k^2 = \hat{\Pi}_k^2 + \frac{\hat{\Lambda}_{k-1}^2}{\cos^2 \alpha_k} + \frac{\hat{l}_k^2}{\sin^2 \alpha_k}, \quad \hat{\Lambda}_1^2 = \hat{l}_1^2, \quad (\text{A.28})$$

$$\hat{\Pi}_k^2 = -\frac{1}{\sin^2 \alpha_k \cos^{3k-4} \alpha_k} \frac{\partial}{\partial \alpha_k} \sin^2 \alpha_k \cos^{3k-4} \alpha_k \frac{\partial}{\partial \alpha_k}. \quad (\text{A.29})$$

A convenient transformation is

$$\hat{\Pi}_k^2 = \frac{1}{\sin \alpha_k \cos^{(3k-4)/2} \alpha_k} \left[ -\frac{\partial^2}{\partial \alpha_k^2} - \frac{9k-10}{2} + \frac{(3k-4)(3k-6)}{4} \tan^2 \alpha_k \right] \sin \alpha_k \cos^{(3k-4)/2} \alpha_k. \quad (\text{A.30})$$

### A.2.3 $N$ particles in $d$ dimensions

Without repeating the steps in the derivation we collect here the results in  $d$  spatial dimensions. In the general dimension the hyperspherical coordinates can be defined in the same way, when applicable, as for three dimensions. This means that for the integer dimensions we have the set of coordinates

$$\mathbf{q} = \begin{cases} (\rho, \alpha_{N-1}, \dots, \alpha_2, \varphi_{N-1}, \dots, \varphi_1, \vartheta_{N-1}, \dots, \vartheta_1) & \text{for } d = 3, \\ (\rho, \alpha_{N-1}, \dots, \alpha_2, \varphi_{N-1}, \dots, \varphi_1) & \text{for } d = 2, \\ (\rho, \alpha_{N-1}, \dots, \alpha_2) & \text{for } d = 1. \end{cases} \quad (\text{A.31})$$

While the coordinates  $\alpha_k \in [0, \pi/2]$  for  $d = 3$  and  $d = 2$ , it is for  $d = 1$  convenient to include the sign of a Jacobi coordinate in the definition of the corresponding hyperangle, and thus the appropriate range for  $d = 1$  is  $\alpha_k \in [-\pi/2, \pi/2]$ . The volume element is given by

$$\prod_{k=1}^{N-1} d\eta_k = d\rho \rho^{d(N-1)-1} d\Omega_{N-1}, \quad d\Omega_k = d\Omega_\alpha^{(k)} d\Omega_\eta^{(k)} d\Omega_{k-1}, \quad (\text{A.32})$$

$$d\Omega_1 = d\Omega_\eta^{(1)}, \quad d\Omega_\alpha^{(k)} = d\alpha_k \sin^{d-1} \alpha_k \cos^{d(k-1)-1} \alpha_k, \quad (\text{A.33})$$

$$d\Omega_\eta^{(k)} = \begin{cases} d\varphi_k d\vartheta_k \sin \vartheta_k & \text{for } d = 3, \\ d\varphi_k & \text{for } d = 2, \\ 1 & \text{for } d = 1. \end{cases} \quad (\text{A.34})$$

The relative Laplacian becomes

$$\hat{\Delta} = \hat{\Delta}_\rho - \frac{\hat{\Lambda}_{N-1}^2}{\rho^2}, \quad \hat{\Delta}_\rho = \frac{1}{\rho^{d(N-1)-1}} \frac{\partial}{\partial \rho} \rho^{d(N-1)-1} \frac{\partial}{\partial \rho}, \quad (\text{A.35})$$

$$\hat{\Lambda}_k^2 = \hat{\Pi}_k^2 + \frac{\hat{\Lambda}_{k-1}^2}{\cos^2 \alpha_k} + \frac{\hat{l}_k^2}{\sin^2 \alpha_k}, \quad \hat{\Lambda}_1^2 = \hat{l}_1^2, \quad (\text{A.36})$$

$$\hat{\Pi}_k^2 = -\frac{1}{\sin^{d-1} \alpha_k \cos^{d(k-1)-1} \alpha_k} \frac{\partial}{\partial \alpha_k} \sin^{d-1} \alpha_k \cos^{d(k-1)-1} \alpha_k \frac{\partial}{\partial \alpha_k}, \quad (\text{A.37})$$

$$\hat{l}_k^2 = \begin{cases} -\frac{1}{\sin \vartheta_k} \frac{\partial}{\partial \vartheta_k} \sin \vartheta_k \frac{\partial}{\partial \vartheta_k} - \frac{1}{\sin^2 \vartheta_k} \frac{\partial^2}{\partial \varphi_k^2} & \text{for } d = 3, \\ -\frac{\partial^2}{\partial \varphi_k^2} & \text{for } d = 2, \\ 0 & \text{for } d = 1. \end{cases} \quad (\text{A.38})$$

Useful transformations of the operators are

$$\hat{\Pi}_k^2 = \frac{1}{\sin^{(d-1)/2} \alpha_k \cos^{l_{d,k}+1} \alpha_k} \left[ -\frac{\partial^2}{\partial \alpha_k^2} + l_{d,k}(l_{d,k}+1) \tan^2 \alpha_k \right. \\ \left. + \frac{(d-1)(d-3)}{4} \cot^2 \alpha_k + \frac{1-d^2(k-1)}{2} \right] \sin^{(d-1)/2} \alpha_k \cos^{l_{d,k}+1} \alpha_k, \quad (\text{A.39})$$

$$\hat{\Delta}_\rho = \frac{1}{\rho^{l_{d,N}+1}} \left[ \frac{\partial^2}{\partial \rho^2} - \frac{l_{d,N}(l_{d,N}+1)}{\rho^2} \right] \rho^{l_{d,N}+1}, \quad l_{d,k} \equiv \frac{d(k-1)-3}{2}. \quad (\text{A.40})$$

with non-negative integers  $\nu_k = 0, 1, 2, \dots$

### A.3 “Hypercylindrical” coordinates

Apart from using the same coordinates as in the spherical case, there are, at least, two alternative methods for describing a system with cylindrical symmetry or different geometries along all three coordinate axes.

#### Combination of one and two dimensions

The relative coordinates, which are important when describing correlations, can be described by the usual  $N-1$  Jacobi vectors, which are now related to two hyperradii and corresponding hyperangles by

$$\boldsymbol{\eta}_k = \begin{pmatrix} \rho_{\perp,k} \sin \alpha_k \cos \varphi_k \\ \rho_{\perp,k} \sin \alpha_k \sin \varphi_k \\ \rho_{z,k} \sin \beta_k \end{pmatrix}, \quad k = 1, 2, \dots, N-1, \quad (\text{A.41})$$

where  $\rho_{\perp,N-1} = \rho_{\perp}$  and  $\rho_{\perp,k} = \rho_{\perp} \cos \alpha_{N-1} \cdots \cos \alpha_{k+1}$  for  $k = 1, 2, \dots, N-2$ . Analogue relations hold for  $\rho_{z,k}$ , especially  $\rho_{z,N-1} = \rho_z$ . The recursions stop at  $\beta_1 = \alpha_1 = \pi/2$ . We collectively denote the angles by  $\Omega$ .\* The volume element

\*The description can be extended to describe deformations along all axes. Then the  $\rho_{\perp}$ -part is separated into  $\rho_x$ - and  $\rho_y$ -parts, that are similar to the  $\rho_z$ -part in the present description.

becomes

$$\prod_{k=1}^{N-1} d\boldsymbol{\eta}_k = d\rho_{\perp} \rho_{\perp}^{2(N-1)-1} d\rho_z \rho_z^{(N-1)-1} d\varphi_1 \times \quad (\text{A.42})$$

$$\prod_{k=2}^{N-1} \left[ d\alpha_k \sin \alpha_k \cos^{2(k-1)-1} \alpha_k d\beta_k \cos^{(k-1)-1} \beta_k d\varphi_k \right].$$

The relative Laplacian operator becomes

$$\hat{\Delta} = \hat{\Delta}_{\rho_z} + \hat{\Delta}_{\rho_{\perp}} - \frac{\hat{\Lambda}_{2,N-1}^2}{\rho_{\perp}^2} - \frac{\hat{\Lambda}_{1,N-1}^2}{\rho_z^2}, \quad (\text{A.43})$$

$$\hat{\Delta}_{\rho_q} = \frac{1}{\rho_q^{d(N-1)-1}} \frac{\partial}{\partial \rho_q} \rho_q^{d(N-1)-1} \frac{\partial}{\partial \rho_q}, \quad (\text{A.44})$$

where  $d = 1$  for  $q = z$ ,  $d = 2$  for  $q = \perp$ , and  $\hat{\Lambda}_{d,N-1}$  is the operator in  $d$  spatial dimensions given previously by equation (A.36). The angles to enter equation (A.36) are for  $d = 1$  the  $\beta_k$ 's, and for  $d = 2$  the  $\alpha_k$ 's and  $\varphi_k$ 's.

Parametrization of the hyperradius

Alternatively, one common hyperradius can be used along with an angle  $\theta$  which parametrizes the axial and plane contributions as follows:

$$\boldsymbol{\eta}_k = \rho \begin{pmatrix} \sin \theta \cos \alpha_{N-1} \cdots \cos \alpha_{k+1} \sin \alpha_k \cos \varphi_k \\ \sin \theta \cos \alpha_{N-1} \cdots \cos \alpha_{k+1} \sin \alpha_k \sin \varphi_k \\ \cos \theta \cos \beta_{N-1} \cdots \cos \beta_{k+1} \sin \beta_k \end{pmatrix}, \quad (\text{A.45})$$

with  $\beta_1 = \alpha_1 = \pi/2$ . The volume element and the relative Laplacian becomes

$$\prod_{k=1}^{N-1} d\boldsymbol{\eta}_k = d\rho \rho^{3(N-1)-1} d\theta \cos^{(N-1)-1} \theta \sin^{2(N-1)-1} \theta \times \quad (\text{A.46})$$

$$d\varphi_1 \prod_{k=2}^{N-1} \left[ d\alpha_k \sin \alpha_k \cos^{2(k-1)-1} \alpha_k d\beta_k \cos^{(k-1)-1} \beta_k d\varphi_k \right],$$

$$\hat{\Delta} = \hat{\Delta}_{\rho} + \hat{\Delta}_{\theta} - \frac{\hat{\Lambda}_{2,N-1}^2}{\rho^2 \sin^2 \theta} - \frac{\hat{\Lambda}_{1,N-1}^2}{\rho^2 \cos^2 \theta}, \quad (\text{A.47})$$

$$\hat{\Delta}_{\rho} = \frac{1}{\rho^{3N-4}} \frac{\partial}{\partial \rho} \rho^{3N-4} \frac{\partial}{\partial \rho}, \quad (\text{A.48})$$

$$\hat{\Delta}_{\theta} = \frac{1}{\rho^2} \frac{1}{\cos^{N-2} \theta \sin^{2N-3} \theta} \frac{\partial}{\partial \theta} \cos^{N-2} \theta \sin^{2N-3} \theta \frac{\partial}{\partial \theta}, \quad (\text{A.49})$$

where  $\hat{\Lambda}_{d,N-1}$  is the operator in  $d$  spatial dimensions as before.

## Appendix B

### Hyperangular matrix elements

#### B.1 Alternative Jacobi trees

For use in the calculation of matrix elements different Jacobi trees have to be chosen [SS77]. The relevant ones in the context of the Faddeev- and angular variational equations are shown in figure B.1.

The coordinates of the standard tree of figure B.1a are defined by

$$\boldsymbol{\eta}_{N-1} = \frac{1}{\sqrt{2}}(\mathbf{r}_2 - \mathbf{r}_1), \quad (\text{B.1})$$

$$\boldsymbol{\eta}_{N-2} = \sqrt{\frac{2}{3}} \left[ \mathbf{r}_3 - \frac{1}{2}(\mathbf{r}_2 + \mathbf{r}_1) \right], \quad \dots, \quad (\text{B.2})$$

$$\boldsymbol{\eta}_1 = \sqrt{\frac{N-1}{N}} \left[ \mathbf{r}_N - \frac{1}{N-1}(\mathbf{r}_{N-1} + \dots + \mathbf{r}_1) \right]. \quad (\text{B.3})$$

In the (12)(34)-tree of figure B.1b two of the vectors are different from the standard tree:

$$\boldsymbol{\eta}_{N-2} = \frac{1}{\sqrt{2}}(\mathbf{r}_4 - \mathbf{r}_3), \quad (\text{B.4})$$

$$\boldsymbol{\eta}_{N-3} = \frac{1}{2}(\mathbf{r}_4 + \mathbf{r}_3 - \mathbf{r}_2 - \mathbf{r}_1). \quad (\text{B.5})$$

In the (123)(45)-tree of figure B.1c two of the vectors differ from the standard tree:

$$\boldsymbol{\eta}_{N-3} = \frac{1}{\sqrt{2}}(\mathbf{r}_5 - \mathbf{r}_4), \quad (\text{B.6})$$

$$\boldsymbol{\eta}_{N-4} = \sqrt{\frac{6}{5}} \left[ \frac{1}{2}(\mathbf{r}_5 + \mathbf{r}_4) - \frac{1}{3}(\mathbf{r}_3 + \mathbf{r}_2 + \mathbf{r}_1) \right]. \quad (\text{B.7})$$

In the (12)(345)-tree of figure B.1d three of the vectors deviate from the standard tree:

$$\boldsymbol{\eta}_{N-2} = \frac{1}{\sqrt{2}}(\mathbf{r}_4 - \mathbf{r}_3), \quad (\text{B.8})$$

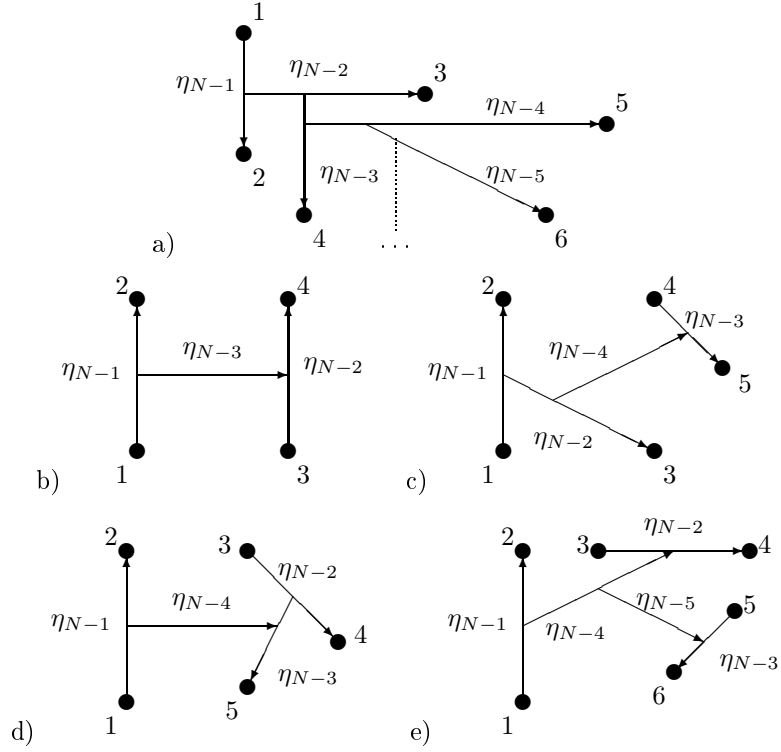


Figure B.1: Jacobi trees: a) standard, b) (12)(34), c) (123)(45), d) (12)(345), and e) (12)(34)(56).

$$\eta_{N-3} = \sqrt{\frac{2}{3}} \left[ r_5 - \frac{1}{2}(r_4 + r_3) \right], \quad (\text{B.9})$$

$$\eta_{N-4} = \sqrt{\frac{6}{5}} \left[ \frac{1}{3}(r_5 + r_4 + r_3) - \frac{1}{2}(r_2 + r_1) \right]. \quad (\text{B.10})$$

In the (12)(34)(56)-tree of figure B.1e four vectors are different:

$$\eta_{N-2} = \frac{1}{\sqrt{2}}(r_4 - r_3), \quad \eta_{N-3} = \frac{1}{\sqrt{2}}(r_6 - r_5), \quad (\text{B.11})$$

$$\eta_{N-4} = \frac{1}{2}(r_4 + r_3 - r_2 - r_1), \quad (\text{B.12})$$

$$\eta_{N-5} = \sqrt{\frac{4}{3}} \left[ \frac{1}{2}(r_6 + r_5) - \frac{1}{4}(r_4 + r_3 + r_2 + r_1) \right]. \quad (\text{B.13})$$

Since only inter-relations between  $\eta_{N-1}$ ,  $\eta_{N-2}$ , and  $\eta_{N-3}$  are needed in evaluating the matrix elements, we use the common notation:

$$\eta_{N-1} = \rho \sin \alpha, \quad \eta_{N-2} = \rho \cos \alpha \sin \beta \quad (\text{B.14})$$

$$\eta_{N-3} = \rho \cos \alpha \cos \beta \sin \gamma, \quad \boldsymbol{\eta}_k \cdot \boldsymbol{\eta}_l = \eta_k \eta_l \cos \vartheta_{k,l}. \quad (\text{B.15})$$

Here  $\vartheta_{k,l}$  is the angle between the  $k$ 'th and  $l$ 'th Jacobi vectors. We abbreviate  $\vartheta_{N-1,N-2} \rightarrow \vartheta_x$ ,  $\vartheta_{N-1,N-3} \rightarrow \vartheta_y$ , and  $\vartheta_{N-2,N-3} \rightarrow \vartheta_z$ . An azimuthal angle  $\varphi$  determining the projection of  $\boldsymbol{\eta}_{N-3}$  onto the plane of  $\boldsymbol{\eta}_{N-1}$  and  $\boldsymbol{\eta}_{N-2}$  is defined in the usual way such that

$$\cos \vartheta_z = \sin \vartheta_x \sin \vartheta_y \cos \varphi + \cos \vartheta_x \cos \vartheta_y. \quad (\text{B.16})$$

With  $\tau = \{\beta, \gamma, \vartheta_x, \vartheta_y, \varphi\}$  a matrix element of an arbitrary function  $f$  of all the variables  $\alpha$  and  $\tau$  then becomes

$$\int d\tau f(\alpha, \tau) = \frac{\int d\tilde{\tau} f(\alpha, \tau)}{\int d\tilde{\tau}}, \quad (\text{B.17})$$

$$\begin{aligned} \int d\tilde{\tau} g(\alpha, \tau) &= \int_0^{\pi/2} d\beta \sin^2 \beta \cos^{3N-10} \beta \int_0^{\pi/2} d\gamma \sin^2 \gamma \cos^{3N-13} \gamma \\ &\times \int_0^\pi d\vartheta_x \sin \vartheta_x \int_0^\pi d\vartheta_y \sin \vartheta_y \int_0^{2\pi} d\varphi g(\alpha, \tau). \end{aligned} \quad (\text{B.18})$$

The normalization is explicitly  $\int d\tau = 1$ . In the following matrix elements we need relations for interparticle distances and therefore define  $\boldsymbol{\eta}_{ij} \equiv (\mathbf{r}_j - \mathbf{r}_i)/\sqrt{2}$  and the angle  $\alpha_{ij}$  related to  $\eta_{ij} = \rho \sin \alpha_{ij} = r_{ij}/\sqrt{2}$ .

## B.2 Matrix elements: Faddeev

Equations (2.73) and (2.74) are evaluated as follows.

In the integral  $\int d\tau \phi(\alpha_{34})$  a convenient choice of coordinates is the alternative Jacobi (12)(34)-tree of figure B.1b. The angle  $\alpha_{34}$  is associated with the distance  $r_{34} = \sqrt{2}\eta_{34}$  by the relation

$$\eta_{34} = \eta_{N-2} = \rho \cos \alpha \sin \beta = \rho \sin \alpha_{34} \iff \sin \alpha_{34} = \cos \alpha \sin \beta. \quad (\text{B.19})$$

The integrand  $\phi(\alpha_{34})$  only depends on  $\alpha_{34}$ , which is a function of  $\alpha$  and  $\beta$ . Therefore at fixed  $\alpha$  equation (B.17) reduces to

$$\begin{aligned} \int d\tau \phi(\alpha_{34}) &= \frac{\int_0^{\pi/2} d\beta \sin^2 \beta \cos^{3N-10} \beta \phi(\alpha_{34})}{\int_0^{\pi/2} d\beta \sin^2 \beta \cos^{3N-10} \beta} = \\ &\frac{4}{\sqrt{\pi}} \frac{\Gamma(\frac{3N-6}{2})}{\Gamma(\frac{3N-9}{2})} \int_0^{\pi/2} d\beta \sin^2 \beta \cos^{3N-10} \beta \phi(\alpha_{34}) \equiv \hat{\mathbf{R}}_{34}^{(N-2)} \phi(\alpha). \end{aligned} \quad (\text{B.20})$$

To describe three particles in  $\int d\tau \phi(\alpha_{13})$  simultaneously, Jacobi vectors of the standard tree are needed. The distance between particles 1 and 3 is related to the corresponding Jacobi vector

$$\boldsymbol{\eta}_{13} = \frac{1}{\sqrt{2}}(\mathbf{r}_3 - \mathbf{r}_1) = \frac{1}{2}\boldsymbol{\eta}_{N-1} + \frac{\sqrt{3}}{2}\boldsymbol{\eta}_{N-2}, \quad (\text{B.21})$$

The hyperangle  $\alpha_{13}$ , associated with the distance between particles 1 and 3 through  $\eta_{13} = r_{13}/\sqrt{2} = \rho \sin \alpha_{13}$ , is then

$$\sin^2 \alpha_{13} = \frac{1}{4} \sin^2 \alpha + \frac{3}{4} \cos^2 \alpha \sin^2 \beta + \frac{\sqrt{3}}{2} \sin \alpha \cos \alpha \sin \beta \cos \vartheta_x, \quad (\text{B.22})$$

where  $\vartheta_x$  is the angle between the Jacobi vectors  $\boldsymbol{\eta}_{N-1}$  and  $\boldsymbol{\eta}_{N-2}$ . Note that  $\phi(\alpha_{13})$ , through  $\alpha_{13}$ , for fixed  $\alpha$  depends on  $\beta$  and  $\vartheta_x$ , which leaves a two-dimensional integral. Therefore equation (B.17) becomes

$$\begin{aligned} \int d\tau \phi(\alpha_{13}) &= \frac{\int_0^{\pi/2} d\beta \sin^2 \beta \cos^{3N-10} \beta \int_0^\pi d\vartheta_x \sin \vartheta_x \phi(\alpha_{13})}{\int_0^{\pi/2} d\beta \sin^2 \beta \cos^{3N-10} \beta \int_0^\pi d\vartheta_x \sin \vartheta_x} \quad (\text{B.23}) \\ &= \frac{2}{\sqrt{\pi}} \frac{\Gamma(\frac{3N-6}{2})}{\Gamma(\frac{3N-9}{2})} \int_0^{\pi/2} d\beta \sin^2 \beta \cos^{3N-10} \beta \int_0^\pi d\vartheta_x \sin \vartheta_x \phi(\alpha_{13}). \end{aligned}$$

This integral can be reduced to one dimension by a partial integration. The final one-dimensional integral becomes

$$\begin{aligned} \int d\tau \phi(\alpha_{13}) &= \frac{4}{\sqrt{3\pi}} \frac{\Gamma(\frac{3N-6}{2})}{\Gamma(\frac{3N-7}{2})} \sin^{-1} \alpha \cos^{8-3N} \alpha \times \\ &\left[ \int_{(\alpha-\pi/3)\Theta(\alpha>\pi/3)}^{\pi/2-|\pi/6-\alpha|} d\alpha_{13} \cos^{3N-9} \gamma^+ \sin \alpha_{13} \cos \alpha_{13} \phi(\alpha_{13}) - \right. \quad (\text{B.24}) \\ &\left. \int_0^{(\pi/3-\alpha)\Theta(\pi/3>\alpha)} d\alpha_{13} \cos^{3N-9} \gamma^- \sin \alpha_{13} \cos \alpha_{13} \phi(\alpha_{13}) \right] \equiv \hat{\mathbf{R}}_{13}^{(N-2)} \phi(\alpha), \end{aligned}$$

where  $\sin^2 \gamma^\pm = 4(\sin^2 \alpha + \sin^2 \alpha_{13} \mp \sin \alpha \sin \alpha_{13})/3$ , and  $\Theta$  is the truth function.

### B.3 Matrix elements: variational

We first divide the integrals of equation (2.81) into similar terms, then compute them in general, and finally in the short-range limit.

#### B.3.1 Numbers of different terms

We have to evaluate the double sums of equation (2.81) including the potential:

$$\sum_{k<l}^N v_{kl} \sum_{i<j}^N \phi_{ij}. \quad (\text{B.25})$$

Three types of terms occur, due to the fact that we vary the wave function component  $\phi_{12}^*$  in equation (2.80): the potential concerning particles 1 and 2, the potential concerning one of the particles 1 or 2 and a third particle and the



potential concerning neither particle 1 nor 2, but a third and a fourth particle. We obtain

$$\begin{aligned} \sum_{k<l}^N v_{kl} &= v_{12} + \sum_{l=3}^N v_{1l} + \sum_{l=3}^N v_{2l} + \sum_{3\leq k<l}^N v_{kl} \\ &\rightarrow v_{12} + 2(N-2)v_{13} + \frac{1}{2}(N-2)(N-3)v_{34}, \end{aligned} \quad (\text{B.26})$$

where the arrow indicates the identity of the terms after integration over all angles except  $\alpha_{12}$ , i.e. analogously to the steps leading up to equation (2.72). Treating each of these in the quadruple sum, where the repeated use of arrows ( $\rightarrow$ ) has the meaning given just above:

Fixing  $\phi_{12}^*$  and  $v_{12}$  yields three different terms:

$$\begin{aligned} v_{12} \sum_{i<j}^N \phi_{ij} &= v_{12} \left( \phi_{12} + \sum_{j=3}^N \phi_{1j} + \sum_{j=3}^N \phi_{2j} + \sum_{3\leq i<j}^N \phi_{ij} \right) \\ &\rightarrow v_{12} \left[ \phi_{12} + 2(N-2)\phi_{13} + \frac{1}{2}(N-2)(N-3)\phi_{34} \right], \end{aligned} \quad (\text{B.27})$$

as shown in figure B.2.

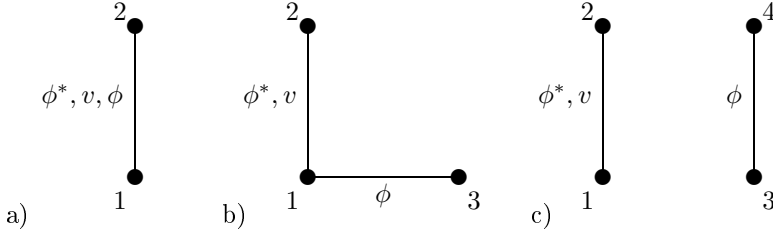


Figure B.2: Illustration of  $\phi_{12}^* v_{12}$ -terms.

Fixing  $\phi_{12}^*$  and  $v_{13}$  yields seven different terms. These can be identified in two steps, the first of which separates into four different sums:

$$v_{13} \sum_{i<j}^N \phi_{ij} = v_{13} \left( \sum_{j=2}^N \phi_{1j} + \sum_{j=3}^N \phi_{2j} + \sum_{j=4}^N \phi_{3j} + \sum_{4\leq i<j}^N \phi_{ij} \right). \quad (\text{B.28})$$

Each of these four terms are then identified as:

$$\begin{aligned} v_{13} \sum_{j=2}^N \phi_{1j} &= v_{13} \left( \phi_{12} + \phi_{13} + \sum_{j=4}^N \phi_{1j} \right) \\ &\rightarrow v_{13} [\phi_{12} + \phi_{13} + (N-3)\phi_{14}], \end{aligned} \quad (\text{B.29})$$

$$v_{13} \sum_{j=3}^N \phi_{2j} = v_{13} \left( \phi_{23} + \sum_{j=4}^N \phi_{2j} \right) \rightarrow v_{13} [\phi_{23} + (N-3)\phi_{24}], \quad (\text{B.30})$$

$$v_{13} \sum_{j=4}^N \phi_{3j} \rightarrow v_{13}(N-3)\phi_{34}, \quad (\text{B.31})$$

$$v_{13} \sum_{4 \leq i < j}^N \phi_{ij} \rightarrow v_{13} \frac{1}{2}(N-3)(N-4)\phi_{45}. \quad (\text{B.32})$$

The resulting seven types are shown in figure B.3.

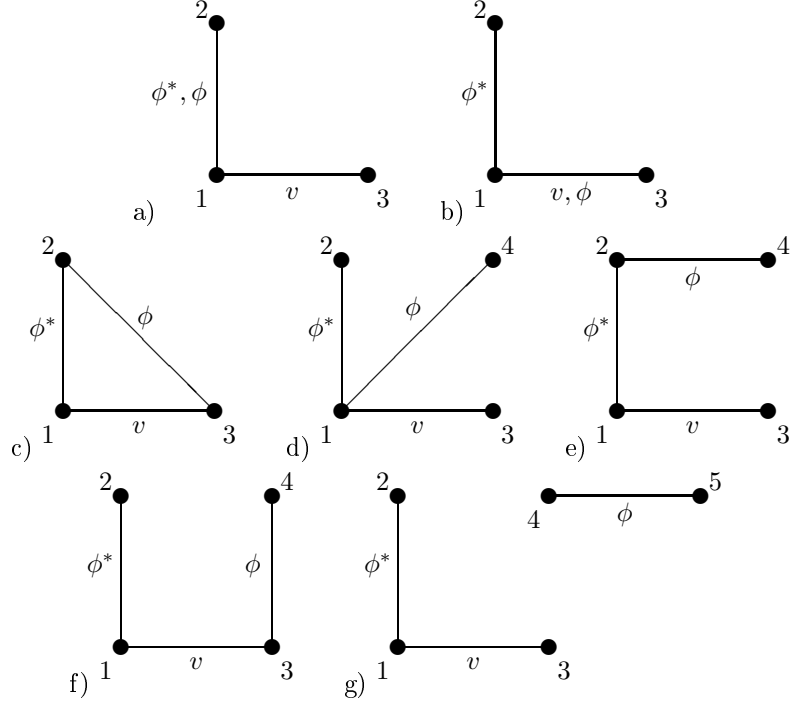


Figure B.3: Illustration of  $\phi_{12}^* v_{13}$ -terms.

Fixing  $\phi_{12}^*$  and  $v_{34}$  yields six different terms, identified as follows. The first step is:

$$v_{34} \sum_{i < j}^N \phi_{ij} = v_{34} \left( \sum_{j=2}^N \phi_{1j} + \sum_{j=3}^N \phi_{2j} + \sum_{j=4}^N \phi_{3j} + \sum_{j=5}^N \phi_{4j} + \sum_{5 \leq i < j}^N \phi_{ij} \right). \quad (\text{B.33})$$

In the next step the sums are treated:

$$v_{34} \sum_{j=2}^N \phi_{1j} = v_{34} \left( \phi_{12} + \phi_{13} + \phi_{14} + \sum_{j=5}^N \phi_{1j} \right)$$

$$\rightarrow v_{34} [\phi_{12} + 2\phi_{13} + (N - 4)\phi_{15}] , \quad (\text{B.34})$$

$$v_{34} \sum_{j=3}^N \phi_{2j} = v_{34} \left( \phi_{23} + \phi_{24} + \sum_{j=5}^N \phi_{2j} \right) \rightarrow v_{34} [2\phi_{13} + (N - 4)\phi_{15}] , \quad (\text{B.35})$$

$$v_{34} \sum_{j=4}^N \phi_{3j} = v_{34} \left( \phi_{34} + \sum_{j=5}^N \phi_{3j} \right) \rightarrow v_{34} [\phi_{34} + (N - 4)\phi_{35}] , \quad (\text{B.36})$$

$$v_{34} \sum_{j=5}^N \phi_{4j} \rightarrow v_{34} (N - 4)\phi_{35} , \quad (\text{B.37})$$

$$v_{34} \sum_{5 \leq i < j}^N \phi_{ij} \rightarrow v_{34} \frac{1}{2} (N - 4)(N - 5)\phi_{56} . \quad (\text{B.38})$$

See the six types in figure B.4.

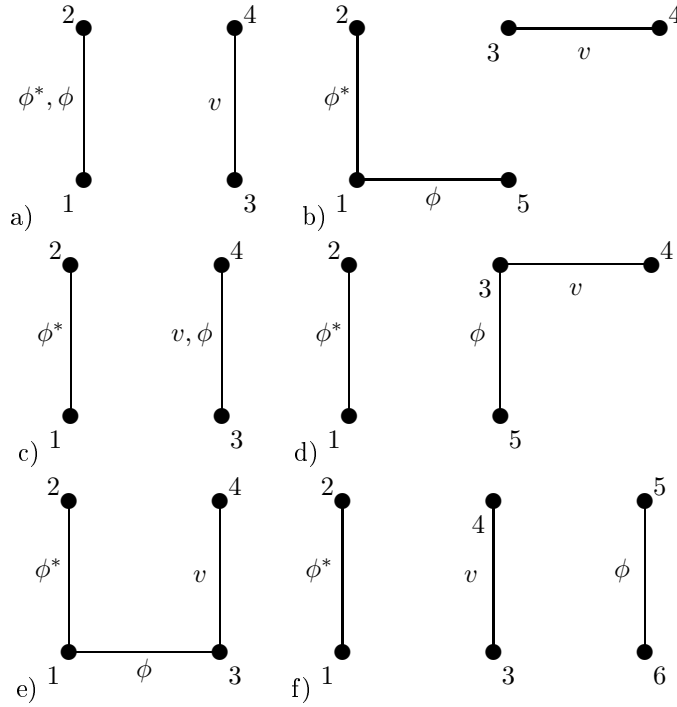


Figure B.4: Illustration of  $\phi_{12}^* v_{34}$ -terms.

### B.3.2 Evaluation of terms

The term of figure B.2a is trivial since the integrand is independent of  $\tau$ . The terms of figures B.2b, B.2c, B.3a, B.3b, B.4a, and B.4c can be evaluated by

equations (B.21) and (B.24).

The term of figure B.3c becomes with the use of the standard Jacobi tree of figure B.1a

$$\int d\tau f(\alpha_{13}) g(\alpha_{23}) = \frac{2}{\sqrt{\pi}} \frac{\Gamma(\frac{3N-6}{2})}{\Gamma(\frac{3N-9}{2})} \times \int_0^{\pi/2} d\beta \sin^2 \beta \cos^{3N-10} \beta \int_0^\pi d\vartheta \sin \vartheta f(\alpha_{13}) g(\alpha_{23}), \quad (\text{B.39})$$

$$\sin^2 \alpha_{13,23} = \frac{3}{4} \cos^2 \alpha \sin^2 \beta + \frac{1}{4} \sin^2 \alpha \pm \frac{\sqrt{3}}{2} \cos \alpha \sin \alpha \sin \beta \cos \vartheta. \quad (\text{B.40})$$

The term of figure B.4f becomes with the use of the alternative (12)(34)(56)-tree of figure B.1e

$$\int d\tau v(\alpha_{34}) \phi(\alpha_{56}) = \frac{2A_N}{\pi} \times \quad (\text{B.41})$$

$$\int d\beta \sin^2 \beta \cos^{3N-10} \beta \int d\gamma \sin^2 \gamma \cos^{3N-13} \gamma v(\alpha_{34}) \phi(\alpha_{56}),$$

$$\sin \alpha_{34} = \cos \alpha \sin \beta, \quad \sin \alpha_{56} = \cos \alpha \cos \beta \sin \gamma, \quad (\text{B.42})$$

$$A_N \equiv (3N-8)(3N-10)(3N-12). \quad (\text{B.43})$$

The terms of figures B.3g, B.4b, and B.4d are evaluated using the (123)(45)- and (12)(345)-trees of figures B.1c and B.1d, so

$$\int d\tau I_5(\alpha, \tau) = \frac{A_N}{\pi} \int_0^{\pi/2} d\beta \sin^2 \beta \cos^{3N-10} \beta \times \int_0^{\pi/2} d\gamma \sin^2 \gamma \cos^{3N-13} \gamma \int_0^\pi d\vartheta_{x,z} \sin \vartheta_{x,z} I_5(\alpha, \tau), \quad (\text{B.44})$$

where  $I_5(\alpha, \tau)$  can be either  $v(\alpha_{34})\phi(\alpha_{35})$  or  $f(\alpha_{13})g(\alpha_{45})$ . The relevant angles are

$$\sin \alpha_{34} = \cos \alpha \sin \beta, \quad \sin \alpha_{45} = \cos \alpha \cos \beta \sin \gamma, \quad (\text{B.45})$$

$$\sin^2 \alpha_{35} = \frac{\cos^2 \alpha}{4} \left( 3 \cos^2 \beta \sin^2 \gamma + \sin^2 \beta + 2\sqrt{3} \cos \beta \sin \beta \sin \gamma \cos \vartheta_z \right), \quad (\text{B.46})$$

and  $\alpha_{13}$  given by equation (B.22). Note the identity  $\int d\tau v(\alpha_{34})\phi(\alpha_{15}) = \int d\tau \phi(\alpha_{13})v(\alpha_{45})$ .

The terms of figures B.3d, B.3e, B.3f, and B.4e are evaluated using the standard Jacobi tree. Then equation (B.17) reduces to, with  $i = 1, 2, 3$ ,

$$\int d\tau f(\alpha_{13}) g(\alpha_{i4}) = \frac{A_N}{4\pi^2} \int_0^{\pi/2} d\beta \sin^2 \beta \cos^{3N-10} \beta \int_0^\pi d\vartheta_x \sin \vartheta_x \times \int_0^{\pi/2} d\gamma \sin^2 \gamma \cos^{3N-13} \gamma \int_0^\pi d\vartheta_y \sin \vartheta_y \int_0^{2\pi} d\varphi f(\alpha_{13}) g(\alpha_{i4}). \quad (\text{B.47})$$

The angles  $\alpha_{ij}$  can be determined by  $\rho \sin \alpha_{ij} = \eta_{ij}$  through the relations

$$\eta_{13} = \frac{\sqrt{3}}{2} \eta_{N-2} + \frac{1}{2} \eta_{N-1}, \quad (\text{B.48})$$

$$\eta_{14} = \sqrt{\frac{2}{3}} \eta_{N-3} + \frac{1}{2\sqrt{3}} \eta_{N-2} + \frac{1}{2} \eta_{N-1}, \quad (\text{B.49})$$

$$\eta_{24} = \sqrt{\frac{2}{3}} \eta_{N-3} + \frac{1}{2\sqrt{3}} \eta_{N-2} - \frac{1}{2} \eta_{N-1}, \quad (\text{B.50})$$

$$\eta_{34} = \sqrt{\frac{2}{3}} \eta_{N-3} - \frac{1}{\sqrt{3}} \eta_{N-2}. \quad (\text{B.51})$$

### B.3.3 Results in the short-range limit

The integrals in the short-range limit, when the range  $b$  of  $V(r_{ij})$  is much smaller than the size scale  $\rho$ , are:

$$\int d\tau v(\alpha_{34}) \phi(\alpha_{13}) \simeq v_1(\alpha) \hat{\mathbf{R}}_{3413}^{(2)} \phi(\alpha), \quad (\text{B.52})$$

$$\int d\tau v(\alpha_{34}) \phi(\alpha_{15}) \simeq v_1(\alpha) \hat{\mathbf{R}}_{13}^{(N-3)} \phi(\alpha), \quad (\text{B.53})$$

$$\int d\tau v(\alpha_{34}) \phi(\alpha_{34}) = \hat{\mathbf{R}}_{34}^{(N-2)} v \phi(\alpha) \simeq v_1(\alpha) \phi(0), \quad (\text{B.54})$$

$$\int d\tau v(\alpha_{34}) \phi(\alpha_{35}) \simeq v_1(\alpha) \hat{\mathbf{R}}_{3435}^{(1)} \phi(\alpha), \quad (\text{B.55})$$

$$\int d\tau v(\alpha_{34}) \phi(\alpha_{56}) \simeq v_1(\alpha) \hat{\mathbf{R}}_{34}^{(N-3)} \phi(\alpha), \quad (\text{B.56})$$

$$\int d\tau v(\alpha_{13}) \phi(\alpha_{13}) = \hat{\mathbf{R}}_{13}^{(N-2)} v \phi(\alpha) \simeq v_2(\alpha) \phi(0), \quad (\text{B.57})$$

$$\int d\tau v(\alpha_{13}) \phi(\alpha_{i4}) \simeq v_2(\alpha) \hat{\mathbf{R}}_{1314}^{(2)} \phi(\alpha); \quad i = 1, 3, \quad (\text{B.58})$$

$$\int d\tau v(\alpha_{13}) \phi(\alpha_{23}) \simeq v_2(\alpha) \phi(\alpha), \quad (\text{B.59})$$

$$\int d\tau v(\alpha_{13}) \phi(\alpha_{24}) \simeq v_2(\alpha) \hat{\mathbf{R}}_{1324}^{(2)} \phi(\alpha), \quad (\text{B.60})$$

$$\int d\tau v(\alpha_{13}) \phi(\alpha_{45}) \simeq v_2(\alpha) \hat{\mathbf{R}}_{1345}^{(1)} \phi(\alpha). \quad (\text{B.61})$$

The integrals are given by

$$\hat{\mathbf{R}}_{ijkl}^{(1)} \phi(\alpha) \equiv \frac{4}{\sqrt{\pi}} \frac{\Gamma(\frac{3N-9}{2})}{\Gamma(\frac{3N-12}{2})} \int_0^{\pi/2} d\gamma \sin^2 \gamma \cos^{3N-13} \gamma \phi(\alpha_{kl}^0), \quad (\text{B.62})$$

where  $\sin \alpha_{35}^0 \equiv \sqrt{3} \cos \alpha \sin \gamma / 2$ ,  $\sin \alpha_{45}^0 \equiv \cos \alpha \cos \beta_0 \sin \gamma$ ,  $\sin \beta_0 \equiv \tan \alpha / \sqrt{3}$ , and

$$\begin{aligned} \hat{R}_{ijkl}^{(2)} \phi(\alpha) &\equiv \frac{2}{\sqrt{\pi}} \frac{\Gamma(\frac{3N-9}{2})}{\Gamma(\frac{3N-12}{2})} \int_0^{\pi/2} d\gamma \sin^2 \gamma \cos^{3N-13} \gamma \\ &\times \int_0^\pi d\vartheta_x \sin \vartheta_x \phi(\alpha_{kl}^0), \end{aligned} \quad (\text{B.63})$$

$$\begin{aligned} \sin^2 \alpha_{14}^0 &\equiv \frac{1}{9} \sin^2 \alpha + \frac{2}{3} \cos^2 \alpha \cos^2 \beta_0 \sin^2 \gamma \\ &+ \frac{2\sqrt{2}}{3\sqrt{3}} \sin \alpha \cos \alpha \cos \beta_0 \sin \gamma \cos \vartheta_x, \end{aligned} \quad (\text{B.64})$$

$$\begin{aligned} \sin^2 \alpha_{24}^0 &\equiv \frac{4}{9} \sin^2 \alpha + \frac{2}{3} \cos^2 \alpha \cos^2 \beta_0 \sin^2 \gamma \\ &+ \frac{4\sqrt{2}}{3\sqrt{3}} \sin \alpha \cos \alpha \cos \beta_0 \sin \gamma \cos \vartheta_x, \end{aligned} \quad (\text{B.65})$$

$$\begin{aligned} \sin^2 \alpha_{13}^0 &\equiv \frac{1}{4} \sin^2 \alpha + \frac{1}{2} \cos^2 \alpha \sin^2 \gamma \\ &+ \frac{1}{\sqrt{2}} \sin \alpha \cos \alpha \sin \gamma \cos \vartheta_x. \end{aligned} \quad (\text{B.66})$$

The two-dimensional integral  $\hat{R}_{ijkl}^{(2)} \phi(\alpha)$  can be reduced to a one-dimensional integral, analogously to equation (B.24), by a transformation of the general form

$$I = \int_0^{\pi/2} d\gamma \sin^2 \gamma \cos^p \gamma \int_0^\pi d\vartheta \sin \vartheta \phi(\alpha'), \quad (\text{B.67})$$

$$\sin^2 \alpha' = f^2(\alpha) + g^2(\alpha) \sin^2 \gamma + 2f(\alpha)g(\alpha) \sin \gamma \cos \vartheta, \quad (\text{B.68})$$

to the one-dimensional integral

$$\begin{aligned} I &= \frac{1}{2f(\alpha)g(\alpha)(p+1)} \left[ \int_{\text{MAX}\{0, \alpha'^-\}}^{\alpha'^+} d\alpha' \sin 2\alpha' \cos^{p+1} \gamma^+ \phi(\alpha') \right. \\ &\quad \left. - \int_0^{\text{MAX}\{0, -\alpha'^-\}} d\alpha' \sin 2\alpha' \cos^{p+1} \gamma^- \phi(\alpha') \right], \end{aligned} \quad (\text{B.69})$$

$$\sin \gamma^\pm \equiv \frac{\pm \sin \alpha' - f(\alpha)}{g(\alpha)}, \quad \sin \alpha'^\pm = f(\alpha) \pm g(\alpha). \quad (\text{B.70})$$

The function  $\text{MAX}\{x, y\}$  outputs the largest of the two numbers  $x$  and  $y$ .

## Appendix C

### Properties of Jacobi functions

The Jacobi function  $\mathcal{P}_\nu^{(a,b)}(x)$  is related to the hyperangular kinetic-energy eigenfunctions. More specifically, an eigenfunction to the operator  $\hat{\Pi}_k^2$  from equation (A.37) is  $\mathcal{P}_\nu^{(a,b)}(x)$  with  $x = \cos 2\alpha_k$ ,  $a = (d-2)/2$ , and  $b = d(k-1)/2 - 1$ . Some relevant properties of these functions in the relation to the hyperspherical treatments are given by Nielsen *et al.* [NFJG01]. The important properties in this context are the following [AS65, NFJG01].

The Jacobi function  $\mathcal{P}_\nu^{(a,b)}(x)$  is a solution to the differential equation

$$(1+x^2)y''(x) + [a+b+(a+b+1)x]y'(x) + \nu(\nu+a+b+1)y(x) = 0. \quad (\text{C.1})$$

A second solution is  $\mathcal{P}_\nu^{(b,a)}(-x)$ , which for integer  $\nu$  is identical to  $\mathcal{P}_\nu^{(a,b)}(x)$ . For non-integer  $\nu$  the Jacobi function  $\mathcal{P}_\nu(x)$  is regular at  $x=1$  and irregular at  $x=-1$ . We will for integer  $\nu$  not consider the irregular solution, which diverges at both  $x = \pm 1$ .

Important relations for the Jacobi function are

$$\begin{aligned} \mathcal{P}_\nu^{(a,b)}(x) &= \frac{\Gamma(\nu+a+1)}{\Gamma(\nu+1)\Gamma(a+1)} \mathcal{F}\left(-\nu, \nu+a+b+1; a+1; \frac{1-x}{2}\right), \quad (\text{C.2}) \\ \mathcal{P}_\nu^{(b,a)}(x) &= \frac{\Gamma(-a)}{\Gamma(\nu+1)\Gamma(-\nu-a)} \mathcal{F}\left(-\nu, \nu+a+b+1; 1+a; \frac{1+x}{2}\right) \\ &\quad + \frac{\Gamma(a)\Gamma(\nu+b+1)}{\Gamma(\nu+1)\Gamma(-\nu)\Gamma(\nu+a+b+1)} \left(\frac{1+x}{2}\right)^{-a} \\ &\quad \times \mathcal{F}\left(\nu+b+1, -\nu-a; 1-a; \frac{1+x}{2}\right), \quad (\text{C.3}) \end{aligned}$$

where  $\mathcal{F}$  is the hypergeometric function  ${}_2F_1$  [AS65].

For small values of the argument  $\alpha_k$  they can be rewritten via

$$\mathcal{P}_\nu^{(a,b)}(x) = \mathcal{P}_\nu^{(b,a)}(-x) \cos \pi\nu - \mathcal{Q}_\nu^{(b,a)}(-x) \sin \pi\nu, \quad (\text{C.4})$$

$$\mathcal{P}_\nu^{(a,b)}(\cos 2\alpha) = \frac{\Gamma(\nu+a+1)}{\Gamma(\nu+1)\Gamma(a+1)}, \quad (\text{C.5})$$

$$\mathcal{Q}_\nu^{(a,b)}(\cos 2\alpha) = \frac{\Gamma(a)\Gamma(\nu+b+1)}{\pi\Gamma(\nu+a+b+1)}\alpha^{-2a} \quad \text{for } a > 0. \quad (\text{C.6})$$

Some properties of the gamma function  $\Gamma(x)$  are  $\Gamma(x+1) = x\Gamma(x)$ ,  $\Gamma(x)\Gamma(1-x) = \pi/\sin(\pi x)$ , and  $\Gamma(A+x)/\Gamma(A) \rightarrow A^x$  for  $A \gg |x|$ .

### Rotation properties

For integer values of the quantum number  $\nu$  the Jacobi function for  $d = 3$  and  $k = N - 1$ , i.e.  $a = 1/2$  and  $b = 3N/2 - 4$ , can be written as the polynomial (omitting upper indices)

$$\mathcal{P}_\nu(\cos 2\alpha) = \sum_{n=0}^{\nu} c_{\nu,n} \sin^{2n} \alpha, \quad (\text{C.7})$$

$$c_{\nu,0} = 1, \quad (\text{C.8})$$

$$c_{\nu,n+1} = -c_{\nu,n} \frac{(3N-5)(\nu-n) + 2(\nu^2 - n^2)}{(n+1)(2n+3)}. \quad (\text{C.9})$$

Some rotation properties of these kinetic-energy eigenfunctions are

$$\hat{\mathbf{R}}_{13}^{(N-2)} \mathcal{P}_0 = \mathcal{P}_0, \quad \hat{\mathbf{R}}_{34}^{(N-2)} \mathcal{P}_0 = \mathcal{P}_0, \quad (\text{C.10})$$

$$\hat{\mathbf{R}}_{13}^{(N-2)} \mathcal{P}_1 = \frac{N-5}{4(N-2)} \mathcal{P}_1, \quad (\text{C.11})$$

$$\hat{\mathbf{R}}_{34}^{(N-2)} \mathcal{P}_1 = -\frac{1}{N-2} \mathcal{P}_1. \quad (\text{C.12})$$

Related properties are

$$\hat{\mathbf{R}}_{13}^{(N-2)} \sin^2 \alpha = \frac{1}{4(N-2)} [3 + (N-5) \sin^2 \alpha], \quad (\text{C.13})$$

$$\hat{\mathbf{R}}_{34}^{(N-2)} \sin^{2n} \alpha = \frac{\Gamma(\frac{3N-6}{2})}{\Gamma(\frac{3N-6}{2} + n)} \frac{\Gamma(\frac{3}{2} + n)}{\Gamma(\frac{3}{2})} \cos^{2n} \alpha. \quad (\text{C.14})$$



## Appendix D

### Numerical scalings of angular potential

Chapter 3 contained an account of the properties of the numerically obtained angular eigenvalues. We collect here some of the details behind the parametrization of the angular eigenvalue in equations (3.37) and (3.38). They were published as a part of a larger article [SFJ03a] and are kept here for completeness.

#### D.1 Effective dependence on the scattering length

The angular eigenvalue spectrum coincides with the free spectrum at both small and large hyperradii; at  $\rho = 0$  because all interactions are multiplied by  $\rho^2$  and at  $\rho = \infty$  because the short-range interaction has no effect at infinitely large distances. Thus, perturbation theory for a Gaussian potential shows that for small  $\rho$  the eigenvalues all change from their hyperspherical values  $\lambda_\nu(0) = 2\nu(2\nu + 3N - 5)$  with  $\nu = 0, 1, \dots$  as

$$\lambda_\nu(\rho) - \lambda_\nu(0) = \frac{mV(0)}{\hbar^2} N(N-1)\rho^2. \quad (\text{D.1})$$

If the two-body potential is attractive, but too weak to support a bound state, the eigenvalues reach a minimum and then return to one of the finite hyperspherical values. For a two-body bound state of energy  $E^{(2)}$  one eigenvalue diverges as  $\lambda = 2mE^{(2)}\rho^2/\hbar^2$ . The corresponding structure describes, appropriately symmetrized, one pair of particles in that bound state and all others far apart from the pair and from each other. In addition to this finite number of such eigenvalues the hyperspherical spectrum emerges at large distances.

To illustrate we show in figure D.1 a number of angular eigenvalues  $\lambda$  as functions of hyperradius for different potentials. The entirely positive (solid line) corresponds to a repulsive Gaussian. The curves diverging at large hyperradii (dotted and thick dot-dashed lines) correspond to potentials with one bound two-body state.

The convergence of  $\lambda$  as  $\rho \rightarrow 0$  is due to the finite range of the potential and depends on the interaction range  $b$ . The deep minima at small to intermediate distances depend strongly on both the number of particles and the strength of

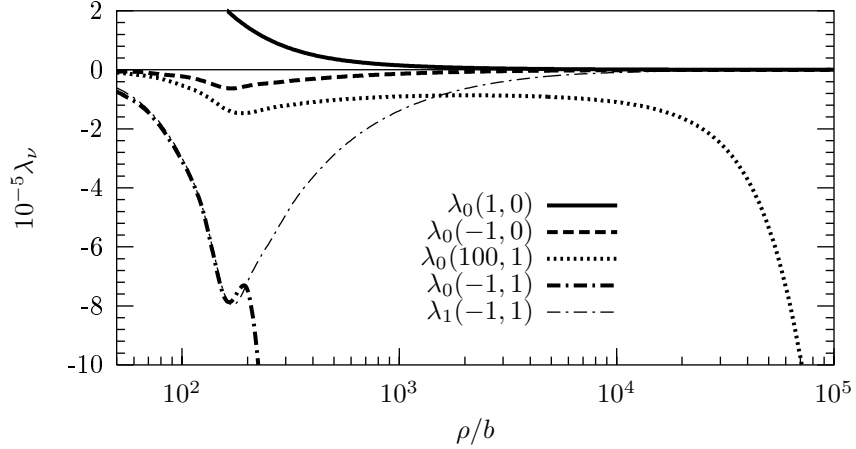


Figure D.1: Angular eigenvalues  $\lambda_\nu$  (divided by  $10^5$ ) as functions of hyperradius divided by interaction range,  $\rho/b$ , for  $N = 100$ , for scattering lengths  $a_s/b$  and numbers of bound two-body states  $\mathcal{N}_B$  indicated as  $\lambda_\nu(a_s/b, \mathcal{N}_B)$  on the figure.

the attraction. Increasing the strength of the attraction leads to larger negative values of  $\lambda$ . This trend continues by increasing the attraction even further until the same scattering length is reached but now with one bound two-body state.

The asymptotic behaviour of  $\lambda$  is compared to the zero-range result  $\lambda_\delta$  in figure D.2. The convergence to the limiting value is fastest for the smallest value of  $a_s$  (dashed curve) already reflecting that the correlations arising for large scattering lengths (dotted line) cannot be accounted for by the simple zero-range result. This is well understood for three particles where the Efimov effect (very large  $a_s$ ) extends correlations in hyperradius to distances around four times the average scattering length [FJ93, JGF97]. These effects are not present in the mean-field type of zero-range expectation value contained in  $\lambda_\delta$ . When  $\rho$  exceeds  $a_s$  by a sufficiently large amount  $\lambda_\delta$  is approached.

The positive scattering length also leads to an eigenvalue approaching  $\lambda_\delta$  at large distance with a similar convergence rate (solid curve). A stronger attraction corresponding to one bound two-body state produces one diverging eigenvalue while the second eigenvalue converges towards the lowest hyperspherical value (dot-dashed curve). It almost coincides with the lowest eigenvalue for the same scattering length but for a potential without bound two-body states (dotted curve).

The deviations from  $\lambda_\delta$  at large distance is in all cases less than 10%. The asymptotic behaviour is very smooth but still originating in systematic numerical inaccuracies which can be cured by increasing the number of integration points in the finite-difference scheme.

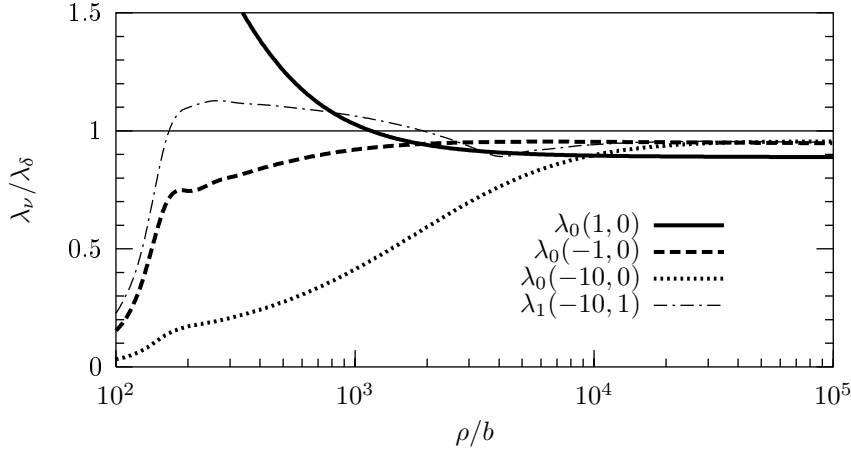


Figure D.2: Same as figure D.1, but the angular potential is shown in units of the zero-range result in equation (3.31).

## D.2 Dependence on the number of particles

The angular eigenvalues increase rapidly with  $N$  as seen from the  $N^{7/2}$ -dependence in  $\lambda_\delta$ , equation (3.31). The major variation in magnitude is then accounted for by using this large-distance zero-range result as the scaling unit. Figure D.3 shows a series of calculations for the same two-body interaction for different numbers of atoms. All curves are similar, i.e. there is a systematic increase in the characteristic hyperradius, where the curves bend over and approach the zero-range result. The large-distance asymptote is determined by the scattering length. A characteristic length  $\rho_a$  is conveniently defined by

$$\rho_a(N) \equiv N^{7/6} |a_s|, \quad (\text{D.2})$$

where the power is obtained numerically to be very close to the indicated value  $7/6$ .

The quality of this scaling is seen in figure D.4 where all curves essentially coincide for distances smaller than  $\rho_a$ . At larger hyperradii the zero-range result of  $+1$  should be obtained. However, here numerical inaccuracies produce systematic deviations from a common curve, i.e. the deviations increase with  $N$ .

The numerical curves can be rather well reproduced by the function

$$\lambda^{(-)}(N, \rho) = |\lambda_\delta(N, \rho)| \cdot g^{(-)}(\rho/\rho_a), \quad (\text{D.3})$$

$$g^{(-)}(x) = g_\infty (1 - e^{-x/x_a}) \left(1 + \frac{x_b}{x}\right), \quad (\text{D.4})$$

where  $g_\infty$  has the value  $-1$  in accurate calculations, because  $a_s < 0$ . The exponential term reproduces the rather steep approach to the asymptotic value

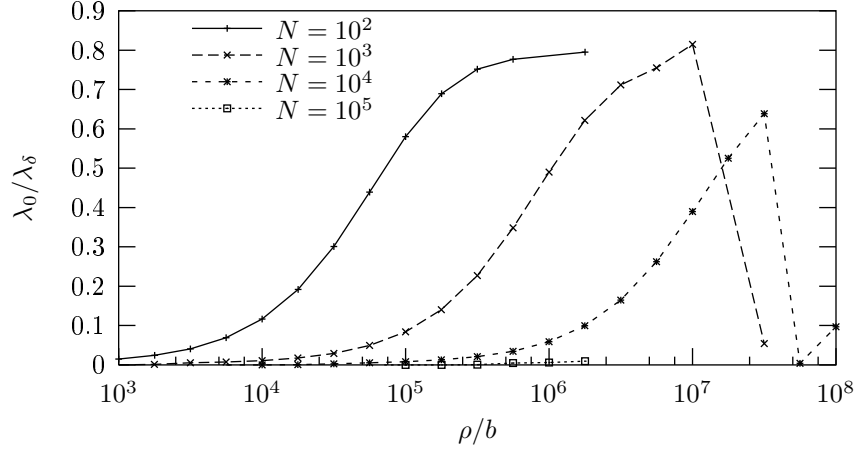


Figure D.3: The lowest angular eigenvalue as a function of hyperradius for  $a_s/b = -401$  for four different numbers of particles  $N = 10^2, 10^3, 10^4, 10^5$ . The angular potentials are in units of  $\lambda_\delta$ .

as seen in figure D.4. The behaviour at smaller distance, depending on the range of the interaction, is here simulated by the  $x_b$ -term. The extreme limit of  $\rho \rightarrow 0$  is not computed and not included in the approximate function in equation (D.4).

The two groups of computations in figure D.4 are reasonably reproduced by the parameter sets  $x_a \simeq 0.74$ ,  $x_b \simeq 2.3 \cdot 10^{-3}$ , and  $g_\infty \simeq -0.8$  or  $g_\infty \simeq -0.4$  for the high and low accuracy, respectively. These parameters may also depend on the scattering length. Table D.1 gives the best choice of parameters for different  $a_s$ .

$a_s/b$	-5.98	-401	-799	-4212
$-g_\infty$	0.99	0.80	0.65	0.30
$x_a$	1.06	0.74	0.59	0.28
$-g_\infty/x_a$	0.93	1.081	1.099	1.077
$x_b$	0.15	$2.3 \cdot 10^{-3}$	$1.15 \cdot 10^{-3}$	$2.2 \cdot 10^{-4}$
$x_b/(b/ a_s )$	0.92	0.922	0.919	0.927

Table D.1: Numerical values of  $g_\infty$ ,  $x_a$ , and  $x_b$  for four scattering lengths.

It should be noticed that  $-g_\infty$  and  $x_a$  both are of order unity, and that the fraction  $g_\infty/x_a$  is almost constant, except for the smallest scattering length. The parameter  $x_b$ , introduced to account for the finite interaction range, is close to  $b/|a_s|$ .

At large hyperradii, where  $x_a \ll \rho/\rho_a$  or equivalently  $\rho \gg N^{7/6}|a_s|$ ,  $\lambda^{(-)}$  approaches  $g_\infty|\lambda_\delta|$ . The expected large-distance asymptotic behaviour is  $\lambda^{(-)} \rightarrow$

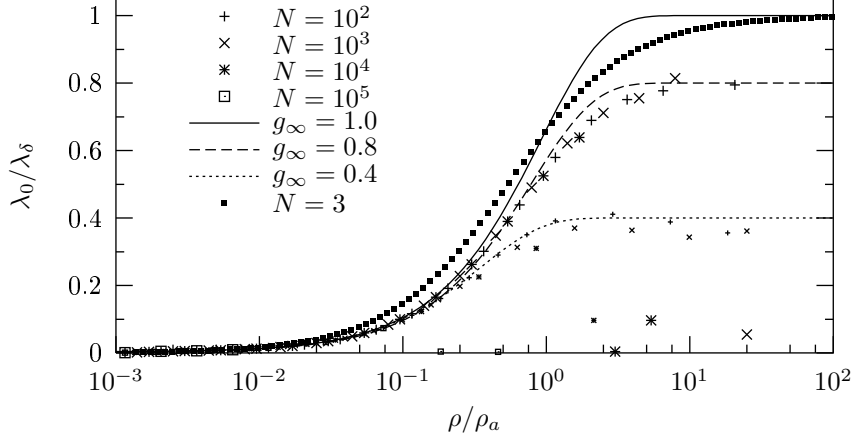


Figure D.4: The same as figure D.3, but with  $\rho$  in units of  $\rho_a$ . The larger points following the intermediate curve ( $g_\infty = -0.8$ ) are calculated with the highest numerical accuracy and the smaller points along the upper curve ( $g_\infty = -0.4$ ) are obtained with lower accuracy. The curve for  $g_\infty = -1.0$  is the expected correct asymptotic behaviour.

$\lambda_\delta$  and  $g_\infty$  should therefore approach  $-1$  in increasingly accurate calculations. The results for  $N = 100$  and different scattering lengths, see figure D.2, confirm this conclusion by deviating less than 10% from  $\lambda_\delta$  at large hyperradii.

A well-established result for  $N = 3$  identical bosons is the large-distance behaviour [JGF97]

$$\lambda_\delta(N = 3, \rho) = \frac{48a_s}{\sqrt{2\pi\rho}}, \quad (\text{D.5})$$

which is in agreement with  $\lambda_\delta$  obtained from equation (3.31) for  $N = 3$ . Then the universal function  $g^{(-)}$  asymptotically approaches  $g_\infty = -1$  for all scattering lengths.

The function  $g^{(-)}$  is almost independent of  $N$ . This combined with the conclusion for  $N = 3$  implies that  $g_\infty = -1$  is valid for all scattering lengths and particle numbers.

The angular eigenvalue is given by  $g^{(-)}(x) \simeq g_\infty x/x_a$  for  $x_b \ll \rho/\rho_a \ll x_a$ . Numerical calculations in this intermediate region of hyperradii therefore rather accurately determines the fraction  $g_\infty/x_a \simeq -1.08$  as given in table D.1. With  $g_\infty = -1$  this implies that  $x_a \simeq 1/1.08 \simeq 0.92$ . The parameters of  $g^{(-)}(x)$  in equation (D.4) can now be collected to be

$$g_\infty = -1, \quad x_a \simeq 0.92, \quad x_b \simeq 0.92 \frac{b}{|a_s|}. \quad (\text{D.6})$$

The accuracy of the parametrization is seen in figures D.5a-d, where the

angular eigenvalues are shown in units of  $\lambda^{(-)}$  with the individual set of parameters from table D.1. A fairly good agreement is found for  $\rho/\rho_a > x_b$ . The remaining deviations occur at small hyperradii, which is not included in the  $g^{(-)}$ -parametrization, and at large hyperradii where the numerical inaccuracy increases with increasing scattering lengths. On the other hand the large-distance behaviour is known from analytic considerations, which renders numerical computations at these distances superfluous.

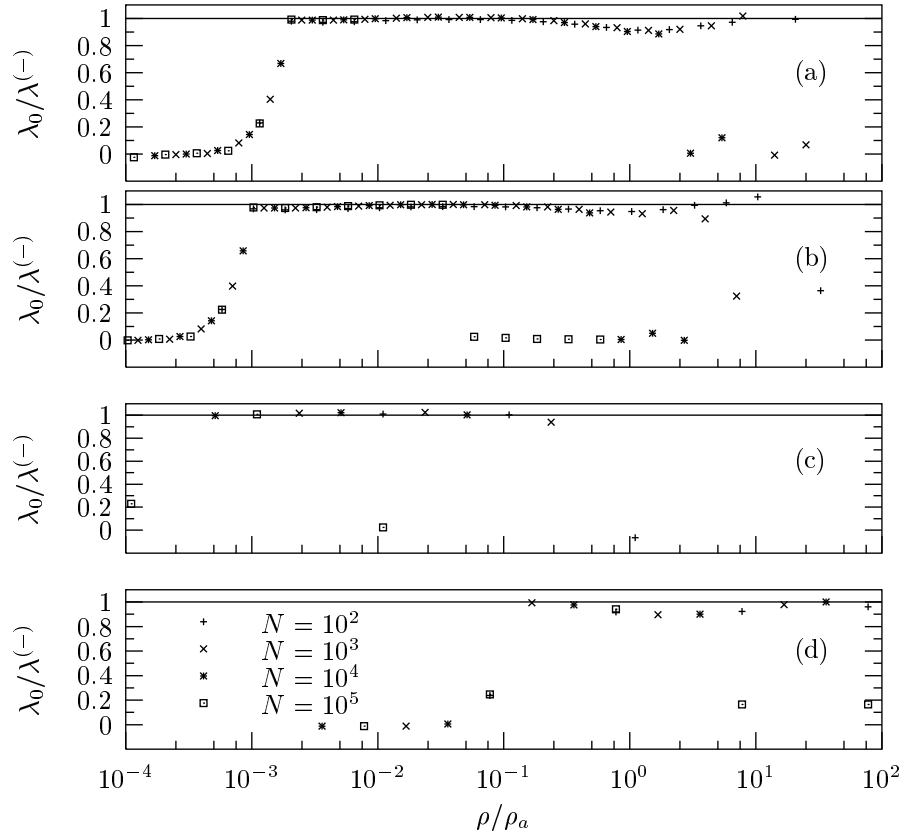


Figure D.5: The lowest angular eigenvalue  $\lambda$  in units of  $\lambda^{(-)}$ , equations (D.3) and (D.4) and table D.1, as functions of the hyperradius in units of  $\rho_a$ , equation (D.2). The scattering lengths are given by a)  $a_s/b = -401$ , b)  $a_s/b = -799$ , c)  $a_s/b = -4212$ , and d)  $a_s/b = -5.98$ . The different  $N$ -values are as indicated.

### D.3 Bound two-body state

In the presence of a bound two-body state one angular eigenvalue eventually diverges at large hyperradii as

$$\lambda^{(2)}(\rho) = \frac{2m\rho^2}{\hbar^2} E^{(2)}, \quad E^{(2)} < 0, \quad (\text{D.7})$$

where  $E^{(2)}$  is the energy of the two-body bound state. In the limit of weak binding, or for numerically large scattering lengths, the energy of the two-body bound state is given by

$$E^{(2)} = -\frac{\hbar^2}{ma_s^2} c, \quad (\text{D.8})$$

where  $c$  approaches unity for large scattering lengths.

The angular eigenvalue corresponding to a two-body bound state is parametrized by an expression similar to equations (D.3) and (D.4). The effect of the bound two-body state only shows up at large distances where the behaviour corresponds to equation (D.8). The small and intermediate distances resemble the behaviour when no bound state is present. Therefore the angular eigenvalue is given by the parametrization

$$\lambda^{(+)}(N, \rho) = |\lambda_\delta(N, \rho)| g^{(+)}(\rho/\rho_a), \quad (\text{D.9})$$

$$g^{(+)}(x) = x \left( 1 + \frac{x_b}{x} \right) \left( \frac{g_\infty}{x_a} - c \frac{4}{3} \sqrt{\frac{\pi}{3}} x^2 \right), \quad (\text{D.10})$$

with the notation and estimates from equation (D.6), i.e.  $x_b \simeq 0.92b/|a_s|$  and  $g_\infty/x_a \simeq -1.08$ . The terms in the second bracket of this expression only aim at the correct behaviour in the limits of small to intermediate and large hyperradii. The exact transition between these regions is not reproduced.

Figure D.6 shows a comparison of the parametrization in equations (D.9) and (D.10) with the computed angular eigenvalues for a potential with one bound two-body state. For the large scattering length in figure D.6a one smooth curve applies for all the particle numbers; numerical inaccuracies set in at larger hyperradii, which is most obvious for the largest particle numbers. This smooth curve is in a large interval of hyperradii at most deviating by 20% from the parametrized form, and even less than 10% at large hyperradii before numerical instabilities set in.

The shape at intermediate distances could be improved for example by inclusion of a linear term in equation (D.10). The smooth curve at small hyperradii is outside the range of validity of the parametrization, i.e. this is within the range of the two-body potential and therefore depends on details of the interaction.

The lowest eigenvalue diverges at large hyperradius as described in connection with figure D.6a and equation (D.9). If the two-body potential only has one bound state the second eigenvalue is expected to approach zero at large

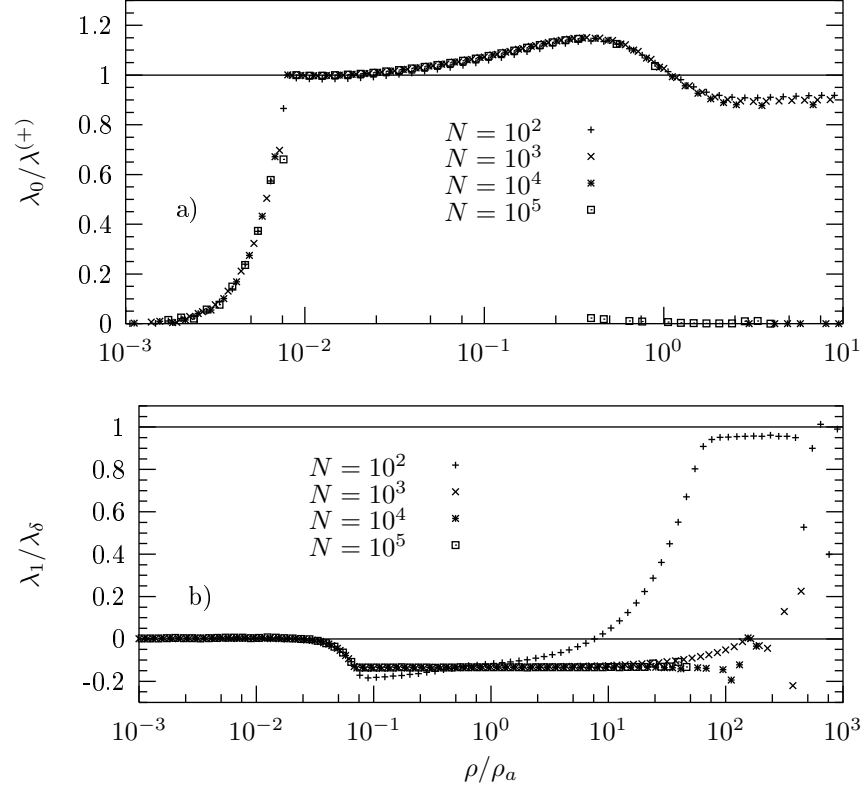


Figure D.6: a) The lowest angular eigenvalue  $\lambda_0$  in units of  $\lambda^{(+)}$ , equations (D.9) and (D.10), for  $a_s/b = +100$  and  $c = 1.02$ , when the potential holds one bound two-body state. The number of particles is indicated on the figure. The parameters are  $g_\infty/x_a = -1.09$  and  $x_b = 9.2 \cdot 10^{-3}$ . b) The first excited angular eigenvalue  $\lambda_1$  in units of  $\lambda_\delta$  for  $a_s/b = +10$ .

distances as  $\lambda_\delta$ . This pattern should be repeated with more than one bound two-body state, i.e. the first non-divergent angular eigenvalue should behave as  $\lambda_\delta$  for large  $\rho$ . Figure D.6b therefore compares the computed first excited angular eigenvalue with  $\lambda_\delta$  for different  $N$ . As in figure D.4 smooth and almost universal curves are obtained at small  $\rho$ , where the approach to unity sets in exponentially fast depending on  $N$ , but now for  $\rho$  one or two orders of magnitude larger than  $\rho_a$ . A parametrization would also here be possible. The large-distance asymptotic behaviour of the first excited state corresponds to a repulsive potential as seen by the approach to +1. However, at small and intermediate hyperradii the potential is attractive ( $\lambda_1 < 0$ ).



## Appendix E

### Derivation of effective dimension

For the case of  $N$  non-interacting identical bosons trapped in a cylindrically deformed harmonic field the Hamiltonian can be written with the choice of coordinates in appendix A.3 as

$$\hat{H} = \hat{H}_\rho + \hat{H}_\theta + \hat{T}_\Omega, \quad (\text{E.1})$$

$$\frac{2m\hat{H}_\rho}{\hbar^2} = -\frac{1}{\rho^{3N-4}} \frac{\partial}{\partial \rho} \rho^{3N-4} \frac{\partial}{\partial \rho} + \frac{\rho^2}{b_\perp^4}, \quad (\text{E.2})$$

$$\begin{aligned} \frac{2m\rho^2\hat{H}_\theta}{\hbar^2} &= -\frac{1}{\cos^{N-2}\theta \sin^{2N-3}\theta} \frac{\partial}{\partial \theta} \cos^{N-2}\theta \sin^{2N-3}\theta \frac{\partial}{\partial \theta} \\ &+ \rho^4 \left( \frac{1}{b_z^4} - \frac{1}{b_\perp^4} \right) \cos^2\theta. \end{aligned} \quad (\text{E.3})$$

Here  $\hat{T}_\Omega$  is the angular kinetic energy operator which is neglected later when there is no dependency on the internal angles. The ground state total wave function is known to be

$$\Psi_{\text{total}} = \prod_{i=1}^N \exp\left(-\frac{r_{i,z}^2}{2b_z^2} - \frac{r_{i,\perp}^2}{2b_\perp^2}\right), \quad (\text{E.4})$$

with  $b_q \equiv \sqrt{\hbar/(m\omega_q)}$ . We change to the coordinates  $\{\rho, \theta\}$  given by  $\rho_z = \rho \cos \theta$  and  $\rho_\perp = \rho \sin \theta$ , see appendix A.3, and obtain the wave function

$$\Psi_{\text{total}} = \exp\left(-\frac{NR_z^2}{2b_z^2} - \frac{NR_\perp^2}{2b_\perp^2}\right) F(\rho, \theta), \quad (\text{E.5})$$

$$F(\rho, \theta) = \exp\left(-\frac{\rho^2}{2b_\perp^2}\right) \exp\left[-\rho^2 \cos^2\theta \left(\frac{1}{2b_z^2} - \frac{1}{2b_\perp^2}\right)\right]. \quad (\text{E.6})$$

We write the Schrödinger equation and integrate over the coordinate  $\theta$  as follows:

$$0 = \int d\theta \Omega_\theta(\theta) F^*(\rho, \theta) (\hat{H}_\rho + \hat{H}_\theta - E) F(\rho, \theta), \quad (\text{E.7})$$

$$\Omega_\theta(\theta) \equiv \cos^{N-2}\theta \sin^{2N-3}\theta. \quad (\text{E.8})$$

Doing this we end up with terms only depending on  $\rho$ . Including formally the integration over hyperradius, but without completing it, we get

$$\begin{aligned} 0 &= \int d\rho \rho^{3(N-1)-1} \int d\theta \Omega_\theta(\theta) F^*(\rho, \theta) \left( \hat{H}_\rho + \hat{H}_\theta - E \right) F(\rho, \theta) \\ &= \int d\rho \rho^{3(N-1)-1} B(\rho) \left[ -E + \frac{\hbar^2}{2m} (N-1)(2C_\perp + C_z) \right], \end{aligned} \quad (\text{E.9})$$

$$B(\rho) \equiv \frac{\Gamma(a)\Gamma(2a)}{2\Gamma(3a)} e^{-C_\perp \rho^2} \mathcal{M}\left(a, 3a, -\Delta_1 \rho^2\right), \quad a \equiv \frac{N-1}{2}, \quad (\text{E.10})$$

where  $\mathcal{M}(a, b, z)$  is the Kummer function, i.e. identical to the confluent hypergeometric function  ${}_1F_1(a, b, z)$  [AS65],  $C_q \equiv 1/b_q^2$ , and  $\Delta_1 \equiv C_z - C_\perp$ . Furthermore, it is clear that

$$E = \frac{\hbar^2}{2m} (N-1)(2C_\perp + C_z) = \hbar\omega_\perp (N-1) + \frac{1}{2} \hbar\omega_z (N-1). \quad (\text{E.11})$$

We desire to write an effective  $d$ -dimensional Hamiltonian as

$$\hat{H}_d = \frac{\hbar^2}{2m} \left[ -\frac{1}{\rho^{d(N-1)-1}} \frac{\partial}{\partial \rho} \rho^{d(N-1)-1} \frac{\partial}{\partial \rho} + \frac{\rho^2}{b_d^4} \right] \quad (\text{E.12})$$

with an effective dimension  $d$  and a general length scale  $b_d$ . The normalization of the corresponding  $d$ -dimensional Schrödinger equation, with eigenvalue  $E_d$ , is

$$\int d\rho \rho^{d(N-1)-1} G_d^*(\rho) \left( \hat{H}_d - E_d \right) G_d(\rho) = 0, \quad (\text{E.13})$$

where  $G_d$  is a  $d$ -dimensional wave function. We want to approximate the correct equation (E.9) by this equation. From the two normalizations we identify the  $d$ -dimensional wave function  $G_d$  by the relation

$$\rho^{3(N-1)-1} B(\rho) = \rho^{d(N-1)-1} |G_d(\rho)|^2. \quad (\text{E.14})$$

Using this in equation (E.13) we obtain

$$\begin{aligned} 0 &= \int d\rho \rho^{d(N-1)-1} G_d^*(\rho) \left( \hat{H}_d - E_d \right) G_d(\rho) \\ &= \int d\rho \rho^{3(N-1)-1} B(\rho) \left\{ -E_d + \frac{\hbar^2}{2m} \left[ (N-1)(2C_\perp + C_z) + v(\rho^2) \right] \right\}, \end{aligned} \quad (\text{E.15})$$

$$\begin{aligned} v(x) &\equiv -x(C_z^2 - C_d^2) - \frac{1}{x} (3-d)a [a(3+d) - 2] \\ &\quad + \frac{4}{3} C_\perp \Delta_1 x \mu(-\Delta_1 x) + \frac{4}{9} \Delta_1^2 x \mu^2(-\Delta_1 x), \end{aligned} \quad (\text{E.16})$$

$$\mu(z) \equiv \frac{\mathcal{M}(a, 3a+1, z)}{\mathcal{M}(a, 3a, z)}. \quad (\text{E.17})$$

If we subtract equation (E.15) from equation (E.9) we get

$$\int d\rho \rho^{3(N-1)-1} B(\rho) \left[ E - E_d + \frac{\hbar^2}{2m} v(\rho^2) \right] = 0. \quad (\text{E.18})$$

We are now in a position to study the three limits i) spherical ( $b_z = b_\perp$ ), ii) two-dimensional ( $b_\perp \gg b_z$ ), iii) one-dimensional ( $b_z \gg b_\perp$ ).

When the external trap is spherically symmetric, i.e.  $b_z = b_\perp$ , we have  $C_z = C_\perp$ ,  $\Delta_1 = 0$ , and  $\mu(0) = 1$ . This yields

$$v(\rho^2) = -\rho^2(C_z^2 - C_d^2) - \frac{a}{\rho^2}(3-d)[a(3+d)-2]. \quad (\text{E.19})$$

The bracket of equation (E.18) is zero for all hyperradii when three conditions are true:

$$E_d = E = \frac{\hbar^2}{2m}(N-1)(2C_\perp + C_z) = \frac{3}{2}\hbar\omega(N-1), \quad (\text{E.20})$$

$$C_d = C_z \iff b_d = b_z = b_\perp, \quad d = 3. \quad (\text{E.21})$$

$E$  is the ground state energy minus the centre-of-mass energy for  $N$  identical non-interacting particles of mass  $m$  in a three-dimensional oscillator of frequency  $\omega$ .

The two-dimensional geometry occurs when the external trap is squeezed along the  $r$ -plane such that  $b_\perp \gg b_z$ . This leads to  $C_z \gg C_\perp$  and  $\Delta_1 = C_z - C_\perp \simeq C_z > 0$ . In this case the hyperradius is determined by the radial trap length, i.e.  $\rho \sim \sqrt{N}b_\perp$ , which implies that typically  $-\Delta_1\rho^2 \sim -NC_z b_\perp^2 = -NC_z/C_\perp \rightarrow -\infty$ . We therefore need the limit of  $\mu(z)$  when  $z \rightarrow -\infty$ :

$$\mu(z) \simeq \frac{3}{2} \left( 1 + \frac{a}{z} + \frac{2a^2 - a}{z^2} \right). \quad (\text{E.22})$$

This leads to

$$v(\rho^2) \simeq -2aC_z - \rho^2(C_\perp^2 - C_d^2) - \frac{a}{\rho^2}(2-d)[a(2+d)-2]. \quad (\text{E.23})$$

The bracket of equation (E.18) becomes to order  $\rho^{-2}$

$$E - E_d + \frac{\hbar^2}{2m} \left\{ -2aC_z - \rho^2(C_\perp^2 - C_d^2) - \frac{a}{\rho^2}(2-d)[a(2+d)-2] \right\}. \quad (\text{E.24})$$

This is zero for all hyperradii when

$$E_d = E - \frac{\hbar^2}{2m} 2aC_z = \frac{\hbar^2}{2m}(N-1)2C_\perp = \hbar\omega_\perp(N-1), \quad (\text{E.25})$$

$$C_d = C_\perp \iff b_d = b_\perp, \quad d = 2. \quad (\text{E.26})$$

The system is effectively one-dimensional when the external trap is squeezed along the  $z$ -axis such that  $b_z \gg b_\perp$ . This leads to  $C_\perp \gg C_z$  and  $\Delta_1 = C_z - C_\perp \simeq$

$-C_\perp < 0$ . In this case the hyperradius is determined by the axial trap length, i.e.  $\rho \sim \sqrt{N}b_z$ , which implies that typically  $-\Delta_1\rho^2 \sim NC_\perp b_z^2 = NC_\perp/C_z \rightarrow +\infty$ . We therefore need the limit of  $\mu(z)$  when  $z \rightarrow +\infty$ :

$$\mu(z) \simeq \frac{3a}{z} \left(1 - \frac{a-1}{z}\right). \quad (\text{E.27})$$

This leads to

$$v(\rho^2) \simeq -4aC_\perp - \rho^2(C_z^2 - C_d^2) - \frac{a}{\rho^2}(1-d)[a(1+d) - 2]. \quad (\text{E.28})$$

The bracket of equation (E.18) becomes to order  $\rho^{-2}$

$$E - E_d + \frac{\hbar^2}{2m} \left\{ -4aC_\perp - \rho^2(C_z^2 - C_d^2) - \frac{a}{\rho^2}(1-d)[a(1+d) - 2] \right\}. \quad (\text{E.29})$$

This is zero for all hyperradii when

$$E_d = E - \frac{\hbar^2}{2m} 4aC_\perp = \frac{\hbar^2}{2m} (N-1)C_z = \frac{1}{2} \hbar \omega_z (N-1), \quad (\text{E.30})$$

$$C_d = C_z \iff b_d = b_z, \quad d = 1. \quad (\text{E.31})$$

The results are collected in table E.1. In all three cases the energy is given

limit	spherical	oblate	prolate
condition	$b_z \simeq b_\perp$	$b_\perp \gg b_z$	$b_z \gg b_\perp$
$z = -\Delta_1\rho^2$	0	$-\infty$	$+\infty$
$\mu(z)$	1	$\frac{3}{2} \left(1 + \frac{a}{z} + \frac{2a^2 - a}{z^2}\right)$	$\frac{3a}{z} \left(1 - \frac{a-1}{z}\right)$
$E_d/(N-1)$	$\frac{3}{2} \hbar \omega$	$\hbar \omega_\perp$	$\frac{1}{2} \hbar \omega_z$
$b_d$	$b_z \simeq b_\perp$	$b_\perp$	$b_z$
$d$	3	2	1

Table E.1: The (typical) values of  $z$ ,  $\mu(z)$ ,  $E_d$ ,  $b_d$ , and  $d$  in the three limits: spherical, oblate, and prolate.

by

$$E_d = \frac{d}{2} \hbar \omega_d (N-1), \quad \omega_d \equiv \frac{\hbar}{mb_d^2}. \quad (\text{E.32})$$

In the general case, when we cannot assume  $b_z = b_\perp$  or  $b_z \gg b_\perp$  or  $b_z \ll b_\perp$ , it is not possible to obtain a simple expansion in  $\rho$  of the bracket in equation (E.18). Instead we study the integrated equation.

We rescale the equation in a convenient length scale  $b_0$  given by

$$b_0^2 \equiv 2b_\perp^2 + b_z^2. \quad (\text{E.33})$$

In the three special limits we found that  $E_d = \hbar^2 ad/(mb_d^2)$  and  $b_d^2 = b_0^2/d$ . We therefore introduce the parameters  $e_d$  and  $\beta_d$  given by

$$E_d \equiv \frac{\hbar^2 a e_d}{m b_0^2}, \quad \beta_d \equiv \frac{b_0^2}{b_d^2}. \quad (\text{E.34})$$

This leads from equation (E.18) to the integrated equation

$$0 = e_d - \frac{1}{2}\beta_d^2 + g(d)f_1(\beta) - f_2(\beta), \quad f_1(\beta) \equiv a^2 I[x^{-2}], \quad (\text{E.35})$$

$$f_2(\beta) \equiv 2\beta_r + \beta_z - \frac{1}{2}\beta_z^2 + \frac{4}{3}\beta_r(\beta_z - \beta_r)I\{x^2\mu[x^2(\beta_r - \beta_z)]\} \\ + \frac{4}{9}(\beta_z - \beta_r)^2 I\{x^2\mu^2[x^2(\beta_r - \beta_z)]\}, \quad (\text{E.36})$$

$$g(d) \equiv (3-d)(3+d-2/a), \quad (\text{E.37})$$

$$\beta \equiv \frac{b_\perp^2}{b_z^2}, \quad \beta_r \equiv \frac{b_0^2}{b_\perp^2} = 2 + \frac{1}{\beta}, \quad \beta_z \equiv \frac{b_0^2}{b_z^2} = \frac{2}{\beta} + 1, \quad (\text{E.38})$$

$$I[f(x)] \equiv \frac{\beta_z^a \beta_r^{2a}}{a\Gamma(3a)} \int_0^\infty dx x^{6a-1} \exp(-\beta_r x^2) \\ \times \mathcal{M}\left[a, 3a, x^2(\beta_r - \beta_z)\right] f(x). \quad (\text{E.39})$$

If we use the expectations that

$$e_d = d^2(1 + \varepsilon), \quad \beta_d = d(\beta + \delta)^{1/2}, \quad \varepsilon \ll 1, \quad \delta \ll 1 \quad (\text{E.40})$$

we get that

$$\mathcal{A}d^2 + \mathcal{B}d + \mathcal{C} = 0, \quad \mathcal{A} \equiv 1/2 + \varepsilon - \delta/2 - f_1(\beta), \quad (\text{E.41})$$

$$\mathcal{B} \equiv 2f_1(\beta)/a, \quad \mathcal{C} \equiv (9 - 6/a)f_1(\beta) - f_2(\beta). \quad (\text{E.42})$$

If we demand only one solution, i.e.  $\mathcal{B}^2 - 4\mathcal{A}\mathcal{C} = 0$ , we get

$$d = -\frac{\mathcal{B}}{2\mathcal{A}} = -\frac{2\mathcal{C}}{\mathcal{B}}. \quad (\text{E.43})$$

The results for various  $N$ -values are shown in figure 7.4.

Furthermore, we check that  $\varepsilon - \delta/2$  is small ( $< 10^{-2}$ ) so the approximations in equation (E.40) are valid. The conclusion is that generally we can use  $E_d = \hbar^2 ad/(mb_d^2)$  and  $b_d^2 = b_0^2/d$  as the relevant energy and length scales, respectively, with  $d$  given by figure 7.4.



## Appendix F

### List of notations

Notation	Description	Chapter
$a_s$	two-body $s$ -wave scattering length	3-7
$a_B$	Born approximation to $a_s$	2,3,5
$a_d$	$d$ -dimensional interaction parameter	7
$a_{1D}$	one-dimensional scattering length	7
$b$	interaction range	2-6
$b_t$	trap length	2-7
$b_d, b_q, b_x, b_y, b_z, b_\perp$	trap lengths	4,7
$d$	spatial dimension	7
$d_c$	condensate length	4,6
$E, E_n$	total relative energy	2,4-7
$E_{\text{total}}$	total energy	5,6
$E^{(2)}$	two-body energy	3
$E_d$	energy in $d$ dimensions	7
$f, f_\nu$	reduced hyperradial wave function	2,4,7
$f_\infty$	Efimov hyperradial wave function	4
$F, F_\nu$	hyperradial wave function	2,4,7
$g, g_2, g_3$	coupling strengths	5,7
$G$	kernel for variational angular equation	2
$G_d$	$d$ -dimensional wave function	7
$\hat{h}_\Omega$	reduced angular Hamiltonian operator	2,3
$\hbar$	Planck's constant	2-7
$\hat{H}, \hat{H}_q$	Hamiltonian operator	2,7
$\hat{H}_d$	Hamiltonian operator in $d$ dimensions	7
$i$	complex number $i = \sqrt{-1}$	2
$i, j, k, l$	indices	2-7
$k_B$	Boltzmann's constant	4
$K = K_{N-1}$	grand hyperangular momentum	2-4
$K_k$	hyperangular momentum	2-3
$l_{N,K}$	generalized angular momentum	4

Notation	Description	Chapter
$l_k$	angular momentum	2
$l_T$	thermal length	4
$l_1, l_2$	trap lengths	7
$L_k$	collection of angular momenta	2
$\tilde{L} = L_{N-1}$	total relative angular momentum	2
$\mathcal{L}$	Laguerre polynomial	4
$m$	particle mass	2-7
$m_k$	projection of angular momentum	2
$M$	total mass	2
$M_k$	projection of $L_k$	2
$\tilde{M} = M_{N-1}$	projection of $\tilde{L}$	2
$n$	single-particle density	2
$n$	density	3,5,6
$n$	hyperradial quantum number	4
$N$	number of particles	2-7
$\mathcal{N}$	number of bound states	4
$\mathcal{N}_B$	number of bound two-body states	3
$\mathcal{N}_E$	number of Efimov-like states	4
$\hat{O}$	operator	2
$p_i$	momentum	2
$\hat{P}$	permutation operator	2
$P_R$	total momentum	2
$\mathcal{P}, \tilde{\mathcal{P}}$	Jacobi function	2,3
$q$	degree of freedom (e.g. $x, y, z$ )	4,7
$Q_{\nu\nu'}$	coupling term	2
$r = r_{12}, r_{ij}$	interparticle coordinates	2-7
$r_i$	particle coordinates	2-7
$\bar{r}, \bar{r}_n$	root-mean-square (rms) distance	4-6
$\bar{r}_R$	rms separation from mass centre	4
$R, R_q$	centre-of-mass coordinates	2,7
$\hat{R}_{ij}, \hat{R}_{ijkl}$	rotation operators	2,3
$R_{\text{eff}}$	effective range	3
$s$	reduced interaction strength	7
$t$	time	6
$T$	temperature	4
$\hat{T}$	kinetic-energy operator	2
$\hat{T}_\rho$	hyperradial kinetic-energy operator	2
$u$	reduced two-body wave function	3
$u$	reduced hyperradial potential	6,7
$U, U_\nu$	hyperradial potential	2-4,6,7
$v, v_{ij}$	reduced two-body potential	2,3
$v_1, v_2$	rotations of potential	2
$V, V_{ij}$	two-body potential	2-3,5,7



Notation	Description	Chapter
$\tilde{V}$	total interaction potential	7
$V_d$	two-body potential in $d$ dimensions	7
$V_{\text{trap}}$	external trapping potential	2,4,7
$V_G$	Gaussian two-body potential	3,5
$V_\delta$	zero-range interaction potential	3,5,7
$V_3$	three-body interaction potential	5
$\mathcal{V}$	volume	6
$w$	variational width	6
$x, y, z$	cartesian axes	2-7
$Y$	spherical harmonics	2
$\mathcal{Y}, \tilde{\mathcal{Y}}$	hyperspherical harmonics	2
$\alpha$	mean-free path	5
$\alpha = \alpha_{N-1} = \alpha_{12}, \alpha'$	primary hyperangle	2,3,7
$\alpha_{ij}$	hyperangle related to $r_{ij}$	2,3,7
$\alpha_k$	hyperangle related to $\eta_k$	2,3
$\beta$	deformation parameter	7
$\gamma$	deformation parameter	7
$\Gamma$	Euler's gamma function	2,3,7
$\Gamma_{\text{rec}}, \Gamma_{\text{tunnel}}, \Gamma_{\text{collapse}}$	decay widths	6
$\delta$	Dirac delta function	3,5,7
$\delta^{(d)}$	$d$ -dimensional delta function	7
$\delta_G$	Gaussian representation of $\delta$	5
$\hat{\Delta}$	Laplacian operator	A
$\varepsilon$	reduced energy	7
$\eta_k$	Jacobi coordinates	2
$\theta$	polar angle for hyperradius	7
$\Theta$	step or truth function	2,3
$\vartheta, \vartheta_k, \vartheta_{ij,k}, \vartheta_{ij}$	polar angle	2,7
$\kappa$	wave vector or wave number	2,3
$\lambda, \lambda_\nu$	hyperangular eigenvalue	2-6
$\lambda_K$	kinetic-energy hyperangular eigenvalue	2-4
$\lambda_\delta$	$\lambda$ with expectation value of $V_\delta$	3-7
$\lambda_\infty$	plateau value for angular eigenvalue	3-6
$\lambda^{(2)}$	angular potential for two-body state	3
$\lambda_{\text{3-body}}$	$\lambda$ from three-body interaction	5
$\hat{\Lambda}_{N-1}$	grand hyperangular momentum operator	2
$\hat{\Lambda}_k$	hyperangular momentum operator	2
$\mu$	chemical potential	5
$\nu = \nu_{N-1}, \nu_k$	hyperangular quantum number	2-4
$\nu_{\text{rec}}$	three-body recombination rate	6
$\nu_{\text{tunnel}}$	macroscopic tunneling rate	6
$\nu_{\text{trap}}, \nu_q, \nu_x, \nu_y, \nu_z$	trap frequencies	3-7
$\xi$	Efimov scale	4

Notation	Description	Chapter
$\tilde{\Pi}, \tilde{\Pi}_k, \tilde{\Pi}_{ij}$	partial hyperangular momenta	2
$\rho$	hyperradius	2-7
$\rho_q, \rho_\perp, \rho_z$	components of hyperradius	7
$\bar{\rho}$	root-mean-square hyperradius	3-6
$\varrho$	planar projection of coordinate	7
$\sigma$	action integral	6
$d\tau$	reduced hyperangular volume element	2,3
$\tau, \tau_{\text{rec}}, \tau_{\text{tunnel}}, \tau_{\text{trap}}$	time scales	6
$\Upsilon$	centre-of-mass wave function	2
$\phi, \phi_\nu$	Faddeev component	2,3,7
$\phi_K$	Faddeev kinetic-energy eigenfunction	3
$\tilde{\phi}$	reduced Faddeev component	3
$\Phi, \Phi_\nu$	angular wave function	2-4
$\Phi_K$	angular kinetic-energy eigenfunction	3
$\varphi, \varphi_k$	azimuthal angle	2
$\chi$	phase shift of two-body wave function	3
$\psi$	wave function component	2,5,6
$\Psi$	total wave function	2,4
$\omega, \omega_x, \omega_y, \omega_z, \omega_q$	angular trap frequencies	2-7
$\Omega, \Omega_{N-1}$	all hyperangles	2-4,7
$\Omega_k$	part of hyperangles	2
$d\Omega_\alpha^{(k)}$	volume element for $\alpha_k$	2,7
$\Omega_\eta^{(k)}$	angles for direction of $\eta_k$	2

## List of Figures

2.1	Jacobi vectors for six particles . . . . .	8
2.2	Simplifications due to short-range potentials . . . . .	27
3.1	Two possible two-body potentials: realistic and simplified . . . . .	30
3.2	Scattering length for Gaussian and square-well potentials . . . . .	32
3.3	Angular kinetic-energy eigenfunctions . . . . .	35
3.4	Angular eigenvalues for twenty particles . . . . .	42
3.5	Angular eigenvalues with two-body bound states . . . . .	43
3.6	Two lowest angular eigenvalues for one bound two-body state . . . . .	44
3.7	Angular eigenvalues for twenty particles (Faddeev calculation) . . . . .	45
3.8	Angular wave functions for two-body bound states . . . . .	46
3.9	Angular wave functions for different interaction parameters . . . . .	47
3.10	Second angular moment as a function of hyperradius . . . . .	48
3.11	Angular eigenvalues from analytical approximation . . . . .	49
4.1	Radial potential for twenty particles and small scattering length . . . . .	56
4.2	Radial potential for one hundred bosons . . . . .	58
4.3	Density profile . . . . .	59
4.4	Radial potentials from the parametrized angular eigenvalue . . . . .	60
4.5	Radial potential and energy-length relations for infinite scattering length . . . . .	61
4.6	Interparticle distance and energy as a function of quantum number . . . . .	65
4.7	Interaction energies . . . . .	66
5.1	Density-dependent coupling strengths . . . . .	73
5.2	Energy and distance from Gross-Pitaevskii equation and two-body correlated model . . . . .	75
5.3	Angular eigenvalue with outlined validity regions . . . . .	78
6.1	Radial potentials as a function of particle number and scattering length . . . . .	82
6.2	Sequence of radial potentials as the barrier vanishes . . . . .	83
6.3	Time scales involved in the macroscopic decay . . . . .	86
6.4	Collapsing many-body wave function in the potential for twenty bosons . . . . .	87

7.1	Contour plots of effective potential for deformed boson system . . .	94
7.2	Effective potential along cuts for different deformations . . . . .	95
7.3	Critical strength as a function of deformation . . . . .	96
7.4	Effective dimension as a function of deformation . . . . .	99
7.5	Effective interaction strength as a function of deformation . . . . .	101
B.1	Various Jacobi trees . . . . .	116
B.2	Diagonal potential terms . . . . .	119
B.3	Semi-diagonal potential terms . . . . .	120
B.4	Non-diagonal potential terms . . . . .	121
D.1	Angular eigenvalues for different scattering lengths . . . . .	128
D.2	Angular eigenvalues in units of zero-range result . . . . .	129
D.3	Angular eigenvalues for different particle numbers . . . . .	130
D.4	Angular eigenvalues as a function of a scaled hyperradius . . . . .	131
D.5	Angular eigenvalues in units of analytical approximation . . . . .	132
D.6	Angular eigenvalues for two-body states in units of approximation	134

## Bibliography

- [ABGG03a] Grigory E. Astrakharchik, Dörte Blume, Stefano Giorgini, and Brian E. Granger. Quantum Monte Carlo study of quasi-one-dimensional Bose gases. *E-print arXiv cond-mat/0310749*, 2003.
- [ABGG03b] Grigory E. Astrakharchik, Dörte Blume, Stefano Giorgini, and Brian E. Granger. Quasi-one-dimensional Bose gases with large scattering length. *E-print arXiv cond-mat/0308585*, 2003.
- [Adh01] Sadhan K. Adhikari. Stability and collapse of a hybrid Bose-Einstein condensate of atoms and molecules. *J. Phys. B: At. Mol. Opt. Phys.*, 34:4231, 2001.
- [Adh02a] Sadhan K. Adhikari. Collapse of attractive Bose-Einstein condensed vortex states in a cylindrical trap. *Phys. Rev. E*, 65:016703, 2002.
- [Adh02b] Sadhan K. Adhikari. Mean-field description of collapsing and exploding Bose-Einstein condensates. *Phys. Rev. A*, 66:013611, 2002.
- [AEM<sup>+</sup>95] M. H. Anderson, J. R. Ensher, M. R. Matthews, Carl E. Wieman, and Eric A. Cornell. Observation of Bose-Einstein condensation in a dilute atomic vapor. *Science*, 269:198, July 1995.
- [AG73] R. D. Amado and F. C. Greenwood. There is no Efimov effect for four or more particles. *Phys. Rev. D*, 7:2517–2519, 1973.
- [AM02] Sadhan K. Adhikari and Paulsamy Muruganandam. Bose-Einstein condensation dynamics from the numerical solution of the Gross-Pitaevskii equation. *J. Phys. B: At. Mol. Opt. Phys.*, 35:2831, 2002.
- [AS65] Milton Abramowitz and Irene A. Stegun, editors. *Handbook of Mathematical Functions*. Dover, New York, 9th edition, 1965.
- [Bar99a] Nir Barnea. Hyperspherical functions with arbitrary permutational symmetry: Reverse construction. *Phys. Rev. A*, 59:1135, 1999.

- [Bar99b] Nir Barnea. Solution of the Schrödinger equation including two-, three- and four-body correlations - Bose systems. *Phys. Lett. B*, 446:185, 1999.
- [BBH00] Paulo F. Bedaque, Eric Braaten, and Hans-Werner Hammer. Three-body recombination in Bose gases with large scattering length. *Phys. Rev. Lett.*, 85:908, 2000.
- [BEG98] John L. Bohn, Brett D. Esry, and Chris H. Greene. Effective potentials for dilute Bose-Einstein condensates. *Phys. Rev. A*, 58:584, July 1998.
- [BG01] Dörte Blume and Chris H. Greene. Quantum corrections to the ground state energy of a trapped Bose-Einstein condensate: A diffusion Monte Carlo calculation. *Phys. Rev. A*, 63:063601, June 2001.
- [BG02] Dörte Blume and Chris H. Greene. Three particles in an external trap: Nature of the complete  $j = 0$  spectrum. *Phys. Rev. A*, 66:013601, 2002.
- [BHM02] Eric Braaten, Hans-Werner Hammer, and Thomas Mehen. Dilute Bose-Einstein condensate with large scattering length. *Phys. Rev. Lett.*, 88:40401, 2002.
- [Bij40] A. Bijl. The lowest wave function of the symmetrical many particles system. *Physica*, 7:869–886, 1940.
- [BJ83] Brian H. Bransden and Charles J. Joachain. *Physics of atoms and molecules*. Longman Scientific & Technical, USA, 1983.
- [BP96] Gordon Baym and Christopher J. Pethick. Ground-state properties of magnetically trapped Bose-condensed rubidium gas. *Phys. Rev. Lett.*, 76:6, 1996.
- [BSTH95] Curtis C. Bradley, Cass A. Sackett, Jeff J. Tollett, and Randall G. Hulet. Evidence of Bose-Einstein condensation in an atomic gas with attractive interactions. *Phys. Rev. Lett.*, 75:1687, August 1995.
- [Bul02] Aurel Bulgac. Dilute quantum droplets. *Phys. Rev. Lett.*, 89:050402, 2002.
- [CBB<sup>+</sup>03] B. Cochet, K. Bennaceur, P. Bonche, T. Duguet, and J. Meyer. Compressibility, effective mass and density dependence in Skyrme forces. *E-print arXiv nucl-th/0309012*, 2003.
- [CC98] F. Ciesielski and J. Carbonell. Solutions of the Faddeev-Yakubovsky equations for the four nucleon scattering states. *Phys. Rev. C*, 58:58, 1998.

- [CCR<sup>+</sup>00] Simon L. Cornish, Neil R. Claussen, Jacob L. Roberts, Eric A. Cornell, and Carl E. Wieman. Stable  $^{85}\text{Rb}$  Bose-Einstein condensates with widely tunable interactions. *Phys. Rev. Lett.*, 85:1795, 2000.
- [CHM<sup>+</sup>02] S. Cowell, Henning Heiselberg, I. E. Mazets, J. Morales, Vijay R. Pandharipande, and Christopher J. Pethick. Cold Bose gases with large scattering lengths. *Phys. Rev. Lett.*, 88:210403, 2002.
- [CKT<sup>+</sup>03] Neil R. Claussen, Servaas J. J. M. F. Kokkelmans, Sarah T. Thompson, Elizabeth A. Donley, Eleanor Hodby, and Carl E. Wieman. Very-high-precision bound-state spectroscopy near a  $^{85}\text{Rb}$  Feshbach resonance. *Phys. Rev. A*, 67:060701, 2003.
- [DCC<sup>+</sup>01] Elizabeth A. Donley, Neil R. Claussen, Simon L. Cornish, Jacob L. Roberts, Eric A. Cornell, and Carl E. Wieman. Dynamics of collapsing and exploding Bose-Einstein condensates. *Nature (London)*, 412:295–299, 2001.
- [DGPS99] Franco Dalfovo, Stefano Giorgini, Lev P. Pitaevskii, and Sandro Stringari. Theory of Bose-Einstein condensation in trapped gases. *Rev. Mod. Phys.*, 71:463, 1999.
- [Din49] Robert B. Dingle. The zero-point energy of a system of particles. *Phil. Mag.*, 40:573, 1949.
- [dlR84] M. Fabre de la Ripelle. Solution of the Schrödinger equation with two-body correlations included. *Phys. Lett. B*, 135:5, 1984.
- [dlRFS88] M. Fabre de la Ripelle, H. Fiedeldey, and S. A. Sofianos. Integro-differential equation for few- and many-body systems. *Phys. Rev. C*, 38:449, 1988.
- [DMA<sup>+</sup>95] K. B. Davis, M.-O. Mewes, M. R. Andrews, N. J. van Druten, D. S. Durfee, Dan M. Stamper-Kurn, and Wolfgang Ketterle. Bose-Einstein condensation in a gas of sodium atoms. *Phys. Rev. Lett.*, 75:3969, November 1995.
- [EB95] Mark Edwards and Keith Burnett. Numerical solution of the non-linear Schrödinger equation for small samples of trapped neutral atoms. *Phys. Rev. A*, 51:1382, February 1995.
- [Efi70] Vitaly Efimov. Energy levels arising from resonant two-body forces in a three-body system. *Phys. Lett. B*, 33(8):563–564, 1970.
- [EG99] Brett D. Esry and Chris H. Greene. Validity of the shape-independent approximation for Bose-Einstein condensates. *Phys. Rev. A*, 60:1451–1462, 1999.
- [Fad60] L. D. Faddeev. Scattering theory for a three-particle system. *J. Exptl. Theoret. Phys.*, 39:1459, 1960.

- [FG02] I. N. Filikhin and A. Gal. Faddeev-Yakubovsky calculations for light lambda-lambda hypernuclei. *Nucl. Phys. A*, 707:491, 2002.
- [FJ93] Dmitri V. Fedorov and Aksel S. Jensen. Efimov effect in coordinate space Faddeev equations. *Phys. Rev. Lett.*, 71:4103, 1993.
- [FJ01a] Dmitri V. Fedorov and Aksel S. Jensen. Correlation-induced collapse of many-body systems with zero-range potentials. *Phys. Rev. A*, 63:063608, 2001.
- [FJ01b] Dmitri V. Fedorov and Aksel S. Jensen. Regularization of a three-body problem with zero-range potentials. *J. Phys. A*, 34:6003–6012, 2001.
- [GB01] Sydney Geltman and A. Bambini. Triplet scattering lengths for rubidium and their role in Bose-Einstein condensation. *Phys. Rev. Lett.*, 86:3276, 2001.
- [GBM<sup>+</sup>01] Markus Greiner, Immanuel Bloch, Olaf Mandel, Theodor W. Hänsch, and Tilman Esslinger. Exploring phase coherence in a 2d lattice of Bose-Einstein condensates. *Phys. Rev. Lett.*, 87:160405, 2001.
- [GFT01] A. Gammal, T. Frederico, and Lauro Tomio. Critical number of atoms for attractive Bose-Einstein condensates with cylindrically symmetrical traps. *Phys. Rev. A*, 64:055602, 2001.
- [GFTA00] A. Gammal, T. Frederico, Lauro Tomio, and F. Kh. Abdullaev. Stability analysis of the  $d$ -dimensional nonlinear Schrödinger equation with trap and two-and three-body interactions. *Phys. Lett. A*, 267:305–311, 2000.
- [GFTC00] A. Gammal, T. Frederico, Lauro Tomio, and Ph. Chomaz. Atomic Bose-Einstein condensation with three-body interactions and collective excitations. *J. Phys. B: At. Mol. Opt. Phys.*, 33:4053–4067, 2000.
- [GVL<sup>+</sup>01] A. Görlitz, J. M. Vogels, A. E. Leanhardt, C. Raman, T. L. Gustavson, J. R. Abo-Shaer, A. P. Chikkatur, S. Gupta, S. Inouye, T. Rosenband, and Wolfgang Ketterle. Realization of Bose-Einstein condensates in lower dimensions. *Phys. Rev. Lett.*, 87:130402, 2001.
- [IAS<sup>+</sup>98] S. Inouye, M. R. Andrews, J. Stenger, H.-J. Miesner, Dan M. Stamper-Kurn, and Wolfgang Ketterle. Observation of Feshbach resonances in a Bose-Einstein condensate. *Nature (London)*, 392:151, 1998.
- [Jas55] Robert Jastrow. Many-body problem with strong forces. *Phys. Rev.*, 98:1479, 1955.



- [JGF97] Aksel S. Jensen, Eduardo Garrido, and Dmitri V. Fedorov. Three-body systems with square-well potentials in  $l = 0$  states. *Few-Body Syst.*, 22(4):193, 1997.
- [KGB03] Thorsten Köhler, Thomas Gasenzer, and Keith Burnett. Microscopic theory of atom-molecule oscillations in a Bose-Einstein condensate. *Phys. Rev. A*, 67:013601, 2003.
- [KH02] Servaas J. J. M. F. Kokkelmans and Murray J. Holland. Ramsey fringes in a Bose-Einstein condensate between atoms and molecules. *Phys. Rev. Lett.*, 89:180401, 2002.
- [KM90] Steven E. Koonin and Dawn C. Meredith. *Computational Physics, Fortran Version*. Addison-Wesley, Reading, MA, 1990.
- [KMW02] N. N. Khuri, A. Martin, and T.-T. Wu. Bound states in  $n$  dimensions (especially  $n = 1$  and  $n = 2$ ). *Few-Body Syst.*, 31:83–89, 2002.
- [LHY57] T. D. Lee, Kerson Huang, and C. N. Yang. Eigenvalues and eigenfunctions of a Bose system of hard spheres and its low-temperature properties. *Phys. Rev.*, 106:1135–1145, 1957.
- [Lin95] C. D. Lin. Hyperspherical coordinate approach to atomic and other Coulombic three-body systems. *Phys. Rep.*, 257:1, 1995.
- [LMDB02] M. D. Lee, S. A. Morgan, M. J. Davis, and Keith Burnett. Energy dependent scattering and the Gross-Pitaevskii equation in two-dimensional Bose-Einstein condensates. *Phys. Rev. A*, 65:043617, 2002.
- [LS02] Elliott H. Lieb and Robert Seiringer. Proof of Bose-Einstein condensation for dilute trapped gases. *Phys. Rev. Lett.*, 88:170409, 2002.
- [LY57] T. D. Lee and C. N. Yang. Many-body problem in quantum mechanics and quantum statistical mechanics. *Phys. Rev.*, 105:1119–1120, 1957.
- [Mac68] Joseph H. Macek. Properties of autoionizing states of He. *J. Phys. B: At. Mol. Phys.*, 1:831, 1968.
- [MM01] Ch. C. Moustakidis and S. E. Massen. Bose-Einstein condensation of correlated atoms in a trap. *Phys. Rev. A*, 65:063613, 2001.
- [MSJ02] Matt Mackie, Kalle-Antti Suominen, and Juha Javanainen. Mean-field theory of Feshbach-resonant interactions in  $^{85}\text{Rb}$  condensates. *Phys. Rev. Lett.*, 89:180403, 2002.

- [MW02] Brett A. McKinney and Deborah K. Watson. Bose-Einstein condensation in variable dimensionality. *Phys. Rev. A*, 65:033604, 2002.
- [NFJG01] Esben Nielsen, Dmitri V. Fedorov, Aksel S. Jensen, and Eduardo Garrido. The three-body problem with short-range interactions. *Phys. Rep.*, 347:373, June 2001.
- [NM99] Esben Nielsen and Joseph H. Macek. Low-energy recombination of identical bosons by three-body collisions. *Phys. Rev. Lett.*, 83:1566, 1999.
- [Ols98] Maxim Olshanii. Atomic scattering in the presence of an external confinement and a gas of impenetrable bosons. *Phys. Rev. Lett.*, 81:938–941, 1998.
- [PBS98] N. P. Proukakis, Keith Burnett, and Henk T. C. Stoof. Microscopic treatment of binary interactions in the nonequilibrium dynamics of partially Bose-condensed trapped gases. *Phys. Rev. A*, 57:1230, 1998.
- [PFTV89] William H. Press, Brian P. Flannery, Saul A. Teukolsky, and William T. Vetterling. *Numerical Recipes in Pascal*. Cambridge University Press, USA, 1989.
- [PHS00] D. S. Petrov, M. Holzmann, and Gora V. Shlyapnikov. Bose-Einstein condensation in quasi-2d trapped gases. *Phys. Rev. Lett.*, 84:2551–2555, 2000.
- [Pit61] Lev P. Pitaevskii. Vortex lines in an imperfect Bose gas. *J. Exptl. Theoret. Phys.*, 40:646–651, 1961.
- [Pou02] Uffe V. Poulsen. *Bose-Einstein Condensates: Excursions beyond the mean field*. PhD thesis, Department of Physics and Astronomy, University of Århus, Denmark, 2002.
- [PS01] D. S. Petrov and Gora V. Shlyapnikov. Interatomic collisions in a tightly confined Bose gas. *Phys. Rev. A*, 64:012706, 2001.
- [PS02] Christopher J. Pethick and Henrik Smith. *Bose-Einstein Condensation in Dilute Gases*. Cambridge University Press, Cambridge, 2002.
- [PS03] Lev P. Pitaevskii and Sandro Stringari. *Bose-Einstein Condensation*. Clarendon Press, Oxford, 2003.
- [RBC<sup>+</sup>01] Jacob L. Roberts, James P. Burke, Jr., Neil R. Claussen, Simon L. Cornish, Elizabeth A. Donley, and Carl E. Wieman. Improved characterization of elastic scattering near a Feshbach resonance in <sup>85</sup>Rb. *Phys. Rev. A*, 64:024702, 2001.

- [RCB<sup>+</sup>98] Jacob L. Roberts, Neil R. Claussen, James P. Burke, Jr., Chris H. Greene, Eric A. Cornell, and Carl E. Wieman. Resonant magnetic field control of elastic scattering in cold  $^{85}\text{Rb}$ . *Phys. Rev. Lett.*, 81:5109, 1998.
- [RCC<sup>+</sup>01] Jacob L. Roberts, Neil R. Claussen, Simon L. Cornish, Elizabeth A. Donley, Eric A. Cornell, and Carl E. Wieman. Controlled collapse of a Bose-Einstein condensate. *Phys. Rev. Lett.*, 86:4211, May 2001.
- [RENG03] D. Rychtarik, B. Engeser, H.-C. Nägerl, and R. Grimm. Two-dimensional Bose-Einstein condensate in an optical surface trap. *E-print arXiv cond-mat/0309536*, 2003.
- [SFJ02a] Ole Sørensen, Dmitri V. Fedorov, and Aksel S. Jensen. Correlated trapped bosons and the many-body Efimov effect. *Phys. Rev. Lett.*, 89:173002, 2002.
- [SFJ02b] Ole Sørensen, Dmitri V. Fedorov, and Aksel S. Jensen. Two-body correlations in  $N$ -body boson systems. *Phys. Rev. A*, 66:032507, 2002.
- [SFJ03a] Ole Sørensen, Dmitri V. Fedorov, and Aksel S. Jensen. Correlated  $N$ -boson systems for arbitrary scattering length. *Phys. Rev. A*, 68:063618, 2003.
- [SFJ03b] Ole Sørensen, Dmitri V. Fedorov, and Aksel S. Jensen. Stability, effective dimensions and interactions for bosons in deformed fields. *E-print arXiv cond-mat/0310462*, revised version will be submitted to *Phys. Rev. A*, 2003.
- [SFJ04] Ole Sørensen, Dmitri V. Fedorov, and Aksel S. Jensen. Structure of boson systems beyond the mean field. *J. Phys. B: At. Mol. Opt. Phys.*, 37(1):93–116, 2004.
- [SFJN02] Ole Sørensen, Dmitri V. Fedorov, Aksel S. Jensen, and Esben Nielsen. Two-body correlations in Bose-Einstein condensates. *Phys. Rev. A*, 65:051601(R), 2002.
- [SGWH99] Cass A. Sackett, J. M. Gerton, M. Welling, and Randall G. Hulet. Measurements of collective collapse in a Bose-Einstein condensate with attractive interactions. *Phys. Rev. Lett.*, 82:876, 1999.
- [SIA<sup>+</sup>99] J. Stenger, S. Inouye, M. R. Andrews, H.-J. Miesner, Dan M. Stamper-Kurn, and Wolfgang Ketterle. Strongly enhanced inelastic collisions in a Bose-Einstein condensate near Feshbach resonances. *Phys. Rev. Lett.*, 82:2422, 1999.
- [SJ87] Phillip J. Siemens and Aksel S. Jensen. *Elements of Nuclei*. Addison-Wesley, Reading, MA, 1987.

- [Smi60] Felix T. Smith. Generalized angular momentum in many-body collisions. *Phys. Rev.*, 120:1058, 1960.
- [Spi68] Murray R. Spiegel. *Schaum's Mathematical Handbook of Formulas and Tables*. McGraw-Hill, New York, 1968.
- [SS77] Yu. F. Smirnov and K. V. Shitikova. The method of  $k$  harmonics and the shell model. *Sov. J. Part. Nucl.*, 8:344, 1977.
- [SSH98] Cass A. Sackett, Henk T. C. Stoof, and Randall G. Hulet. Growth and collapse of a Bose-Einstein condensate with attractive interactions. *Phys. Rev. Lett.*, 80:2031, 1998.
- [TOH<sup>+</sup>03] B. Laburthe Tolra, K. M. O'Hara, J. H. Huckans, W. D. Phillips, S. L. Rolston, and J. V. Porto. Observation of reduced three-body recombination in a fermionized 1D Bose gas. *E-print arXiv cond-mat/0312003*, 2003.
- [US03] Masahito Ueda and Hiroki Saito. A consistent picture of a collapsing Bose-Einstein condensate. *J. Phys. Soc. Jpn.*, 72 suppl. C:127–133 (*E-print arXiv cond-mat/0305242*), 2003.
- [WM99] Deborah K. Watson and Brett A. McKinney. Improved large- $N$  limit for Bose-Einstein condensates from perturbation theory. *Phys. Rev. A*, 59:4091–4094, 1999.
- [Yak67] Oleg A. Yakubovskii. On the integral equations in the theory of  $N$  particle scattering. *Sov. J. Nucl. Phys.*, 5:937, 1967.